null allele results in 50% perinatal lethality and 50% postnatal lethality, with one quarter surviving to a viable and fertile but growth restricted adulthood (*377*). Expression of *Dlk1, Dio3* and *Rtl1* are decreased in the paternal null offspring. Surprisingly homozygous null offspring, generated from F1 hybrid crosses of viable paternal knockout offspring, survive but have lower birth weights (*377*). Because the *Meg3* null mutation does not affect methylation at the *Dlk1* DMD it is unlikely that there is *de facto* loss of imprinting (*377*). It is hypothesized that maternal *Meg3* promoter CGI deletion results in direct loss of ncRNA products and derepression of *Rtl1* in *trans* (*377*). However, paternal inheritance of the *Meg3* null allele is thought to lead to repression of *Dlk1* and *Dio3 in cis* due to ablation of the secondary DMD (*377*). There is a need for finer mutations targeting individual miRNAs and snoRNAs to better understand the function of ncRNAs in this cluster.

Deletion of the *Dlk1* DMD that resides between the 3′ end of *Dlk1* and the *Meg3* promoter, results in developmental defects based on parental inheritance (*367*). Maternal *Dlk1* DMD null conceptuses have late gestation lethality (~E16) with increased expression of *Dlk1*, *Rtl1* and *Dio3*, and decreased *Meg3*, snoRNA and miRNA expression (*367*). However, paternal inheritance results in normal transcriptional profiles and viable offspring (*367*). These results indicate that the *Dlk1* DMD is the primary germline-DMD regulating the 12qF1 cluster, and that its deletion effectively creates a paternal (methylated) allele (*367*)

Additional research on the importance of the *Dlk1* imprinting cluster in fetal and placental development is warranted. The *Dlk1* cluster has been implicated in animal husbandry research as the genetic determinant of the *calligpye* allele in sheep, which has parent of origin effects that result in lean muscle hypertrophy (*378*). In humans, maternal and paternal UPD14 cases can also be caused by *Dlk1* DMD deletion and hypomethylation (*362, 363*). Intriguingly,

one of the phenotypes associated with UPD14 is placentomegaly (*363*). The fetal and placental phenotypes observed in the *Dlk1*, *Rtl1*, *Meg3* and DMD deletions discussed above demonstrate that the *Dlk1* cluster has a critical role in prenatal development. Lastly, there are only 2 paternal imprinted DMDs shared in mouse and human (*H19* and *Dlk1*), and both are required for embryonic development from induced pluripotent stem cell and bimaternal embryonic development in mouse (*379-381*). These disparate but important phenomenon may be related to modulation of placental function by the *Dlk1* imprinted loci.

1.5.14 *Igf2r*

The insulin receptor growth factor type 2, *Igf2r*, is maternally expressed and resides within the larger *Tme* locus that when deleted in maternal lineages is lethal at E15.5 (*10, 382*). *Igf2r* and its human homolog are found on chromosomal bands17qA1 and 6q25.3 respectively. The *Igf2r* DMD is maternally methylated in both species, however in humans and other primates *Igf2r* is biallelically expressed in the majority of individuals ((*383*) and references therein). A maternally methylated DMD sequence within intron 2 of *Igf2r* can confer imprinting of YAC transgenes in mice (*384, 385*). The *Igf2r* DMD is situated at the promoter of *Airn* (antisense *Igf2r* RNA), a long antisense ncRNA (*385, 386*). Transcription of *Airn* occurs on the unmethylated paternal allele that is associated with a silenced *Igf2r* (*385, 386*). Truncation of the *Airn* transcript by insertion of poly-adenylation sequences mitigates *Igf2r* silencing independent of DNA methylation (*387, 388*). It is therefore hypothesized that the act of *Airn* transcription is directly responsible for *Igf2r* maternal inactivation (*387*). However, it has also been noted that in the placenta full length but not truncated *Airn* ncRNA associates with the *Slc22a3* promoter and recruits the H3K9 methyltransferase EHMT2 to invoke lineage-specific imprinting (*389*).

In the majority of embryonic and adult tissues imprinting at the *Igf2r* locus is limited to the expression of *Igf2r* and *Airn*. However, in the placenta and extra embryonic visceral yolksac the downstream *Slc22a2* and *Slc22a3* transcripts, encoding molecular transporters of unknown function, are preferentially expressed from the maternal allele (*307, 309, 390*). The expansion of the imprinted locus in extraembryonic tissues is similar to that found at other loci including *Kcnq1, Igf2, Peg10* and *Grb10* (*309*). The IGF2R protein is a receptor for IGF2 expressed in SynT as both a plasma membrane and cleaved soluble form (*391*). IGF2R exerts negative inputs to IGF2 signaling by acting to bind and clear excess IGF2, but may also have signaling properties (*391*). Targeted deletion of *Igf2r* (deletion of exons 13-18) when maternally inherited results in fetal and placental overgrowth (*392, 393*). Maternal *Igf2r* null conceptuses have elevated levels of IGF2 and IGF2-binding proteins (*392*). Deletion of the *Igf2R* DMD generates an allele that effectively mimics the maternal methylated state, and when paternally inherited results in increased *Igf2r* expression and embryonic and neonatal growth restriction (*394*). Due to increased *Igf2r* expression, paternally inherited the *Igf2r* DMD deletion can rescue maternally inherited *Tme* mutations (*394*). Based on these studies *Igf2r* is a growth suppressor. Based on the importance of the *Igf2r* locus in growth and its expanded boundaries in extraembryonic tissues it is important to determine the effects of loss of imprinting at the *Igf2r* DMD in placental development

1.5.15 *Impact*

The *Impact* gene resides on chromosomal band 18qA1 and is equated with parent-of-origin specific embryonic developmental delays observed with patUPD in studies of Robertsonian translocations involving chromosome 18 (*395, 396*). The paternally imprinted and ubiquitously

expressed *Impact* contains 11exons, and has a maternally methylated DMD within its first intron (*397*). *Impact* is adjacent to the non-imprinted proximal *Osbpl1* and the distal *Hrh4* (*398*). In humans, *IMPACT* is found in the same genomic context on chromosome band 18q11.2-12.1 but is not imprinted and lacks an intronic DMD (*397, 398*). Intriguingly a similar arrangement of *Osbpl2* and *Hrh3* but lacking an *Impact* paralog is found between the tandem duplicated *Lama3* and *Lama5* genes on mouse chromosome 2qH4 near the *Nnat* and *Gnas* clusters, and within a syntenic region on human chromosome 20q13.3 (*398*). Expression of *Impact* is much higher in rodent species where it is imprinted (*e.g.* mouse, rat and rabbit) than in pigs and primates where it is not (*399*). This suggests that the regulation of *Impact* gene dosage can explain the difference in imprinting status between mammalian clades (*399*).

The IMPACT protein is homologous to the ancestral yeast protein YIH1 involved in nutrient starvation responses (*395, 397*). In fact, IMPACT participates in the same translational regulation molecular pathways as its yeast homolog. IMPACT binds to GCN1 and inhibits the activity of GCN2 inactivating phosphorylation of Ser51 on the eukaryotic translational initiation factor 2 (eIF2α) (*400*). Unphosphorylated eIF2α inhibits translation of many proteins and activates translation of a few stress response genes (*400*). High levels of IMPACT in the hypothalamus and low levels of phosphorylated eIF2α are thought to be involved in nutrient deprivation and feeding behavior stress responses (*400*). In addition, IMPACT associates with ribosomes in post-differentiation neurons to promote neuritogenesis (*401*). Given the expression of *Impact* within the placenta and its role in mediating nutrient stress response it is plausible this gene has important functions within this essential organ.

A. *Nnat* 2qH4

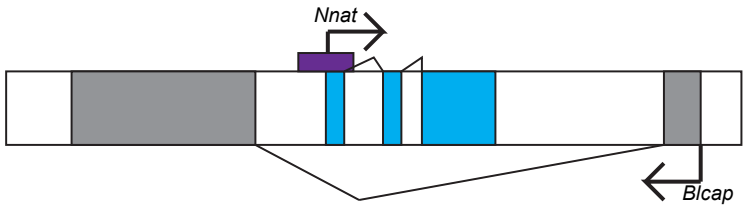

B. *Gnas* 2qH4

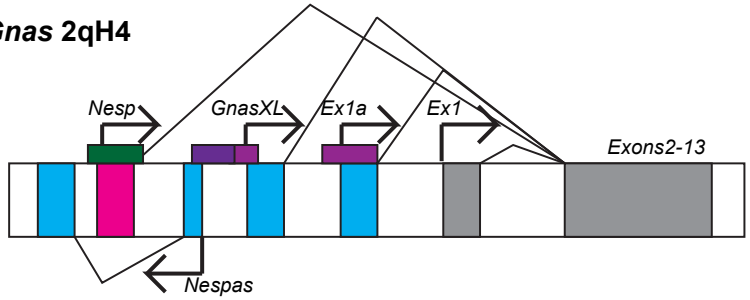

C. *Mest* 6qB3

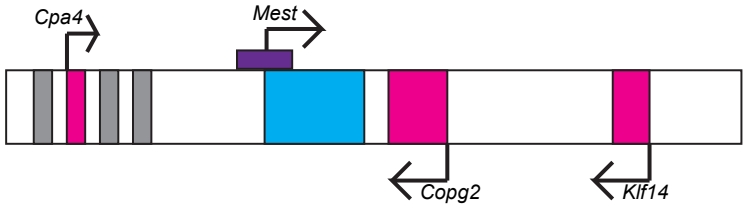

D. *Nap1l5* 6qB3

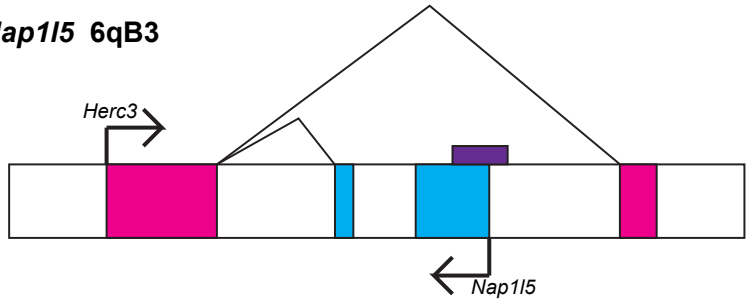

E. *Peg10* 6qA1

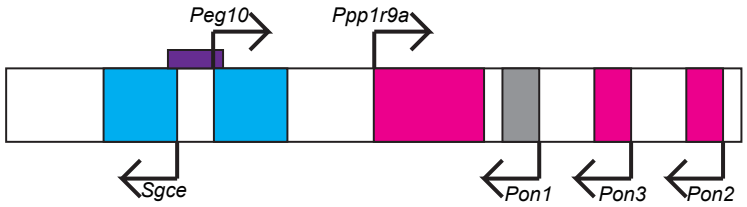

F. *H19* 7qF5

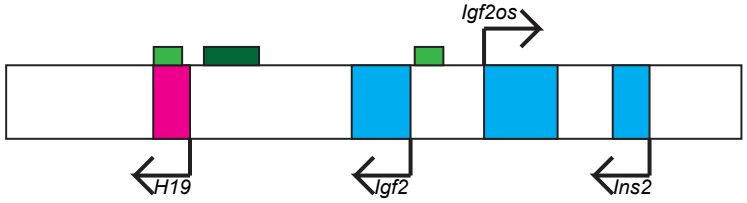

G. *Kcnq1* 7qF5

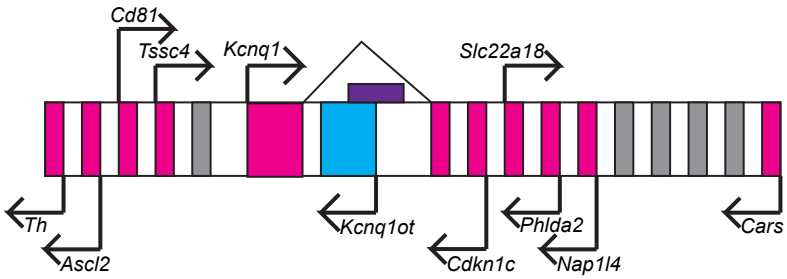

H. *Snrpn* 7qB5-7qC

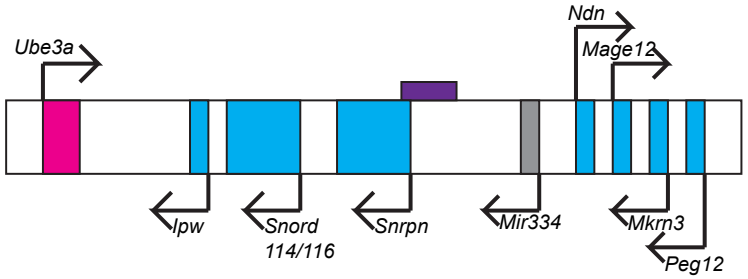

I. *Peg3* 7qA1

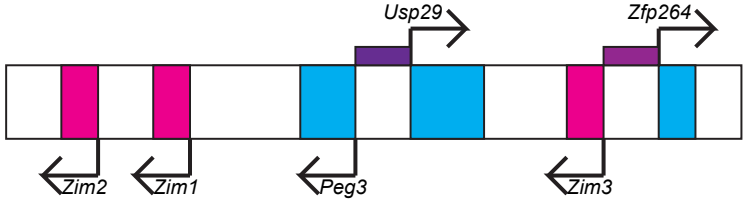

J. *Plagl1* 10qA2

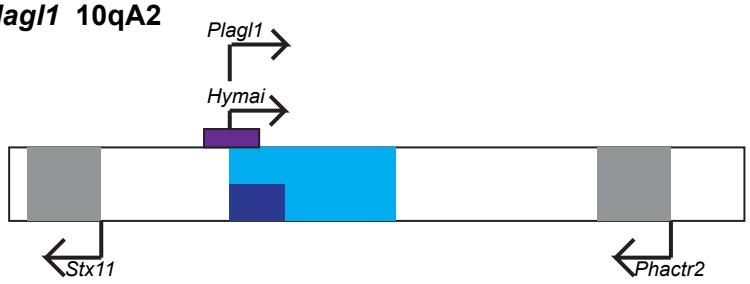

K. *Grb10* 11qA1

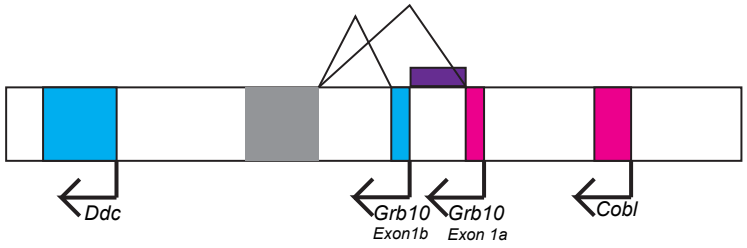

L. *Zrsr1* 11qA3.2

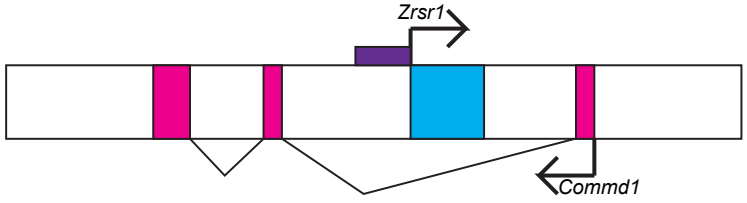

M. *Dlk1* 12qF1

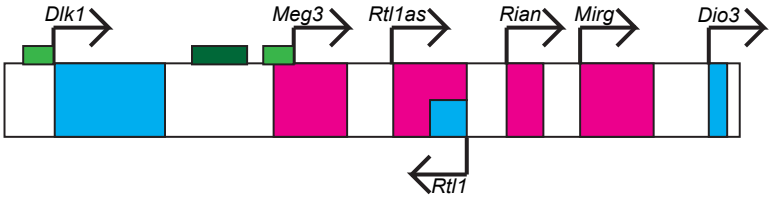

N. *Igf2r* 17qA1

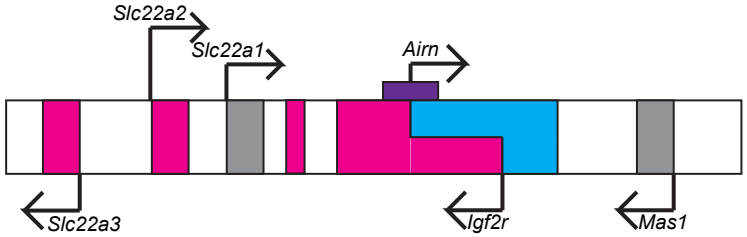

O. *Impact* 18qA1

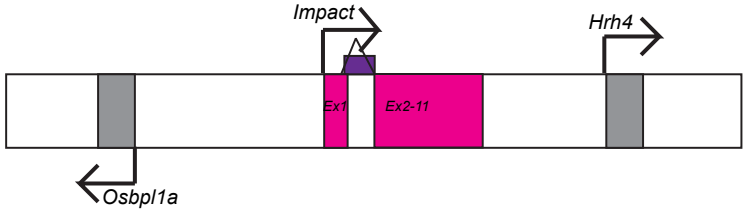

Figure 2. 15 Imprinted gene clusters. (A-O) 15 imprinted loci implicated in placental development are labeled by mouse chromosomal bands and refseq gene names. Each gene is represented by a filled rectangle and arrows give transcriptional direction. The color of each gene box indicates its imprinting status as maternally expressed (Pink), paternally expressed (Blue) or biallelic (Gray). DMDs are indicated as rectangle of lesser height outside above the gene diagram and are colored as to indicate their DNA methylation as maternal (purple) or paternal (green) in origin with secondary DMDs in lighter shades. Triangulated lines indicate alternative splicing, where relevant to genomic imprinting. This figure is the summation of the numerous works cited within section 1.5.1-15. Figure not drawn to scale.

1.6 SPECIFIC AIMS

My dissertation research tests the hypothesis that genomic imprints are essential during placental development and aims to define their importance in this fundamental mammalian organ. In my introduction I have described the importance of genomic imprinting in mammalian development and human disease. I have discussed the dynamics of methylation changes during germ cell and preimplantation development with a focus on imprinted DMD methylation. In addition, I have reviewed the function and development of the mouse placenta highlighting aspects relevant to modeling the human placenta. Herein, I have also described in detail fifrteen imprinted gene clusters with possible involvement in placental development. The placental function of imprinted gene clusters as an integrated unit, including both imprinted genes and the DMD methylation that controls their parent-of-origin specific expression, are incompletely understood. My thesis research builds off the knowledge presented within the introduction and seeks to identify the roles of genomic imprints in placental development by studying placental development in their absence.

In Chapters 2 and 3 of my dissertation I address the first two aims of my dissertation which examine the effects of partial loss of genomic imprints on placental development using the

Dnmt1$^{\Delta 1o}$ maternal effect model. The first aim of my dissertation research is to determine which placental processes are influenced by genomic imprinting. To these ends I described the range of placental morphological and molecular phenotypes of *Dnmt1*$^{\Delta 1o}$ maternal effect (DNMT1o-deficient) placentas across murine gestation from E9.5 to E17.5. Considerable emphasis was placed on quantifying changes in the following attributes: cellular composition, fetal viability, labyrinth vascularity, glycogen and lipid deposition, and gene expression. This section reveals many aspects of placental development are dependent on normal genomic imprinting as a whole.

The second aim of my thesis is to identify specifically which imprints are responsible are responsible for placental phenotypes associated with loss of imprinting. I started by describing the spectrum of mosaic loss of genomic imprinting in DNMT1o-deficient placentas by assaying imprinted gene expression and DMD methylation levels Then I tested for associations between placental phenotypes quantified in Chapter 2 and loss of imprints at specific DMDs using linear regression analysis. These results enabled the direct interpretation of functional significance of individual imprinted clusters in placental biology.

My third, and final dissertation research aim is to generate and describe a novel targeted deletion of the imprinted *Klf14* gene. This allele was designed and engineered using recombineering and was used to test the maternal-specific expression of *Klf14* in the placenta, and to record any phenotypes associated with its loss of expression. These results aide in the understanding of the role of the *Mest* imprinting cluster in its entirety in placental biology. The sum of my thesis aims is to provide pillars of evidence that unequivocally demonstrate the importance of genomic imprinting in placental development and identify specific placental functional and developmental processes that genomic imprints regulate.

2.0 PLACENTAL PHENOTYPES OBSERVED IN THE *DNMT1$^{\Delta 1o}$* MOUSE MODEL

2.1 SUMMARY

The *Dnmt1$^{\Delta 1o}$* maternal effect model produces DNMT1o-deficient embryos with partial loss of genomic imprints and grossly abnormal morphology (*60, 104, 105, 402*). As a consequence, DNMT1o-deficient fetuses do not survive until birth except on rare occasion. It is suspected that the poor developmental outcome of DNMT1o-deficient embryos is in part due to the failure of normal placental development. In this chapter I show that DNMT1o-deficient placentas exhibit variable abnormal phenotypes throughout gestation. Early in gestation *Dnmt1$^{\Delta 1o}$* maternal effect mutant placentas were found to have considerable loss of LZ development and an increased abundance of TGCs. In mid to late gestation DNMT1o-deficient placentas were found to have ectopic SpT extensions into the LZ, dilated fetal blood vessels, SynT lipid droplet accumulation and increased glycogen cell abundance. The balance of placental and fetal growth was dysregulated in late gestation *Dnmt1$^{\Delta 1o}$* maternal effect placentas. In addition, placental gene expression patterns were altered revealing that the imprinted gene network regulates important transcriptional pathways including oxidative stress response, molecular transport, lipid transport, and lipid metabolism. This evidence that placental development is disrupted in the *Dnmt1$^{\Delta 1o}$* maternal effect model is interpreted as support for the hypothesis that genomic imprints regulate key processes in trophoblast differentiation and placental development.

2.2 INTRODUCTION

2.2.1 The *Dnmt1*$^{\Delta 1o}$ model

The *Dnmt1* oocyte-specific isoform deletion (*Dnmt1*$^{\Delta 1o}$) model is a unique genetic system in which absence of the maternal effect DNMT1o protein in oocytes results in offspring with partial and mosaic loss of imprinted DMD methylation. It is unique in that its primary genetic mutation compromises the integrity of epigenetic inheritance of genomic imprints. This model is particularly useful because it yields a myriad of loss of imprinting epigenotypes unlike other available genetic models used to study genomic imprinting. Inactivating mutations of *Dnmt1*, which eliminate maintenance methyltransferase activity throughout development, are embryonic lethal and erase all imprinted DMD methylation as well as other genomic methylation (*101-103*). In addition, offspring of the *Dnmt3l* null maternal effect model are homogenous in their complete loss of maternal imprints and early embryonic lethality at E9.5 due to placental failure (*94, 97, 99*). Furthermore, nearly all DMD deletion models (reviewed in section 1.5) acquire the imprinted state of the methylated allele. The *Dnmt1*$^{\Delta 1o}$ model provides a means to directly study the effects of loss of DMD methylation on embryonic and placental development.

2.2.2 Identification of *Dnmt1o*

DNA methylation is perpetuated during each mitotic S-phase by the maintenance DNA methyltransferase DNMT1 at replication foci (*403*). The DNMT1 protein contains the modular

RFTS, CxxC Zn finger, BAH, and methyltransferase catalytic domains from N- to C-terminal as well as a disordered domain between amino acids 100 and 400 (*27, 83-85, 110*). DNMT1 is a component of multimeric complexes that dynamically modulate the epigenome through its interactions with other epigenetic regulators including DMAP, ZFP57, TRIM28, and DNMT3 isoforms (*75, 76, 107*). At least three mRNA isoforms of *Dnmt1* are produced from transcription of alternative promoters yielding different 5′ exons (*62*). The mouse somatic, *Dnmt1s* isoform is transcribed in the majority of tissues and encodes a 1620 amino acid protein (DNMT1s) with a molecular weight of 190kDa. Two sex-specific isoforms are generated from alternative promoters of *Dnmt1* in germ cells (*62*). Spermatagonia at the pachytene stage transcribe *Dnmt1p* from a downstream promoter immediately adjacent to the *Dnmt1* exon 1s 3′ splice juncture (*62*). The *Dnmt1p* exon 1p contains a much weaker translation initiation sequence and does not produce DNMT1 protein (*62*). The *Dnmt1o* promoter initiates approximately 7.5kb upstream from the *Dnmt1s* promoter and yields a protein product that is shortened by 118 amino acids at the N-terminus (*62*)

The oocyte specific DNMT1o isoform was first identified by the discovery of a truncated DNMT1 protein isoform in oocytes and preimplantation embryos that had a molecular weight of approximately 175kDa (*404*). The truncated N-terminus of DNMT1o as compared with DNMT1s ablates the sequences required for interaction with DMAP but enables the interaction of the N-terminus with annexin V (ANXA5) (*62*). The importance of the interaction between DNMT1 and DMAP is particularly important based on the epistatic lethality of the $Dnmt1^{v}$ (constitutive *Dnmt1o* expression) and *Dmap1* null alleles (*107*). ANXA5 is a phospholipid binding protein at the plasma membrane of mature oocytes, and has been shown to interact with DNMT1o but not DNMT1s, suggesting that the longer N-terminus of DNMT1s may block this

interaction (*62, 405*). The ANXA5-DNMT1o interaction is likely responsible for the sequestration of DNMT1o to the cytoplasm and plasma membrane in oocytes until it translocates to the nucleus at the 8-cell stage (see section 2.2.4) and may explain differences in maternally produced DNMT1s and DNTM1o stability and activity in preimplantation embryos (*62, 63, 104*). The research presented in the remaining introduction ascribes the primary function of DNMT1o to maintain imprinted DMD methylation during the rapid preimplantation genomic demethylation event.

2.2.3 Targeted deletion of *Dnmt1o*

The *Dnmt1*$^{\Delta 1o}$ allele was generated using homologous recombination in ESCs to eliminate a 260bp region spanning *Dnmt1* exon 1o and part of the 5′ 1o promoter (*104*). The targeting construct contained a loxp-neo-TK-loxp cassete in place of the 260bp to be deleted. Homologous recombinant ESCs were positively selected using neomycin and then transfected with a CRE expressing plasmid to induce deletion and then negatively selected for using the thymidine kinase substrate ganciclovir. These ESCs were used to derive a line of chimeric males that passed the *Dnmt1*$^{\Delta 1o}$ allele through the germline to establish a colony that was backcrossed onto the 129Sv background. Heterozygous and homozygous offspring of crosses between heterozygous parents develop normally, however homozygous females had progeny that could not survive, indicating a maternal effect.

Howell *et al.*(2001) studied DNMT1o-deficient embryos, derived from the *Dnmt1*$^{\Delta 1o}$ maternal effect model, for changes in their DNA methylation patterns (*104*). Methylation sensitive Southern blot analysis showed that global methylation was unchanged. Furthermore, both γ-satellite and IAP repetitive elements were proven to be normally methylated by

methylation sensitive Southern blotting and bisulfite sequencing in DNMT1o-deficient embryos. Genomic imprints on the other hand were not normally methylated in the *Dnmt1*$^{\Delta 1o}$ maternal effect offspring.

A severe reduction in genomic imprinting was observed in DNMT1o-deficient embryos (*104*). A single nucleotide polymorphism extension assay using conceptuses derived from crosses between the C57/B6 *mus musculus* homozygous *Dnmt1*$^{\Delta 1o}$ females and *mus castenous* wild-type males provided evidence of biallelic *H19* and *Snrpn* expression in an example DNMT1o deficient embryo. Using the same interspecific crosses an approximately fifty percent loss of methylation was observed at the *H19, Snrpn* and *Peg3* DMDs by bisulfite genomic sequencing. Imprinting in oocytes was shown to be normal, indicating a failure to maintain imprints in the zygote rather than a defect in the establishment of maternal imprints. Transplantation of DNMT1o-deficient pro-nuclei into wild-type oocytes resulted in full rescue of the methylation defect. The majority of *Dnmt1*$^{\Delta 1o}$ maternal effect progeny die between E12.5 and term and very few survive through the neonatal period of development.

2.2.4 Localization of DNMT1 in preimplantation embryos

Early studies on DNMT1 using the PATH-52 anti-DNMT1 antibody found that oocytes and preimplantation embryos express a shorter form (later named DNMT1o) than somatic cells (*404*). Immunoflourescense of oocytes and preimplantation embryos using the PATH-52 antibody showed that DNMT1 was concentrated in the subcortical cytosplasm in oocytes and 2-cell embryos, in cytoplasmic granules at the 4-cell stage and nuclear at the 8-cell stage (*62, 404*). Further studies using C-terminal truncated *Dnmt1*-β-galactosidase fusion genes identified regions required for cytoplasmic sequestration C-terminal to the RFTS domain (*406*).

Two new anti-DNMT1 antibodies, UPTC21 and UPT82, enabled a clearer picture of DNMT1 localization during preimplanation development (*63*). These antibodies have greater sensitivity than PATH52, and UPT82 can distinguish between full length somatic DNMT1 and the shorter DNMT1o. UPTC21 is an antiserum raised against DNMT1 amino acids 636-1108 and recognizes all DNMT1 isoforms, whereas UPT82 is an antiserum raised against the DNMT1 118 N-terminal amino acids and thus recognizes the longer somatic form of DNMT1 (DNMT1s) but not DNMT1o. The presence of a UPT-82 band in western blot analysis of oocytes showed that oocytes express DNMT1s in addition to the shorter DNMT1o isoform identified with the PATH-52 isoform. Immunofluorescence revealed UPT82 signal within ooplasm and 2-cell nuclei indicating maternal DNMT1s present and likely to be active early in zygotic development. UPTC21 immunoflourescene was detected in ooplasm and in the zygote cytoplasm up until the 8-cell stage, results interpreted to mean that DNMT1o is sequestered within the cytoplasm during early cleavage events. The amount of maternal effect DNMT1o protein far exceeds maternal DNMT1s in oocytes and preimplantation embryos, and provides an explanation for observations of the apparent absence of DNMT1s in the nucleus of 2- and 4- cell embryos using pan DNMT1 antibodies. Furthermore replacement of the 1o exon with the 1s coding sequence increased the amount of DNMT1s in 4-cell embryos. Reverse transcription PCR was also used to confirm expression of both *Dnmt1s* and *Dnmt1o* isoforms in the mouse oocyte (*63*).

The *Dnmt1*$^{\Delta 1o}$ and *Dnmt1*^{v} models provided an excellent confirmation of the above immunofluorescence assays (*60*). Wildtype embryos from 2 to 8-cells had nuclear UPT82 staining, whereas embryos from homozygous *Dnmt1*^{v} dams showed no UPT82 staining at the 1-cell stage and only gradually increased through the morula stage. Additionally, heterozygous *Dnmt1*^{v} females crossed with homozygous *Dnmt1*^{v} males all had nuclear UPT82 signal in the 1-

cell embryo, but only half had maintained UPT82 signal beyond that point. These results indicate that maternally derived DNMT1s is a nuclear protein during early cleavage prior to zygotic *Dnmt1s* transcriptional activation. Furthermore, loss of DMD methylation at *H19* and *Snrpn* DMDs could be prevented in *Dnmt1*$^{\Delta 1o}$ maternal effect offspring by transgenic overexpression of *Dnmt1s* in occytes driven by the zona pelucida *Zp3* promoter. This result was interpreted as evidence that there may not necessarily be anything inherently different between maternally acquired DNMT1o and DNMT1s recognition of methylation targets. Rather, DNMT1o is more effectively stored in oocytes, thus ensuring accurate maintenance of imprints (DMDs) in 8-cell embryos.

2.2.5 Preimplantation function of DNMT1o

The role of DNMT1o during preimplantation development is to maintain the integrity of genomic imprints. The initial report of loss of DMD methylation in *Dnmt1*$^{\Delta 1o}$ maternal effect offspring showed a fifty percent loss at three different DMDs in the analysis of a handful of samples and speculated that loss of methyltransferase activity at the 8-cell stage and random chromosomal assortment at the 5th mitosis would result in mosaic partial loss of genomic imprinting (*104*). A more thorough analysis confirmed these findings and found a profound level of epigenetic mosaicisim in *Dnmt1*$^{\Delta 1o}$ maternal effect offspring (*402*). Loss of *Snrpn* and *H19* DMD methylation could be detected as early as the morula stage by allele-specific bisulfite genomic sequencing and ranged from 13% to 65% methylation on the normally fully methylated parental alleles. The TR2+3 /*Igmyc* maternally imprinted transgene was crossed onto *Dnmt1*$^{\Delta 1o}$ females and used to determine that loss of methylation occurs as early as the 8-cell embryo and resolves to approximately 51% methylation at the blastocyst stage (*402*). Combined bisulfite

sequencing and restriction analysis (COBRA) was used to further validate that different DNMT1o-deficient ESC derived lines had varying levels of *H19* and *Snrpn* DMD methylation. At E9.5 loss of imprinted methylation at the *H19* and *Snrpn* DMD in DNMT1o-deficient embryos and placentas was observed alongside loss of monoallelic imprinted gene expression patterns. These studies firmly established the role of DNMT1o in preventing epigenetic variation at imprinted loci during preimplantation development and provided the framework for our current understanding of the *Dnmt1*$^{\Delta 1o}$ maternal effect model (Figure 3).

2.2.6 Fetal development of *Dnmt1*$^{\Delta 1o}$ maternal effect offspring

It is not surprising that the epigenetic mosaic predicted in the maternal effect model results in profound and variable embryonic morphology. A study of DNMT1o-deficient embryos focusing on fetal development at E9.5 revealed that mutant fetuses scored lower in nearly all morphological developmental features as compared to wild-type (*105*). DNMT1o-deficient fetuses were developmentally delayed on average 12hrs, had shorter crown-rump lengths and decreased number of somites. Although there were DNMT1o deficient fetuses that were morphologically normal, others had features such as failure of axial rotation, failure of anterior neuropore closure, poor heart morphogenesis and some that were in states of disintegration and reasbsorption. This varied and mosaic nature of DNMT1o-deficient fetal defects were in line

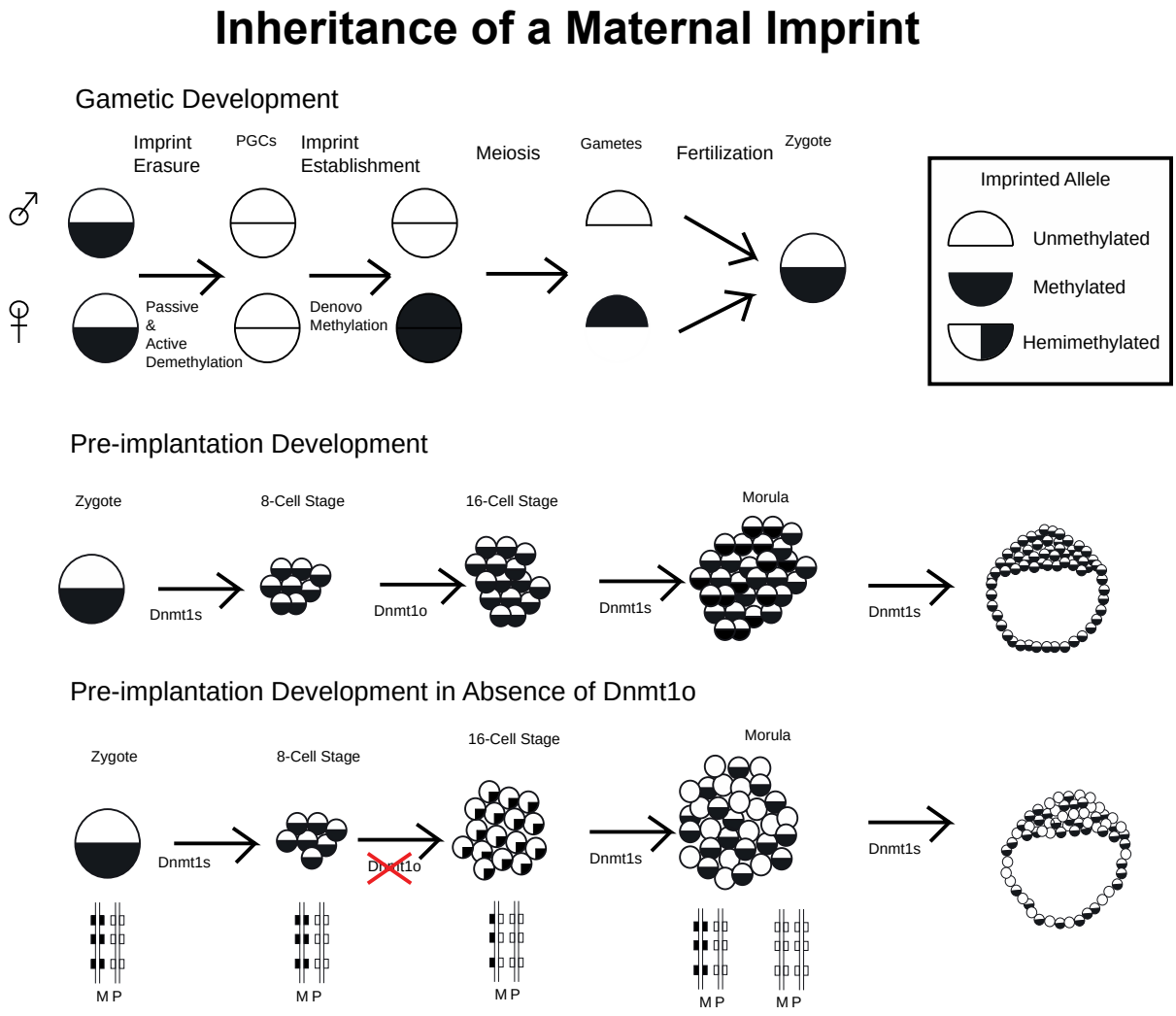

Figure 3. Inheritance of a maternal imprint in normal and *Dnmt1*$^{\Delta 1o}$ maternal effect embryos. During gametic development genomic imprints are erased in primordial germ cells and then reestablished in a sex-specific manner, such that in this example the maternal gamete contains a methylated imprint. In the wild-type zygote the combined action of maternally inherited DNMT1s, DNMT1o and zygotic DNMT1s account for maintenance of imprinted DMD methylation during preimplantation development. In DNMT1o-deficient conceptuses the lack of DNMT1o at the 4th mitotic event generates hemimethylated DNA that is then replicated, generating a mosaic of cells with half completely lacking the maternal imprint. Because this occurs at 24 different imprints scattered on various independently segregating autosomes, a great number of partial loss of imprinting permutation of can occur. Therefore, each DNMT1o-deficient 32-cell morula contains 16-normal cells and a mosaic of 16 cells with unique loss of imprinting epigenotypes.

with the molecular model of partial and varied loss of genomic imprinting and suggest a numerous roles for imprinted loci in early fetal development.

2.2.7 Placental development of *Dnmt1$^{\Delta 1o}$* maternal effect offspring

Initial reports also suggest that the placental compartment is affected by loss of imprinting in the *Dnmt1$^{\Delta 1o}$* maternal effect model. DNMT1o-deficient fetal and placental epigenomes are not always congruent. In fact, in a small set of E9.5 DNMT1o-deficient embryos, neither *H19* nor *Snrpn* DMD methylation was eqivalent in corresponding fetal and placental DNA samples (*402*). Preliminary research on placental morphology in E9.5 *Dnmt1$^{\Delta 1o}$* maternal effect offspring revealed that many DNMT1o-deficient placentas had shell shaped placentas draped around the conceptuses suggestive of trophoblast hyperplasia (*407*). This phenotype was more common in female than male conceptuses. Further studies examining loss of X-chromosome imprinting in extraembryonic lineages and placental trophoblast hyperplasia and diminished LZ development were performed by McGraw and colleagues (2013) contemporaneously with my own dissertation work (*408*).

2.2.8 Chapter 2 aims

The aim of this section is to utilize the *Dnmt1$^{\Delta 1o}$* maternal effect model of partial loss of imprinting to better understand the role of genomic imprints in placental biology. The *Dnmt1$^{\Delta 1o}$* maternal effect model is based on a genetic mutation that manifests loss of DMD methylation as the primary defect. This model produces a mosaic of epigenetic mutants that provide an opportunity to study the effects of loss of imprinting as a whole on placental development. In this

chapter I have tested the functional significance of genomic imprints in placental biology and tried to determine what layers and cell lineages are affected by describing DNMT1o-deficient placentas across gestation from E9.5 to E17.5. To assess placental efficiency and the balance of fetal and placental growth wet weight measurements of DNMT1o-deficient placentas and fetuses were made. To examine placental layer and cell type composition DNMT1o-deficient placentas were histologically analyzed using an array of tissue staining techniques. Placental metabolism in DNMT1o-deficient placentas was studied by triglyceride quantification and qualitatively by lipid and glycogen histological staining. The description and analyses of DNMT1o deficient placentas has been performed to delineate which placental processes genomic imprints are involved in and to lay the foundation for further research and modeling of the role of genomic imprints in placental development.

2.3 MATERIALS AND METHODS

2.3.1 Animal husbandry

All mice were maintained and used in accordance with guidelines from the Institutional Care and Use Committee (IACUC) at the University of Pittsburgh. The *Dnmt1*$^{\Delta 1o}$ allele was maintained on a 129Sv (Taconic) background by backcrossing heterozygous females to 129Sv males. Placentas from crosses between heterozygous *Dnmt1*$^{\Delta 1o}$ females and 129Sv males were used as wild-type (wt) controls. Crosses between homozygous *Dnmt1*$^{\Delta 1o}$ females and 129Sv males generated DNMT1o-deficient (*Dnmt1*$^{\Delta 1o}$ maternal effect) mutant (mt) conceptuses.

2.3.2 Genotyping

Genotyping was carried out on DNA isolated by phenol-chloroform extraction and ethanol precipitation of tails snipped at weaning or during embryonic collection. In addition, the genotype of pregnant mouse dams that were dissected for placental analysis was confirmed using DNA isolated from tail and spleen extracted at the time of dissection. *Dnmt1*$^{\Delta 1o}$ genotyping PCR used 350ng of starting genomic DNA and used the following thermocylcer program with Taq polymerase (Invitrogen): 95°C 5′ denaturing followed by 35 cycles of 95°C 30″, 56°C 30″; 72°C 45″, a 72°C 10′ final extension and indefinite hold at 4°C. PCR products were run on a 1 or 1.5% agarose gel to look for the presence of a wild-type (380bp) or mutant (120bp) band. Sex genotyping of embryos was performed using primers specific to the *Zfy* gene on the male sex chromosome. PCR conditions were as follows: 95°C 5′ denaturing followed by 35 cycles of 95°C 30″, 56°C 30″; 72°C 30″, a 72°C 7′ final extension and indefinite hold at 4°C. PCR products from the *Zfy* reaction were run on a 2% agarose gel to look for the presence of a 200bp band indicating male identity. The PCR primer sequences used for genotyping are given in Appendix A.

2.3.3 Collection of placentas

Embryonic day 0.5 (E0.5) was established based on the presence of a post-copulatory vaginal plug. Fertilization was assumed to have occurred at 12am based on the nocturnal nature of mating in *Mus* species. Pregnant females were sacrificed by CO_2 asphyxiation and conceptuses were collected at embryonic day 9.5, 12.5, 15.5 and 17.5 (E9.5, E12.5, E15.5 and E17.5). Dissections were carried out under low magnification (0.8X-2.5X) with a 350MZ dissection

microscope (Leica) using fine 8mm forceps. The whole uterus of sacrificed pregnant dams was isolated following cesarean section. Incision at the fat pad of each ovary and at the cervix facilitated removal of the uterus, which was placed in a 10cm petri dish of phosphate buffer saline (PBS) pH 7.5.

Each individual conceptus was removed from the uterine myometrium and placed in a 60mm petri dish with PBS leaving the embryo, yolk sac, placenta and decidua and inner myometrium intact. Whole E9.5 conceptuses were immediately placed in 4% paraformaldehyde (4% PFA). E12.5, E15.5 and E17.5 placentas were collected by the below protocol. The inner myometrium was carefully removed leaving the embryonic tissues and decidua intact. The yolk sac was excised away from the base of the placenta leaving the embryo exposed. The umbilical cord was pinched for 20″ to stop blood flow and stimulate clotting to stem leakage from both the fetus and placenta. The umbilical cord was then cut at the base of the chorionic plate and fetal abdomen. Each placenta and fetus was then weighed to the nearest tenth of a milligram. A small tail piece was cut and used for embryonic sex genotyping. Placentas were immersed in PBS again, then paced on a glass microscope slide with labyrinth facing down and cut in half with a sterile razor blade. One half was then placed back in fresh PBS and the other in 4% PFA for fixation. The half immersed in PBS was then cleaned of the decidua cap and any remaining yolk-sac and allantois. The E12.5 half samples were placed in RNA later, whereas the E15.5 and E17.5 samples were cut into two quarters, one placed in RNA later and the other snap frozen on dry ice for lipid extraction. Samples at each gestational age were labeled by litter (Letter A-G) and individual embryo (Number 1-8) for those used in DMD methylation analysis in Chapter 3.

2.3.4 Cryo-histology

Following fixation in 4% PFA, placental halves were suspended through a sucrose gradient up to 20% weight per volume, and then embedded in Tissue-Tek O.C.T compound (Sakura). Placental cryosections of 5μm and 10μm thickness were cut with a CM1850 cryostat (Leica) for histological analysis. Regressive hematoxylin and eosin (H&E; Sigma or Leica) staining was performed on a series of 5 micron meridian placental sections. In brief cryosections were fixed with O-Fix (Leica) for 30″, flushed with tap water for 30″, placed in hematoxylin for 45″ then washed for 1′ in water, placed in bluing reagent for 1′, water for 30″ and then 70% EtOH for 7-dips, alcoholic eosin for 16″, 95% EtOH for 7-dips, two washes in 100% EtOH of 7-dips and two washes in xylene of 7-dips before being mounted in a xylene based mounting medium. Periodic Acid-Schiff (PAS; Sigma) staining was carried out on E15.5 samples using standard instructions with the addition of a 5′ methyl-green (0.5%) nuclear staining prior to dehydration steps. In brief, PAS staining was carried out in coplin jars by placing cryosections in O-Fix for 1′, washing with water for 1′, placing in periodic acid solution for 5′, washing with water for 1′,, placing in Schiff's reagent for 15′, washing with water for 5′, placing in distilled deionized water for 1′, in 5′ methyl-green (0.5%) for 5′, rinse in water for 1′, and then run through 95-100-100% EtOH dehydration steps of 7-dips and then cleared in xylene for 7-dips twice and coverslipped in xylene based medium. All E9.5 and E12.5 histology was performed on cryosections, however some E15.5 and E17.5 H&E, PAS and immunocytochemistry was performed on paraffin embedded samples with the assistance of the MWRI histology core.

2.3.5 *In situ* hybridization

A series of 10μm sections were stained by *in situ* hybridization (ISH) with Digoxigenin-11-dUTP (Roche) labeled antisense RNA probes. ISH probes of the placental marker genes *Tpbpa, Tfeb, LepR, Pchdh12, Mest, Prl2c2, Prl3b1 and Prl3d1* were in-vitro transcribed (Promega) from cDNA cloned into pBluescript, and used to identify the labyrinth (*Tfeb*), SpT (*Tpbpa*), SynT (*LepR*), GCs (*Pchdh12*), fetal vascular (*Mest*) and TGCs (*Prl2c2, Prl3b1 and Prl3d1*) respectively. ISH probes of the imprinted genes *Ascl2, Phlda2* and *Igf2* were similarly generated. RNA probes were purified using a G50 column (GE Healthcare) to remove unincorporated nucleotides, ammonium acetate ethanol precipitation, and dissolved in 30μl of water. RNA concentration was then determined by using a nanovue spectrometer (GE Healthcare) and diluted in ISH hybridization buffer (50% Formamide, 5X SSC, 5X Denhardt's, 0.25mg/ml tRNA, 0.5mg/ml herring sperm DNA) to a concentration of 200ng/μl.

Cryosections were stored at -70°C and warmed to 30°C to dry before starting ISH processing. Slides were fixed in 4% PFA for 10′, washed with PBS 3x for 3′ and digested with proteinase K for 5′. Following digestion slides were placed back into 4% PFA for 5′, washed 3x with PBS and then placed in an acetylation reaction (200ml aqueous solution of 0.1M triethanolamine and 0.2M HCl, initiated with 500μl of acetic anhydride immediately prior to use) for 10′. Slides were then washed with PBS 3x for 5′, tissue sections outlined with a pap-pen and were pre-incubated with ISH buffer for 2h at room temperature. At the end of 2h ISH probes were heated to 75-80°C for 5′ on hot beads, placed on ice for 3′ and spun down and then diluted (10μl probe +140μl ISH buffer per section). 125μl of diluted probe was added to each slide, a cover slip placed on top, the slides placed in a humidified slide box wrapped with paraffin tape and incubated overnight at 65°C. The following day slides were washed with 5x SSC to remove

coverslips, and incubated with 0.2X SSC for 2h at 70°C. After cooling down to room temperature samples were incubated with buffer B1 (0.1M Tris pH7.5 and 0.15M NaCl) for 5′ then incubated with B2 (B1 +5% Fetal Goat Serum) for 1 hour and then with B1 + anti-DIG alkaline phosphatase (AP) conjugated antibody (1:5000) overnight at 5°C. On the third day slides were washed three times with B1 and then equilibrated with B3 (0.1M Tris pH9.5, 0.1M NaCl and 50mM $MgCl_2$) for 5′. Slides were then incubated in the dark with B4 (B3+levamisole and NBT/BCIP) for 3-24 hours depending on strength of probe. AP reactions were stopped using TE buffer, the slides air-dried, passed through an ethanol dehydration gradient and xylene clearing step and cover slipped with a xylene based media.

2.3.6 Immunohistochemistry

E17.5 10μm paraffin sections were stained by immunohistochemistry (IHC) using an anti-CD31 antibody. Briefly, samples were processed according to IHC kit instructions (Pierce): Slides were deparaffinized and rehydrated using xylene and ethanol washes, then were washed with exposed 3% hydrogen peroxide for 10′, washed with PBST (PBS + 1% Tween 20) blocked with horse serum, incubated overnight with 1:200 rabbit polyclonal anti-CD31 (Vector Labs) at 4°C, washed, incubated with biotinylated secondary, washed and then stained using the Vectastain ABC reagent (Pierce), and counter stained with hematoxylin.

2.3.7 Immunofluorescence

E17.5 cryosections were stained with a combination of DAPI, LipidTOX (Invitrogen) and anti-CD31 fluorescent reagents. Briefly samples were washed with PBST, blocked with 5% goat

serum, incubated with primary anti-CD31 (Jackson ImmunoResearch Labs) overnight at 4°C, washed with PBST, incubated with 1:200 alexa-555 or -488 goat anti-rat IgG (BD) for 1h at room temperature, washed with PBST, stained with 1:250 LipidTOX for 30′ in the dark, washed with PBST and then coverslipped with DAPI containing medium. E12.5 samples were stained with DAPI and coverslipped to count TGCs.

2.3.8 Stereology and morphometrics

All images of placental tissue sections were taken using a DMI4000B inverted microscope (Leica) using 1.6x, 5x, 10x, 20x or 40x objectives and a 10x multiplier. Morphometric area measurements were made using the Image J (NIH) grid tool. The area of JZ and LZ layers were determined using random grid sampling within 2-3 central 50x or 16x fields of view of H&E stained sections for E12.5 and E15.5 placentas respectively. H&E images were overlaid with a random offset grid with 0.050 or 0.125mm^2 per point respectively based on image magnification. The placental cell layer of each point (or upper left quadrant at boundary areas) was determined based on cell morphology of JZ (compact diploid SpT layer) or LZ (integrated SynT, fetal vasculature and maternal blood spaces). The chorionic plate was excluded from LZ measurements. Areas were integrated across the known distance (~250μm) between serial sections to generate a central LZ and JZ volume metric. Area and volume measurements were confirmed by analysis of adjacent slides stained by ISH of lineage markers. P-TGCcount measurements were obtained from 2-3 central 10μm DAPI stained sections. The polyploidy P-TGC nuclei were readily distinguished from the diploid nuclei of the neighboring decidua and SpT cells at greater than 100x total magnification. The average cell count per 10μm section was

used as the reported metric. The identity of trophoblast giant cells was confirmed with ISH of adjacent sections.

2.3.9 Lipid extraction

Placenta samples cleaned of maternal decidua were stored at -70C for up to 3 months prior to lipid extraction. Samples were weighed and reduced to 25mg total weight. Samples were then placed in a dounce homogenizer with 250µl of deionized water with 5% NP40 and completely homogenized. Samples were then transferred with a Pasteur pipette to a clean glass test tube and cycled through a beaker of hot (80-100°C) water and room temperature two times to precipitate cell debris. The samples were then transferred to microcentrifuge tubes and centrifuged at 13000rpm for 5′ to pellet debris. Supernatant was transferred to a clean glass test tube, covered with paraffin film and stored for up to 1 week at 5°C. A triglyceride assay kit (Biovision) was used to quantify lipid content using a colorimetric assay in 96 well flat bottom plates. Duplicate standard controls of 10, 20, 30, 40 and 50 ng/well were used to generate a standard curve. Samples were plated in triplicate using 10µl of placental triglyceride extract and 40µl of sample buffer per well. Samples and controls were incubated with 2µl of lipase for 20′ at room temperature and then incubated with a reaction mix containing 46µl of buffer, 2µl of triglyceride probe and 2µl of enzyme mix per well and incubated for 1 hour at RT with gentle shaking. Absorbance at 570nm was the colormetric readout. Sample concentrations were back calculated as nmol triglyceride per mg of tissue using the standard curve and known mg per volume of sample.

2.3.10 Biostatistics

Mean mutant and wild-type phenotypic averages were calculated for all quantitative traits. The phenotypic data was also subdivided into dead/alive and male/female subgroups to determine the influence of fetal viability and sex on placental phenotypes. The distribution of each data set was tested for normality using the Kolmogorov-Smirnov, Shapiro-Wilk and Anderson-Darling tests of normality. When distributions approximated normality the students t-test was used to compare the distribution of mutant and wild-type phenotypes as well as the phenotypes observed in subgroups. Likewise, where the data was non-normally distributed the Mann-Whitney U (Rank-sum) test was used to compare the sample averages. Phenotypic data is most often displayed in charts showing mean + SEM.

2.3.11 Microarray analysis

E17.5 placental halves cleaned of maternal decidua were used to analyze global gene expression. Four wild-type controls, four low E/P DNMT1o-deficient and four high E/P DNMT1o-deficient placentas were analyzed. An even number of males and females were included in each group to minimize sex-specific expression differences. RNA was extracted from placental samples using a DNA/RNA combined kit (Qiagen). Illumina mouse WG-6-V2.0 Expression bead chips were used for whole genome expression profiling of 45,200 transcripts. Data was normalized and then mean expression values were determined for each subgroup. Ingenuity pathway analysis (IPA) was used to determine which biological pathways had altered gene expression patterns in low and high E/P ratio DNMT1o-deficient placentas.

2.4 RESULTS

2.4.1 *Dnmt1*$^{\Delta 1o}$ maternal effect embryonic viability

DNMT1o-deficient placentas exhibited a large spectrum of phenotypic abnormalities in the placental compartment across gestational development from E9.5 to E17.5. The number of live DNMT1o-deficient embryos decreased across gestation such that a greater number of litters was required late to collect the same number of placental samples for each gestational age (Table 2). These results revealed a strong selection event between E9.5 and E12.5 that reduced the number of viable embryos. The results reported here differ slightly from those I published in Developmental Biology (*409*) and PLoS One: Epigenetics (*410*) because of less stringent viability criteria at E9.5 used herein.

A diverse array of placental phenotypes was observed in the *Dnmt1*$^{\Delta 1o}$ maternal effect across gestation from E9.5 to E17.5. Early in development I observed decreases in the central volume of JZ and LZ layers and expansion of trophoblast giant cells. While placentas were smaller than average at E12.5, those recovered at E17.5 were overgrown. At mid (E15.5) and late (E17.5) gestational time points DNMT1o-defiicent placentas had reduced fetal vascular surface area, labyrinth hemorraghing, increased GCs abundance, increased lipid content and a prevalence of SpT extensions within the LZ. In addition, the balance of fetal and placental growth was disrupted

Gestational Age (dpc)	# Litters	# Placentas(a)	#Live Embryos(b)
E9.5	4	30	29
E12.5	3	24	10
E15.5	4	23	11
E17.5	5	23	14

Table 2. Survival of DNMT1o-deficient embryos and placentas. (a) Only intact placentas that were not necrotic, reabsorbing or hydatidiform moles were counted. (b) Based on structural integrity at E9.5 and presence of active circulation at E12.5 and later.

2.4.2 E9.5 Phenotypes

I performed histological analysis on E9.5 whole mount cryo-embedded conceptuses from 3 *Dnmt1*$^{\Delta 1o}$ maternal effect litters. A single example of a DNMT1o-deficient litter with 7 conceptuses (M1-M7) is shown in Figure 4 alongside an exemplary wild-type (wt) control. Abnormalities in placental layers were identified in central placental H&E stained sections. Central sections were determined based on presence of the maternal spiral artery, a triangular shaped maternal artery at the apex of trophoblast implantation. Maternal and fetal blood was distinguished by the presence of hematoxylin stained nuclei in fetal erythrocytes and absence in erythrocytes of maternal origin. In wild-type placenta a large maternal artery was observed for all samples and each placental layer was intact (wt; Figure 4). Not all mutant placentas observed had a dilated maternal artery, indicating a defect in implantation (DNMT1o-deficient mutants M2, M5 and M7; Figure 4). Poor structural integrity of the labyrinth and expansion of trophoblast giant cells was noticeable in many of the mutants. DNMT1o-deficient placentas M2, M3, M4, M5 and M7 had underdeveloped LZ. DNMT1o-deficient placentas M2 and M7 had an easily discernible overabundance of trophoblast giant cells.

To confirm the cell identities and phenotypes interpreted from H&E histology I performed in situ hybridization with a set of trophoblast lineage markers (Figure 4). The prolactin family member *Prl2c2* was used as a TGC marker. Expansion of the TGC layer from 1-

3 cells thick to 5-6 cells was observed in DNMT1o-deficient mutants M2 and M7 (Figure 4). An antisense probe to the transcription factor *Tfeb* cDNA was used to identify EXE derived chorionic plate and SynT progenitors. DNMT1o-deficient mutant M2, M3, M4, M5 and M7 showed decreased expression and less structural development of maternal blood spaces (Figure 4). In wild type placenta *Tfeb* had a complex spatial expression pattern of raised and convoluted chorionic trophoblast, whereas the abnormal DNMT1o-deficient placentas displayed flattened labyrinth chorionic trophoblast. An antisense probe for the ectoplacental cone specific transcription factor *Tpbpa* was used to identify SpT and progenitors. In wild-type placentas *Tpbpa* marks an apex area around the maternal spiral artery. DNMT1o-deficient mutants M3 and M4 have a marked decrease in *Tpbpa* expression.

In conjunction with ISH of placenta lineage markers I probed adjacent E9.5 whole-mount DNMT1o-deficient placenta with antisense probes to the imprinted genes *Ascl2, Phlda2* and *Igf2* (Figure 4). We expected and observed a decrease in the spatial expression pattern for each imprinted genes. *Ascl2* is expressed in the EPC in wild-type E9.5 placentas whereas *Phlda2* is expressed primarily in the labyrinthine EXE derived lineages. Loss of methylation at the *Kcnq1* DMD should have the predicted effect of decreased *Aslc2* and *Phlda2*. DNMT1o-deficient mutants M3 and M4 had severely restricted expression of both *Aslc2* and *Phlda2* (Figure 4). *Igf2* is ubiquitously expressed in placental and embryonic tissues. Loss of *H19* DMD methylation is expected to result in diminished *Igf2* expression. The majority of DNMT1o-deficient mutants had minimal *Igf2* staining, with the exceptions being M6 and M7 (Figure 4). Discordant *Igf2* expression patterns were observed between placenta and fetus and also between EPC (SpT and TGC) and EXE (chorion and SynT) derived trophoblast lineages. These results indicate that the

DNMT1o-maternal effect model has early wide-ranging phenotypes in placental structure and imprinted gene expression.

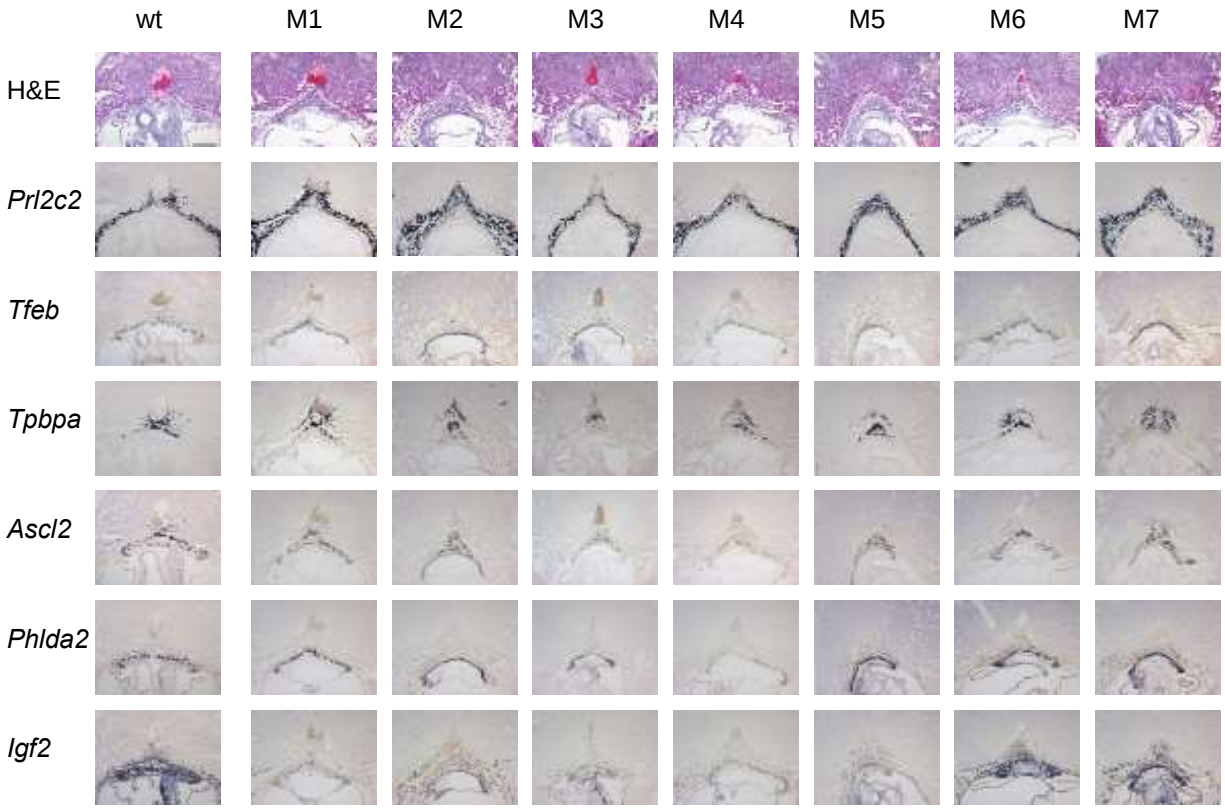

Figure 4. E9.5 Histology of wild-type (wt) and DNMT1o-deficient placentas (M1-M7). A broad range of morphologic and gene expression abnormalities is present in an exemplary single litter of E9.5 DNMT1o-deficient placentas. H&E staining and ISH of adjacent central placental sections are shown. ISH probes are listed on the left bar include placenta lineage markers Prl2c2 (TGCs), Tpbpa (EPC), Tfeb (Chorion) and imprinted genes Ascl2, Phlda2 and Igf2. Scale bar 500um.

2.4.3 E12.5 Phenotypes

I performed histological analysis on 24 E12.5 whole mount cryo-embedded conceptuses from 3 *Dnmt1*$^{\Delta 1o}$ maternal effect litters (E12.5 Litters A-C). Two wild-type litters, with a total of 16 conceptuses were used as controls. H&E staining was used to observe overall abnormalities and

in situ hybridization in order to confirm cell type identities. DNMT1o-deficient and wild-type placentas differed in many ways at E12.5, particularly in weight, central JZ volume, central LZ volume and number of TGCs (Figure 5). There was a trend toward decreased placental weight in DNMT1o-deficient placentas ($P<0.05$; Figure 5A). Additionally, there were significant decreases in measured central LZ volume ($P<0.005$; Figure 5B) and central JZ volume ($P<0.005$; Fig 5B) in the DNMT1o-deficient placentas compared to wild-type controls. A marked increase in the number of TGCs per central section was measured in the E12.5 DNMT1o-deficient placentas compared to wild-type controls ($P<0.01$; Figure 5C). These findings are in line with my previous findings of distorted placental layer development at E9.5 (Section 2.4.2; (*409*)).

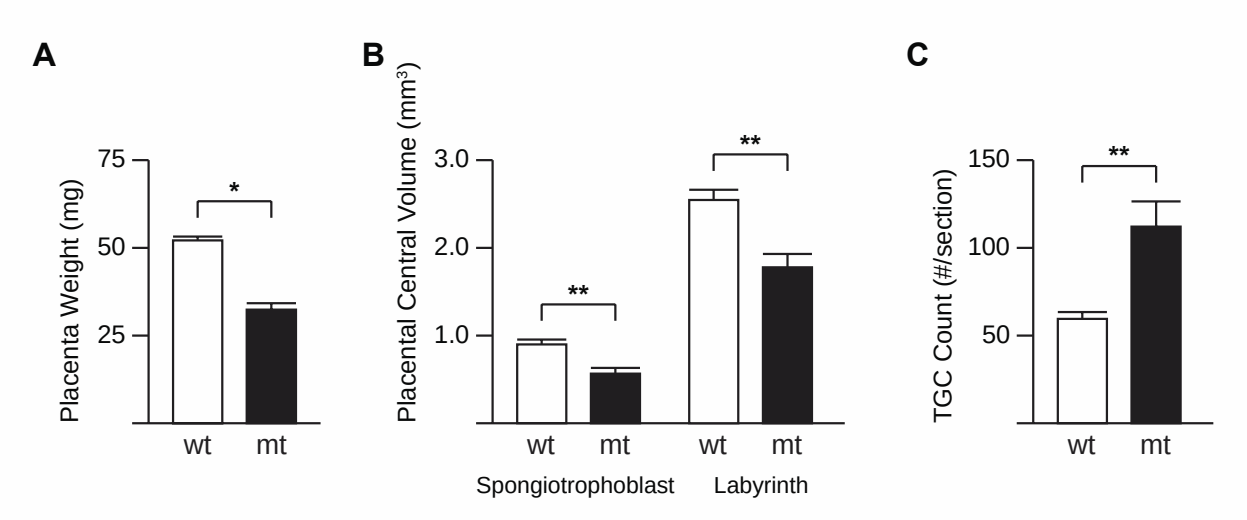

Figure 5. Phenotypic comparison of wild-type (wt) and DNMT1o-deficient (mt) placentas at E12.5. (A) Measurements of wet placenta weight, (B) Spongiotrophoblast and Labyrinth central volume, and (C) the number of TGCs per slide of a cohort of wt and mt placentas are displayed as open and filled bars respectively. Data are plotted as mean +SEM. *($P<0.05$) and **($P<0.005$) denote significant differences between wt and mt averages by the Rank-sum test, wt n=21 for placental weights and wt n=12 for layer volumes, mt n=24 for all.

To determine the effects of fetal viability and sex on placental phenotypes in the *Dnmt1*$^{\Delta 1o}$ maternal effect mouse model we compared live/dead and male/female mutant and wild-type cohorts (Figures 6 and 7). We compared the phenotypes of DNMT1o-deficient

placentas that harbored live and dead fetuses and found that those placentas that did not support a viable fetus had less labyrinth volume than those that did support a live fetus (Figure 6). In a sex comparison of DNMT1o-deficient placentas we discovered that female placentas on average had smaller central LZ volumes than mutant males ($P<0.05$; Figure 7). In addition, DNMT1o-deficient females had significant differences from wild-type counterparts at all measured phenotypes whereas mutant males only differed from wild-type males in LZ central volume and TGC number (Figure 7). These results are in line with preliminary reports earlier placental phenotypes that are more prominent in female than male *Dnmt1*$^{\Delta 1o}$ maternal effect offspring (*407*).

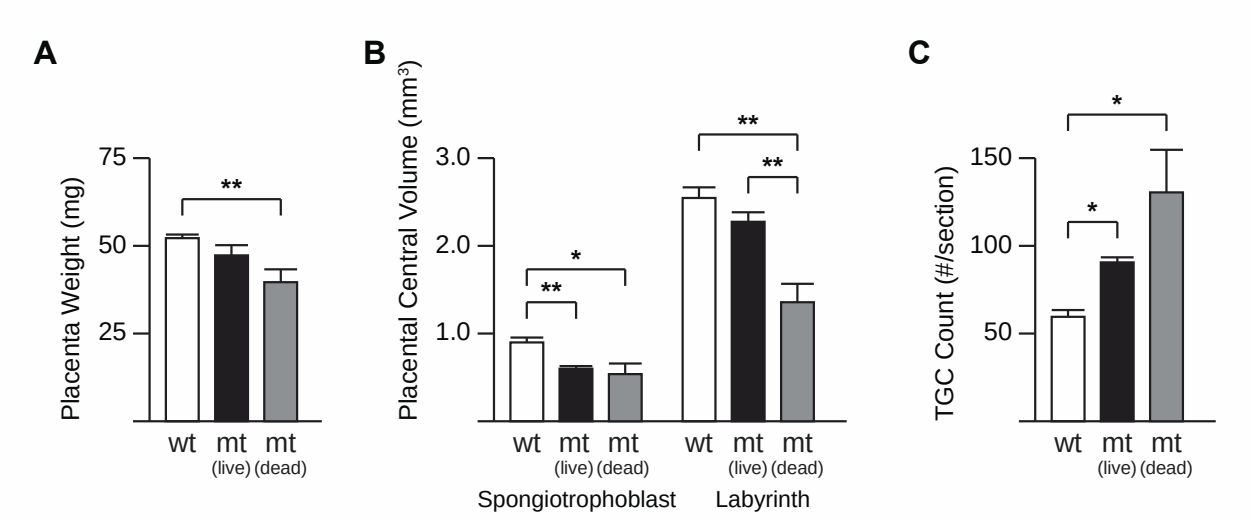

Figure 6. Phenotypic comparison of wild-type (wt) and DNMT1o-deficient (mt) live and dead placentas at E12.5. (A) Measurements of wet placenta weight, (B) Spongiotrophoblast and Labyrinth central volume, and (C) the number of TGCs per slide of a cohort of wt and mt-Live and mt-Dead placentas are displayed as white, black and gray bars respectively. Data are plotted as mean + SEM. *($P<0.05$) and **($P<0.005$) denote significant differences between wt, mt-live and mt-dead averages by the Rank-sum test. wt n=21 for placental weights, n=12 for layer volumes, mt(live) n= 11, mt(dead) n=13.

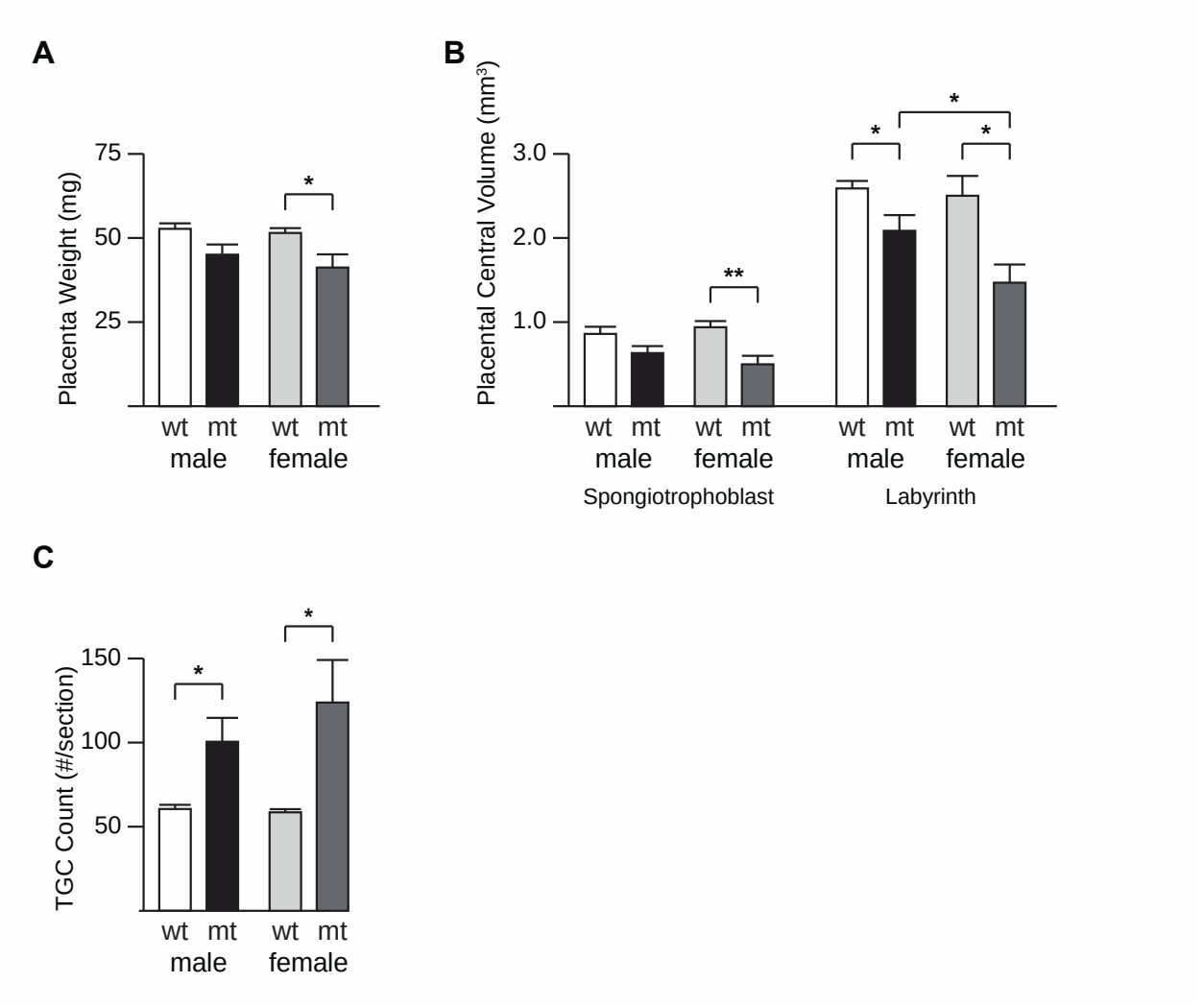

Figure 7. Phenotypic comparison of wild-type (wt) male and female, and DNMT1o-deficient (mt) male and female placentas at E12.5. (A) Measurements of wet placenta weight, (B) Spongiotrophoblast and Labyrinth central volume, and (C) the number of TGCs per slide of a cohort of wt-male, mt-male, wt-female and mt-female placentas are displayed as white, black, light-gray and dark-gray bars respectively. Data are plotted as mean + SEM. *($P<0.05$) and **($P<0.005$) denotes significant differences between wt-male, wt-female, mt-male and mt-female averages by the Rank-sum test. wt-male n=11 and wt-female n=10 for placental weights, wt-male n=6 and wt-female n=6 for layer volumes, mt-male n=12, mt-female n=12.

Labyrinth morphology was noticeably abnormal with hemorrhaging of maternal blood pools and poor fetal vasculature development (see Figure 37 in section 3.4.5 for H&E staining of DNMT1o-deficient placentas associated with loss of *Peg10* DMD methylation). To confirm the poor vascular development in DNMT1o-deficient samples ISH with an RNA probe antisense to

the *Mest* transcript was used to identify fetal vessels. Although *Mest* is an imprinted gene, its expression is expected to increase rather than decrease with loss of methylation at the *Mest* DMD. Therefore, any reduction in expression observed should be due to loss of fetal vasculature and not loss of imprinting at the *Mest* locus. In one maternal effect litter of eight (Figure 8 C1-C8), four have normal fetal vessel branching (C1, C5, C6 and C7), two have stumped and underdeveloped vasculature (C2 and C3) and two completely lacked vasculature (C4 and C8). Not surprisingly the placentas with diminished or no vasculature did not support a viable fetus. Although these results indicate imprinting is important for placental fetal vasculature development it does not tell us whether it is imprinting within the fetal derived vascular endothelium or trophoblast components of the placenta that is critical.

The spongiotrophoblast layer was examined by ISH expression analysis of *Tpbpa* and *Ascl2* (Figures 9 and 10). In wild type placentas a distinct JZ layer was present at the boundary of the LZ and maternal decidua consisting of SpT that stained strongly for *Tpbpa* (WT; Figure 9). ISH staining for *Tpbpa* in DNMT1o-deficient placentas ranged from normal (C2 and C7; Figure 9) to abnormal, showing ectopic expression in the LZ or decidua (C1, C6, C7 and C8; Figure 9) and/or diminished and dispersed signal (C1, C3 and C4 and C8; Figure 9). Expression of *Ascl2* marks SpT but does not stain as strongly in wild-type placentas at E12.5 than at E9.5 (wt, Figures 4 and 10). However, at E12.5 *Ascl2* is also detected in C-TGCs and S-TGCs and remaining TSC populations embedded in the LZ (WT; Figure 10). DNMT1o-deficient mutant placentas exhibited a wide spectrum of *Ascl2* spatial expression patterns (C1-8; Figure 10). *Dnmt1*$^{\Delta 1o}$ maternal effect mutants showed near normal (C1), partial loss (C3, C6, C8) or complete loss (C4) of *Ascl2* expression, consistent with varying degrees of partial loss of *Kcnq1* DMD methylation. Intriguingly, DNMT1o-deficient placenta C3 has partial loss of *Ascl2*

expression on the same junctional zone side that lacks *Tpbpa* expression, and has stunted vascular development; whereas DNMT1o-deficient placenta C4 with complete loss of *Ascl2* has neither *Tpbpa* expression nor vascular development. Some DNMT1o-deficient placentas had stronger than normal *Ascl2* staining with the LZ (C1, C5 and C7) suggesting that undifferentiated EPC progenitors, C-TGCs or S-TGCs may be accumulating.

Excessive abundance of TGCs is shown in three examples of DNMT1o-deficient placentas by DAPI nuclear staining (Figure 11; also See Figure 38 in section 3.4.5) for H&E and in situ analysis of TGC accumulation in E12.5 placentas with loss of *Kcnq1* DMD methylation). DAPI TGC nuclei were counted for 2-3 central sections and averaged for each placenta. Wild-type and $Dnmt1^{\Delta 1o}$ maternal effect mutant cohort TGC count averages were compared with extended analysis of live/dead and male/female subgroubs (Figures 5C, 6C, and 7C). Accumulation of TGCs in DNMT1o-deficient placentas was most evident in placentas lacking a viable fetus, and was significant in both male and female conceptuses. DNMT1o-deficient placentas C1, C3 and C8 had elevated TGC counts and abnormal (although not absent) *Ascl2* and *Tpbpa* expression. These results suggest that the maldevelopment of each layer is interdependent in DNMT1o-deficient placentas.

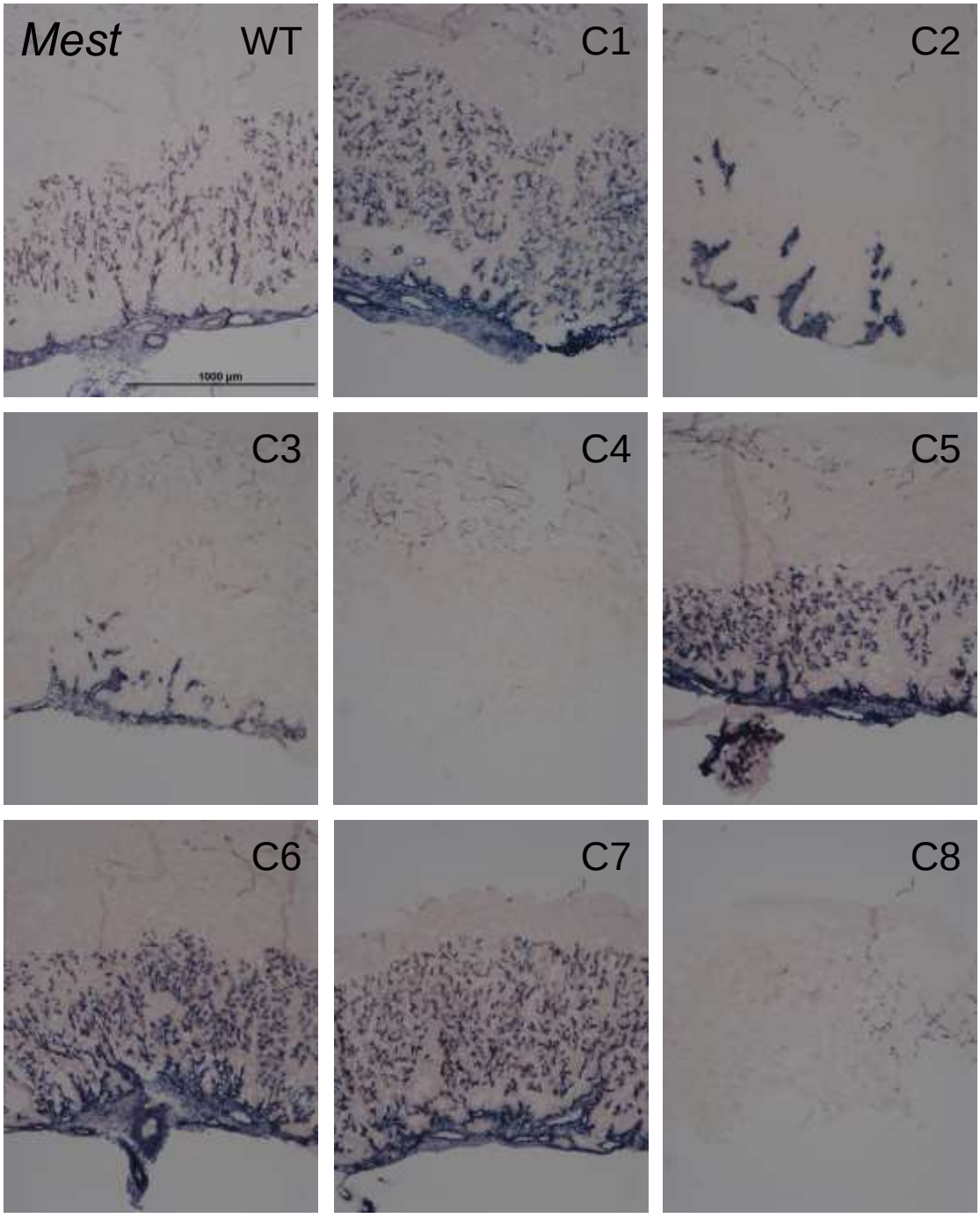

Figure 8. E12.5 *Mest* ISH of a Wild-type (WT) and a litter of eight DNMT1o-deficient (C1-C8) placentas. *Mest* expression marks fetal endothelium and chorionic plate. Note the normal fetal vessel branching patterns in WT and C1, C5, C6, and C7, stumped in C2 and C3, and lack of in C4 and C8. 4x objective Scale bar is 1000um.

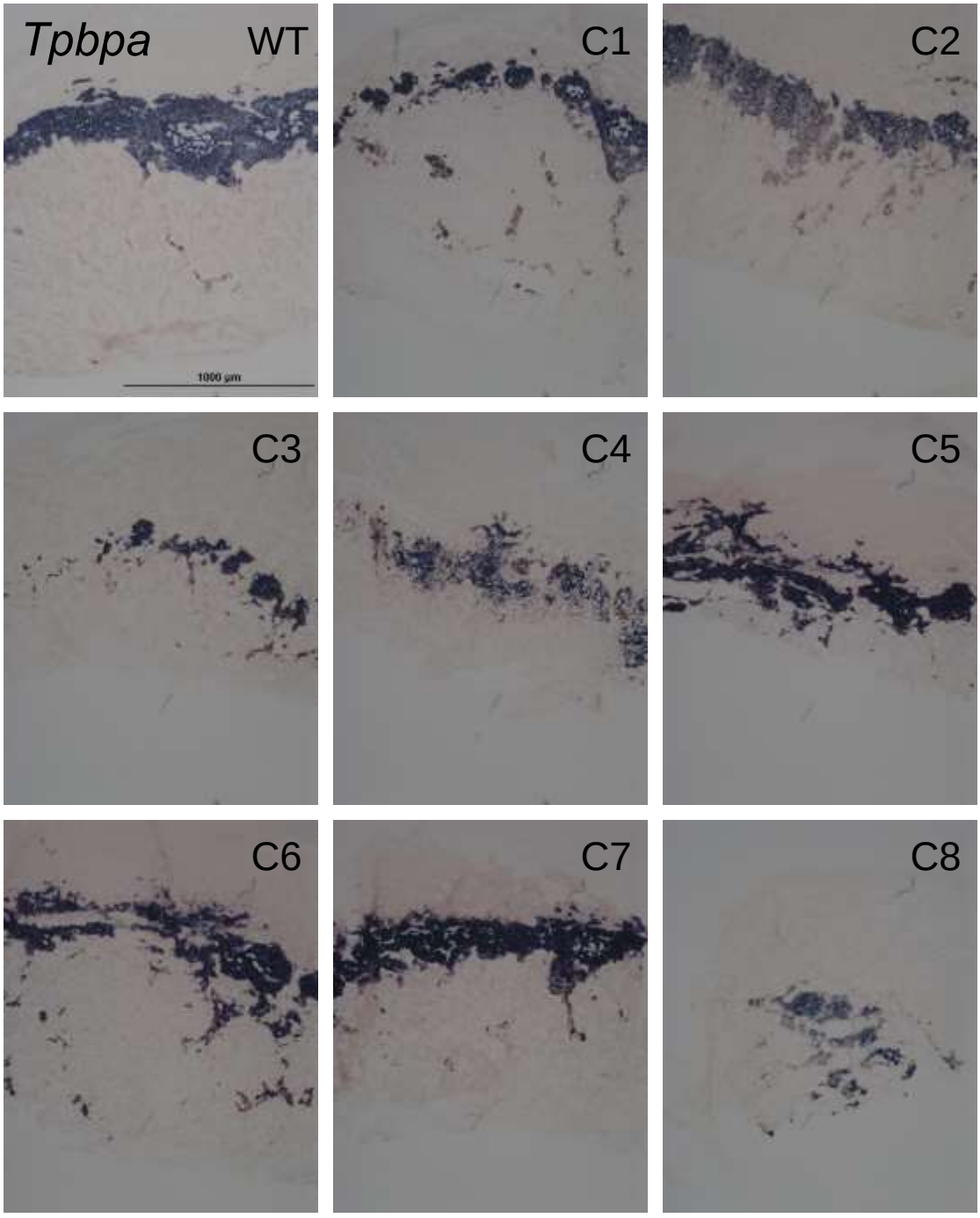

Figure 9. E12.5 *Tpbpa* ISH of a Wild-type (WT) and a litter of eight DNMT1o-deficient (C1- C8) placentas. *Tpbpa* expression marks the spongiotrophoblast. Notice the strong staining and compact layer in WT and mutant C2. However, other DNMT1o-deficient placentas show Ectopic (C6) diffuse (C1, C3, C4 and C8) or ectopic (C5, C6 and C7) expression. 4x objective Scale bar is 1000um

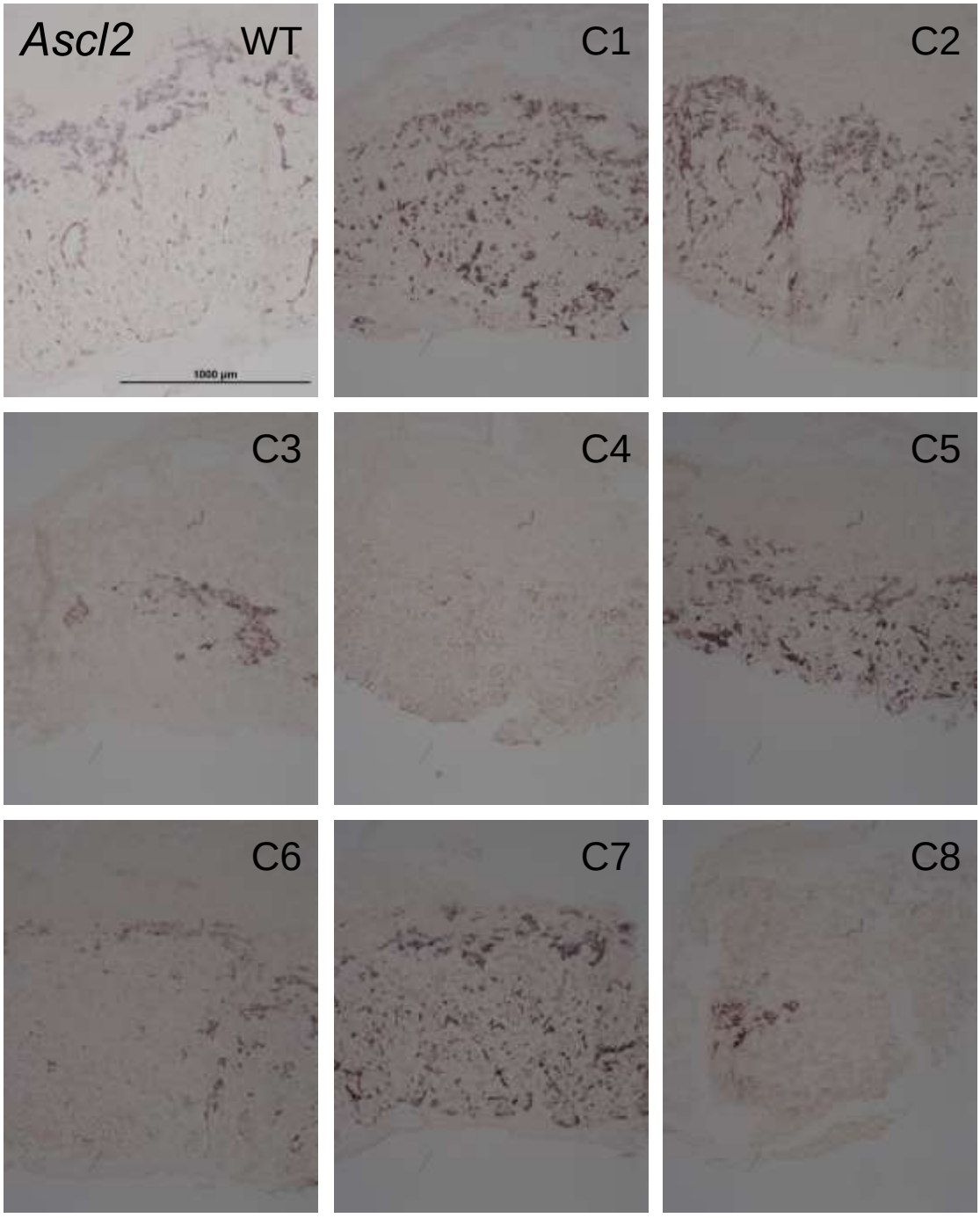

Figure 10. E12.5 *Ascl2* ISH of a Wild-type (WT) and a litter of eight DNMT1o-deficient (A-H) placentas. *Ascl2* marks primarily the spongiotrophoblast and scattered S-TGCs and C-TGCs in the labyrinth Notice the compact SpT layer in WT and DNMT1o-deficient placentas C1, C2, 5 and C7; whereas placentas C3, C4, C6 and C8 have have a range of loss of Ascl2 expression from partial to complete. 4X objective, scale is 1mm.

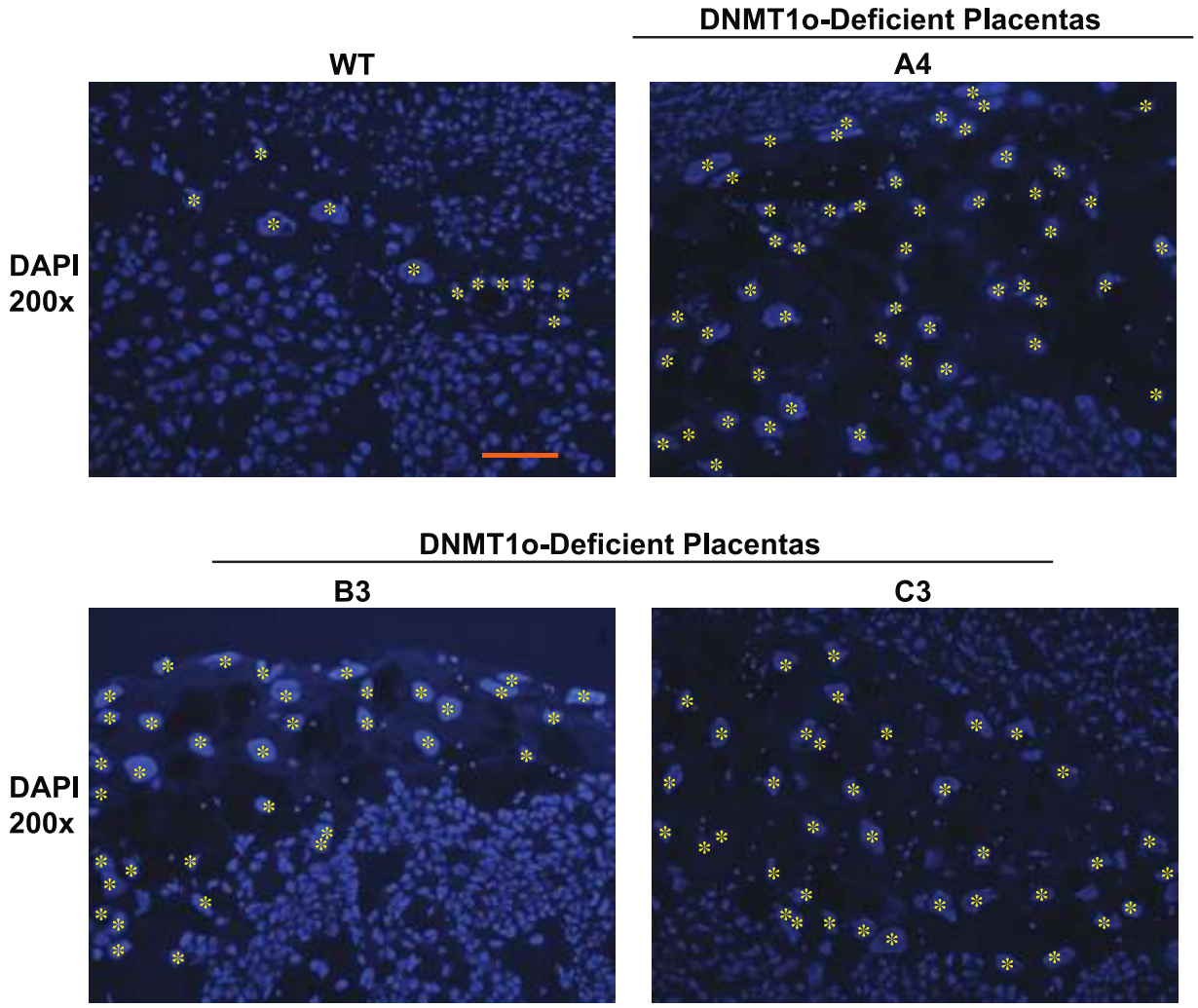

Figure 11. DAPI nuclear staining of TGCs in a wild-type (WT) and three DNMT1o-deficient E12.5 placentas. A yellow asterisk highlights the nucleus of each TGC. 20X objective, orange scale bar is 100μm.

2.4.4 E15.5 phenotypes

The variability in phenotypic metrics observed at E15.5 was smaller than that seen at E12.5.

Specifically, at E15.5 neither JZ central volume nor LZ central volume phenotypic metrics

significantly differed between wild-type and mutant cohorts (Figure 12C). However, there was an increase in both placental and fetal weights in DNMT1o-deficient placentas compared to gestational age matched controls (Figures 12A and 12B). In the comparison of live and dead mutants, viable DNMT1o-deficient placentas and fetuses were overgrown ($P<0.005$; Figures 13A and 13B). Mutant female placentas weighed more than wild-type females ($P<0.05$) but males did not differ from their wild-type counterparts (Figure 14A).

Although there was no quantitative difference in JZ central volume between wild-type and DNMT1o-deficient placentas (Figure 12C), there were noticeable qualitative changes. Wild-type *Tpbpa* ISH staining in E15.5 controls showed a single compact layer of JZ (WT; Figure 15). DNMT1o-deficient placentas ranged from having a thin JZ layer (C3; Figure 15), to having an increased JZ layer (C6 and D2; Figure 15). Many of the E15.5 $Dnmt1^{\Delta 1o}$ maternal effect placentas exhibited extensions of *Tpbpa* positive SpT within the LZ. Much of the SpT including the extensions were rich in GCs. Three examples of GC rich placentas are shown with PAS staining to highlight glycogen content (Figure 16). These findings suggest that volumetric estimates may not be indicative of the full phenotypic spectrum of placental layer development.

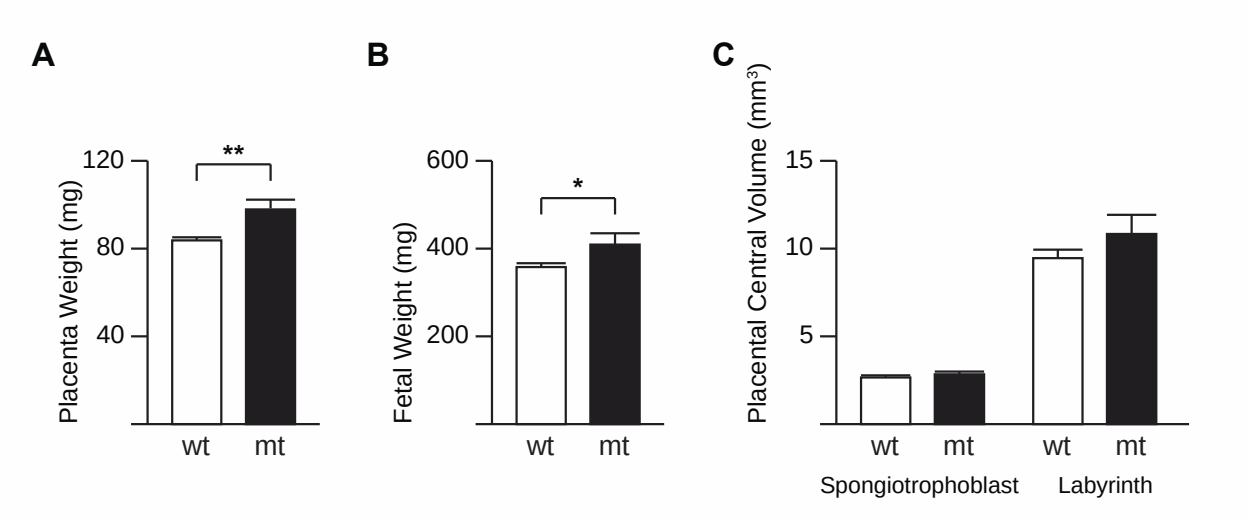

Figure 12. Phenotypic comparison of wild-type (wt) and DNMT1o-deficient (mt) placentas and fetuses at E15.5. (A) Wet placental weight, (B) Wet fetal weight, (C) Spongiotrophoblast volume and labyrinth zone volume of a cohort of wt and mt samples are displayed as open and filled bars respectively. Data are displayed as mean + SEM. * ($P<0.05$) and **($P<0.005$) denote significant differences between wt and mt averages by the Rank-sum test. wt n=27 for placental and fetal weights, wt n=9 for layer fractions, and mt n=21 for all measurements

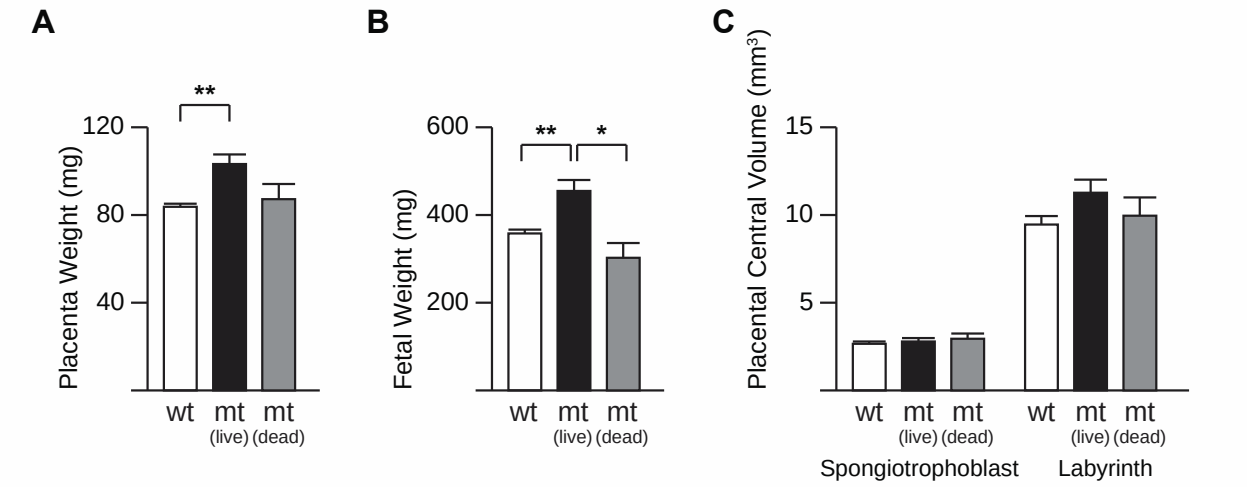

Figure 13. Phenotypic comparison of wild-type (wt) and DNMT1o-deficient (mt) live and dead placentas at E15.5. (A) Measurements of wet placenta weight, (B) Wet fetal weight and (C) Spongiotrophoblast and Labyrinth central volume of a cohort of wt and mt-live and mt-dead placentas are displayed as white, black and gray bars respectively. Data are plotted as mean + SEM. *($P<0.05$) and **($P<0.005$) denote significant differences between wt, mt-live and mt-dead averages by the Rank-sum test. wt n=27, mt-live n= 14 and mt-dead n=7.

The concentration of triacylcglycerides (lipids) within E15.5 DNMT1o-deficient placentas was measured. This analysis compared four wild-type and twenty *Dnmt1*$^{\Delta 1o}$ maternal effect placentas. Wild-type E15.5 placentas had an average triacylglyceride concentration of 5.70 nmol/mg compared to the DNMT1o-deficient placental average of 7.36 nmol/mg ($P>0.05$; Figure 17A). Additionally, neither fetal viability nor embryonic sex significantly differed from wild-type nor within mutant subgroups ($P>0.05$; Figures 17B and 17C). This data is interpreted as evidence that there may be changes to trophoblast lipid accumulation at E15.5 but that elevated levels may not occur to a great enough degree or in a sufficient fraction of samples to reach significance in a comparison of means. LipidTOX fluorescence of E15.5 DNMT1o-deficient placenta shows that lipid droplets primarily accumulate in SynT rather than CD31 positive fetal endothelium (Figure 18).

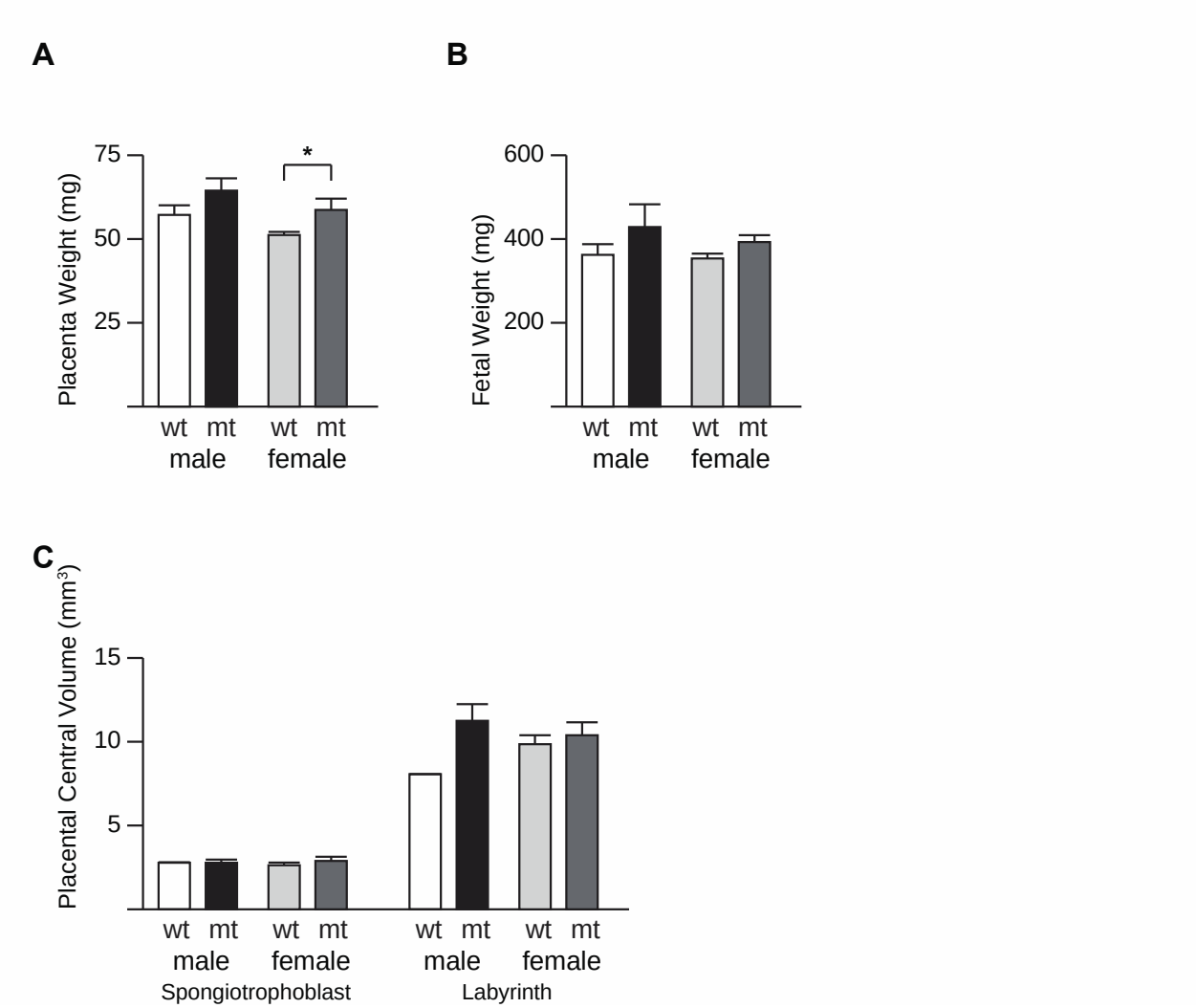

Figure 14. Phenotypic comparison of wild-type (wt) male and female, and DNMT1o-deficient (mt) male and female placentas at E15.5. (A) Measurements of wet placenta weight, (B) wet fetal weight and (C) spongiotrophoblast and labyrinth central volume of a cohort of wt-male, mt-male, wt-female and mt-female placentas are displayed as white, black, light-gray and dark-gray bars respectively. Data are plotted as mean + SEM. *($P<0.05$) and **($P<0.005$) denotes significant differences between wt-male, wt-female, mt-male and mt-female averages by the Rank-sum test. wt-male n=4 and wt-female n=17 for placental and fetal weights, wt-male n=2 and wt-female n=7 for layer fractions, mt-male n=9 and mt-female n=12 for all measurements.

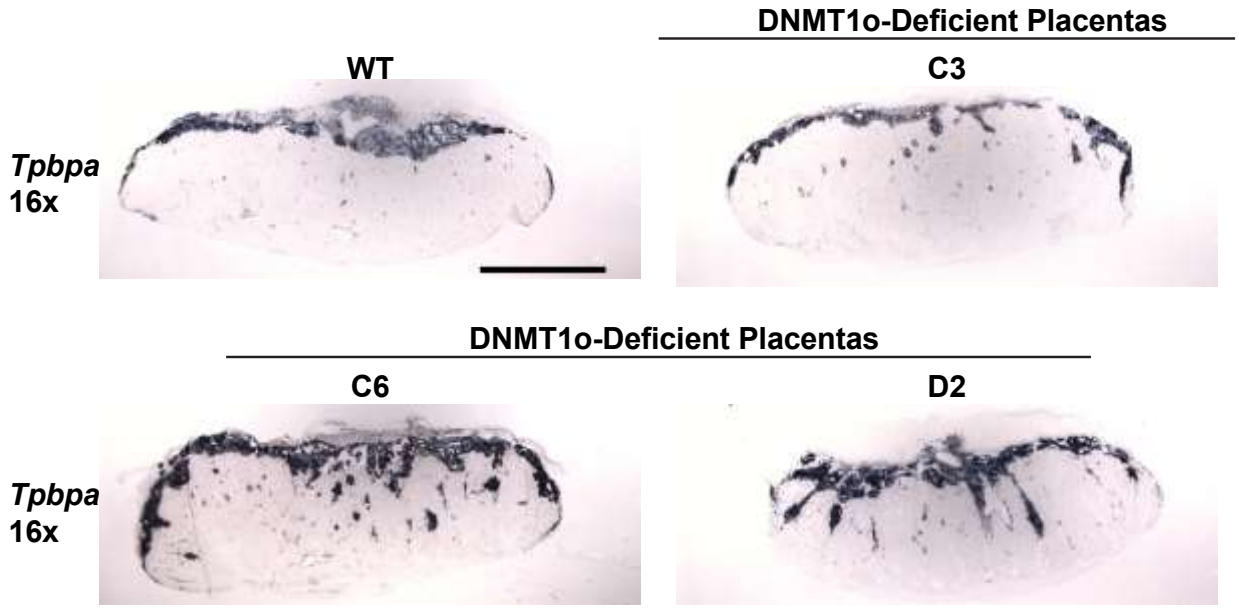

Figure 15. *Tpbpa* ISH of wild-type (WT) and DNMT1o-deficient E15.5 placentas. *Tpbpa* is a marker of spongiotropbhoblast, which is present as a compact layer in WT but ranges from a thin layer to thickened and having projections in to the labyritnth in DNMT1o-deficient mutant placentas. Scale bar is 2mm. 1.6X objective.

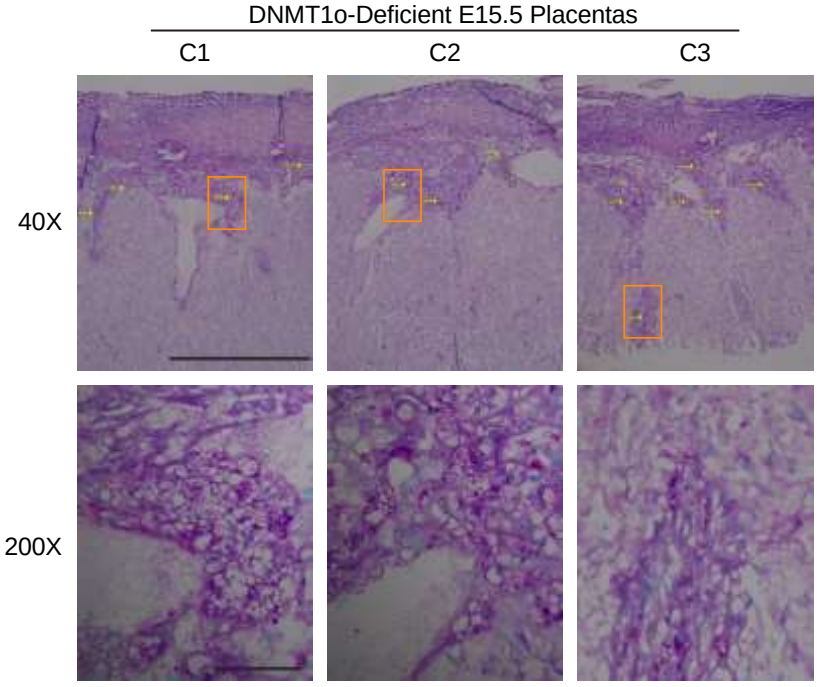

Figure 16. PAS in E15.5 DNMT1o-deficient placentas. Vacuolated and glycogen rich (purple) GCs indicated by Yellow arrows and zoomed in areas in orange boxes. Scale bars 1mm and 100μm.

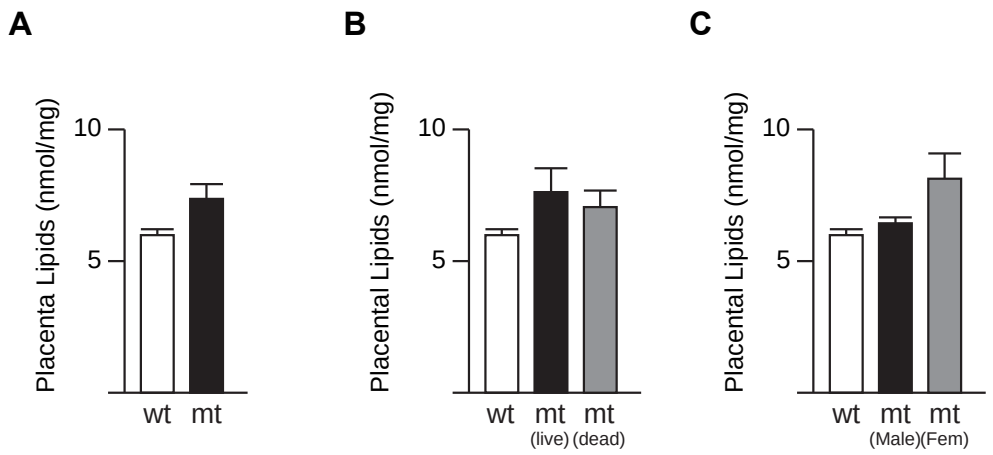

Figure 17 E15.5 triacylglyceride Levels. (A) Comparison of wild-type (wt) and DNMT1o-deficient (mt) placental lipid concentrations. (B) Comparison of wt and mt-live and mt-dead placentas. (C) Comparion of wt and mt-male and mt-female placentas. Mean and SEM of each sample distribution are shown. All comparions were not siginificant (P>0.05) by rank sum test. wt n=4, mt n=20, mt-live n=13, mt-dead n=7, mt-male n=9, mt-female n=11

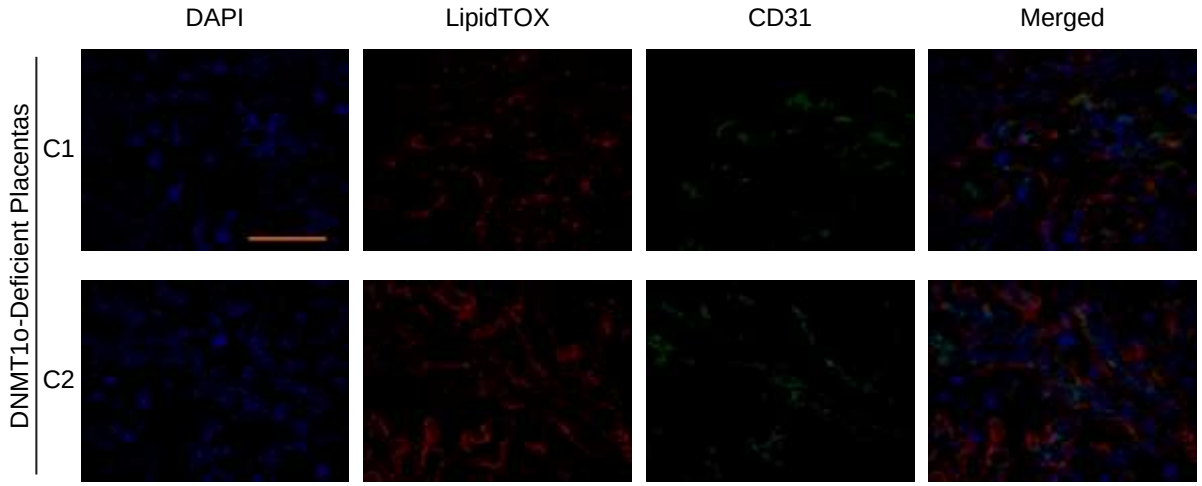

Figure 18. Fluorescent imaging of E15.5 DNMT1o-deficient placentas. Nuclei are shown in blue (DAPI), lipid droplets in red (LipdTOX), fetal vasculature in green (CD31) and composite RBG merged image. Note that lipid droplets occur primarily in SynT that are negative for CD31 staining. Images taken with 40X objective, orange scale bar is 100μm.

2.4.5 E17.5 placental phenotypes

Placental and fetal weights at of DNMT1o-deficient placentas recovered at E17.5 were greater than wild-type controls ($P<0.005$; Figure 19A). Conceptuses supporting live fetuses harbored heavier placentas ($P<0.005$) and fetuses ($P<0.005$) than those that were not viable (Figures 20A and 20B). Both male and female mutant placentas were heavier than wild-type controls ($P<0.005$ and $P<0.05$; Figure 21A). These results suggest that DNMT1o-deficient placentas that survive into late-gestation are overgrown.

The ratio of embryonic to placental weight (E/P) is a standard metric of placental efficiency as it directly measures the placental capacity to support fetal growth normalized to the amount of placenta present. An analysis of fetal and placental weights from 17 wild-type and 62 DNMT1o-deficient placentas revealed that mutant placentas are widely variable in their placental efficiency. Wild-type placentas had an average an E/P ratio of 9.99 and when plotted cluster into a tight group (Figures 22A and 22B). DNMT1o-deficient placentas showed a wide range in E/P ratios with a significantly lower than wild-type average of 6.08 and when plotted show a scattered distribution ($P<0.001$; Figures 22A and 22B). Not surprisingly mutant placentas that did not support growth had a lower E/P ratio than those that could (E/P of 3.13 versus 8.36), and formed distinct groups when plotted (Figures 22A and 22B).

To determine if the wild-type, mutant-live and mutant-dead samples formed distinct E/P groups the Kmeans clustering algorithm was applied to all E17 embryo and placenta data. The number of clusters (K) was set to 5, because the data as plotted in Figure 22B appeared to have one wild-type placenta group and four DNMT1o-deficient groups: normal placenta with large embryo, large placenta with large embryo, normal placenta with small embryo, and small placenta with small embryo. Kmeans clustering returned these expected groups (Figure 22C). Cluster 2

included all wild-type samples, along with one live mutant and one dead mutant and had a centroid E/P ratio of 9.62, close to that of wild-type samples (Figure 22C). Cluster 1 contained 18 live mutants and one dead mutant, and had a centroid E/P ratio of 8.78 with enhanced fetal growth (Figure 22C). Cluster 3 contained 14 live mutants with a centroid E/P ratio of 8.5 with large placentas and fetuses (Figure 22C). Cluster 4 had 7 dead mutants and a centroid E/P ratio of 2.9; these samples had extremely small placentas and fetuses (Figure 22C). Lastly, Cluster 5 contained 18 deceased mutants and one live mutant with a centroid E/P ratio of 2.7; these samples had normal placental weights but small fetuses and therefore were very inefficient (Figure 22C). These results highlight that DNMT1o-maternal effect placentas without a viable fetus are very inefficient, whereas those that survive are slightly less efficient than normal but can be extremely overgrown. The range of fetal weights found in cluster 1 show that within the live-mutant population that have slightly above average placental weights some placentas are more efficient (supporting higher fetal weight) than others (supporting lower fetal weight). Placentas within cluster 1 with high and low E/P are compared in transcriptional analysis described at the end of this results section.

In a cohort of E17.5 DNMT1o-deficient placentas substantial phenotypic variance was unearthed. The volume fraction of JZ increased whereas the volume fraction of the LZ layer decreased ($P<0.05$; Figures 23B and 23C). Strong qualitative phenotypes were also noticed. The JZ layer of many placentas had ectopic extensions of SpT into the LZ visible on H&E and *Tpbpa* ISH histological sections (left column; Figure 24). Much of the excess SpT was positive for the glycogen cell marker *Pcdh12* (data not shown) and contained glycogen vacuoles visible in PAS staining (right columns; Figure 24).

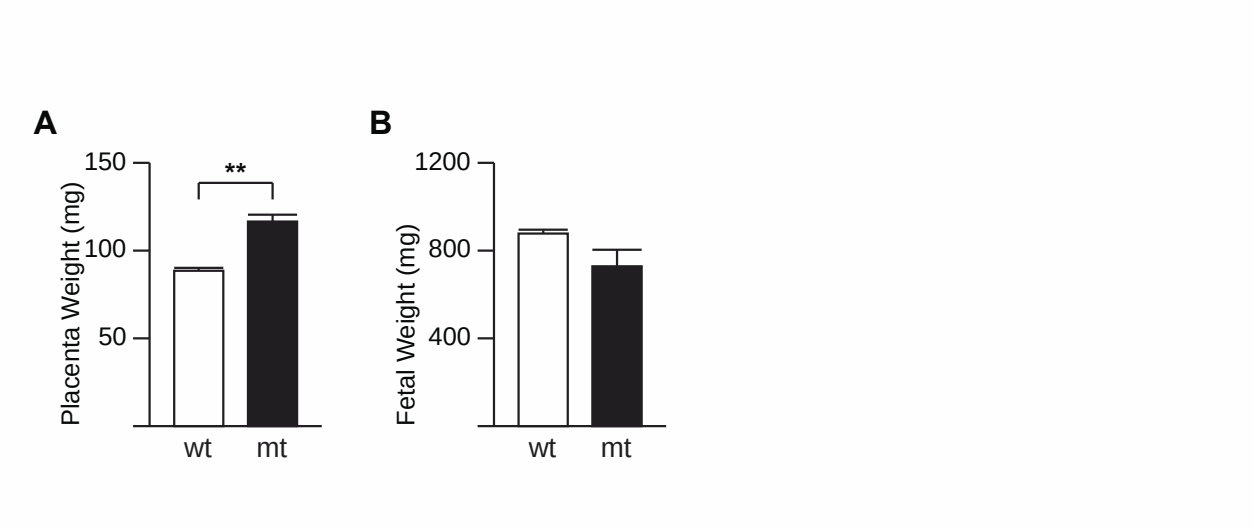

Figure 19. Comparison of wild-type (wt) and DNMT1o-deficient placental and fetal weights at E17.5. (A) Wet placental weights and (B) wet fetal weights of wt and mt cohorts are shown as open and filled bars respectively. Data are displayed as mean +SEM. ** (P<0.001) by the Rank-Sum test, wt n=17, mt n=23.

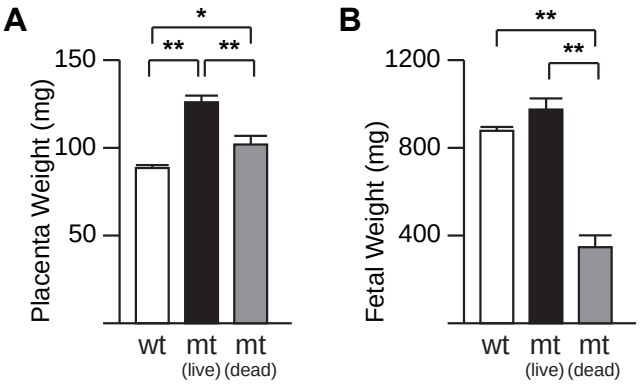

Figure 20. Phenotypic comparison of wild-type (wt) and DNMT1o-deficient (mt) live and dead placentas at E17.5. (A) Measurements of wet placenta weight and (B) Wet fetal weights of wt and mt cohorts are shown as open and filled bars respectively. Data are displayed as mean +SEM. ** (P<0.001) by the Rank-Sum test. wt n=17, mt-live n=14 and mt-dead n=9.

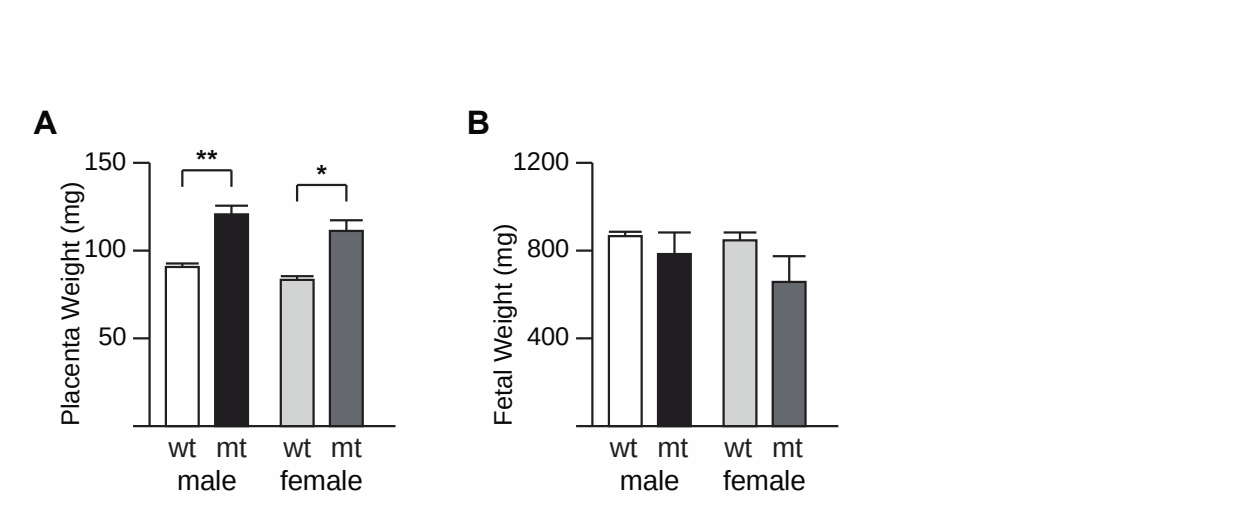

Figure 21. Phenotypic comparison of wild-type (wt) male and female, and DNMT1o-deficient (mt) male and female placentas at E17.5. (A) Measurements of wet placenta weight and (B) Wet fetal weights of wt and mt cohorts are shown as open and filled bars respectively. Data are displayed as mean +SEM. ** ($P<0.001$) by the Rank-Sum test. wt-male n=12, wt-female n=5, mt-male n=13 and mt-female n=10.

The labyrinth layer of E17.5 DNMT1o-deficient placentas was also abnormal. Expression of SynT marker *Lepr* was sporadic or diminish to varying degrees in mutant placentas (left column; Figure 25). IHC staining with antibodies against the fetal vascular endothelium marker CD31(VECAM) enabled detailed resolution of both fetal vessels and maternal blood pools (right column; Figure 25). This IHC analysis showed that many DNMT1o-deficient placentas have dilated maternal blood sinuses (asterisks; Figure 25). However, it was of note that unlike at E12.5 all placentas at E17.5 had intact fetal vasculature, indicating that those showing severe labyrinth defects at E12.5 cannot survive to E17.5. Taken together this evidence demonstrates that DNMT1o-deficient placentas exhibit variable abnormal labyrinth morphology.

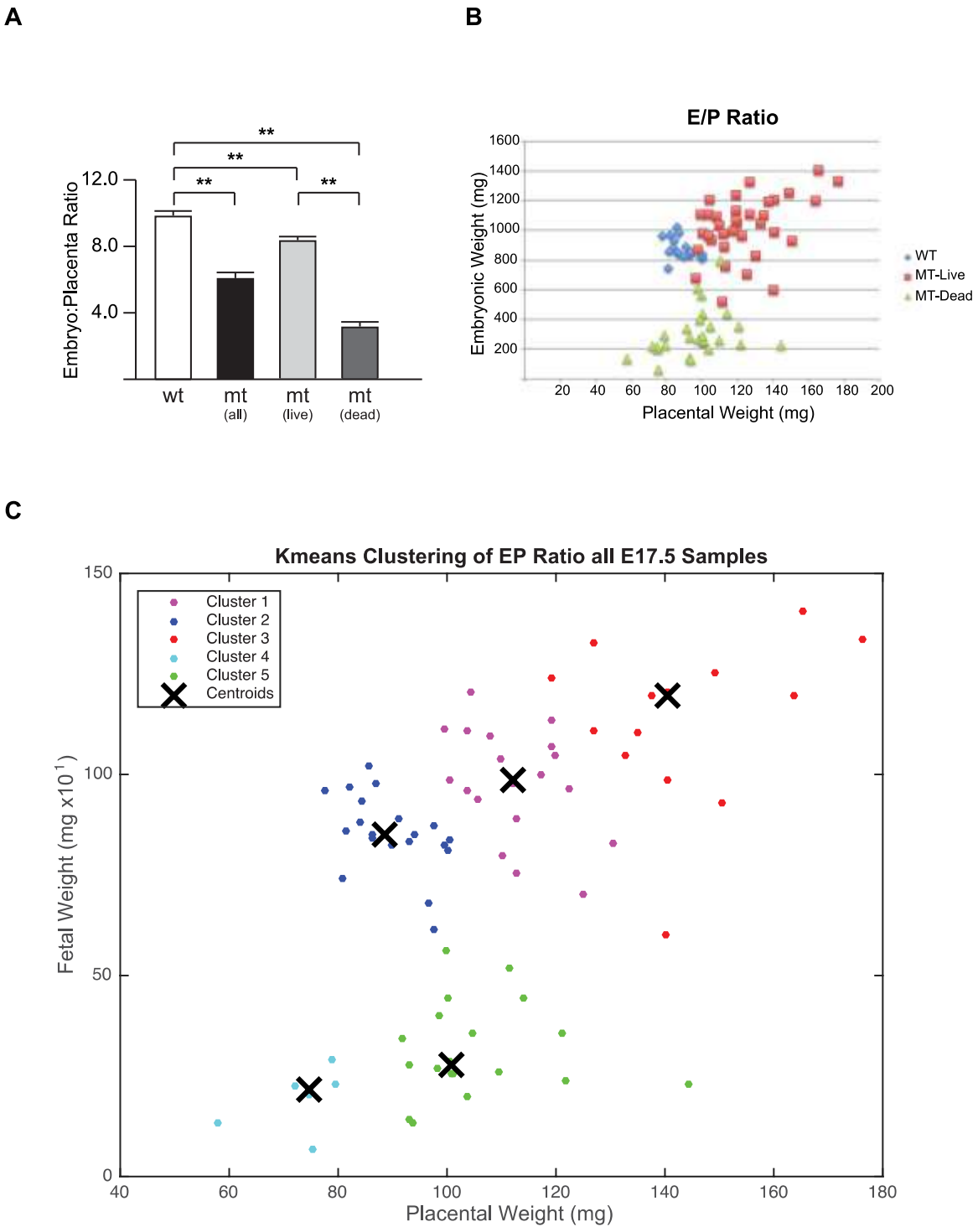

Figure 22. Analysis of E/P ratio in wild-type and DNMT1o-deficient E17.5 offspring. (A) Bar chart of E/P ratio in wild-type, mutant live and mutant dead samples. (B) Plot of E/P ratio for each subgroup: wt n=17, mt-live n=67, mt-dead n=34. (C) Kmeans clustering with K=5. **P<.001 with two tailed unequal variance T-test.

Histological analysis of E17.5 DNMT1o-deficient placentas by ORO staining revealed an abundance of lipids in the LZ (Figure 26A-D). There was a wide range in the staining from extremely abundant staining to similar levels as wild-type. Quantification of triaclyclgeride content revealed an overabundance of lipids in DNMT1o-deficient placentas that was statistically significant (P<0.0 Figure 26E). The robust lipid deposition combined with the overabundance of GCs is evidence that the metabolic states of late gestation DNMT1o-deficient placentas are altered.

A microarray gene expression analysis was performed to determine what cellular pathways are altered in the $Dnmt1^{\Delta 1o}$ maternal effect model in E17.5 placentas with high and low E/P ratios (Figure 27). Hierarchical clustering analysis of all samples revealed a structured hierarchy in which wild-type samples were highly similar, and high and low E/P samples separated into distinct mutant sub-groups (Figure 27A). Of the genes down-regulated 1.3 fold or more there was significant overlap in the low and high E/P groups (Figure 27B); and these were enriched in genes involved in oxidative response (Figure 27C). On the other hand there was less overlap in genes up-regulated by both low and high E/P ratio DNMT1o-deficient placentas placentas (Figure 27B). Genes involved in lipid metabolism were up-regulated by both groups. In contrast, only high E/P ratio had up-regulated genes enriched for molecular transport and lipid metabolism pathways. Overall, my description of DNMT1o-deficient at E17.5 and throughout mid-gestation demonstrate a large gamut of placental developmental and structural defects.

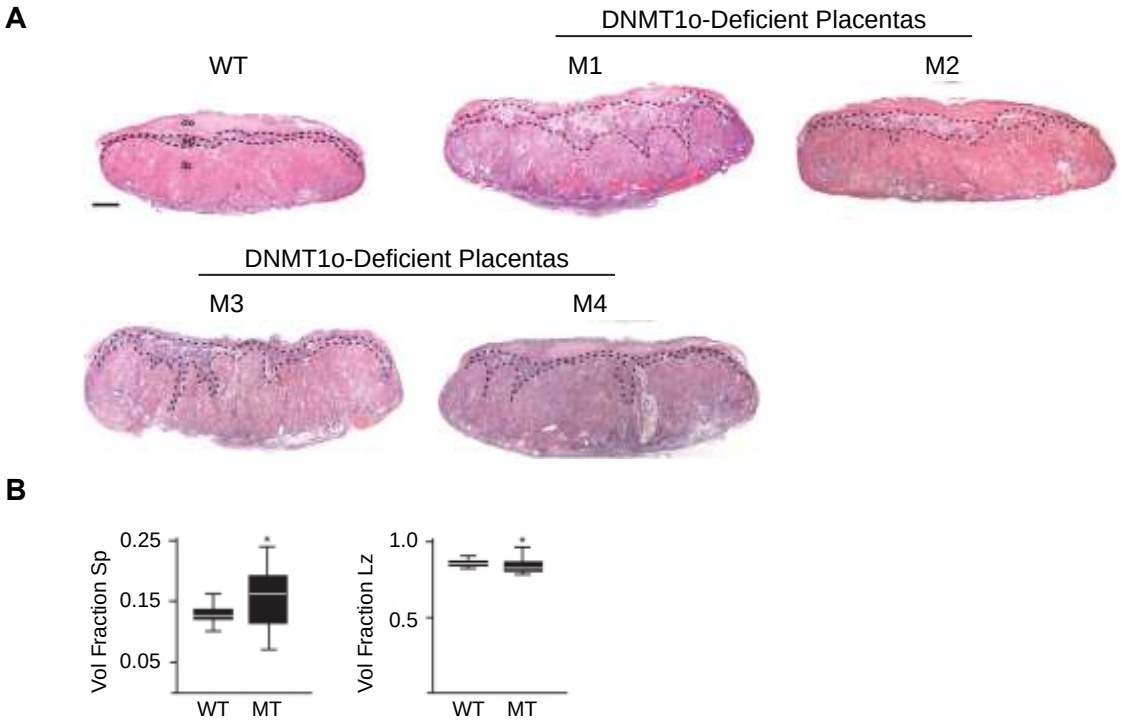

Figure 23. H&E Histology and volume fraction measurements of E17.5 DNMT1o-deficient placentas. (A) Histology of H&E stained paraffin embedded wild-type (WT) and DNMT1o-deficient (M1-M4) placentas. (B) Box plots showing spongiotrophoblast and labyrinthine wild-type and DNMT1o-deficient volume fractions medians and upper and lower quartiles. Abbreviations de decidua; sp spongiotrophoblast; lb labyrinthine.1.6X ojective, Scale is 400μm *P<0.05 Kruskal-Wallis

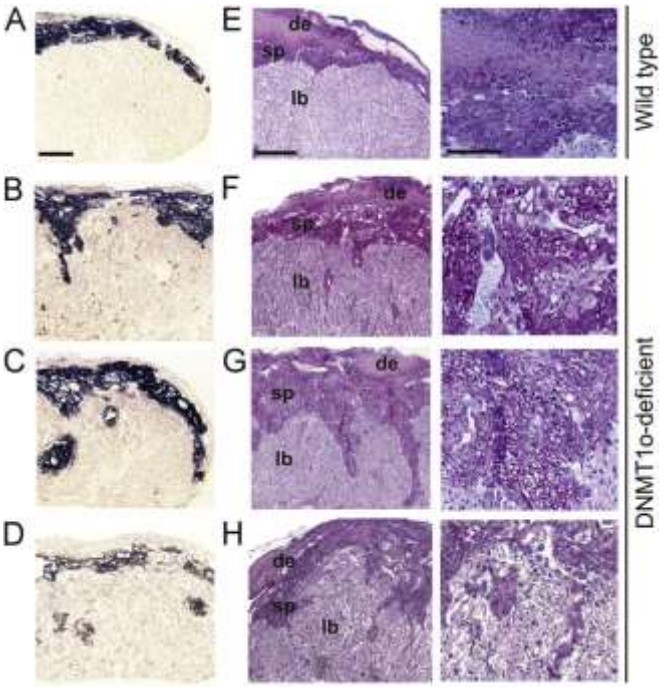

Figure 24. *Tpbpa* ISH and PAS staining of a wild-type and three E17.5 DNMT1o-deficient placentas. (A-D) *Tpbpa* ISH of a wild-type and 3 representative DNMT1o-deficient placentas. (E-H) Adjacent sections from the same samples with PAS glycogen staining. Abbreviations: de decidua; sp spongiotrophoblast; lb labyrinthine. Left and center panels 5x objective, scale bar is 400μm; Right panel 10X objective scale bar is 100μm.

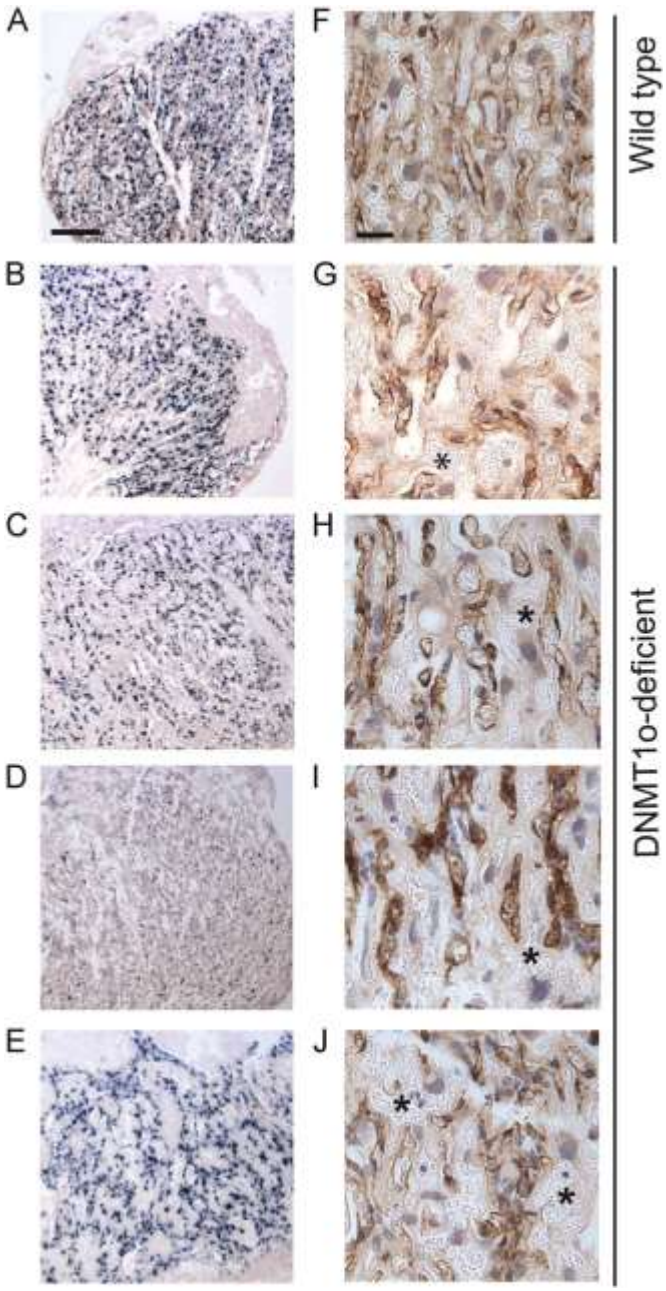

Figure 25. *Lepr* ISH and CD31 IHC histology of DNMT1o-deficient E17.5 placentas. (A-E) *Lepr* ISH staining of SynT in a wild-type and four representative DNMT1o-deficient placentas. (F-J) CD31 IHC staining of fetal vessels in a different set of representative DNMT1o-deficient placentas. Left panel 5X objective, scale bar is 400μm. Right panel 40X objective, scale bar is 50μm. * dilated maternal blood pools.

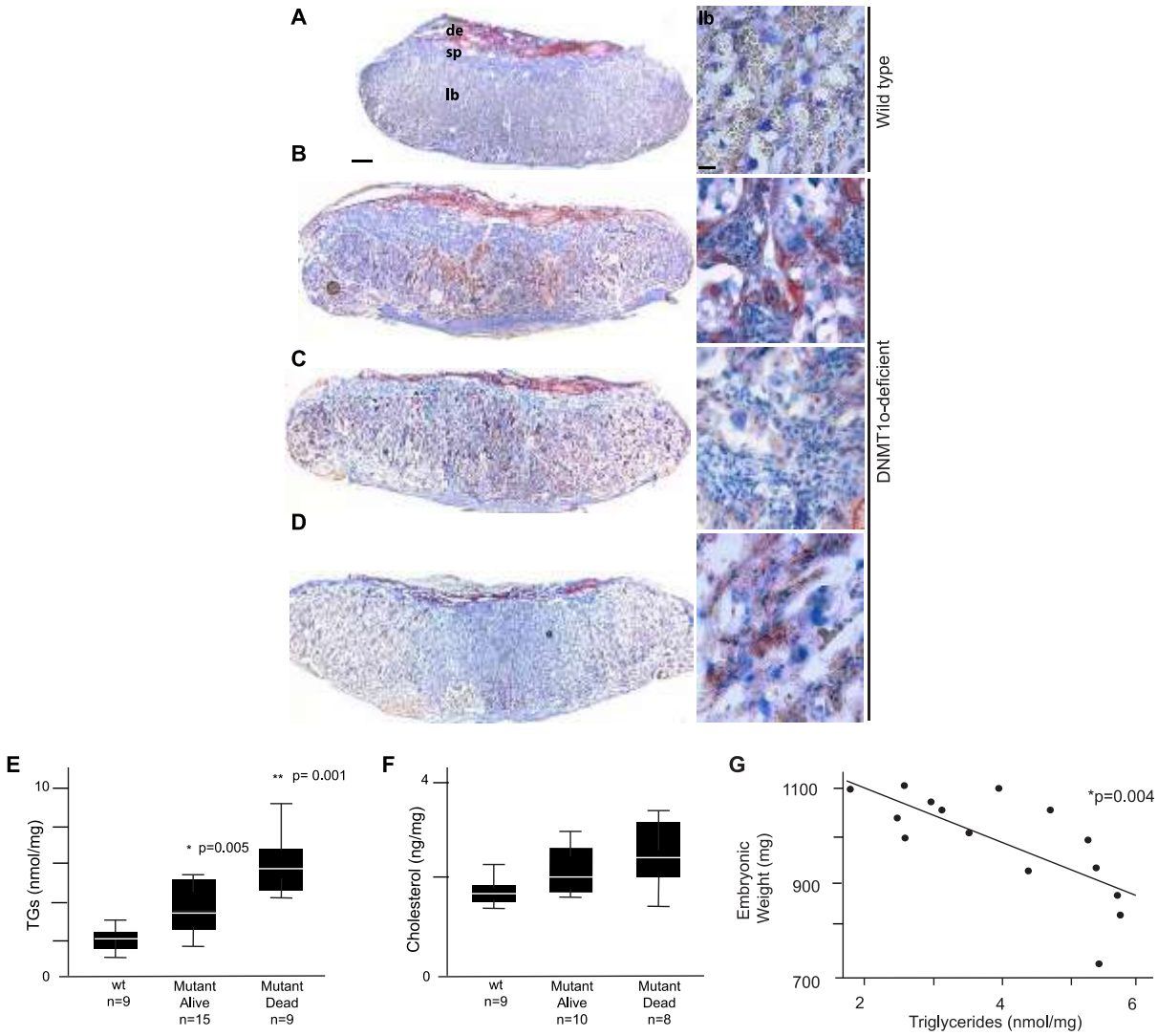

Figure 26. Lipid accumulation in E17.5 DNMT1o-deficient placentas. (A-D) Staining with Oil-Red-O in a single wild type and three DNMT1o-deficient placentas. (E) Quantification of triaclyglyceride concentrations. (F) Quantification of cholesterol concentrations. (G) Inverse relationship of triglyceride concentration and embryonic weight revealed by linear regression. Abbreviations: TGs Trigylcerides; wt Wild-type; de decidua; sp spongiotrophoblast; lb labyrinthine. Left panel 1.6X objective, scale is 400um. Right panel 40x objective, scale is 100μm. * P-values from Kruskal-Wallis test.

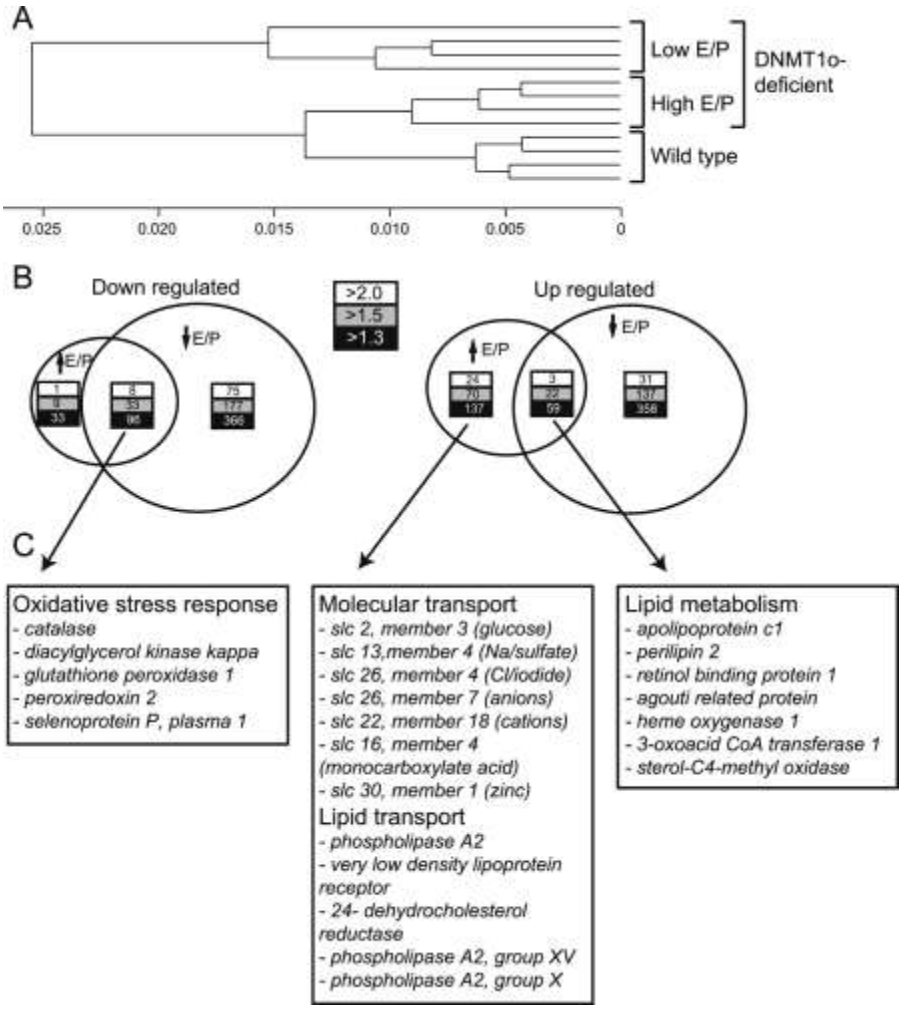

Figure 27. E17.5 microarray analysis of DNMT1o-deficient placentas. (A) Hierachical clustering derived dendrogram describing genome-wide expression patterns. The X-axis is 1 minus the correlation coefficient. (B) Ven diagrams showing overlapping subsets of genes common to low and high E/P ratio DNMT1o-deficient placentas and (C) enriched gene ontology pathways determined by Ingenuity Pathway Analysis.

2.5 DISCUSSION

2.5.1 Fetal viability and growth

Partial mosaic loss of imprinting in the *Dnmt1*$^{\Delta 1o}$ maternal effect model has a profound impact on placental development and fetal growth that progresses across gestation. The most prominent and obvious phenotype in DNMT1o-deficient placentas was the inability to support a viable fetus. At E9.5 the majority of embryos are alive, at E12.5 roughly half of each litter is deceased, and by E15.5 and E17.5 only a fraction of normal litter sizes are recovered (Table 2). This gradual mid-gestation lethality points to a temporal juncture between E9.5 and E12.5 in genomic imprinting that is critical for proper development. While the embryonic lethality observed in the *Dnmt1*$^{\Delta 1o}$ maternal effect model is likely due to loss of imprinting in both the fetal and placental compartment, given the severe placental abnormalities and similar stage of gestational developmental arrest in known placental lethal mutants (*e.g. Ascl2*, *Rtl1*, *Peg10*, *Pparδ* and *Pparγ*) it is likely that placental development is the major factor.

At E12.5 *Dnmt1*$^{\Delta 1o}$ maternal effect litters were similar in size to wild-type litters in having 8 conceptuses. The partial embryonic lethality observed at E12.5 was an opportunity to observe placental abnormalities associated with loss of fetal viability. Two distinct groups of placentas were observed in a representative E12.5 DNMT1o-deficient litter that were either able to support a viable fetus (C1, C5, C6 and C7; Figures 8, 9 and 10) or were unable to (C2, C3, C4, C8; Figures 8, 9 and 10). Notably expression of the fetal endothelium marker *Mest* was normal to

slightly expanded in placenta with viable fetuses but stunted or nearly absent placenta from non-viable conceptuses (Figure 8). Likewise, three out of four non-viable placentas had diminished *Ascl2* staining and abnormal *Tpbpa* spatial gene expression patterns (C3, C4, and C8; Figures 9 and 10). I interpret these results to indicate that fetal vasculature in the labyrinth is an absolute requirement for fetal development. In addition, I interpret these results as evidence that that loss of placental *Ascl2* imprinting resulting in lower expression may predispose embryonic lethality through abnormal JZ and LZ layer development. However, these results do not enable the determination as to whether the absence of fetal vasculature is the cause or effect of loss of imprinting in the fetus proper, extraembryonic mesoderm derived fetal vessels or trophoblast derived cellular subtypes.

The parental conflict hypothesis, put forth by Haig and Moore suggests that genomic imprinting evolved to balance maternal health and fetal growth (*411*). The majority of mammalian species are not monogamous, therefore having multiple less taxing litters over a long lifetime increases maternal reproductive fitness by increasing the total number of offspring, whereas having vigorous fecund offspring with little regard to maternal resources and post-nurturing maternal health increases male reproductive fitness by ensuring robust and viable offspring. Imprinted genes generally follow the canonical dogma of the parental conflict hypothesis with maternally expressed genes restricting placental and fetal growth (e.g. *Phlda2*, *Igf2r*) and paternally expressed genes enhancing placental and fetal growth (e.g. *Igf2*, *Mest*, *Grb10*). Based on this theory, a widespread disruption of genomic imprinting such as predicted in the $Dnmt1^{\Delta 1o}$ maternal effect model, should result in a broad range of placental and fetal weights.

In fact, this is exactly what was observed in DNMT1o-deficient placentas (Figures 22). At E12.5 DNMT1o-deficient placentas were on average growth restricted, particularly those associated with either non-viable or female conceptuses (Figures 5A, 6A and 7A). At E15.5 DNMT1o-deficient placentas and fetuses were overgrown, particularly with those associated with either a viable or female conceptus (Figures 12A, 12B, 13A, 13B and 14A and 14B). However, at E17.5 only placental weight, but not fetal weight was significantly increased in DNMT1o-maternal effect placenta (Figures 19A, 19B, 20A, 20B, 21A and 21B). At E17.5 placenta efficiency (E/P ratio) trended lower and showed great variation between samples (Figure 22). It was lowest in conceptuses associated with a non-viable fetus (Figure 22). The E/P ratio of wild-type samples was clustered in a tight group but in DNMT1o-deficient mutants formed expansive clusters segregated by fetal viability (Figures 22B and 22C). In addition, we found specific gene ontology pathways (i.e. oxidative stress response and lipid metabolism) that were altered in high and low E/P placentas and others that were specific to high E/P placenta (molecular transport and lipid metabolism) suggesting that loss of placental imprinting has major effects on placental metabolism (Figure 27). These findings were further corroborated in analysis of placental glycogen and lipid content in the JZ and LZ layers. A number of imprinted genes have been implicated in regulating placental efficiency including *Igf2* (enhances efficiency) and *Grb10* (represses efficiency) (*347, 412, 413*). Overall these results suggest that the balance of fetal and placental growth is disrupted in the $Dnmt1^{\Delta 1o}$ maternal effect partial loss of imprinting model.

2.5.2 Placental labyrinth phenotypes

In early gestation DNMT1o-deficient placentas exhibit under development of the placenta LZ. At E9.5 the labyrinth marker *Tfeb* as well as the imprinted gene *Phlda2* show a decreased and less convoluted labyrinth structure in the majority of DNMT1o-deficient samples (M2, M3, M4, M5 and M7; Figure 4). While the chorionic plate appears intact, there is poor integration of the EXE derived chorionic trophoblast and fetal derived vessels with the EPC, resulting in less definition of maternal blood spaces and diminished percolation of maternal blood. At E12.5 the phenotype is pronounced as evidence of the overall decrease in placental LZ central volume and decreased penetration and branching of fetal vessels (Figures 5B and Figure 8). The decrease in LZ central volume is most pronounced in female DNMT1o-deficient placentas (Figure 7B). These findings of an exacerbated phenotype in female DNMT1o-deficient placenta are similar to those made by a group led by Trasler (*408*). In their study a coarse scoring system was used to show that female placentas had reduced LZ development (*408*). In addition they found female placentas to have placental hyperplasia at E9.5 indicative of TGC proliferation (*408*). Many of the E9.5 and E12.5 DNMT1o-deficient placentas studied herein had a combination of diminished labyrinth development and expanded TGCs, indicating that these two phenotypes are connected.

Late in gestation DNMT1o-deficient placentas that lacked fetal vasculature were not recovered. In contrast E15.5 placentas had nearly normal LZ central volumes and E17.5 placentas displayed a large range of LZ volume fractions that were on average slightly lower than wild-type. However strong qualitative differences were observed in the structure of the LZ. For instance, many DNMT1o-deficient placentas had engorged maternal blood spaces and dilated fetal vessels. Furthermore, ultrastructural SEM of DNMT1o deficient placentas, performed by colleagues, showed that SynT basement membrane was thickened (*414*). The

findings presented here demonstrate that loss of genomic imprinting is detrimental to both LZ structural development and suggest that the placental SynT development is more robust and less of an absolute requirement than fetal vessels in the partial absence of genomic imprints.

In addition to the structural defects both E15.5 (not significant) and E17.5 ($P<.001$) had increased triacylglyceride content (Figures 18 and 26E). These triglycerides accumulated in SynT within lipid droplet organelles as seen in both LipidTOX and ORO staining (Figures 18 and 26B-D). A broader metabolomics survey of DNMT1o-placental tissue performed by my colleague Katherine Himes, MD., revealed accumulation of mitochondrial metabolites (*414*). Excess carnitine derivatives in DNMT1o-deficient placentas indicated disrupted β-oxidation of triacylglycerols. Reduced acontinase activity and accumulation of the TCA cycle intermediate citrate suggested mitochondrial oxidative stress. These results were interpreted as evidence that triacylglycerides accumulate in lipid droplets because their catabolism by β-oxidation and the TCA cycle is blocked. In combination with ultrastructual findings that mitochondria were bloated, Dr. Himes has hypothesized that the mitochondria of DNMT1o-deficient placenta are dysfunctional. Furthermore, the transcriptional changes to molecular transport and lipid metabolism genes in high and low E/P placenta provide two additional lines of evidence that genomic imprints directly regulate fetal and placental growth through metabolic pathways (Figure 27).

The disorganized and abnormal labyrinth structure seen in DNMT1o-deficient placentas is similar to targeted deletions of both imprinted and non-imprinted genes. For example, *Peg10*, *Ascl2* and *Rtl1* genes are imprinted genes that when deleted have detrimental consequences on LZ placental development and embryonic survivorship. *Peg10* is an imprinted gene within a cluster of imprinted genes on chromosome 6 (Section 1.5.5) that is expressed in many

trophoblast cell types. When *Peg10* is paternally deleted the resulting phenotype is embryonic lethal at E9.5-E10.5 due to vastly diminished LZ development as well as a near complete absence of JZ (*293*). However, the connection with the DNMT1o-deficient phenotype is counterintuitive because loss of *Peg10* DMD methylation on the maternal allele should result in an increase in *Peg10* expression rather than a decrease. *Ascl2* is a maternally expressed transcription factor within the *Kcnq1* imprinting cluster (Section 1.4.7) that is expressed in the EPC, and when maternally deleted results in diminished LZ and JZ layers and an expanded TGC population (*222*). *Rtl1* is a paternally expressed gene within the *Dlk1* cluster (Section 1.4.13) that is expressed in the fetal endothelium (*374*). Paternal deletion of *Rtl1* results in a trophoblast phagocytic response to invading fetal endothelium, placental infarction, and late-gestation growth restriction and lethality (*374*). Based on my results in combination with the information garnered from individual imprinted gene deletions it is evident that imprinted genes are important both for early SynT differentiation and LZ development as well as normal late gestation LZ integrity.

It is also of note that some DNMT1o-deficient placentas exhibited phenotypes similar to targeted deletion of ***Pparγ***, *Pparδ* and *Rxrα* (Section 1.3.5). Deletion of ***Pparγ*** is embryonic lethal at E10.5 due to maternal blood space hemorrhaging and lack of fetal vasculature, two phenotypes commonly observed in E12.5 DNMT1o-deficient placentas (*218*). The *Pparδ* null model shows attenuated chorio-allantoic fusion, which is also observed in many E9.5 DNMT1o-deficient placentas (*220*). Lastly, both ***Pparγ*** and *Rxrα* mutants display an accumulation of lipid droplets within the SynT (*218, 221*). I interpret these common phenotypes to indicate that loss of genomic imprinting may alter the genetic pathways vitally important for placental development

2.5.3 Placental junctional zone phenotypes

Early in placental development at E9.5 and E12.5 *Dnmt1*$^{\Delta 1o}$ maternal effect placentas exhibited mosaic, patchy and sporadic SpT layers that often extended into the LZ. At E9.5 *in situ* hybridization with the SpT marker *Tpbpa*, and the imprinted EPC marker *Ascl2* revealed that many placentas had decreased SpT with corresponding decreases of both markers (Figure 4). At E12.5 these phenotypes progressed into overt structural abnormalities. On average E12.5 DNMT1o-deficient placentas had a diminished SpT central volume (Figure 6B). E12.5 placentas stained with *Tpbpa* showed very distinct patterns with some having minimal SpT development (C3 and C8; Figure 9), others having a sporadic staining patterns (C4; Figure 9), while others had expanded SpT with LZ extensions (C2, C6 and C7; Figure 9). The staining pattern for *Tpbpa* matched the pattern of sporadic *Ascl2* (Figure 10). I interpret these results to indicate that reduction in *Ascl2* expression, as modulated by loss of imprinting at the *Kcnq1* cluster, has a direct impact on SpT development. However, it is also plausible that the changes in *Ascl2* spatial expression patterns are passive secondary changes associated with abnormal SpT development due to loss of imprinting at other loci.

In mid- to late-gestation, DNMT1o-deficient placentas had either a thinner layer of SpT or an expanded layer of SpT with LZ extensions and accumulation of GCs (Figures 9, 15, 16 23, 24). A transition from diminished JZ central volume at E12.5 to no difference at E15.5 to an increase in JZ volume fraction at E17.5 occurs in DNMT1o-deficient cohorts. This indicates that those DNMT1o-deficient placentas with severely diminished SpT layers either compensate during mid-gestation or do not survive. While some E12.5 DNMT1o-deficient placentas show SpT extensions into the LZ, it is much more pronounced at E15.5 and E17.5 (Figures 9, 15, 23A, 24A-D). Both the junctional zone as well as the ectopic extensions are enriched in GCs and

glycogen content (Figures 16, 24E-H). There generally appears to be a correlation between GC enrichment and SpT volume, although this has not been quantified. These results, in combination with the previously discussed accumulation of lipid droplets, suggest that loss of genomic imprinting alters placental energy storage.

The diminished spongiotrophoblast observed herein is similar to phenotypes observed in *Ascl2* and *Peg10* targeted deletion models that disrupt both JZ and LZ development, indicating that early placental layer developent are dependent on each other (*222, 293*). *Igf2* and *Igf2p0* null placentas also have decreased SpT development (*303*). The mid- to late-gestation SpT and GC expansion phenotypes observed in DNMT1o-deficient placentas have similarities and differences with *Phlda2* deletion and overexpression models (*316, 317*). Ablation of *Phlda2* expression promotes placental and fetal overgrowth with excessive SpT and GCs (*317*). Given the endocrine role of spongiotrophoblast one interpretation is that expansion of this layer and increased glycogen stores due to loss of genomic imprinting enhances fetal growth. In contrast, overexpression of *Phlda2* in mouse results in growth restriction with reduced SpT and GCs, however protrusion of SpT into the LZ, similar to that seen in the $Dnmt1^{\Delta 1o}$ maternal effect model does occur (*316*). It has been suggested by Tunster *et al*., that these ectopic SpT and GCs within the late gestation LZ are due to failure of these cells to migrate (*316*).

2.5.4 Trophoblast giant cell phenotypes

Early in development at E9.5 and E12.5 there was a marked increase in the number of P-TGCs found between the JZ and decidua (Figures 4 and 5C). The accumulation of P-TGCs was often accompanied by a lack of LZ development. However, at E15.5 and E17.5 none of the recovered placentas displayed an abundance of P-TGCs (data not shown). These findings suggest a

selection event against placentas with an overabundance of P-TGCs early in development. These results can also be interpreted to indicate that TGC accumulation is a common response to failing embryonic development and may facilitate reabsorption. The similarities to placental development in the absence or muted *Ascl2* expression implies a direct role of this imprinted gene in the dysregulation of TGCs in DNMT1o-deficient placentas (*222*, *311*). In addition, the accumulation of TGCs was the most prominent phenotype in *Dnmt3l* maternal effect placentas at E9.5, suggesting that this is the strongest early phenotype caused by loss of maternal imprints (*95*, *97*, *99*).

2.5.5 Conclusion

The wide range of placental phenotypes observed in DNMT1o-deficient placentas begs the question of what are the causative epigenetic changes that drive these abnormalities. Previous work in the Chaillet lab has shown that the *Dnmt1*$^{\Delta 1o}$ maternal effect model generates a mosaic of conceptuses with partial loss of genomic imprinting (*60*, *402*), however no prior attempts to link these alterations with phenotypic measurements have been made. Herein I have quantified placental phenotypic metrics in across mid to late-gestation which will enable using quantitative measurement of imprinted gene expression and DMD methylation the association of specific phenotypes and epigenotypes. The array of distinct phenotypes ranging from early lethality to overgrowth, as well as specific placental layer disruptions fits in with the model in which each placenta of a litter has a unique set of DMDs with loss of imprinting. While it may be difficult to make 1:1 associations between loss of imprinted DMD methylation and placental metrics in order to better understand the role of genomic imprinting in placental biology.

3.0 LOSS OF GENOMIC IMPRINTING IN DNMT1o-DEFICIENT PLACENTAS IS ASSOCIATED WITH SPECIFIC PLACENTAL ABNORMALITIES

3.1 SUMMARY

My dissertation results in Chapter 2 revealed that the *Dnmt1*$^{\Delta 1o}$ maternal effect model produces varied and abnormal placentas. Previous studies, focusing primarily on the fetus, determined that the *Dnmt1*$^{\Delta 1o}$ maternal effect model generates a mosaic and partial loss of imprinting. In this section I have confirmed that DNMT1o-deficient placentas are also subjected to this mosaic partial loss of imprinting by measuring imprinted gene expression by quantititative RT-PCR, by allele specific DMD methylation analysis by bisulfite genomic sequencing, and by quantifying imprinted methylation at a broad array of DMDs using EpiTYPER-mass array technology. Imprinted gene expression was altered at many imprinted gene clusters examined but did not always fit the pattern expected to be associated with loss of DMD methylation late in gestation. Regression analysis revealed a direct association between *Mest* expression and E/P ratio, and an inverse association between *Ascl2* expression and E/P ratio. Allele specific methylation analysis revealed partial loss of methylation on the normally methylated allele of the *H19, Snrpn, Peg1*, and *Kcnq1* DMDs in some but not all DNMT1o-deficient placentas, and provided no evidence of compensatory methylation of the normally unmethylated allele. EpiTYPER DNA methylation analysis of 15 DMDs in E12.5, E15.5 and E17.5 DNMT1o-deficient placental cohorts revealed a

mosaic partial loss of genomic imprinting. Methylation of some imprinted DMDs, most notably *Dlk1*, was nearly normal in mid-gestation DNMT1o-deficient placentas, consistent with the notion that cells having lost methylation on these DMDs do not contribute significantly to placental development. Most imprinted DMDs however showed a wide range of methylation loss among DNMT1o-deficient placentas. Furthermore, I have revealed significant associations between strong placental phenotypes and loss of methylation at specific imprinted loci. At E12.5 two striking associations were observed. First, loss of DNA methylation at the *Peg10* imprinted DMD associated with decreased embryonic viability and decreased LZ volume. Second, loss of methylation at the *Kcnq1* imprinted DMD was strongly associated with TGC expansion. I conclude that the *Peg10* and *Kcnq1* ICRs are key regulators of mid-gestation placental function.

3.2 INTRODUCTION

3.2.1 Loss of genomic imprinting in DNMT1o-deficient placentas

The *Dnmt1*$^{\Delta 1o}$ maternal effect model generates offspring with a mosaic and partial loss of genomic imprinting due to the absence of DNMT1o maintenance methyltransferase activity during preimplantation development (Section 2.2 for full review). This has previously been confirmed at a small subset of DMDs in the embryonic (*H19*, *Snrpn*, *Mest* and *Dlk1*) and placental (*H19* and *Snrpn* only) compartments. DNMT1o-deficient placentas have profoundly abnormal phenotypes (Section 2.3 for description). At E9.5 and E12.5 attenuated LZ development and TGC accumulation is common in DNMT1o-deficient placentas. Later in

gestation, at E15.5 and E17.5, SpT extensions, dilated fetal vessels, and triacylgylceride accumulation are prevalent features. It is of note that *Dnmt1*$^{\Delta 1o}$ maternal effect offspring have sporadic phenotypes with large variation within and between litters that is similar to the predicted mosaic nature of imprinting in this model. In this chapter, I test the hypothesis that the wide-ranging phenotypes are associated with loss of imprinted methylation at specific DMDs in DNMT1o-deficient placentas.

Loss of genomic imprinting in the *Dnmt1*$^{\Delta 1o}$ maternal effect model has previously been validated by DNA methylation and gene expression analysis at a limited set of imprinted loci. Bisulfite genomic sequencing, bisulfite converted restriction analysis, and methylation Southern blots provided the original evidence that the *Dnmt1*$^{\Delta 1o}$ maternal effect model generates partial loss of methylation at DMDs but not other genomic loci (*e.g. Iap* and *Line1* repetitive elements) (*104*, *402*). Restriction fragment polymorphisim analysis of RT-PCR products of imprinted genes within the *Kcnq1* cluster of *Dnmt1*$^{\Delta 1o}$ maternal effect trophoblast and embryo displayed biallelic maternally biased expression of the normally exclusively paternally expressed *Kcnq1ot* but had no effect on allelic bias of maternally expressed genes within the cluster (*415*). Quantitative RT-PCR gene expression analysis of *Kcnq1ot* and seven maternally expressed genes (*Osbpl5*, *Phlda2*, *Cdkn1c*, *Kcnq1*, *Tssc4*, *Cd81* and *Ascl2*) within the *Kcnq1* cluster revealed that in DNMT1o-deficient E10.5 trophoblast *Kcnq1ot* expression was increased, while the expression of the maternally expressed genes decreased (*415*). Intriguingly, despite this transcriptional repression, the H3K4me3 active chromatin mark levels at these maternally imprinted genes was not statistically altered in DNMT1o-deficient trophoblast (*415*). In addition, loss of *H19*, *Igf2* and *Snrpn* imprinting has been observed in a handful of *Dnmt1*$^{\Delta 1o}$ maternal

effect placentas (*402*). However, transcriptional analysis of the majority of imprinted gene clusters has not been performed in either DNMT1o-deficient embryonic or placental lineages.

3.2.2 Transcriptional analysis of imprinted genes

Out of the 24 confirmed genomic imprints in mouse there are reasons to suspect at least 15 of them harbor imprinted genes that are integral to placental development (Section 1.5). There is particularly strong genetic evidence derived from targeted gene deletion mouse models for the involvement of imprinted genes in the *Kcnq1*, *H19, Peg10, Mest, Grb10*, *Dlk1* and *Igf2r* clusters in placental developmental pathways (*222, 274, 293, 302, 312, 313, 347, 374, 392*). In this chapter, quantitative RT-PCR was used to test the hypothesis that *Dnmt1*^{41o} maternal effect placentas have loss of imprinted gene expression, with some transcripts increasing in expression (presumably biallelic), while others becoming fully repressed. Specifically, imprinted gene expression from the following clusters were analyzed: *Peg10* (*Peg10*, *Sgce* and *Pon2*), *Dlk1* (*Dlk1*, *Meg3*, and *Rtl1*), *H19* (*H19* and *Igf2*), *Igf2r* (*Igf2r* and *Slc22a2*), *Mest* (*Mest* and *Klf14*), *Kcnq1* (*Phlda2* and *Ascl2*) and *Grb10* (*Grb10*).

3.2.3 Imprinted DMD methylation analysis

The exact genomic coordinates of DMDs in oocyte and embryonic genomes are overlapping but significantly different, suggesting that the physical extent of differential methylation is dynamic during embryonic development (*58*). Both gametic and embryonic DMD boundaries are defined by biallelic methylated regions (*58*). It is unclear if the exact DMD coordinates in the genome of trophoblast lineages are closer to those in gametes or embryos. In my dissertation research I have

examined imprinted DNA methylation at sequences that are common to both germline and embryonic DMDs. Bisulfite genomic sequencing was used to confirm loss of imprinting in the placenta compartment. A survey of DNA methylation at 15 DMDs across gestation was performed using EpiTYPER technology to quantify DMD methylation at 15 different loci in cohorts of mid-gestation DNMT1o-deficient placentas and to correlate loss of methylation with placental phenotypic metrics.

Imprinted DNA methylation patterns have been analyzed over the years using an array of techniques. Early studies performed methylation sensitive Southern blots that utilized isoschizomeric restriction enzyme pairs in which one enzyme is methylation-sensitive (*e.g.* HpaII) and the other is methylation-insensitive (*e.g.* MspI) and sequence specific genomic probes. This approach analyzes a handful of CpG dinucleotides at a time. The use of sodium bisulfite ($NaSO_4$) based techniques enabled methods of DNA methylation analysis that can provide a readout of multiple CpGs at specific sequences (*416*). High sodium bisulfite concentrations at elevated (85°C) temperatures and low pH (5.0) deaminate unmethylated cytosine nucleosides to uracil (*416*). PCR amplification of bisulfite treated genomic DNA using targeted primers replicates the ribonucleoside uracil into the deoxy-ribonucleoside thymidine (*416*). These bisulfite treated DNA amplicons can be analyzed by DNA sequencing (BGS: bisulfite converted genomic sequencing) or by restriction analysis (COBRA: combined bisulfite restriction analysis) to infer the ratio of unmethylated to methylated CpG methylation by the amount of C→T converted and unconverted product (*416, 417*). Both BGS and COBRA have their limitations: BGS requires the sequencing of many amplicons to obtain a good representation of the allelic population; and the COBRA assay, similar to methylation sensitive Southern blotting, only analyzes a handful of CpGs at a time (*416, 417*).

EpiTYPER analysis is a novel technique that provides a readout of many CpGs at a time from the whole allelic population of a sample (*418*). Ehrich and colleagues (2005) invented EpiTYPER DNA methylation analysis as a high-throughput bisulfite conversion based method to identify methylation differences of targeted sequences in normal and neoplastic lung tissue (*418*). In brief, EpiTYPER analysis is performed as follows: DNA is treated with bisulfite reagent; targeted genomic regions are PCR amplified using sequence specific primers with a T7 polymerase promoter attached; ssRNA is in vitro transcribed from the bisulfite PCR amplicon templates; the ssRNA is then cut with a nucleotide specific RNase; and the digestion products are analyzed by mass spectrometry to determine the sizes of the products (which are different if they incorporated a C or a T) (*418*). This technique gives a readout of 8-25 informative mass spectrometry fragments containing 1-4 CpGs each across amplicons ranging from 200-800bp (*418*).

Bisulfite converted DNA has also been used to measure genome wide methylation patterns using reduced representation bisulfite genomic sequencing (RRBS; a technique that cuts DNA with methylation insensitive MspI, and sequences 200-250bp fragments enriched in CpG islands) and by microarray analysis (*e.g.* Illumina 450k human array), however these approaches are not as cost efficient for detailed analysis of small sets of genomic sequences such as imprinted loci which represent a minute fraction of the genome (*419, 420*).

3.2.4 Association of loss of imprinting and placental phenotypes

In the results of Chapter 2 (Section 2.3) I quantified phenotypic metrics in cohorts of mid-gestation *Dnmt1*$^{\Delta 1o}$ maternal effect placentas. Herein, the DMD methylation profiles of individual placentas from the same DNMT1o-deficient cohorts were quantified by EpiTYPER

analysis. A separate cohort of E17.5 DNMT1o-deficient placentas had both phenotypic measurements and quantified imprinted gene expression. Linear regression was used to examine the relationship between E/P ratio and expression of imprinted genes in those E17.5 placentas. Having the phenotypic and DMD methylation data sets enabled me to test for meaningful phenotype-epigenotype associations. Logistic regression analysis was used to determine if fetal viability, a binary variable, was associated with methylation at any individual DMD. Likewise, linear regression analysis was used to test for meaningful associations between continuous placental metrics (*e.g.* weight, layer volumes, TGC counts and triacylglyceride content) and loss of methylation at specific DMDs. It was expected that only the strongest phenotype-epigenotype associations would emerge due to the complications of epigenetic pleiotropic and epistatic interactions associated with mosaic loss of DMD methylation in the *Dnmt1*$^{\Delta 1o}$ model.

3.2.5 Chapter 3 aims

In this chapter I have analyzed placental DMD methylation patterns in the *Dnmt1*$^{\Delta 1o}$ maternal effect model. This analysis aimed to confirm loss of imprinting in DNMT1o-deficient placentas consistent with prior observations in the embryo and limited preliminary extraembryonic analysis using a combination of quantitative RT-PCR and BGS. The extent of epigenetic mosaicism in DNMT1o-deficient placentas was probed using EpiTYPER analysis of 15 different DMDs. This enabled logistic regression analysis of which epigenotypes are viable and which are not. Ultimately, I attempted to connect loss of DNA methylation at specific DMDs to quantitative placental phenotypic metrics using linear regression analysis. The overarching goal of this section was to gain insight into the collective and individual role of genomic imprints in placental biology and identify those imprints most crucial for normal placental development.

3.3 MATERIALS AND METHODS

3.3.1 DNA and RNA purification

Genomic DNA was extracted from placenta tissues cleaned of maternal decidua contamination and with minimal umbilical cord and yolksac membranes. Samples were stored in RNA later (Sigma-Adlrich) prior to extraction. Whole (E9.5) half (E12.5), or quarter (E15.5 and E17.5) placenta samples weighing <30mg were minced with a razor on a glass microscope slide and placed in 600ml of RLT buffer pre mixed with 6ul of 2'mercaptoethanol in a 2ml microcentrifuge tube with homogenization microbeads, and then homogenized using two 45second cycles with a mini-beadbeater (Biospec). Nucleic acids were then extracted using the DNA/RNA combined extraction mini kit (Qiagen) or the RNeasy kit (Qiagen) following the manufacturer's protocols.

3.3.2 Imprinted gene quantitative real-time RT-PCR

Quantitative real-time reverse transcription PCR (qPCR) was carried out on purified RNA samples from E9.5, E12.5, E15.5 and E17.5 wild-type and DNMT1o-deficient placentas using the standard methods described below and gene specific primers (Appendix B). Contaminating DNA was digested either on column during purification (with the RNeasy kit) or using an RQ1 RNase free DNase digest before cDNA preparation. cDNA was prepared from 1μg of RNA using the high capacity cDNA reverse transcription kit (Applied Biosystems). qPCR was

performed in triplicate using SYBR Green PCR Master Mix (Applied Biosystems) in total reaction volume of 10µl on the 7900HT Fast Real-Time PCR machine. Dissociation curves were run on all reactions to ensure amplification of a single product. A control without RT (-RT) was run for each sample and a control without template (-template) was run for each primer set. Samples were analyzed using the ΔΔct method method relative to the *Rpl32* housekeeping gene. Five wild-type placentas were analyzed at each gestational age (*421*).

3.3.3 Bisulfite genomic sequencing

Genomic bisulfite conversion was carried out using an EpiTect bisulfite conversion kit (Qiagen). 500ng to 1µg of genomic DNA was converted based the amount extracted from each sample. The DNA was diluted with water to 20µl volume, and mixed with 85µl of bisulfite conversion mix and 35µl of DNA protect buffer. Conversion was carried out in 200µl PCR tubes using the following thermocycler program: 99°C 5′, 60°C 25′, 99°C 5′, 60°C 85′, 99°C 5′, 60°C 90′, 20°C hold. Columns and reagents provided by the EpiTect bisulfite kit were used per manufacturers instruction to purify converted DNA in 100µl of elution buffer. Nested bisulfite converted genomic PCR was used to amplify targeted DMDs (primers in Appendix C). The first round of nested PCR used 125ng of bisulfite converted DNA and in a 25 µl Taq Polymerase (Invitrogen) reaction with the following thermocycler program: Precycle: 94°C 4′, 55°C 2′ , 72°C 2′, 94°C 4′, 55°C 2′, 72°C 2′; followed by 35 amplification cycles: 94°C 1′, 55°C 2′, 72°C 2′; and a short 72°C 30″ extension and indefinite hold at 4°C. The second round of nested PCR was primed from 2.5 or 5µl of the first PCR and used a standard thermocycler program: 95°C 5′ denaturing followed by 35 cycles of 95°C 30″, 60°C 30″; 72°C 30″, a 72°C 7′ final extension and indefinite hold at 4°C. Bisulfite PCR reactions were run on 1.5% agarose gels at 80V and the appropriate

sized bands excised and gel purified using Qiaquick gel extraction kits (Qiagen). PCR amplicons were cloned using the TOPO-TA cloning kit (Invitrogen), transformed into competent *E.coli* cells, and plated onto LB + ampicillin agar plates coated with β-galactose and IPTG. 15-30 white opaque colonies were picked and sequenced in both directions using M3 and T7 promoter primers. Sequences were viewed and shortened to include only relevant genomic (and not plasmid) sequence and positioned in the same DNA strand orientation using CLC sequence viewer (CLC Bio). Bisulfite PCR amplicons from each placenta were aligned to fully converted DMD sequences with the Clustalomega multi-sequence alignment program and then exported to a text document where CG dinucleotides were underlined to easily identify converted and unconverted CpGs. Maternal and paternal DMD alleles were determine by use of SNPs between *Mus musculus domesticus* (maternal) and *M.m castenous* (paternal) strains. Results were transcribed into original figures in adobe illustrator.

3.3.4 Epityper analysis

EpiTYPER DNA methylation was used as a high-throughput bisulfite conversion based method to identify DMD methylation differences between wild-type and DNMT1o-deficient placentas (See section 3.1.3 for review). Genomic bisulfite conversion, bisulfite converted genomic PCR, and EpiTYPER (TM – Sequenom) mass-array DNA methylation analysis was performed at the Center for Genetics and Pharmacology at the Roswell Park Cancer Institute. Pre-validated bisulfite PCR primers for imprinted DMD genomic regions were used for the imprinted methylation analysis (Appendix D). All bisulfite amplcion sequences overlapped known primary imprinted DMDs ((*26*), and references therein). Bisulfite converted PCR amplification primers for all but *H19* were chosen from a publicly available mouse imprinted panel (Sequenom). *H19*

primer sequences were originally published by McGraw et al. (2013) (*408*). Each EpiTYPER amplicon was further validated by internal control wild-type placenta DNA (50% imprinted DMD methylation), *Dnmt1*-null (*Dnmt1*$^{c/c}$) ES cell DNA (0% imprinted DMD methylation) and 1:2 (16.6% imprinted DMD methylation) and 2:1 (33.3% imprinted DMD methylation) mixtures of the two. Only amplicons that produced a linear relation between control genomic DNA expected and observed methylation fractions were selected for use in this study

3.3.5 Biostatitics and bioinformatics

EpiTYPER absolute methylation levels were calculated as the unweighted average CpG methylation fraction across each individual imprinted DMD amplicon. Overall imprinted DMD methylation was determined from 12 non-redundant DMD EpiTYPER amplicons (Appendix D) To determine if the wild-type and mutant sample methylation levels were normally distributed Kolmogorov-Smirnov, Shapiro-Wilk and Anderson-Darling tests of normality were applied to the data in Matlab (Mathworks). Because the mutant data were non-normally distributed we compared distributions using a Mann-Whitney U (Rank-Sum) test. In addition Fisher's exact test was used to compare the number of low DMD methylation (less than 0.75 or 0.5 wild-type levels) placentas for each individual DMD across gestation. Bar graphs and scatter plots of overall and individual imprinted DMD methylation levels were originally generated with Matlab and then adapted into Adobe Illustrator.

To display the variability in DMD methylation intrinsic to the *Dnmt1*$^{\Delta 1o}$ maternal effect model we constructed heat maps. Mutant imprinted DMD methylation levels were normalized to wild-type by dividing each sample's imprinted DMD absolute methylation fraction by the average wild-type methylation level for that imprinted DMD and gestational age. The relative

methylation levels were then log2 transformed and clustered using the clustergram function in Matlab. Each clustergram was adapted into a grayscale Adobe Illustrator file.

To associate individual placental DMD methylation defects with particular placental phenotypic abnormalities I performed regression analyses in Matlab. Logistic regression was performed to find associations between individual imprinted DMD methylation levels and the binary fetal viability variable. Bivariate linear regression analysis was used to associate imprinted DMDs with the continuous phenotypic metrics for LZ volume, JZ volume, trophoblast giant cell count and fetal/placental weights. Similarly, P/E ratio and aberrant imprinted gene expression was tested for meaningful associations using linear regression analysis. Stepwise forward linear regression modeling was performed to generate models that explain the *Dnmt1*$^{\Delta 1o}$ maternal effect phenotypic variation based on DNA methylation of the least number of significant DMDs. Phenotypes with strong associations ($P<0.05$) identified by bivariate regression were plotted against DMD methylation or imprinted gene expression.

3.4 RESULTS

3.4.1 Loss of imprinted gene expression

The epigenotypes of DNMT1o-deficient placentas showed a wide-range of loss of imprinting across gestation. Expression of genes from 7 imprinted loci (*Peg10*, *Dlk1*, *H19*, *Igf2r*, *Mest*, *Kcnq1* and *Grb10*) were analyzed by qPCR with the expectation that loss of DMD methylation at any imprinted cluster would cause expression of some imprinted genes to increase and others to

decrease. The observed average imprinted gene expression patterns of cohorts of DNMT1o-deficient placentas are shown in Figure 28. The expected loss of imprinting gene expression patterns are displayed at the bottom of Figure 28. Abnormal imprinted gene expression patterns were observed by qPCR as early as E9.5 and continued through mid (E12.5 and E15.5) and late (E17.5) gestation. Early in gestation many imprinted genes behaved in the manner expected with loss of methylation at neighboring ICRs. For example, placental expression of *Pon2, Igf2, Igf2r, Klf14* and *Grb10* were down regulated in DNMT1o-deficient placentas relative to wild type at E9.5 (Figure 28). However, by E17.5 the expected loss of imprinted gene expression patterns was not as encompassing. At E17.5 DNMT1o-deficient placentas showed loss of imprinted gene expression within the *Mest* cluster congruent with expected results; with *Mest* expression up regulated and *Klf14* down regulated. In contrast, within the *Peg10* cluster, *Sgce* and *Pon2* were up regulated in a manner incoherent with loss of *Peg10* DMD methylation (Figure 28). Unexpected upregulation was also observed for *Dlk1, Phlda2* and *Ascl2* but did not reach significance compared to wild-type (Figure 28). This transcriptional analysis is evidence that the partial loss of imprinting observed in the *Dnmt1*$^{\Delta 1o}$ maternal effect model changes across gestation.

Linear regression was used to determine if the expression of any imprinted gene was associated with the E/P ratio placental efficiency metric in DNMT1o-deficient placentas. Both *Ascl2* and *Mest* expression were significantly associated with E/P ratio ($P<0.01$; Figure 29). Expression of *Ascl2* had an inverse association with with E/P ratio (Figure 29A), whereas expression of *Mest* had a direct association (Figure 29B). Furthermore, in multivariate linear regression modeling the expression of *Ascl2* and *Mest* accounted for 82% of the variance in E/P

ratio. These relationships were maintained when controlling for gender ($P<0.001$; data not shown).

3.4.2 Bisulfite genomic sequencing

DMD methylation patterns were also disrupted in DNMT1o-deficient placentas. Allele specific loss of DMD methylation as measured by BGS was observed at E9.5 and E17.5 (Figures 30 and 31). Strict parent-specific DMD methylation was observed for both paternally imprinted (*H19*) and maternally imprinted (*Kcnq1*, *Snrpn*, and *Mest*) DMDs in a wild-type placentas. In contrast, significant deviations from parent-specific methylation were observed in DMDs of all DNMT1o-deficient placentas analyzed. For example, at E9.5 nearly complete loss of *Mest* DMD methylation was observed in all DNMT1o-deficient placentas (M1-M3; Figure 30). A large range of variation in the extent of methylation loss at individual DMDs was observed across placental samples. For example, whereas M1 showed a pattern of strict parent-specific methylation for the *Snrpn* DMD, M2 showed a near complete loss. In any individual E9.5 placenta there was no correlation among the four different DMDs for the extent of methylation loss. For example, M1 showed nearly complete loss of DMD methylation of the *H19* and *Mest* DMDs, yet normal methylation of the *Snrpn* DMD, whereas M2 showed nearly complete loss of DMD methylation

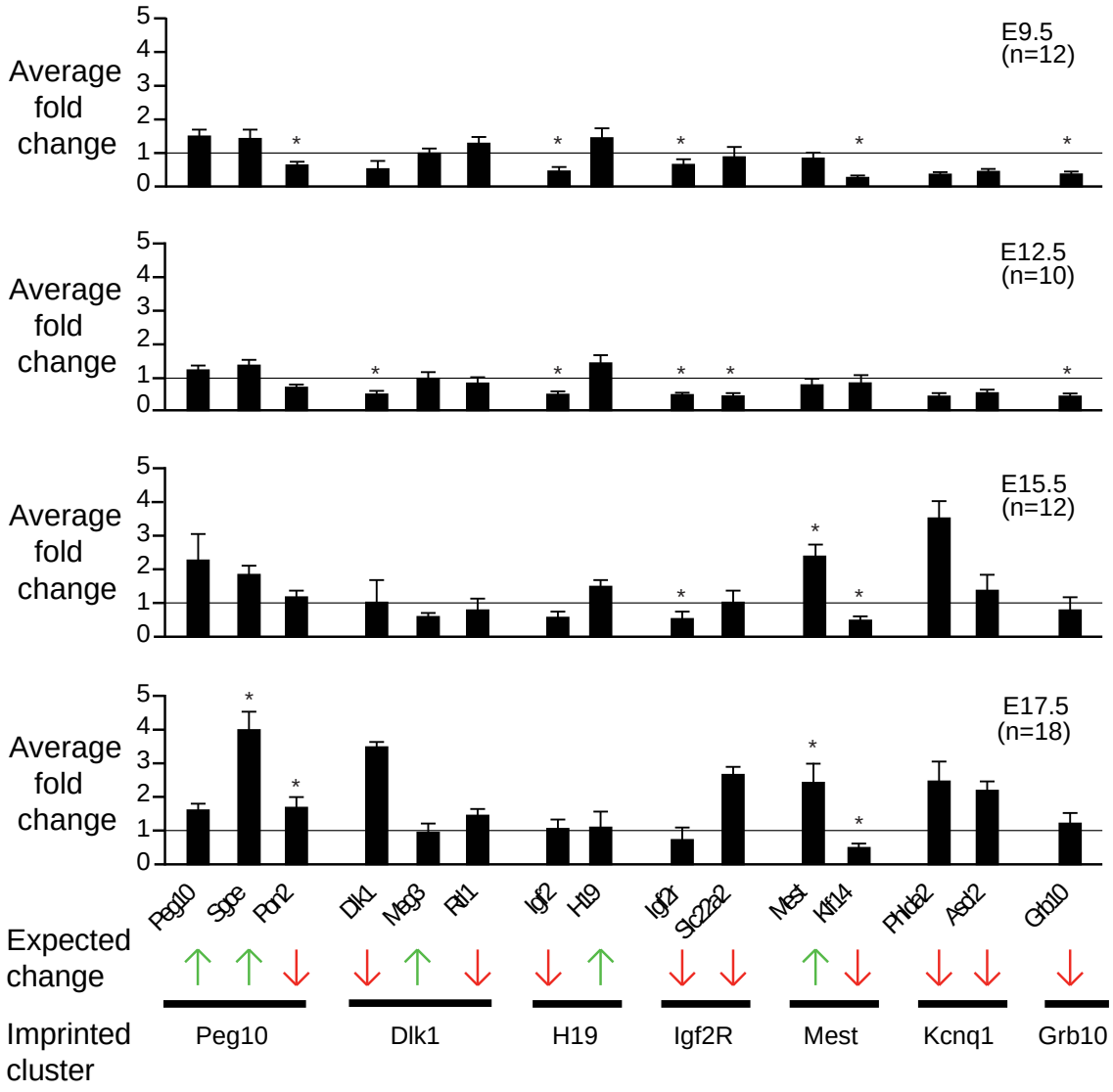

Figure 28. Imprinted gene expression patterns in DNMT1o-deficient placentas across gestation. Bar graph columns show mean expression (+SEM) of 15 imprinted genes in DNMT1o-deficient placentas compared to wild-type (n=5). Normalization to the Rpl32 gene using the ΔΔct method. (*n* = the number of DNMT1o-deficient placentas studied). * Denotes significant (P<0.05) differences in expression between DNMT1o deficient and wild-type ascertained by Kruskal Wallis test. Expected expression changes with loss of DMD methylation for each imprinted gene cluster. Green up arrows indicates expected increase in expression; Red down arrows represent expected decreased expression.

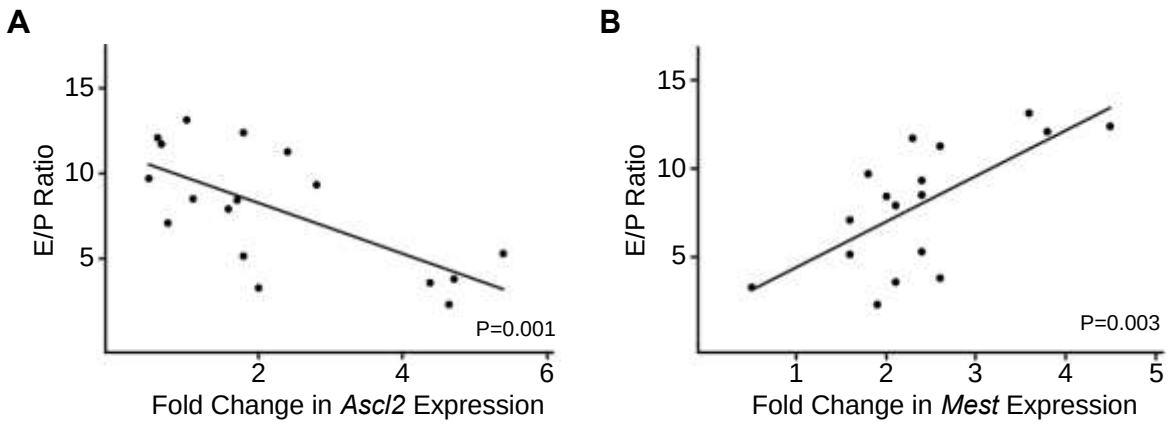

Figure 29. Linear regression of E/P Ratio and imprinted gene expression in E17.5 DNMT1o-deficient placentas. (A) Negative association between *Ascl2* expression and E/P ratio. (B) Positive association between *Mest* expression and E/P ratio.

of the *Mest*, *Kcnq1*, and *Snrpn* DMDs, yet near normal methylation of the *H19* DMD. Finally, there was no evidence in wild-type or in DNMT1o-deficient placentas of methylation on the normally unmethylated parental allele. In summation, these results indicate that DNMT1o-deficient placentas develop as cellular epigenetic mosaics with loss of DMD methylation during the first half of gestation.

At E17.5, the type and extent of DMD methylation changes were distinct from those obtained from E9.5 DNMT1o-deficient placentas (Figure 31). Loss of methylation at the *Snrpn* DMD was observed at a single DNMT1o-deficient placenta (M1) whereas the *Mest* DMD was variable in all three mutants analyzed (M1-M3; Figure 31). The *H19* and *Kcnq1* DMDs did not significantly lose methylation in the 3 analyzed E17.5 DNMT1o-deficient placentas. This finding is notably different than the variation in loss of *H19* and *Kcnq1* DMD methylation observed in E9.5 DNMT1o-deficient placentas. There was no evidence for gain of methylation on the normally unmethylated allele at any of the four DMDs. Based on these results, I conclude that while DMD epigenetic mosaicism is found in late gestaional DNMT1o-deficent placentas, the

precise makeup of mosaics transforms during the second half of gestation such that it is uncommon to recover certain patterns of DMD methylation.

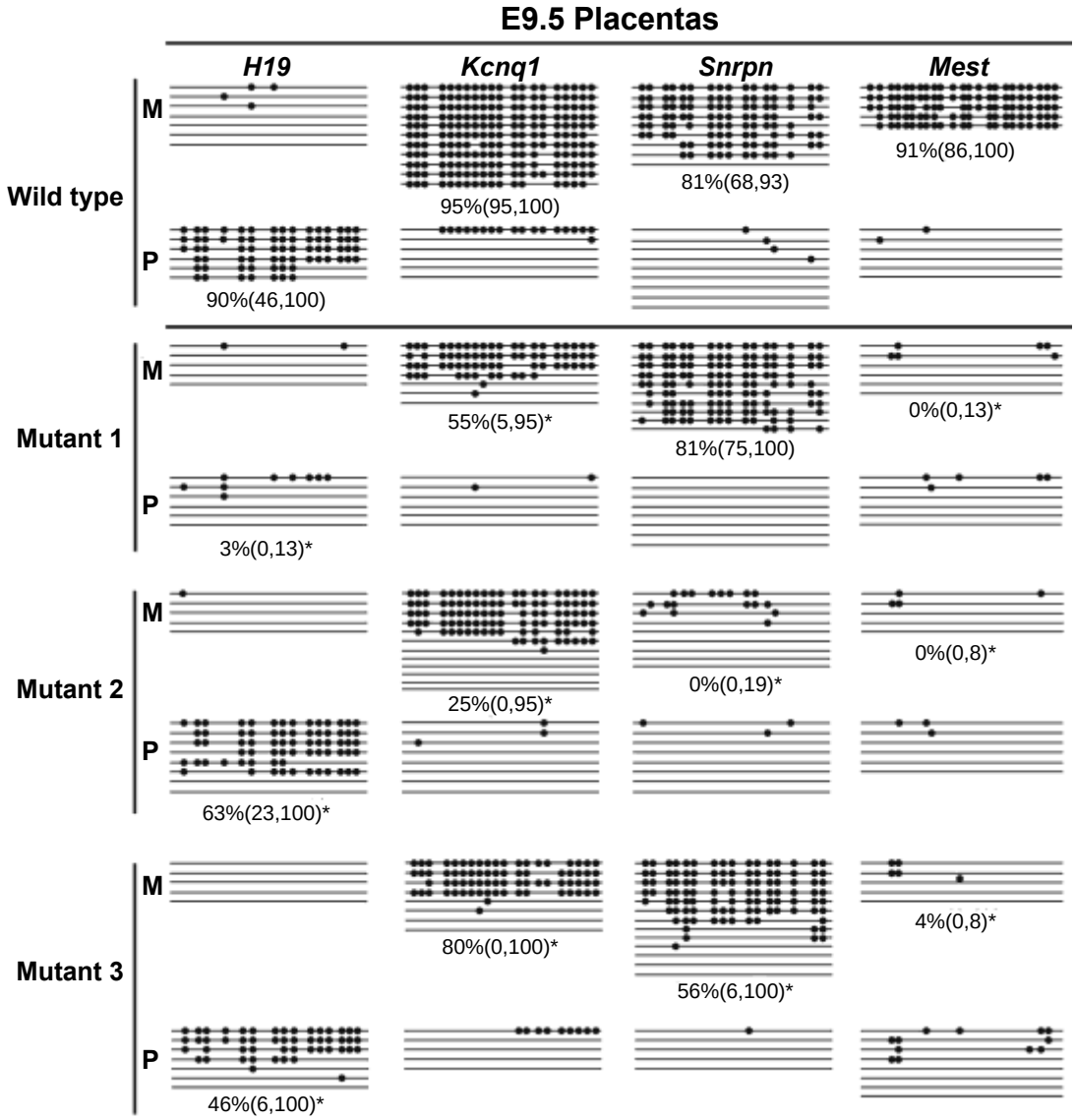

Figure 30. Variable loss of DMD methylation in E9.5 DNMT1o-deficient placentas. Bisulfite genomic sequencing of the H19, Kcnq1, Snrpn and Mest DMDs in a wild-type and three DNMT1o-deficient placentas. Abbreviations: M Maternal allele, P Paternal allele. Position of methylated CpGs are indicated as filled circles. Parantheses indicate intraquartile range. (*) significantly lower methylation than wild-type by Kruskal Wallis ($P<0.05$).

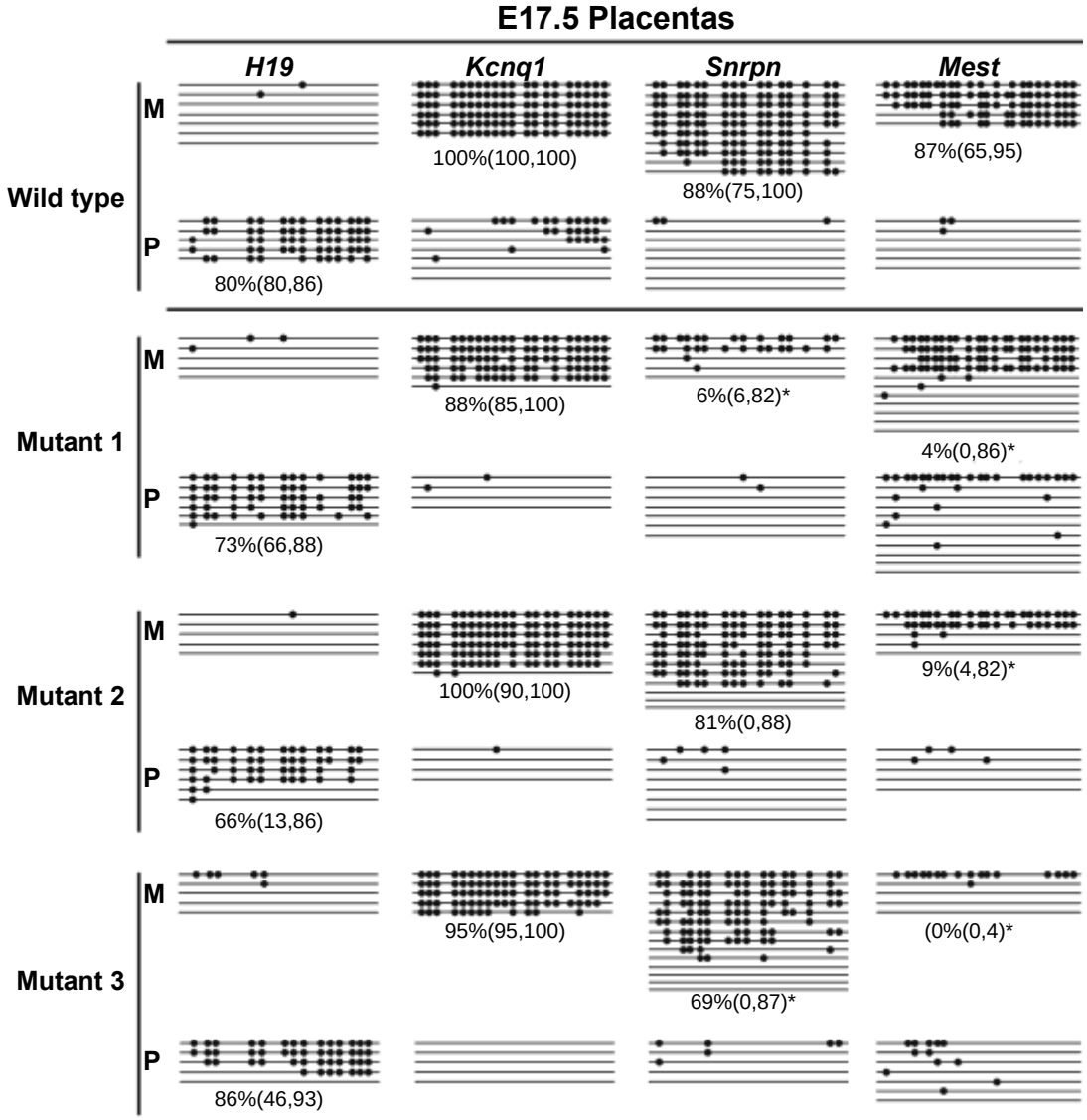

Figure 31. Variable loss of DMD methylation in E17.5 DNMT1o-deficient placentas. Bisulfite genomic sequencing of the H19, Kcnq1, Snrpn and Mest DMDs in a wild-type and three DNMT1o-deficient placentas. Abbreviations: M Maternal allele, P Paternal allele. Position of methylated CpGs are indicated as filled circles. Parantheses indicate intraquartile range. (*) significantly lower methylation than wild-type by Kruskal Wallis ($P<0.05$).

3.4.3 EpiTYPER imprinted DMD methylation analysis

To understand the role of imprinted methylation on the wide-range of placental abnormalities seen in the *Dnmt1*$^{\Delta 1o}$ model, DNA methylation was measured at 14 imprinted DMDs at three times during the latter half of gestation. The average methylation fraction across 12 non-redundant DMD EpiTYPER amplicons was calculated for both wild-type and DNMT1o-deficient placental samples at each time point. Methylation was reduced in DNMT1o-deficient placentas at E12.5, E15.5 and E17.5 (Figure 32A). At E12.5 there was a significant decrease in the average methylation across all DMDs ($P<0.001$) from 0.388 for wild-type to 0.232 for mutant placentas. In a collection of 23 E15.5 DNMT1o-deficient placentas, the average DMD methylation was 0.283, significantly lower than the wild-type average of 0.382 ($P<0.001$). Similarly in a collection of 24 E17.5 placentas average DMD methylation was 0.272, significantly lower than the wild-type average of 0.407 ($P<0.001$). There was a trend toward mutants approaching wild-type levels of imprinted DMD methylation levels as gestation progressed; average DMD methylation increased from E12.5 to E15.5 ($P<0.01$) and from E12.5 to E17.5 ($P<0.001$) but not from E15.5 to E17.5 (not significant). These findings show that total DMD methylation levels in DNMT1o-deficient placentas do not remain constant across gestation but rather resolve to more normal levels, suggesting selection against low DMD methylation epigenotypes that do not support placental development and function.

There was a large range in loss of DMD methylation at most, but not all, individual imprinted DMDs in DNMT1o-deficient placentas. The hypergeometric distribution was used to categorize DMDs as being enriched, depleted or within the expected range of loss of methylation (<0.75 wild-type levels) at E12.5 as compared to the total E12.5 DMD measurements. The *Grb10, Plag1, Igf2r, Kcnq1,* and *H19* DMDs had a number of low methylation samples within

the expected range (Figures 32B-F). Other DMDs including *Peg10*, *Peg1*, *Peg3*, and *Impact* were hyper-variable and had a greater number of samples with low methylation values (Figures 32G-K). A third group of DMDs was hypovariable and depleted for low methylation values, these included *Dlk1*, *Nespas*, and *Snrpn* (Figures 32L-P). Adjacent DMD amplicons were analyzed to confirm the hypervariable *Impact* and hypovariable *Nespas* and *Dlk1* measurements. These findings are interpreted as evidence for early selection against loss of *Nespas, Snrpn* and *Dlk1* DMD methylation in trophoblast.

Concomitant with the increasing average imprinted DMD methylation from E12.5 to E15.5 in DNMT1o-deficient placentas (Figure 32A), I observed a steady reduction in the range of methylation among the examined placentas for many but not all individual DMDs (Figures 32B-P). Based on this, three distinct temporal patterns of methylation were defined by comparing median methylation levels across gestation for each DMD with the Rank-sum test. A group of five DMDs had higher average methylation at E15.5 than at E12.5 (*Mest*, *Snrpn*, *Dlk1*.A, *Dlk1*.B, and *Nespas*.B; $P<0.025$; Figures 32 G, L, O and P). Other DMDs had a more gradual increase in methylation from E12.5 to E17.5 (*Peg10*, *H19* and *Peg3*; $P<0.025$; Figures 32D, H and K). Five DMDs comprise a third DMD class that did not significantly change their average methylation across gestation in DNMT1o-deficient placentas (*Igf2r, Kcnq1 Plagl1*, *Impact*.A, *Impact*.B, *Nespas*.A, and *Nespas*.B; Figures 32B, C, F, I, J, M and N). Out of the three imprinted DMDS for which duplicate adjacent EpiTYPER amplicons were selected (*Dlk1*, *Impact* and *Nespas*), only *Nespas* showed a discordant trend with *Nespas*.A not differing between gestational cohorts and *Nespas*.B transitioning to higher average methylation between E12.5 and E15.5 (Figures 32M and N). Additionally the *Grb10* DMD displayed opposing

changes from E12.5 to E15.5 and E15.5 to E17.5, and did not significantly differ between E12.5 and E17.5 (Figure 32E).

Fisher's exact test was used to confirm these temporal patterns by comparing the number of low methylation placentas using a cutoff of <0.75 or <0.5 wild-type levels. These findings were slightly different. Using a low methylation cutoff of <0.5 wild-type the Fisher's exact test revealed that *Mest* and *Kcnq1* DMDs had significantly fewer low methylation samples at E15.5 than at E12.5, and the *Peg3* DMD had a significant gradual decrease in low methylation samples from E12.5 to E17.5. With a less stringent low methylation cutoff of <0.75 the Fisher's exact test revealed that *Nespas* and *Mest* had a significant decrease in low methylation samples between E12.5 and E15.5, and *Dlk1*.B had a significant decrease in low methylation samples between E12.5 and E17.5. No significant changes were unearthed within the E15 to E17 transition using Fisher's exact test with either cutoff. These results indicate selective pressure against loss of methylation of the *Mest*, *Kcnq1*, *Nespas*, *Peg3* and *Dlk1* DMDs during mid-gestation.

Three additional imprinted DMDs were examined in E12.5 and E15.5 cohorts (*Zrsr1*, *Nnat* and *Nap1l5*), and only *Zrsr1* had a significant difference between wild-type and the *Dnmt1*$^{\Delta 1o}$ mutant average methylation levels (Figures 32Q-S). Each of these DMDs is within a putative microimprinted domain (Section 1.5.1, 1.5.4 and 1.5.12; Figures 2A, D and L). In DNMT1o-deficient placentas *Zrsr1* remained variable and did not differ between E12.5 and E15.5. Overall, the observed trends in DMD methylation during gestation suggest that there are strong biological influences blocking the loss of imprints at specific DMDs during mid-gestation.

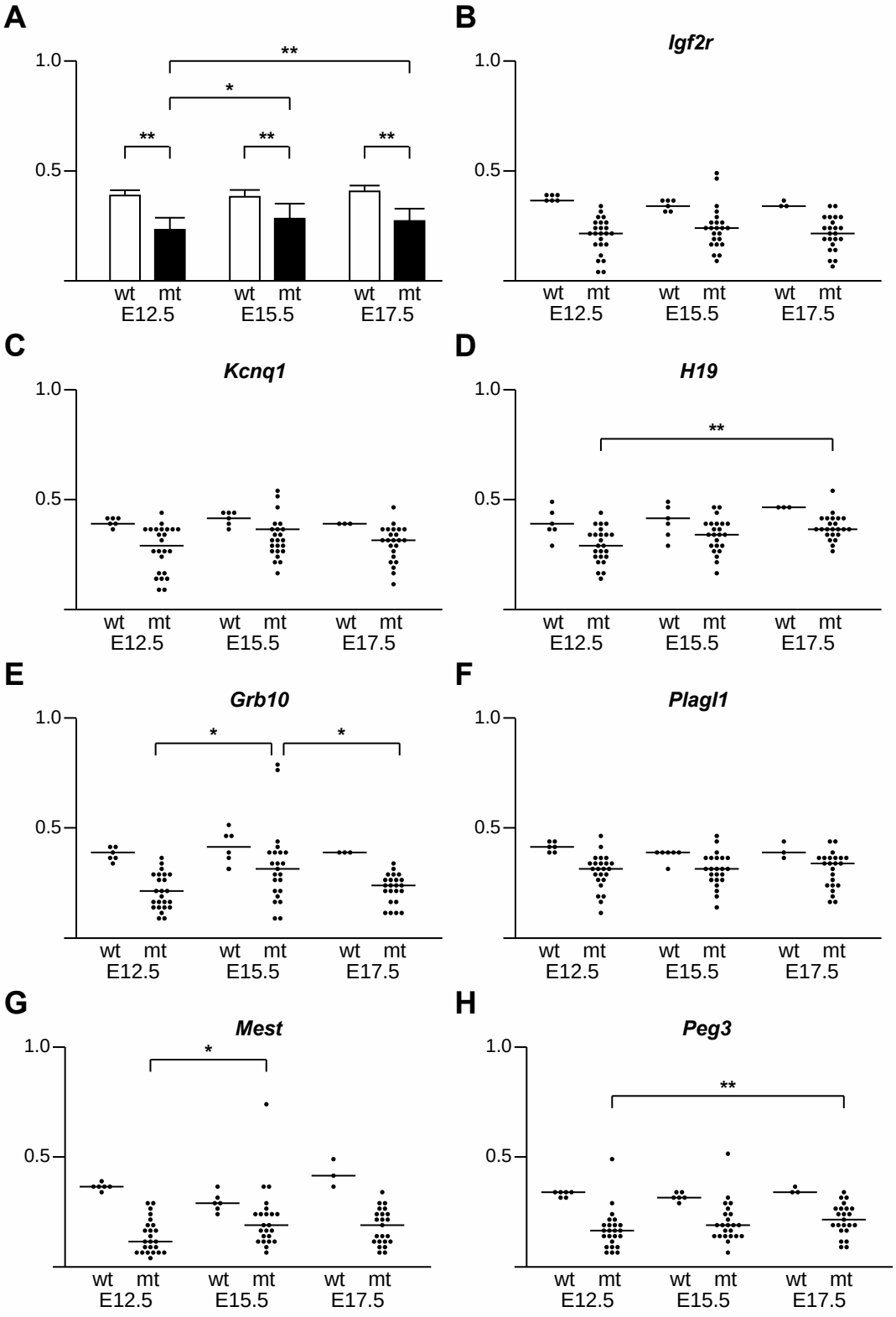
A
B
Igf2r
C
Kcnq1
D
H19
E
Grb10
F
Plagl1
G
Mest
H
Peg3
1.0
0.5
wt mt
E12.5
E15.5
E17.5
*
**

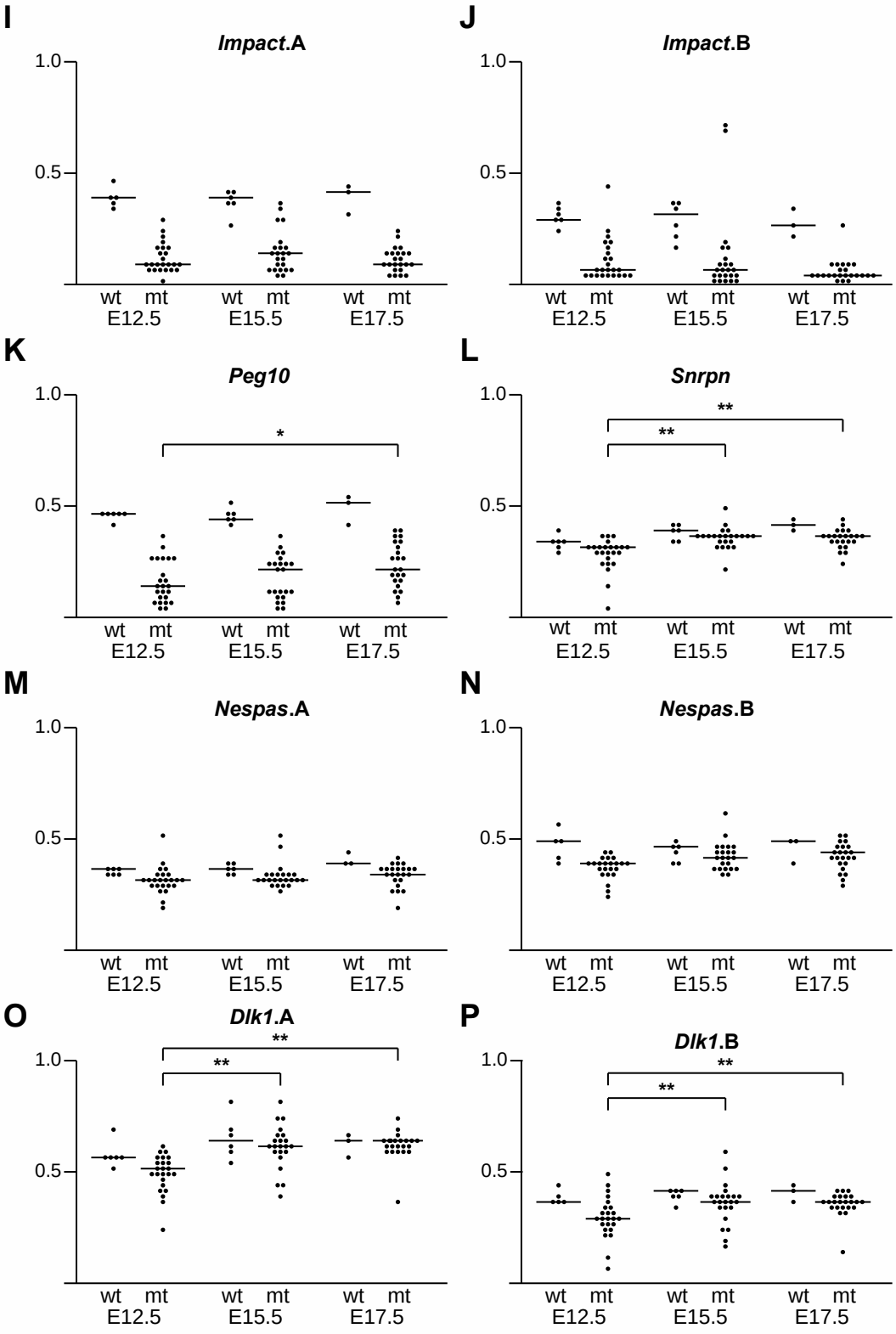
I
Impact.A
J
Impact.B
K
Peg10
L
Snrpn
M
Nespas.A
N
Nespas.B
O
Dlk1.A
P
Dlk1.B
1.0
0.5
wt mt
E12.5
E15.5
E17.5
*
**

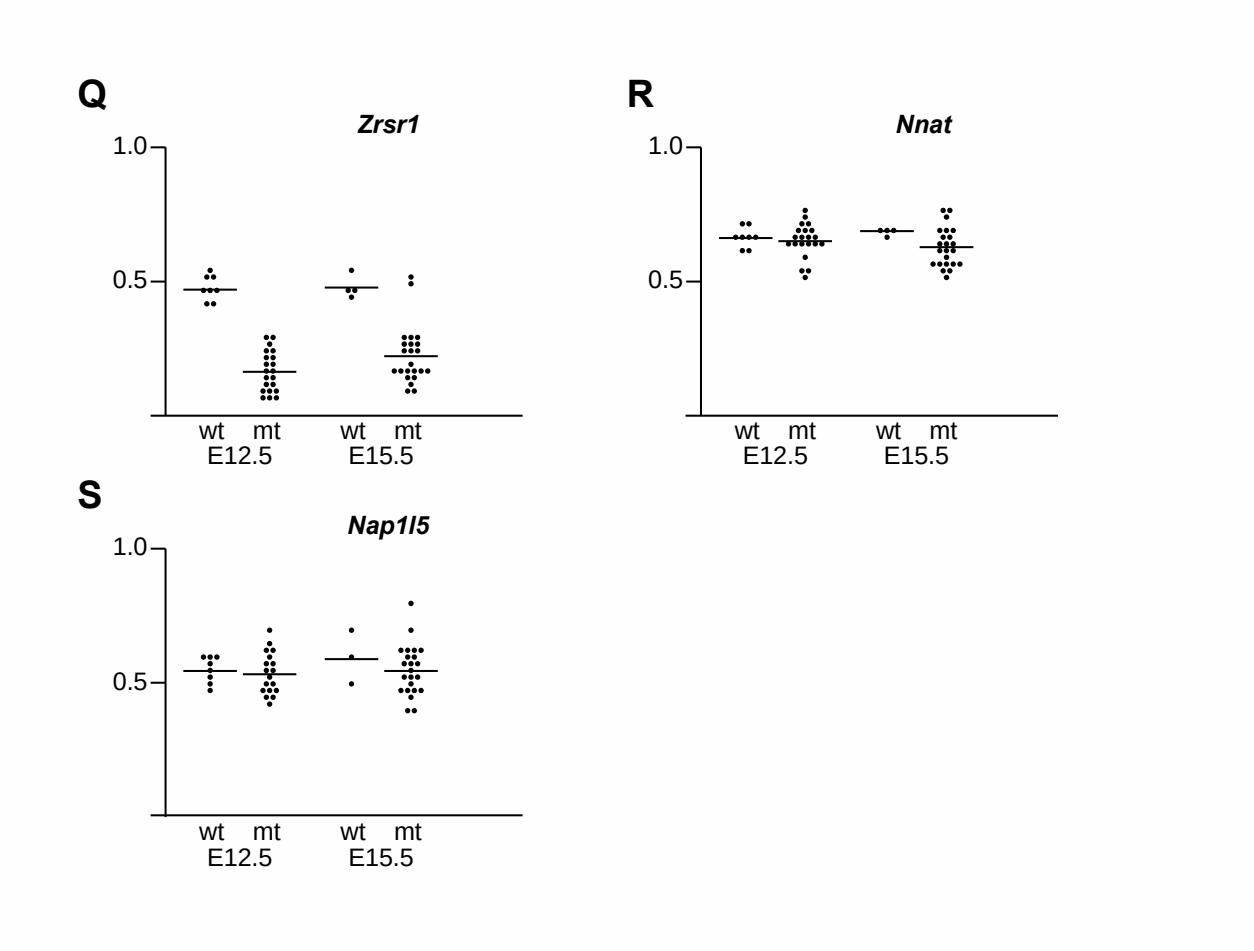

Figure 32. Imprinted DMD methylation levels in wild-type (wt) and DNMT1o-deficient (mt) placentas across mid gestation (E12.5, E15.5 and E17.5). (A) Bar graphs showing average mean and standard deviation of total imprinted DMD methylation of wt (open bars) and mt (filled bars) across mid-gestation. (B-S) Binned scatter plot showing individual wt and mt placentas across mid-gestation and the sample mean for the following imprinted DMDs: (B) *Igf2r*, (C) *Kcnq1*, (D) *H19*, (E) *Grb10*, (F) *Plagl1*, (G) *Mest* (H) *Peg3* (I) *Impact.*A, (J) *Impact.*B, (K) *Peg10*, (L) *Snrpn*, (M) *Nespas.*A, (N) *Nespas.*B, (O) *Dlk1*.A, (P) *Dlk1*.B, (Q) *Zrsr1*, (R) *Nnat*, and (S) *Nap1l5*. Small brackets indicate significant differences between gestational age matched sample populations of wt and mt DMD methylation medians. Larger brackets indicate significant differences between mutant DMD methylation medians at different gestational ages. * ($P<0.01$), and ** ($P<0.001$) denote significant differences of mutant median imprinted DMD methylation compared to wild type, or between gestational ages of mutant sample population by the Rank-sum test. DMDs are organized by hypergeometric distribution as having a number of low methylation samples falling within the expected range (B-F), greater than the expected range (G-K) or less than expected range (L-P).

The spectrum of methylation among 12 DMDs for each individual E12.5 DNMT1o-deficient placenta is displayed in the form of a heat map clustergram (Fig 33). Among the 24 E12.5 placentas represented in this manner, the majority of placentas have a unique DMD methylation profile not found in other placentas, although there are a few cases of high similarity. For example placentas A8 and B2 have identical DMD methylation profiles. Placentas A4 and B5 differ only at *Grb10, Kcnq1* and *H19* DMDs, and placentas A3 and C1 are unique at only the *Plagl1* DMD. Clustering of the DMDs at E12.5 indicate the genetically linked *Peg10* and *Mest* DMDs as well as the linked *Kcnq1* and *Snrpn* DMDs vary in conjunction. Although there is a trend toward more normal DMD methylation levels at E15.5 and E17.5, each DNMT1o-deficient placenta at these stages still has a unique imprinted epigenotype (Figures 33 and 34). These comparisons among placentas across the latter half of gestation point out the intrinsic power of the $Dnmt1^{\Delta 1o}$ maternal effect model to produce diverse and abnormal patterns of imprinted DMD methylation.

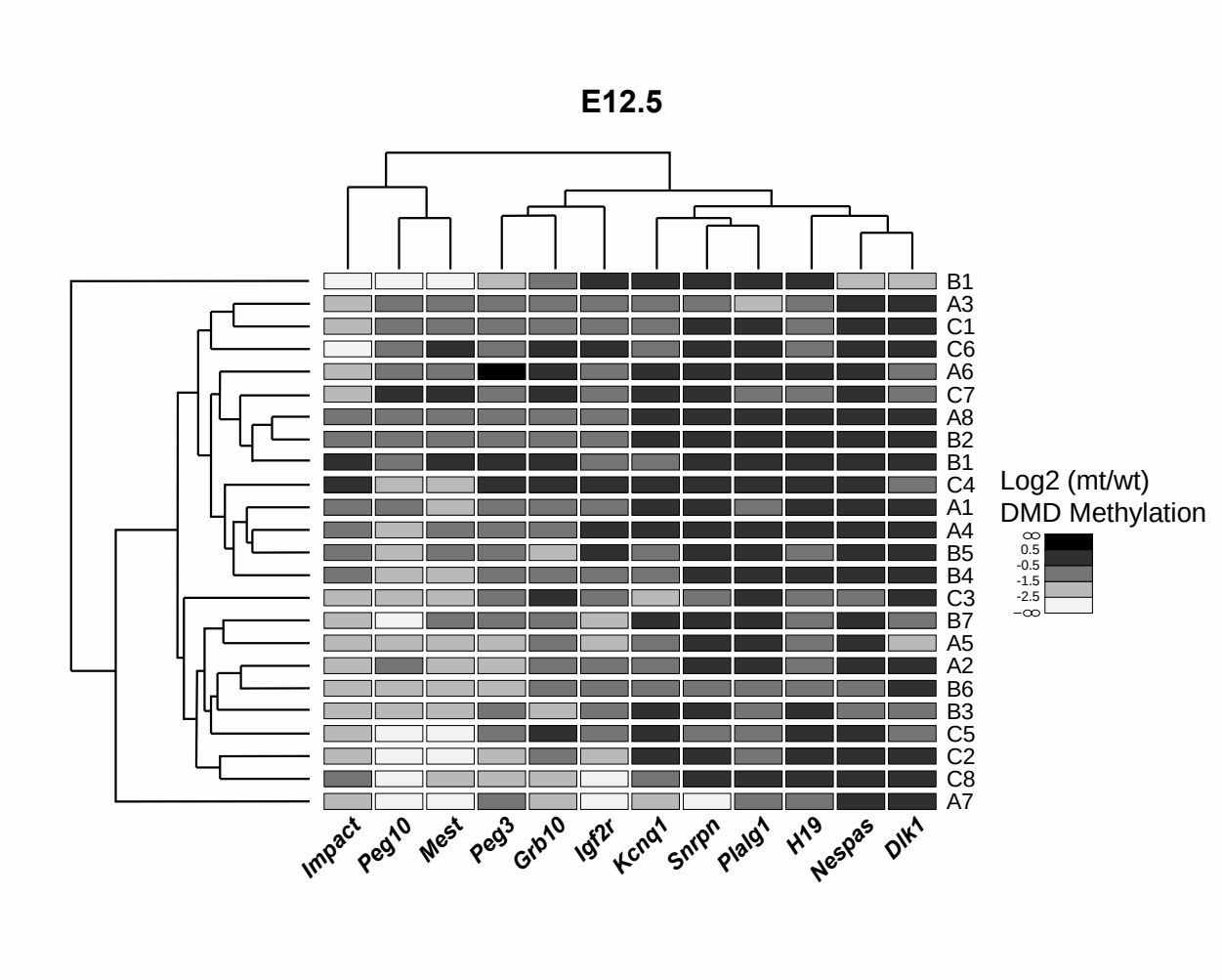

Figure 33. Hierarchical clustering of 24 E12.5 DNMT1o-deficient placentas based on DMD methylation. Data is shown as the log2 transformed ratio of mt:wt DMD methylation. The heat map displays normally methylated DMDs as dark boxes whereas loss of methylation is indicated by lighter shades. The upper and side dendrograms display linkage between imprinted DMDs and DNMT1o-deficient samples respectively. Imprinted DMDs are labeled across the bottom axis. DNMT1o-deficient samples are labeled down the right hand side by cohort litter (Letters A-C) and conceptus (Numbers 1-8).

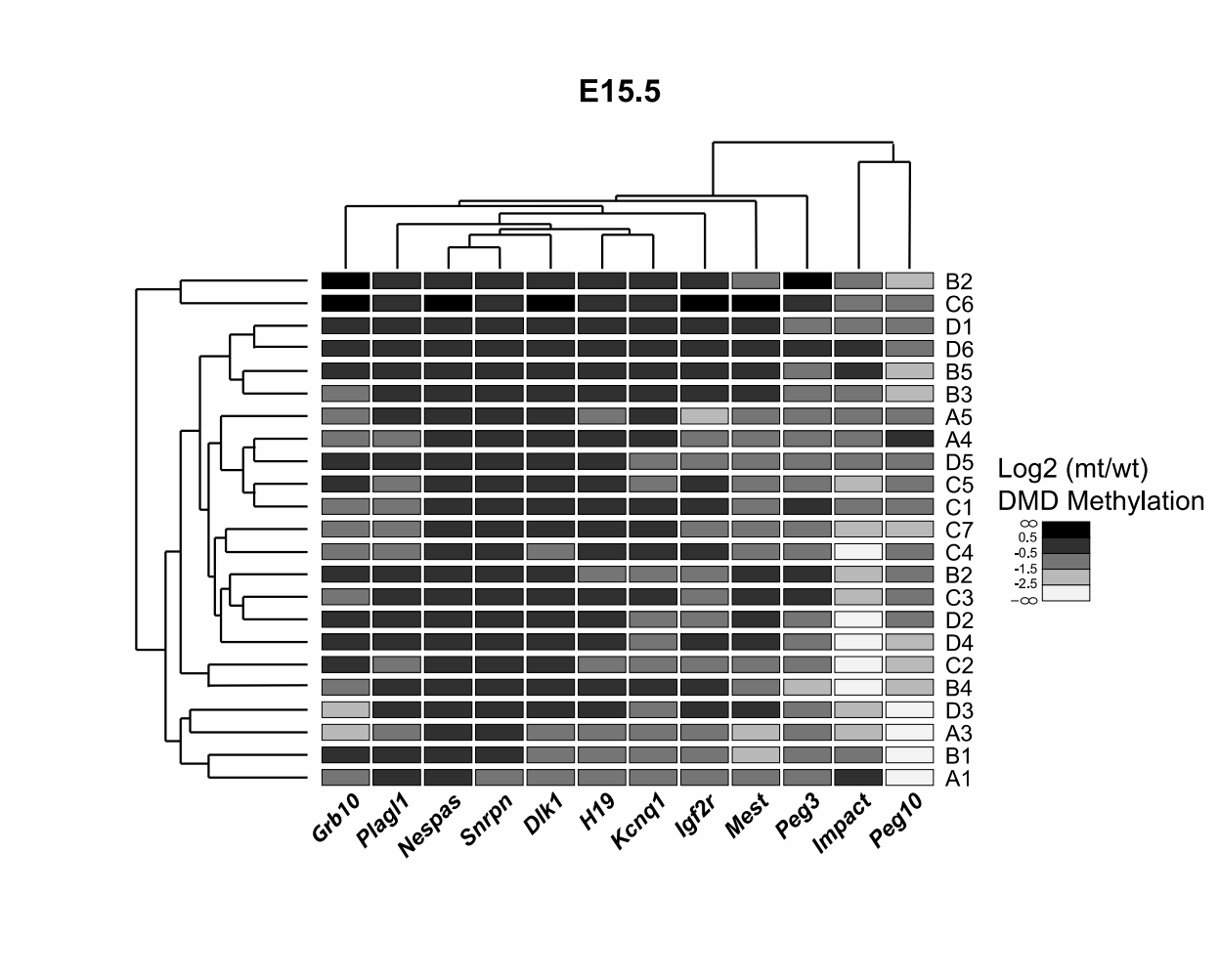

Figure 34. Hierarchical clustering of 23 E15.5 DNMT1o-deficient placentas based on DMD methylation. Data is shown as the log2 transformed ratio of mt:wt DMD methylation. The heat map displays normally methylated DMDs as dark boxes whereas loss of methylation is indicated by lighter shades. The upper and side dendrograms display linkage between imprinted DMDs and DNMT1o-deficient samples respectively. Imprinted DMDs are labeled across the bottom axis. DNMT1o-deficient samples are labeled down the right hand side by cohort litter (Letters A-D) and conceptus (Numbers 1-8).

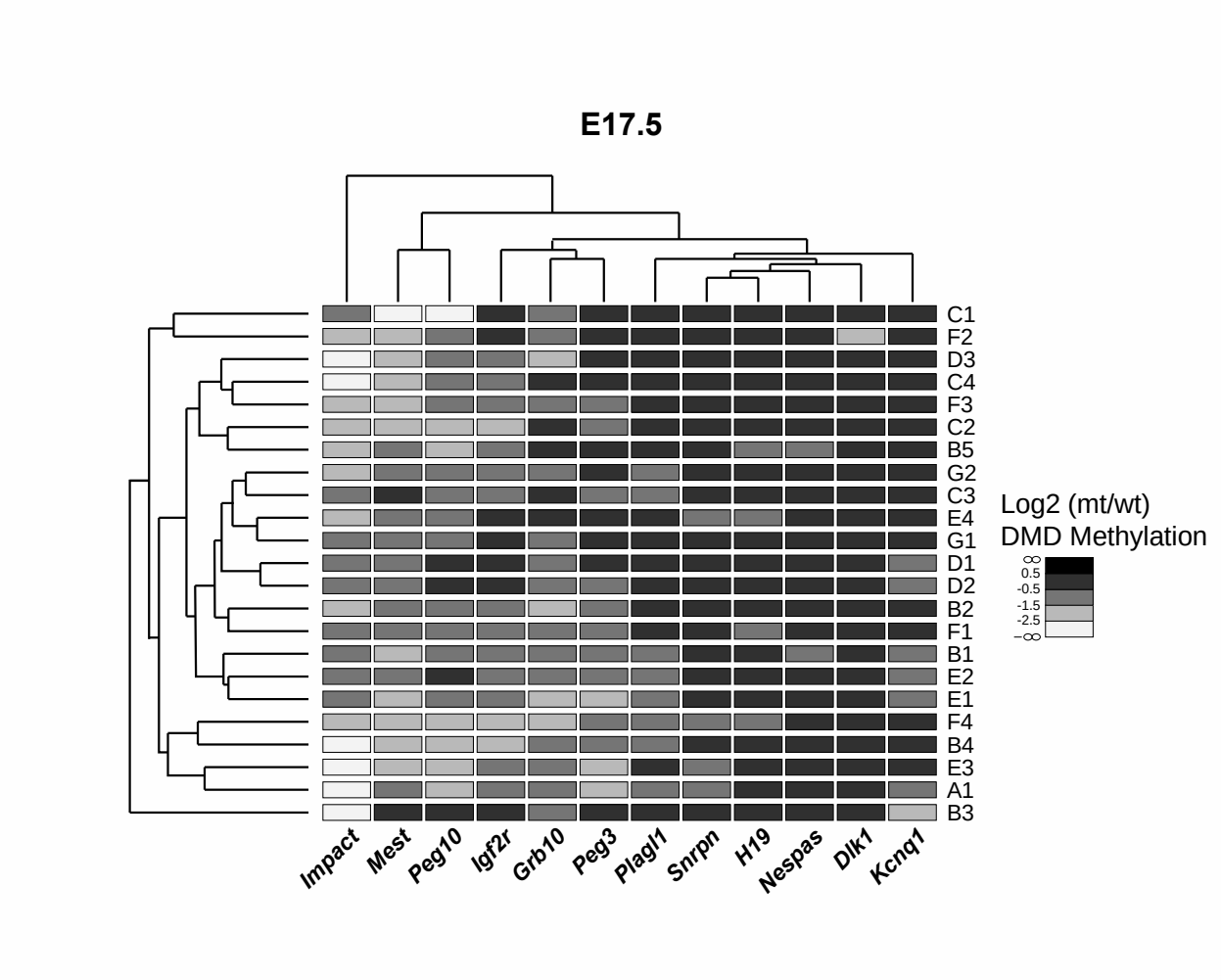

Figure 35. Hierarchical clustering of 23 E17.5 DNMT1o-deficient placentas based on DMD methylation. Data is shown as the log2 transformed ratio of mt:wt DMD methylation. The heat map displays normally methylated DMDs as dark boxes whereas loss of methylation is indicated by lighter shades. The upper and side dendrograms display linkage between imprinted DMDs and DNMT1o-deficient samples respectively. Imprinted DMDs are labeled across the bottom axis. DNMT1o-deficient samples are labeled down the right hand side by cohort litter (Letters A-G) and conceptus (Numbers 1-8).

3.4.4 Decreased fetal viability is associated with loss of *Peg10* DMD methylation

Logistic regression was used to identify those imprinted DMDs that exerted the greatest influence on fetal viability at E12.5 through placental imprinting (Table 3). The logistic regression coefficient (logit) is reported as a measure of the effect of DMD methylation levels on the odds ratio of fetal survival. A positive association was discovered between *Peg10* DMD methylation and fetal viability at E12.5 ($P<0.05$) indicating that placentas with loss of the *Peg10* methylation imprint are less likely to support a viable fetus. A negative association between *Nnat* DMD methylation and fetal viability was observed ($P<0.05$). The only significant association identified between imprinted DMD methylation and fetal viability at either E15.5 or E17.5 was a negative association between *Nespas*.B DMD methylation and viability at E15.5 ($P<0.05$; Table 3). These findings suggest that in the context of the *Dnmt1*$^{\Delta 1o}$ maternal effect mouse model, nearly normal *Nnat* and *Nespas* imprinting may decrease viability.

Gestational Age	DMD	Logit	P-Value
E12.5 (n=24)	*Peg10*	+2.17	3.25E-02
	Nnat	-2.49	4.12E-02
E15.5 (n=23)	*Nespas*.B	-1.05	3.69E-02
E17.5[a] (n=23)			

Table 3. Logistic regression of E12.5, E15.5 and E17.5 DNMT1o-deficient placentas based on DMD methylation and fetal viability. Only significant ($P<0.05$) associations established by logistic regression analysis between dependent fetal viability and independent imprinted DMD methylation values are shown. The log odds ratio(logit) is the coefficient indicating the direction and strencth of the relationship. ([a]) no significant associations were found at E17.5.

3.4.5 Placental abnormalities are associated with loss of DMD methylation

Because of the broader range of abnormal DMD methylation, histomorphological abnormalities and effects on fetal viability at E12.5 I focused primarily on phenotype-epigenotype regression analysis at the E12.5 time point. Bivariate linear regression analysis was used to determine which imprinted DMDs underlie the observed E12.5 placental abnormalities. The most significant ($P<0.05$) DMD associations for each phenotype are displayed in Table 3 and Figure 36. The regression coefficient (β) is reported as the change in phenotype associated with modulation of the DMD methylation fraction (0 to 1.0). Placenta weight is negatively associated with DMD methylation at *Nespas*.A (Table 4 and Figure 36A) although not at *Nespas*.B. For each 1% decrease in *Nespas*.A DMD methylation (0.01 methylation fraction) placental weight increased by a corresponding 1.275 milligrams (95% CI: 0.648, 1.902). Spongiotrophoblast volume was negatively associated with both analyzed *Nespas* regions as well as the *H19* DMD (Table 4 and Figures 36B-D). Each 1% decrease in DMD methylation at *Nespas*.A, *Nespas*.B and *H19* increased JZ volume by 0.0399 (95% CI: 0.0258, 0.054), 0.0266 (95% CI: 0.035, 0.0497) and 0.0170 (95% CI: 0.0017, 0.0323) mm^3 respectively.

Linear regression analysis revealed a strong association between *Peg10* DMD methylation and LZ volume (Table 4 and Figure 36E). Diminishment of *Peg10* DMD methylation by 1% corresponds to a 0.0217 (95% CI: 0.002, 0.066) mm^3 decrease in LZ central volume. Labyrinth structures in three DNMT1o-deficient placentas with low *Peg10* DMD methylation are shown in Fig 4. Labyrinths in these samples are noticeably smaller, disorganized and hemorrhagic. Notably, methylation of the *Nnat* DMD is negatively associated with LZ volume (Table 4 and Figure 36F), counter to the observed trend of decreased LZ in DNMT1o-

deficient placentas; a 1% decrease in *Nnat* DMD methylation resulting in a 0.0249 (95% CI: 0.043, 0.111) mm^3 increase in LZ central volume.

Placental Phenotype	DMD	β	P-Value
Placental Weight (mg)	*Nespas*.A	-127.5	6.21E-04
Spongiotrophoblast Central Volume (mm^3)	*Nespas*.A	-3.99	1.41E-05
	Nespas.B	-2.65	3.54E-02
	H19	-1.7	4.08E-02
Labyrinth Central Volume (mm^3)	*Peg10*	+3.58	3.12E-02
	Nnat	-7.72	2.82E-04
Trophoblast Giant Cell Count (#/section)	*Kcnq1*	-508	1.87E-05
	Snrpn	-674	2.31E-04
	Plagl1	-438	1.97E-02
	Nespas.B	-575	4.38E-02

Table 4. Bivariate regression analysis of 24 E12.5 DNMT1o-deficient placentas based on DMD methylation and placental phenotypes. Only significant ($P<0.05$) associations established by bivariate regression analysis between dependent placental phenotypes and independent imprinted DMD methylation values are shown. β is the linear regression coefficient.

Bivariate regression analysis revealed a significant negative association between *Kcnq1* DMD methylation and accumulation of TGCs (Table 3 and Figure 36G). A 1% decrease in *Kcnq1* DMD methylation corresponds to an increase of 5.08 (95% CI: 3.25, 6.91) TGCs per histological section. Representative H&E and *ISH* stained histological sections of wild-type and DNMT1o-deficient placentas with very low *Kcnq1* DMD methylation and pronounced expansion of parietal TGCs bordering the JZ are displayed in Figure 5. Positive *ISH* staining for the pan-TGC transcripts *Prl2c2* and *Prl3b1* was observed in both parietal TGCs and JZ layers (Figure 5). Intriguingly, the early TGC marker Prolactin-1 (*Prl3d1*) was ectopically expressed in the parietal TGCs of DNMT1o deficient placentas with low *Kcnq1* DMD methylation, where as it should be restricted to TGCs embedded within maternal spiral arteries by E12.5.

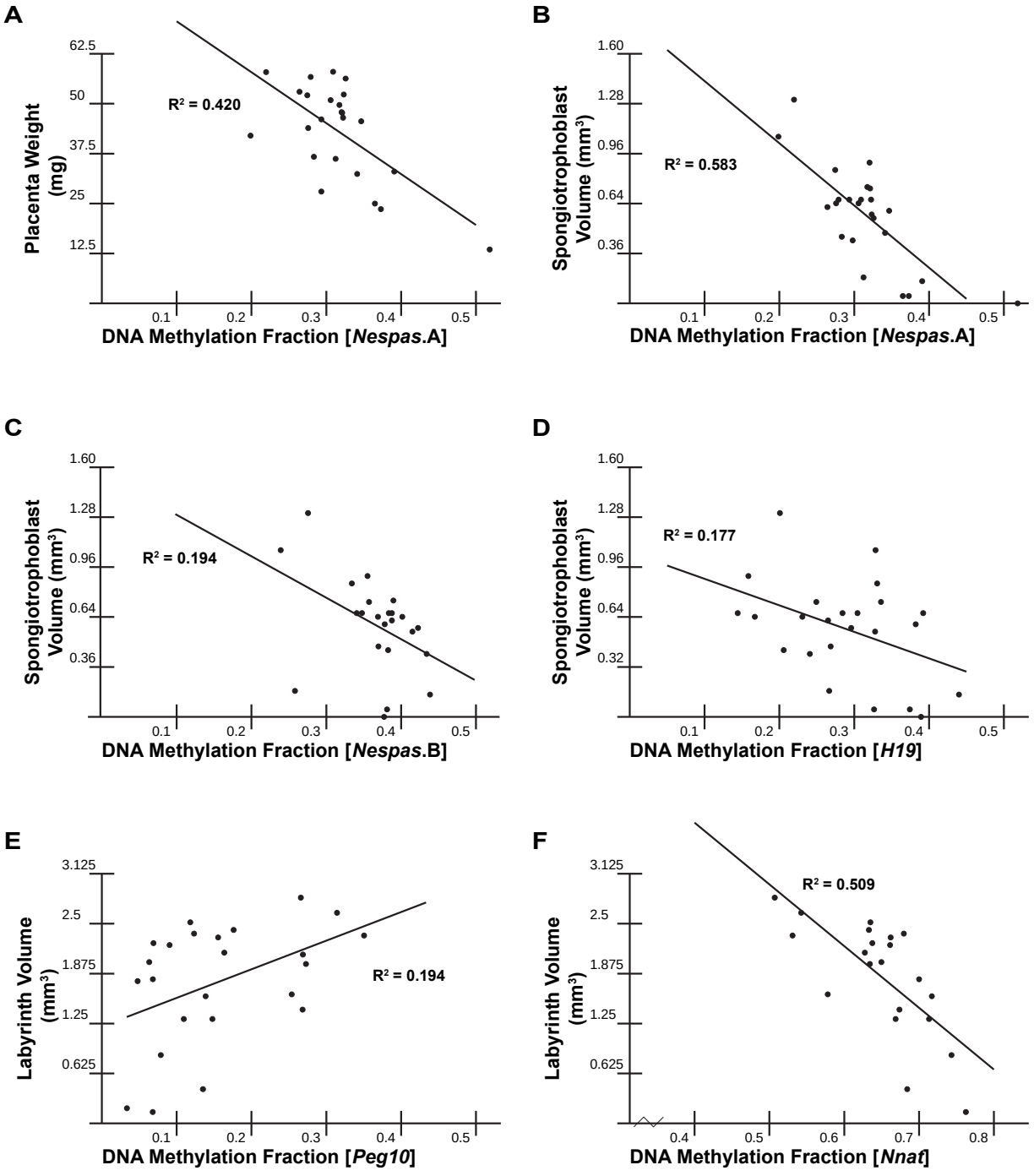
A
Placenta Weight (mg)
62.5
50
37.5
25
12.5
R² = 0.420
0.1
0.2
0.3
0.4
0.5
DNA Methylation Fraction [Nespas.A]
B
Spongiotrophoblast Volume (mm³)
1.60
1.28
0.96
0.64
0.36
R² = 0.583
0.1
0.2
0.3
0.4
0.5
DNA Methylation Fraction [Nespas.A]
C
Spongiotrophoblast Volume (mm³)
1.60
1.28
0.96
0.64
0.36
R² = 0.194
0.1
0.2
0.3
0.4
0.5
DNA Methylation Fraction [Nespas.B]
D
Spongiotrophoblast Volume (mm³)
1.60
1.28
0.96
0.64
0.32
R² = 0.177
0.1
0.2
0.3
0.4
0.5
DNA Methylation Fraction [H19]
E
Labyrinth Volume (mm³)
3.125
2.5
1.875
1.25
0.625
R² = 0.194
0.1
0.2
0.3
0.4
0.5
DNA Methylation Fraction [Peg10]
F
Labyrinth Volume (mm³)
3.125
2.5
1.875
1.25
0.625
R² = 0.509
0.4
0.5
0.6
0.7
0.8
DNA Methylation Fraction [Nnat]

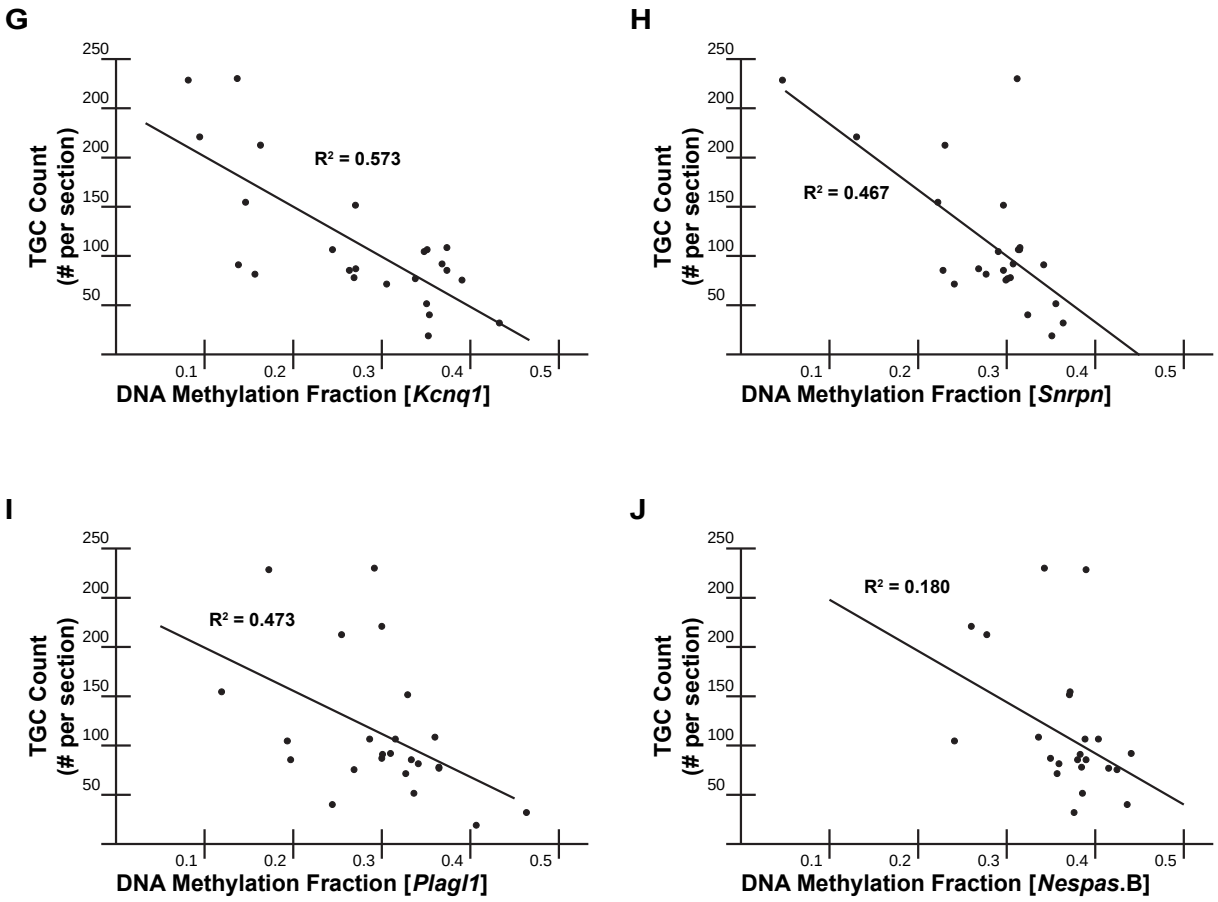

Figure 36. Linear regression plots of imprinted DMD methylation versus placental phenotypic metrics in a cohort of E12.5 DNMT1o-deficient placentas. (A) Negative association between *Nespas*.A DMD methylation and placental weight. (B) Negative association between *Nespas*.A DMD methylation and spongiotrophoblast volume. (C) Negative association between *Nespas*.B DMD methylation and spongiotrophoblast volume. (D) Negative association between *H19* DMD methylation and spongiotrophoblast volume. (E) Positive association between *Peg10* DMD methylation and labyrinth volume. (F) Negative association between *Nnat* DMD methylation and labyrinth volume. (G) Negative association between *Kcnq1* DMD methylation and TGC counts. (H) Negative association between *Snrpn* DMD methylation and TGC counts. (I) Negative association between *Plagl1* DMD methylation and TGC counts. (J) Negative association between *Nespas*.B DMD methylation and TGC counts. R^2 is unadjusted R-square value.

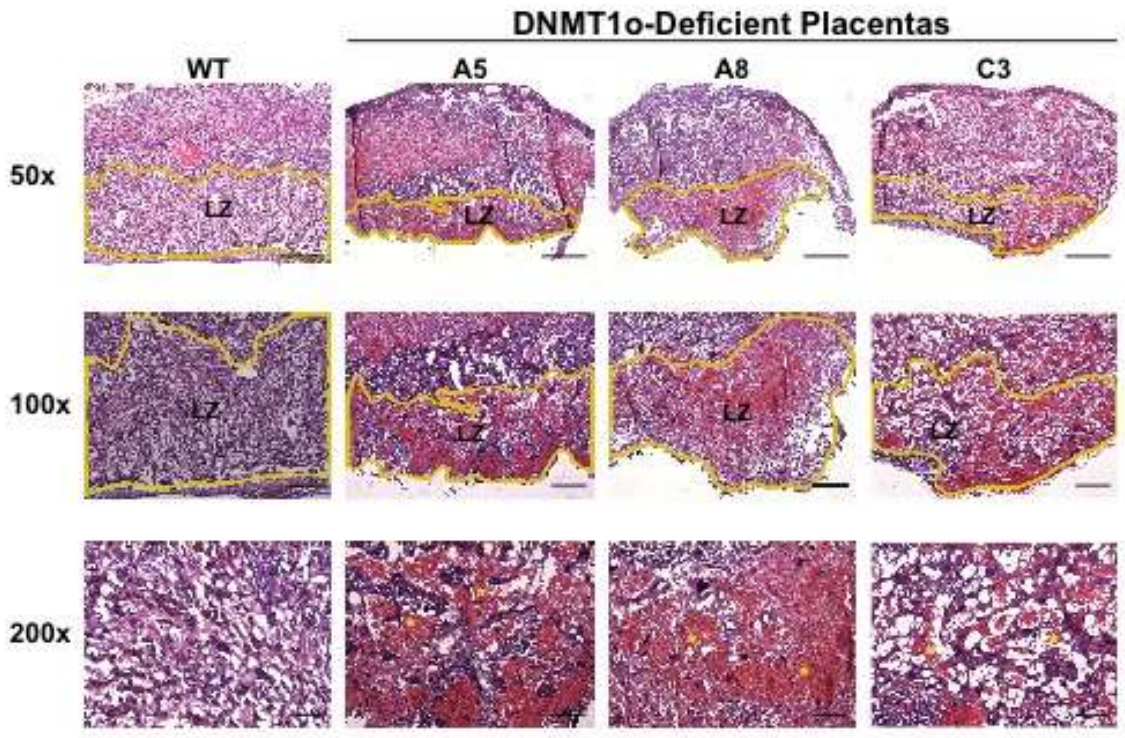

Figure 37. Histology of hematoxylin and eosin (H&E) stained labyrinth of one wild-type (wt) and three DNMT1o-deficient low-*Peg10* DMD methylation placentas. The scale bars for 50X, 100X and 200X magnification are 500, 200 and 100 μm respectively. Yellow lines in 50x and 100x magnification images outline the labyrinthine zone (LZ).

DNA methylation at the genetically linked *Snrpn* DMD (both *Kcnq1* and *Snrpn* DMDs are on mouse chromosome 7) also inversely associated with TGC accumulation (Table 3 and Figure 36H). For every 1% decrease in *Snrpn* DMD methylation there is a corresponding increase of 6.74 (95% CI: 3.73, 9.75) TGCs per section. A weaker inverse association between both *Plagl1* and *Nespas*.B DMD methylation and TGC number was also identified (Table 3 and Figures 36I and 36J). Decreases of 1% methylation at *Plagl1* and *Nespas*.B modulate an increase in TGCs per section of 4.38(95% CI: 0.970, 7.79) and 5.75(95% CI: 0.500, 11.0) respectively. Imprinted DNA methylation at the *Peg3* DMD, which like *Kcnq1* and *Snrpn* is a maternally derived methylation imprint on mouse chromosome 7, was not significantly associated with TGC

accumulation (P=0.40). Linear regression model building confirmed the major DMD methylation influence of TGC accumulation to that of just the *Kcnq1* and *Snrpn* DMDs (S2 Table).

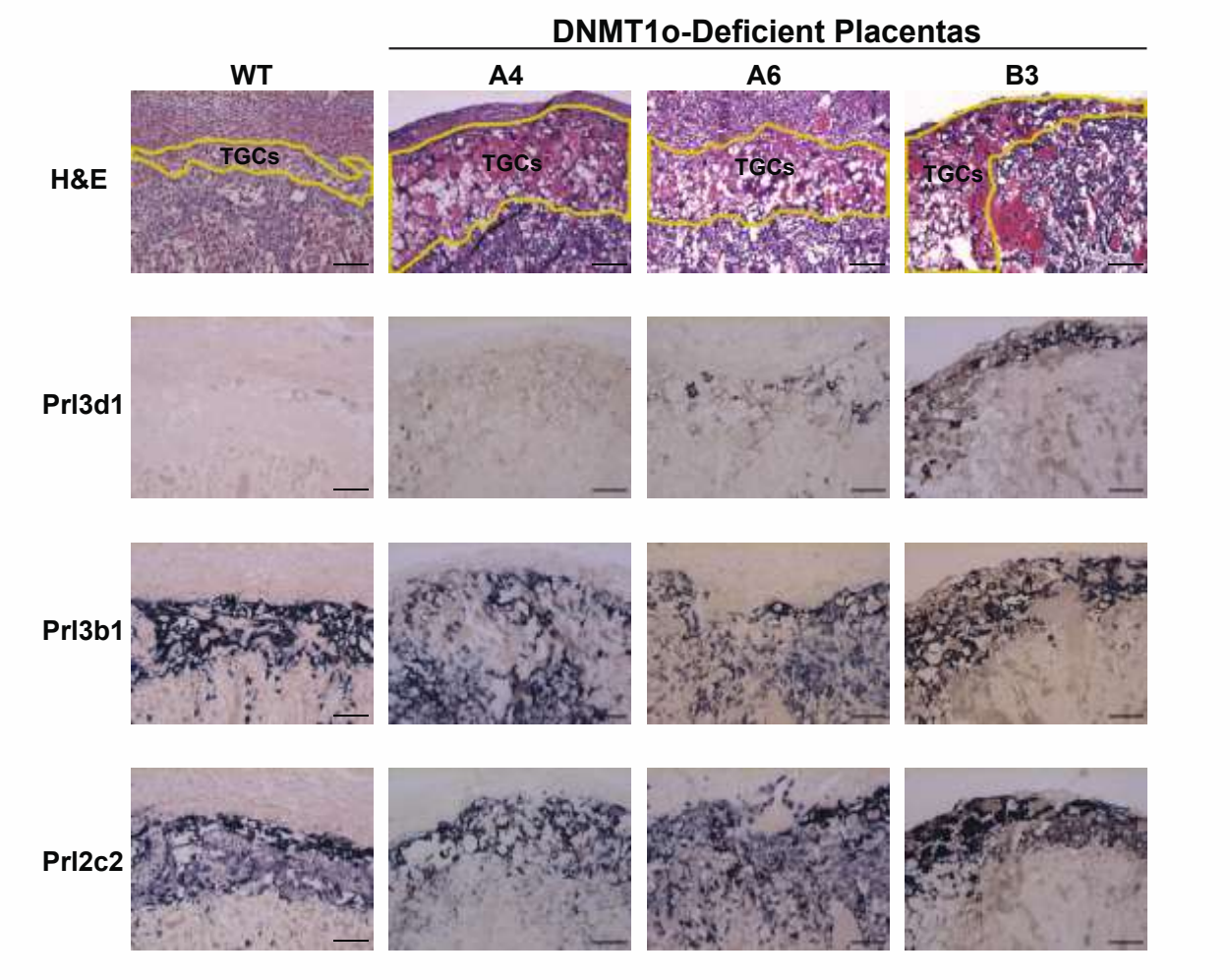

Figure 38. In situ hybridization analysis of TGCs in E12.5 wild-type and DNMT1o-deficient placentas with low *Kcnq1* DMD methylation. All images were taken at 100X magnification. The scale bar is 100μm. Yellow lines delineate the layer containing trophoblast giant cells (TGCs) in the top row displays histology of hematoxylin and eosin (H&E) stained sections. *ISH* for the prolactin gene family members *Prl3d1*, *Prl3b1* and *Prl2c2* on adjacent sections to H&E are shown in the lower three rows.

Parameter	Estimate	SE	P-Value
Intercept	+310	36.8	3.54E-08
Kcnq1 Regression Coefficient (β)	-364	109	3.11E-03
Snrpn Regression Coefficient (β)	-350	160	4.01E-02

Table 5. Stepwise forward linear regression analysis of associations between imprinted DMD methylation and TGC accumulation in E12.5 DNMT1o-deficient placentas. N=24, df=21, model P-value=1.54×10^{-5}

I performed bivariate linear regression to determine if there were any phenotype-epigenotype associations at E15.5 and E17.5. Spongiotrophoblast central volume inversely associated with *Impact*.B and *Mest* methylation at E15.5 ($P<0.05$; Table 6). Each 1% decrease in *Impact*.B and *Mest* methylation increased JZ central volume by 0.0717 (95% CI: 0.043, 0.1004) and 0.0449 (95% CI: 0.0275, 0.0623) mm^3 respectively. Using a relaxed significance threshold only three meaningful phenotype-epigenotype associations were found at E17.5 ($P<0.075$; Table 7). Placental weight was positively associated with *Dlk1*.A methylation: each 1% decrease in *Dlk1*.A methylation corresponded to a 1.166 (95% CI: 0.591, 1.741) milligram decrease in placental weight. Fetal weight was associated with placental methylation at the *Igf2r* and *Mest* DMDs: for each 1% decrease in *Igf2r* and *Mest* methylation fetal weight decreased by 20.40 (95% CI: 11.17, 29.63) and 16.81 (95% CI: 8.05, 25.57) milligrams respectively.

Placental Phenotype	DMD	β	P-Value
Spongiotrophoblast Central Volume (mm^3)	*Impact*.B	-7.72	1.45E-02
	Mest	-4.49	1.87E-02

Table 6. Bivariate Regression analysis of 21 E15.5 DNMT1o-deficient placentas based on DMD methylation and placental phenotypes. Only significant ($P<0.05$) associations established by bivariate regression analysis between dependent placental phenotypes and independent imprinted DMD methylation values are shown. β is the linear regression coefficient.

Placental Phenotype	DMD	β	P-Value
Placental Weight (mg)	*Dlk1*.A	+116	5.52E-02
Fetal Weight (mg)	*Igf2r*	+2041	3.82E-02
	Mest	+1668	7.07E-02

Table 7. Bivariate regression analysis of 23 E17.5 DNMT1o-deficient placentas based on DMD methylation and placental phenotypes. Only significant (P<0.075) associations established by bivariate regression analysis between dependent placental phenotypes and independent imprinted DMD methylation values are shown. β is the linear regression coefficient.

Linear regression analysis revealed an association between loss of *Mest* DMD methylation and triacylglyceride accumulation in E17.5 DNMT1o-deficient placentas (Figure 29B). *Mest* was the only DMD that associated with lipid accumulation. In contrast to the prior regression analysis the methylation variable used in this regression analysis was normalized as the ratio of mutant:wild-type. In section 3.3.1 I showed that imprinted gene expression within the *Mest* imprinting cluster is altered at E17.5 in a manner indicative of loss of imprinting. Both *Mest* and *Klf14* encode factors with functions in lipid metabolism as a putative lipid hydrolase and as a key metabolic transcription factor respectively. However, these results leave open the possibilities that loss of *Mest* DMD methylation causes placental lipid accumulation in a direct fashion through abnormal *Mest* and *Klf14* imprinted gene expression or via an indirect developmental defect (*e.g.* poor SynT or fetal vessel development).

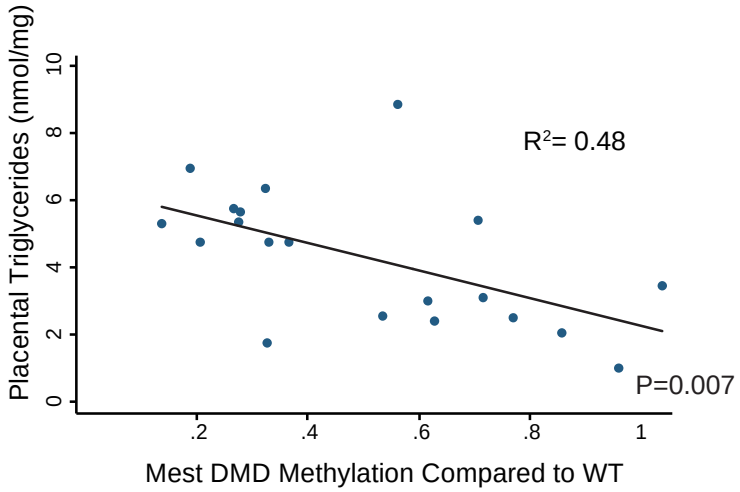

Figure 39. Linear regression plot of *Mest* DMD methylation and placental triglycerides at E17.5. Loss of methylation at *Mest* is associated with elevated placental triacylglycerol concentrations.

3.5 DISCUSSION

3.5.1 A broad spectrum of loss of imprinting is revealed in DNMT1o-deficient placentas

In the results of Chapter 3 I expected and found a large range of loss of imprinting between DNMT1o-placentas and individual DMDs underscoring the mosaicism of this model. Analysis of imprinted gene expression from 7 different imprinted loci revealed many of the expected patterns of loss of imprinting that yielded increased (biallelelic) or reduced (diminished monoallelic) expression at E12.5 (Figure 28). However, at E15.5 and to a greater extent at E17.5, imprinted gene expression was not as expected with certain genes behaving in unexpected and opposite ways (Figure 28). I reconcile these results to indicate that the primary effects of loss of DMD methylation in the *Dnmt1*$^{\Delta 1o}$ maternal effect model are manifested directly on gene

expression early in development, but become increasingly influenced by secondary factors such as trophoblast layer distribution and undefined compensatory mechanisms. In addition, novel associations were revealed between the expression of the *Mest* and *Ascl2* genes with E/P ratio (Figure 29). DMD methylation was also highly variable but not static between gestation ages. My initial BGS results show variable methylation levels at all DMDs analyzed in at least some DNMT1o-deficient placentas at E12.5 but not for every DMD at E17.5, suggestive of an changing population of surviving DNMT1o-deficient placentas in late gestation in terms of both imprinted gene expression and DMD methylation (Figure 30 and 31). These results are further corroborated by EpiTYPER analysis of 14 DMDs in larger cohorts of DNMT1o-deficient mid- and late- placentas.

Quantitative EpiTYPER DNA methylation analysis was used to ascribe placental functions for DMDs in two ways: by identifying nearly normal DMD methylation in DNMT1o-deficient placentas; and by correlating highly variable DMD methylation with placental phenotypes. We expected total wild-type placental DMD methylation to be approximately 50%, but found the wild-type average to be just under 40% at each time point. These results are consistent with the slightly lower levels of DMD methylation found in control placentas than embryos in prior studies (*408*). E12.5 Wild-type placentas showed a large range of methylation across individual DMDs with *Peg3* (32.7%) on the low end and *Dlk1*.A (57.7%) on the high. Based on the current understanding of DNMT1o action it is predicted that on average a 50% loss of methylation at each DMD should be observed in cohorts of DNMT1o-deficient placentas (*60, 104, 402*). However, using the hyper-geometric distribution, I found that the *Dlk1*, *Nespas* and *Snrpn* DMDs were hypovariable and near normal in their methylation levels in E12.5 DNMT1o-deficient placentas (Figures 32G-K). These findings suggest that many epigenotypes with these

DMDs poorly methylated may be incompatible with early trophoblast survival and/or proliferation resulting in selection against specific epigenotypes at the cellular and organismal level.

Interrogation of the association of DMD methylation and placental phenotypes by regression analysis confirmed the importance of DMD methylation in placental development and function. Significant associations were observed between diminished imprinted methylation of the DMDs *Peg10*, *Kcnq1*, *H19* and *Nespas*, and specific placental phenotypes in DNMT1o-deficient E12.5 placentas (Tables 3, 4 and 7; Figure 36). Additional associations were found between the *Impact*.B, *Mest*, *Dlk1*, and *Igf2r* DMDs and placental phenotypes at E15.5 and E17.5 (Tables 6 and 7; Figure 39). Importantly, this approach using the *Dnmt1*$^{\Delta 1o}$ maternal effect model to gain insight into the role of imprinted genes in placental development and function is fundamentally different in two significant ways from genetic approaches that either inactivate single imprinted genes or remove ICRs. First, the *Dnmt1*$^{\Delta 1o}$ maternal effect model produces epigenetic mutant offspring with loss of DMD methylation, while retaining the genetic sequence of ICRs and imprinted genes. Second, the *Dnmt1*$^{\Delta 1o}$ maternal effect model produces broadly variable methylation effects across many DMDs. This permits DMD methylation to be treated as a continuous variable in a quantitative trait analysis, thus revealing strong associations between loss of methylation at particular DMDs and histo-morphological placental phenotypes. The recognition of these associations offers new insights into the integral role of genomic imprints on placenta development.

3.5.2 Association between *Ascl2* and *Mest* gene expression with E/P ratio

Overall my findings of wide-ranging E/P ratios in DNMT1o-deficient conceptuses supports the idea that a subset of imprinted genes is vitally important in placental function. Expression of *Ascl2* and *Mest* accounts for a significant proportion of the observed variation in E/P ratio observed in DNMT1o-deficient offspring. There was a direct correlation between *Mest* expression and E/P ratio, and an inverse correlation between *Ascl2*expression and E/P ratio. Furthermore, *Mest* expression is predicted to increase with loss of methylation at the *Mest* DMD. In mouse placentas, *Mest* expression is limited to the fetal derived extraembryonic mesoderm and is most prominent in mid to late gestation placentas in the capillary endothelial cells of the LZ. Investigations suggest that *Mest* is involved in angiogenic sprouting in the LZ (*275*). An insertional disruption of the *Mest* gene when paternally inherited is associated with fetal and placental growth restriction at E18.5 of 86.4% and 87.5% respectively compared to wild-type (*274*). However, *Mest* null mutant placentas contained congruent LZ and JZ layers indicative a general growth defect rather than a disruption of a single layer. Loss of *Mest* DMD methylation, and concomitant upregulation of *Mest*, may thus be expected to increase the size of both embryo and placenta, and perhaps increase the placenta efficiency resulting an out-sized effect on fetal growth. It is also possible that *Mest* expression is a proxy for loss of imprinting of other genes within the *Mest* cluster (e.g. *Cpa4*, *Copg2* or *Klf14*) that are actually the main effectors. Although expression of *Klf14* is reduced in E17.5 placentas, no association was made between its expression and E/P ratio.

The inverse association between *Ascl2* expression and E/P ratio is more difficult to rationalize due to the unexpected increase in average methylation levels. Taken at face value the expected decrease in *Ascl2* expression associated with loss of *Kcnq1* DMD methylation should

be most similar to either the *Ascl2* null or hypomorphic alleles depending on how uniform the loss of imprinting is (*222*, *311*). Maternally inherited deletion of *Ascl2* is embryonic lethal at E10.5 due to excessive TGC accumulation and a lack of LZ and JZ layer development (*222*). *Ascl2* hypomorphs on the other hand are viable but growth restricted with a lesser degree TGC expansion and diminished LZ (*311*). One explanation for the inverse relationship would be that decreased *Ascl2* expression restricts placental growth disproportionately compared to fetal growth. However, there is also a cluster of four placental samples that have elevated *Ascl2* expression and lower E/P ratio, suggesting elevated *Ascl2* expression may be indicative or causative of inefficient placentas. It is also plausible that *Ascl2* expression is a proxy for other maternally expressed genes in the *Kcnq1* cluster (e.g. *Cdkn1c* and *Phlda2*). Although expression of *Phlda2* was also unexpectedly upregulated, its expression did not associate with E/P ratio. Intriguingly, transgenic over-expression of either *Phlda2* or *Cdkn1c* results in placental growth restriction (*314-316*). Lastly, it is important to note that the unexpected increase in the maternally expressed members of the *Kcnq1* cluster at E17.5 may be due to compensatory changes in placental layer contribution, selection for particular epigenotypes or gene expression patterns.

3.5.3 *Peg10* viability and labyrinth phenotypes

A strong association was observed between loss of *Peg10* DMD methylation and decreased fetal viability and LZ volume at E12.5 (Tables 3 and 4; Figure 36). Most placentas with loss of *Peg10* DMD methylation and decreased LZ volume were unable to support fetal development. I interpret these associations, and the gradual trend toward normal *Peg10* DMD methylation levels from E12.5 to E17.5 (Figure 32K), as a progressive requirement for *Peg10* methylation to sustain fetal viability during later gestation. The decreasing *Peg10* DMD methylation variability and

lack of phenotypic association at E15.5 and E17.5 could be explained by selection against certain low *Peg10* DMD methylation epigenotypes. The DMD methylation epigenotype of placentas with low *Peg10* methylation at E12.5 is different than the epigenotype of placentas with low *Peg10* DMD methylation recovered at E15.5 and E17.5 (Figures 33, 34 and 35). The combination of low *Peg10* DMD methylation (<50% wild-type level) plus low *Dlk1*, *Kcnq1*, *Nespas* or *Snrpn* DMD methylation (<50% wild-type) was observed at E12.5 (samples A5, A7, B1 and C3; Fig 33) but does not occur in any DNMT1o-deficient placentas at either E15.5 or E17.5 (Figures 34 and 35). In summary, my analysis of DNMT1o-deficient placentas reveals a novel link between placentas with low *Peg10* DMD methylation, poor LZ development and the inability to sustain fetal development.

A strong linkage between *Mest* and *Peg10* DMD methylation was found at E12.5 and E17.5 (Figures 34 and 35). This was expected given the proximity of the two DMDs on mouse chromosome 6, however *Mest* did not show significant associations with early placental phenotypes in this study. This observation does not preclude a role for *Mest* later in gestation, and in fact several associations were made between *Mest* DMD methylation and placental phenotypes at E15.5 and E17.5. An inverse association between *Mest* DMD methylation and spongiotrophoblast volume at E15.5, and a positive association between *Mest* and fetal weight at E17.5 were uncovered (Tables 6 and 7). Furthermore, regression analysis revealed a link between loss of *Mest* DMD methylation and placental lipid accumulation at E17.5 (Figure 39). I suggest that *Mest* and *Peg10* DMDs may exert their influence on placental development in a serial manner; loss of *Peg10* DMD methylation impairs LZ development early in gestation, which predisposes these placentas to metabolic abnormalities associated with lost *Mest* DMD methylation later in gestation.

The lethality and labyrinth failure in DNMT1o-deficient placentas with low *Peg10* DMD methylation is similar to the phenotype observed in chromosome 6 translocations and *Peg10* null mice (*10, 261, 262, 293*). Although the expected result of loss of *Peg10* DMD methylation is increased *Peg10* expression, I failed to detect significant changes in *Peg10* expression in DNMT1o-deficient placentas at any time point between E9.5 and E17.5 (Figure 28). However, I did observe a significant increase in *Sgce* and *Pon2* expression in late gestation DNMT1o-deficient placentas (Figure 28). It is difficult to correlate DMD methylation with imprinted gene expression in *Dnmt1*$^{\Delta 1o}$ maternal effect placentas because of the confounding factors of a mosaic model, cell-type expression biases and differential effects of loss of DMD methylation. Based on my direct observation that partial loss of a maternally methylated *Peg10* imprint is detrimental to placental development, I suggest that strict monoallelic dosage of *Peg10*, and/or other imprinted genes within the *Peg10* imprinted cluster is critical for placental development.

3.5.4 Loss of *Kcnq1* DMD methylation and TGC expansion

Mouse chromosome arm 7q contains three maternally methylated DMDs from proximal to distal: *Kcnq1*, *Snrpn* and *Peg3*. Not surprisingly, we found that the methylation status of the *Kcnq1* and *Snrpn* DMDs was linked at E12.5 in DNMT1o-deficient placentas (Figure 33). However, Peg3 is situated closer to *Snrpn* than *Kcnq1* but does not show linkage to the other two at any time point and is hypomethylated in DNMT1o-deficient placentas (Figure 32H and Figures 33-35). I found A strong association between DNA methylation at both the *Kcnq1* and *Snrpn* DMDs and accumulation of TGCs (Tables 4; Figure 36). Based on our forward step-wise regression model the combination of DMD methylation levels of *Kcnq1* and *Snrpn* is the best predictor of TGC abundance (Table 5). I speculate that the association between *Snrpn* methylation and TGC

accumulation is a passive effect due to close linkage with the *Kcnq1* cluster and consistent with lack of known placental function for *Snrpn* (*422*), although the possibility of the involvement of the *Snrpn* in TGC development cannot be ruled out completely. The *in situ* staining of TGCs for *Prl3d1* in DNMT1o-deficient placentas, an early TGC marker, indicates that not only is proliferation altered but also TGC differentiation (Figure 38). The morphology of DNMT1o-deficient placentas with low *Kcnq1* DMD methylation is similar to those described in null and hypomorphic *Ascl2* mouse models in which expansion of TGCs was observed (*222, 311*). These findings are substantiated by the diminished expression of *Ascl2* in DNMT1o-deficient E9.5 and E12.5 placentas (Figure 28).

The accumulation of TGCs observed in the $Dnmt1^{\Delta 1o}$ maternal effect model shown herein is remarkably similar to placentas derived from *Dnmt3L* null mothers, which lack all maternal imprinted DMD methylation (*97, 99*). One mechanistic explanation of the TGC expansion that is common between the $Dnmt1^{\Delta 1o}$, *Dnmt3L* and *Ascl2* models is that a decrease in *Ascl2* expression (by gene deletion or loss of *Kcnq1* DMD methylation) results in derepression of *Hand1*, a transcription factor that promotes differentiation of the EPC, and terminal differentiation of SpT into TGCs (*188, 231, 234*). Loss of *Kcnq1* DMD methylation in DNMT1o-deficient placentas has a distinct phenotype from paternal deletion of the *Kcnq1* ICR, which mimics a maternal (methylated) state with resulting increased maternal expression of *Ascl2*, *Phlda2*, and *Cdkn1c*, and growth restriction (*310*). Regression analysis did not reveal meaningful associations between loss of *Kcnq1* DMD methylation and placental overgrowth at E15.5 or E17.5 that might be expected based on targeted deletion mouse models of *Phlda2* and *Cdkn1c*, which exhibit pronounced placental overgrowth (*312, 313*). These findings taken together with prior research suggest that the imprinted gene *Ascl2* is a focal point for early placental development.

3.5.5 Loss of *Nespas* and *H19* DMD and junctional zone development

In addition to the effects of reduced *Peg10* and *Kcnq1* DMD methylation discussed above, regression analysis revealed weaker, but nonetheless significant, associations between loss of imprinted *Nespas* and *H19* DMD methylation and increased JZ volume (Table 4, and Figures 36B-D). Although both *Nespas* DMD amplicons assayed associated significantly with JZ expansion at E12.5 (Table 4 and Figures 36B and C), an association was not observed at E15.5 (Table 6), indicating this phenotype may resolve to a more normal one during development.

The observed association between loss of *H19* DMD methylation and JZ expansion bordered the significant cutoff (P=0.048, Table 4 and Figure 36D). *H19* DMD methylation gradually increased from E12.5 to E17.5 in DNMT1o-deficient placentas, indicating selection against loss of imprinting at this cluster (Figure 32D). Loss of methylation at the *H19* DMD is expected to depress transcription of the growth factor *Igf2*. Expression of of *Igf2* in DNMT1o-deficient placentas was reduced at E9.5 and E12.5 but was near normal levels at E15.5 and E17.5 (Figure 28). It is known that *Igf2* is paternally expressed throughout the placenta, and that the placenta specific isoform (*Igf2P0*) is expressed exclusively in SynT (*302, 303*). Paternal inheritance of either the *Igf2* null or *Igf2P0* null allele results in placenta with reduced JZ volume (*303*) . Based on this knowledge one explanation for the observed trend is that spongiotrophoblast is less dependent on IGF2 signaling than labyrinthine cell types, and may increase as an early compensatory mechanism to low placental *Igf2* expression. The association between *H19* DMD methylation and JZ volume is not found at E15.5 reflecting the resolving of both *H19* methylation levels and JZ volume toward normal levels.

3.5.6 No placental phenotypes associated with *Dlk1*, *Igf2r* or *Grb10* DMD methylation

At the onset of performing regression analysis I expected to find associations between imprinted DNA methylation at the *Dlk1* DMD and LZ development, and between both the *Grb10* and *Igf2r* DMDs and placental growth based on evidence from genetic models (*347, 374, 393*). In DNMT1o-deficient placentas imprinted DNA methylation at the *Dlk1* DMD did not significantly differ from wild-type although it did increase across gestation (Figures 32O and 32P). This pattern is perhaps indicative of early selection against cellular epigenotypes with loss of *Dlk1* DMD methylation during trophoblast differentiation and proliferation. No associations were found between *Dlk1* DMD methylation and placental phenotypes at E12.5 nor at E15.5, but a positive association between *Dlk1*.A methylation and placental weight at E17.5 was revealed (Table 7), indicating loss of *Dlk1* methylation restricts placental growth. Although there was substantial variation in DMD methylation at the *Igf2r* and *Grb10* DMDs (Figures 36B and 36E), associations between placental weight and DMD methylation were not significant for either loci at E12.5 and at E15. However, I discovered a positive relationship between *Igf2r* DMD methylation and fetal weight at E17.5 (Table 7), a counter intuitive finding given that loss of *Igf2r* methylation should repress expression of this growth suppressor. Regression analysis failed to identify DMDs responsible for the overgrowth of late gestation placentas and embryos but rather identified ones that promoted growth restriction. I interpret these results as evidence that in the context of the *Dnmt1*$^{\Delta 1o}$ mosaic loss of imprinting model, the mid to late gestation growth effects of the *Grb10* and *Igf2r* DMDs may be obscured by epigenetic epistatic interactions with loss of imprinting at other prominent DMDs within both placental and embryonic compartments. The clinically relevant dysregulation of placental and fetal growth associated with loss of imprinting previously highlighted in Chapter 2 is likely due to these complex interactions

between imprinted regions. In contrast, the stronger associations between both *Peg10* and *Kcnq1* and E12.5 placental phenotypes were not occluded by confounding epistatic effects.

3.5.7 *Zrsr1* is an imprinted DMD in placenta but *Nnat* and *Nap1l5* are not

We measured the DNA methylation levels of three additional imprinted DMDs (*Zrsr1*, *Nnat* and *Nap1l5*) in wild-type and DNMT1o-deficient E12.5 and E15.5 placentas (Figures 36Q-S). The mouse genomic coordinates for these three DMDs were previously established (*26*), but were not examined in placenta. EpiTYPER analysis showed that the *Commd1* DMD was methylated at a level consistent with imprinting in wild-type placenta, which was then lost in DNMT1o-deficient placentas (Figure 36Q). Both the *Nnat* and *Nap1l5* DMDs showed a methylation pattern that was not indicative of imprinted DMDs (Figure 36R and 36S). Both DMDs also had higher methylation levels in wild-type placentas than other imprinted DMDs tested (DMD methylation fraction >0.7), and furthermore, neither DMD lost methylation in DNMT1o-deficient placentas. We conclude that *Nnat* and *Nap1l5* are not imprinted DMDs that are perpetuated from gametes to mature trophoblast lineages, and that although the *Zrsr1* DMD is imprinted in the placenta, loss of imprinting at this locus is tolerated. Recent genome methylation studies have provided evidence that the *Nap1l5* but not the *Nnat* DMD retains its imprinted status in the human placenta (*423, 424*).

3.5.8 Conclusion

In summary, I have validated the placental epigenetic variability inherent in the *Dnmt1*$^{\Delta 1o}$ maternal effect model using a broad survey of imprinted gene expression and DMD methylation.

I revealed that the expression of both *Mest* and *Ascl2* are associated with E/P ratio at E17.5. I also discovered a novel association between loss of imprinting at the *Peg10* loci with fetal viability and placental labyrinth maldevelopment. In addition, I found a strong association between loss of imprinting at the *Kcnq1* cluster and TGC accumulation, validating prior genetic models. I conclude from the lack of *Dlk1* DMD methylation variability at E12.5 that *Dlk1* has an essential early trophoblast function. This chapter highlights the direct epigenetic effects of loss of imprinting on placenta development. My findings provide additional rationale to further dissect the *Peg10* and *Kcnq1* imprinting clusters for their roles in placental development.

4.0 *KLF14* IS AN IMPRINTED GENE REGULATING PLACENTAL GROWTH

4.1 SUMMARY

In the previous chapter I revealed two strong associations between loss of imprinting at the *Mest* locus and placental phenotypes. First, *Mest* gene expression was directly associated with the placental efficiency metric E/P ratio. Second, *Mest* DMD methylation was inversely associated with placental triacylglyceride levels. In this chapter I sought to interrogate the role of *Klf14*, a maternally expressed gene within the *Mest* imprinted locus, to determine if loss of its expression recapitulated any of the phenotypes observed in DNMT1o-deficient placentas. To these ends I generated a novel targeted deletion of *Klf14* in mouse. Using this new model, I confirmed that *Klf14* is an imprinted gene expressed from the maternal allele in the placenta. Although the *Klf14* gene appears to be non-essential based on the near Mendelian inheritance observed in heterozygous intercrosses, there were some placental differences. Homozygous late gestation placentas were larger than either heterozygous or wild-type littermates, suggesting a role for *Klf14* in limiting placental growth. No differences in placental layer fractions were observed between genotypes indicating that the placental overgrowth was symmetrical and not localized to one trophoblast cell type. In addition, placental triacylglyceride levels were unchanged in heterozygous intercrosses, however increased levels were observed in maternal null offspring

from homozygous null mothers fed a high fat diet. These results leave open the possibility that *Klf14* may regulate placental growth and mediate metabolic responses to dietary inputs.

4.2 INTRODUCTION

4.2.1 *Klf14* is part of the *Mest* imprinting cluster

Klf14 is a paternally imprinted (maternally expressed) gene within the *Mest* imprinted loci at mouse 6qB3 (See section 1.5.3; Figure 2C). Bimaternal inheritance of Robertsonian 6q translocations is embryonic lethal [10]. The proximal 6q *Peg10* imprinting cluster is most likely responsible for the lethal phenotype, whereas a more subtle intrauterine growth retardation phenotype is observed in embryos with bimaternal inheritance of the subproximal 6q region encompassing *Mest* (*262*). Epigenetic analysis of this region revealed that the *Mest* DMD is located in the promoter and exon 1 of the *Mest* gene and is maternally methylated (*265*). Multiple imprinted genes are regulated by the *Mest* DMD within a 400MB region including the paternally expressed *Mest* and the maternally expressed *Copg2*, *Cpa4*, and *Klf14* (*265*-*270*).

The *Klf14* gene was first identified as a maternally expressed transcript in mouse using RT-PCR restriction length polymorphism analysis of offspring of JF1 and BL6 inter-strain crosses (*270*). Maternal-specific expression of *Klf14* is dependent on *Mest* DMD methylation and is lost in *Dnmt3a*$^{null/+}$ maternal effect offspring (*270*). Additionally, I have shown that DNMT1o-deficient placentas show a strong reduction in *Klf14* expression throughout mid-gestation (Figure 28). Maternal-specific *Klf14* expression has also been confirmed in humans by sequence

comparison of maternal and fetal *Klf14* cDNAs using informative SNPs (*270*). Furthermore, human monochromosomal somatic cell hybrids with exclusively maternal or paternal chromosome 7 show either elevated or absent *Klf14* expression respectively (*270*). These results in mouse and man demonstrate a conserved *Klf14* imprinting mechanism and maternal-specific expression.

4.2.2 The *Mest* imprinting cluster is implicated in placenta development

In the previous chapter I uncovered four novel associations between loss of imprinting at the *Mest* locus and mid to late gestation placental phenotypes. At E15.5 *Mest* DMD methylation inversely associated with JZ central volume (Table 6). At E17.5 the placental efficiency metric E/P ratio is directly associated with *Mest* expression (Figure 29B). In addition, I found that methylation at the *Mest* DMD is positively associated with fetal weight (Table 7) and inversely associated with placental triacylglyceride levels (Figure 39). These results, using the *Dnmt1*$^{\Delta 1o}$ maternal effect model, suggest a role of the *Mest* imprinting cluster in regulating placental growth and metabolism.

The *Mest* gene itself is well studied, although the exact function of its encoded putative α/β hydrolase protein is unclear (*119, 266, 268, 271-276*). The *Mest* gene is expressed in the vascular endothelium of the mouse placenta where it is thought to influence branching morphogenesis (*275*). When paternally inherited insertional mutagenesis of the *Mest* gene completely eliminates its expression, and results in placental growth restriction (*274*). These prior studies, corroborated by my findings in Chapter 3, suggest that *Mest* expression modulates placental and fetal growth. However, they do not fully explain the phenotypic findings of fetal growth restriction and labyrinth lipid accumulation in DNMT1o-deficient offspring.

4.2.3 KLF14 is a transcription factor regulating metabolism

There are 17 mammalian genes encoding Krüppel-like factors (KLFs) including *Klf14* (*425, 426*). KLF proteins share a conserved C-terminal DNA-binding domain composed of a triad of C2H2 type zinc fingers. Each zinc finger is a 23-25 amino acid ββα peptide fold that coordinates a Zn^{2+} cation in a tetrahedral arrangement. The conserved KLF DNA-binding domains recognize similar CACCC or CGCCC sequence motifs and therefore may compete for DNA-binding sites (*425*). KLFs are classified into clades based on their N-terminal peptide sequences. The N-termini of KLFs are known sites of interactions with DNA-binding cofactors. Many KLFs harbor CTBP binding sites whereas others have SIN3A binding motifs. KLF14 falls into the latter group with a putative, although biochemically unconfirmed SIN3A interacting motif (an α-helical AA/VXXL peptide). SIN3a is a histone deacetylase repressive cofactor that acts as a multi-domain scaffold for HDAC1/2, NCOR, SMRT, IKAROS MAD, UMA6 and other chromatin modulators. KLF14 is most closely related to KLF16 based on peptide sequence homology. Moreover, because *Klf14* is an intronless gene, it has been suggested that it arose through retrotransposition during early protoeutherian evolution, whereby it acquired imprinting due to proximity of the *Mest* DMD (*270*). Intriguingly, *Klf14* has undergone recent human specific evolution with genetic changes predominantly in the N-terminal coding region (*270*).

The *Cabut* KLF-like family member in *Drosophila* is a TGFβ responsive developmental regulator and evolutionary precursor to mammalian KLFs 9, 10, 11, 13, 14 and 16 (*427, 428*). These proteins contain a similar tripartite transcriptional regulatory domain (TRD) (*428*). The N-terminal TRD1 contains SIN3A and HDAC interacting motifs whereas the more centrally located C-terminal contains proline rich domains that interact with WW and WD40 domain

containing proteins including numerous GTPases (*428*). The zinc finger domain, or TRD2, interacts with both DNA and histone acetyltransferases (*428*). The mammalian Cabut-related genes are divided into TGFβ inducible early growth response genes (*Klf10* and *Klf11*) and basic transcription factors (*Klf9, 13,14* and *16*) (*428*). The conservation of metabolic regulation is exemplified by *Klf11* which is mutated in maturity onset diabetes of the young (MODY7; OMIM 610508) and neonatal diabetes (*428*).

Although *Klf14* is not thought to be a TGFβ inducible early growth response gene it is involved in TGFβ signaling (*429*). In a human pancreatic epithelial cancer cell line (Panc-1) *KLF14* and *TGFβRII* are upregulated by exposure to TGFβ ligand (*429*). However, rapid upregulation of *TGFβRII* is tempered by the delayed transcription of *Klf14* in an inhibitory feedback circuit. Within TGFβ stimulated Panc-1 cells expression of a luciferase reporter driven by the *TGFβRII* promoter is repressed by KLF14 bound at CG rich sequences (*429*). Furthermore, TGFβ stimulation increases the presence of the repressive histone modification H3K20me3 and decreases the amount of the active histone marks H3K9ac and H4ac at the endogenous *TGFβRII* promoter (*429*). It was also revealed *in vitro* that FLAG-tagged KLF14 in Panc-1 cells pulls down SIN3A and HDAC2 (*429*). In addition, co-stimulation of Leydig cells with TGFβ and progesterone increases *Klf14* expression and leads to increased KLF14 based activation of the endoglin gene promoter (*430*). The endoglin protein is a co-receptor for ALK1 a component of larger TGFβ receptor complexes (*430*). These two studies show that KLF14 is a non-canonical (*i.e.* non-SMAD) protein effector of TGFβ that has both positive and negative feedback on TGFβ signaling. They also provide direct evidence that KLF14 can function as either an activator or repressor of transcription.

The mammalian family of KLFs have diverse physiological functions in cardiovascular, respiratory, digestive, hematological, and immune organ systems as well as in stem cells and tumor biology (*425*). It has recently been suggested that KLF14 is a master transcriptional regulator of adipose metabolism based on genome wide association studies (GWAS). Two separate microarray based studies utilizing human SNPs revealed strong parent-of-origin effects for allelic variants at rs4731702 and rs972283, roughly 14kb upstream of the *KLF14* promoter, that are associated with increased risk of type 2 diabetes when maternally inherited (*279, 281*). In the case of rs4731702, correlations were also made to elevated HDL levels (*280*). Furthermore, it has been shown that both of these risk alleles are associated with decreased adipose expression of *Klf14* in *cis*, when maternally, but not paternally inherited; thereby confirming that these alleles are parent-specific expressed quantitative trait loci (eQTLs) (*279, 281*).

To determine the mechanism by which the *KLF14* eQTL modulates metabolic activity researchers looked for *trans* changes in gene expressions associated with rs 4731702 (*282*, *283*). This approach was justified based on the assumption that *KLF14* encodes a transcription factor that modulates expression of a network of genes. This approach identified 10 genome wide significant trans (GWST) parent-of-origin specific associations between rs4731702 and the following genes in adipose tissue: *TPMT, ARSD, PRMT2, SLC7A10, C8ORF82, APH1B, NINJ2, KLF13, GNB1* and *MYL5*. Nearly all these genes were up-regulated (with SLC7A10 the lone exception) in conjunction with the rs4731702 risk allele suggesting that *KLF14* is in fact a repressor at this set of genomic loci. Furthermore, amongst these 10 genes, the majority were independently associated with other metabolic syndrome traits in GWAS studies. The promoters associated with a set of 50 GWST associations with a relaxed significance threshold, were enriched with CACCC KLF binding motifs. These results taken together suggest that *Klf14*

expression is imprinted and that it regulates a network of genes that modulate insulin response in adipose tissue. With this in mind it is important to understand whether *Klf14* has a similar role in regulating metabolism in mouse placental physiology given its high expression within the tissue, and to ascertain what targets it may regulate there.

4.2.4 Recombineering is a genetic engineering technique

I employed recombineering technology to construct a targeting vector and generate $Klf14^{flox}$ and $Klf14^{null}$ alleles. Recombineering utilizes bacterial strains that induce gap-repair recombination enzymes under certain conditions (*i.e*. temperature) that catalyze recombination between homologous 200-500bp sequences (homology boxes) enabling efficient exchange of sequences from one vector to another (for reviews see (*431, 432*)). A 13.5kb region encompassing *Klf14* and surrounding sequences was retrieved from a bacterial artificial chromosome (BAC) onto a plasmid adjacent to a diphtheria toxin gene (Dta). I then engineered plasmids to insert LNL and LFNTF cassettes to generate a targeting allele. Standard methods of ES cell transfection, homologous recombination, Flp electroporation, Neomycin/Ganciclovir positive/negative selection and blastocyst injection were used to generate a novel transgenic $Klf14^{flox}$ mouse line. This line was then crossed with *Sox2:CRE* transgenic females to generate a constitutive null allele ($Klf14^{null}$). I then used this novel mouse line to study the imprinted expression profile and functional role of *Klf14* in placental biology. Further details on the generation of this mouse line are provided in the material and methods (Sections 4.3.1-4.3.4).

4.2.5 Aims of chapter 4

I genetically engineered a novel targeted deletion to determine if *Klf14* downregulation was responsible for any of the placental phenotypes associated with loss of imprinting at the *Mest* loci in the *Dnmt1*$^{\Delta 1o}$ maternal effect model. This model was used to address important open questions including whether *Klf14* is an essential gene that when deleted results in a lethal phenotype. I also examined litters of heterozygous *Klf14*^{null} intercrosses at E16.5 for abnormal placental growth, layer development and lipid content. In addition, I attempted to provide absolute genetic proof of the maternal-specific expression of *Klf14* in mouse placentas. These efforts explored the functional role of *Klf14* in placenta biology.

4.3 MATERIALS AND METHODS

4.3.1 Recombineering

Primers were designed to amplify homology boxes (HB1-6) containing unique nonrepetitive DNA sequences with 5′ extensions that added restriction endonuclease sites and GCGC clamps (Appendix E). HB1-6 were amplified from a murine 129Sv BAC containing an 80KB genomic contig including *Klf14* (bMQ6044J02; Source Bioscience Lifesciences). HB1 primers were designed to amplify a region 5.5kb downstream of the *Klf14* 3′ UTR and added 3′ BglII and 5′ MluI restriction sites. HB2 primers amplified a region 4.4kb upstream of the *Klf14* TSS and added 5′ HindIII and 3′ MluI restriction sites. Both HB1 and HB2 were cloned into the HindIII and BglII restriction sites in place of the PGKneo and adjacent to the PGKdta cassettes in

plasmid vector PGKneolox2DTA.2 (addgene plasmid #13449). The resulting PGKHB2HB1DTA.2 was linearized with MluI and used as a *Klf14* retrieval plasmid. Prior to retrieval, *E.coli* strain SW106 was transfected with bMQ6044J02, selected for by chloramphenicol, and verified by PCR. On the day of retrieval, the bMQ6044J02 transfected SW106 was heat induced at 42°C and then directly co-transfected with the linearized *Klf14* retrieval plasmid. Positive recombinants were selected for by ampicillin resistance, then cloned and verified to contain PGKDta2 with a 13kb retrieved *Klf14* region by restriction digest and DNA sequencing.

Primers to generate HB3 and HB4 amplified adjacent 400bp regions centered less than 300bp downstream from the *Klf14* 3′UTR and incorporated 5′BamHI and 3′ internal KpnI and external BssHII restriction sites for HB3, and 5′SalI and 3′HindIII restriction sites for HB4. Restriction digested HB3 and HB4 amplicons, derived from PCRs using BMQ6044J02 as a substrate, were cloned together with a BssHII and XhoI digested loxp-frt-neomycin-TK-frt-loxp (LFNTF) cassette and a BamHI and HindIII linearized pBluscript backbone in a quadruple ligation reaction.

Primers to generate HB5 and HB6 amplified adjacent 400bp regions roughly 3kb from the TSS and incorporated 5′BglII and 3′KpnI restriction sites for HB3, and 5′SalI and 3′HindIII restriction sites for HB6. In addition, an endogenous BglII restriction site was removed from the 3′ end of HB3. Restriction digested HB3 and HB4 amplicons derived from PCRs using BMQ6044J02 as a substrate were cloned together with a loxp-neomycin-loxp (LNL) cassette (isolated by restriction digest of by KpnI and XhoI) and a BamHI and HindIII linearized pBluscript backbone in a quadruple ligation reaction.

HB5-LNL-HB6 was excised from pBS with NotI and XhoI, transfected into heat induced SW106 cultures pre-transfected with the *Klf14* positive retrieval plasmid and then plated onto Kanamycin/Ampicillin agar plates. Colony PCR was used to select clones with LNL inserted into the correct region upstream of *Klf14* within the retrieval plasmid, and then subcloned to ensure a single *Klf14* positive retrieval plasmid with a LNL cassette. The neomycin cassette of the LNL was then removed by transfection into SW106 arabinose inducible strain followed by ampicillin selection, and confirmation by HB5/6 PCR and lack of Kanamycin resistant colonies. Electrocompetent heat induced PGK-*Klf14*-5′loxp-Dta.2 transformed SW106 were transfected with linearized HB3LFNTFHB4 and plated onto dual Kanamycin/Ampicillin agar plates and subcloned to individual single vector colonies harboring the primary *Klf14* targeting plasmid. The *Klf14* targeting construct was confirmed by restriction digest analysis and full sequence coverage of the plasmid. To confirm the LFNTF cassette and *Klf14* gene could be deleted, the targeting construct was transfected into SW106 with arabinose induced FLP and SW105 with arabinose induced CRE respectively. Recombineering plasmid maps are shown in Figure 40 for clarity.

4.3.2 Transfection and selection of ESCs

30μg of the *Klf14* targeting construct was linearized by NotI and electroporated into murine J1 ESCs using standard protocols (30μg of pDNA) and plated at various dilutions on irradiated murine fibroblasts. After 48 hours, positive selection with G418 was initiated to eliminate non recombinant ESCs. Within 7-10 days individual colonies were picked and plated onto 96-well plates which were then passaged into 24-well plates after 70% confluence was observed. Homologous recombinants were screened by Southern blot using 5′ and 3′ probes external to the

targeting construct in conjunction with BglII and KpnI digests (Section 4.3.4). The LFNTF cassette was deleted (leaving behind a *loxp* site and ~100bp of additional sequence) by transient transfection of a Flp recombinase plasmid. Colonies surviving ganciclovir negative selection were determined to have deletion of the Neo-TK selectable marker, which was confirmed by PCR and ScaI based Southern digest.

4.3.3 Mouse colony establishment and CRE induced deletion

All mice were humanely cared for in adherence to IACUC guidelines at the University of Pittsburgh. Mouse 129Sv ESCs heterozygous for the *Klf14*^{flox} allele were injected into wild-type B6 blastocysts. Male chimeric offspring were bred with B6 females to test whether recombinant ESCs had been incorporated in the germline which manifests as yielding *agouti* offspring in those crosses. *Agouti* offspring were then genotyped for the presence of the *Klf14*^{flox} allele. Male heterozygous *Klf14*^{flox} offspring were mated to *Sox2:CRE* transgene positive females and the resultant offspring were screened for the combined presence of *Sox2:CRE* (via PCR), and null alleles (via ScaI Southern and PCR). The *Klf14*^{flox} and *Klf14*^{null} alleles, once established in mice, were backcrossed as heterozgotes for greater than five generations to both 129Sv and C57BL/6 (Taconic) strains prior to use in experiments.

4.3.4 *Klf14* genotyping

Southern blot genotyping was carried out using standard protocols utilizing agarose gel electrophoresis, capillary based transfer in alkaline buffer to charged nylon membranes, and hybridization with P^{32} radiolableled DNA probes. Primers that amplified probe templates from

bMQ6044J02 are shown in Appendix E. Probes were generated using random hexamer primed Klenow fragment polymerase based PCR with a nucleotide mixture with radiolableled cytosine (Perkin Elmer). Southern blots were exposed to X-ray film from 2hrs to 2 weeks depending on signal strength. Homologous recombinant ESCs were identified by Southern blotting using 10μg of genomic DNA digested with BglII, run on a 0.7%gel and probed with an external 5′ probe (*Klf14*^{wt} band of 4kb and *Klf14*^{targ} of 9.4kb). Incorporation of the 3′ targeting region was confirmed with a KpnI digest and 3′ external probe (*Klf14*^{wt} band of 16.1kb and *Klf14*^{targ} of 13.3kb). ScaI digestion and 5′ probes showed deletion of the PGKneo-tk marker (*Klf14*^{wt} and *Klf14*^{flox} bands of 11kb and *Klf14*^{targ} band of 12.7kb). Floxed alleles were confirmed by Southern blotting of BglII digests with an external 5′ probe (*Klf14*^{wt} band of 4kb and *Klf14*^{flox} band of 9.2kb). Null alleles were distinguished from wild-type and floxed alleles by Southern blot of ScaI digested genomic DNA with an external 5′ probe (*Klf14*^{wt} and *Klf14*^{flox} bands of 11kb and *Klf14*^{null} band of 6kb).

Klf14 floxed, null and wild-type alleles were also genotyped by semi-nested PCR using primers abutting homology boxes 4, 5 and 6 (Appendix A) using 350ng of genomic DNA and the following thermocycler program: 95°C 5′ denaturing followed by 35 cycles of 95°C 30″, 60°C 30″, 72°C 30″, a 72°C 7′ final extension and an indefinite hold at 4°C. PCR products were run on a 1.5% agarose gel to look for the presence of 200bp (*Klf14*^{wt}), 300bp (*Klf14*^{flox}) and 400bp (*Klf14*^{null}) alleles. *Sox2:CRE* transgenes were also genotyped by PCR using primers provided by the Barak lab (Appendix E)

4.3.5 RT-PCR

Nucleic acids were isolated using All-Prep or RNeasy kits (Qiagen) as previously described from fresh placental tissues, and other embryonic and adult tissues isolated by microdissection. Prior to reverse transcription, RNA was treated with RQ1 DNase for 1h to remove genomic contaminants. Reverse transcription was carried out using MMLV-RT (Promega) from approximately 500ng to 1ug of RNA template oligo dT primers. RT-PCR of *Klf14* was performed using Taq polymerase, approximately 200ng, and primers previously reporter by Parker-Katiraee et al. ((*270*) ; Appendix B)). The housekeeping gene *Gapdh* was used as a positive control. The RT-PCR themocycle was the following: 95°C 5′ denaturing followed by 30 cycles of 95°C 30″, 60°C 30″, 72°C 60″, a 72°C 7′ final extension and an indefinite hold at 4°C. PCR products were run on a 2.0% agarose gel and examined for the presence of an 800bp *Klf14* band.

4.3.6 *Mest* DMD methylation analysis

The methylation status of the *Mest* DMD in wild-type and null placentas was examined by BGS and COBRA assays. Bisulfite genome conversion and PCR of wild-type and $Klf14^{null}$ placental DNA was carried out as previously described using the same reagents and nested primers (Section 3.3.3, Appendix C). The BstBI restriction enzyme was utilized to cut 1ug of bisulfite converted *Mest* PCR amplicon in order to examine for the presence of unconverted (methylated) sites within the *Mest* DMD. Bisulfite genomic sequencing of the same populations of alleles and generation of dot-pot figures was performed as previously described (Section 3.3.3).

4.3.7 Embyronic and placental analysis

Placental analysis focused on the offspring of heterozygous *Klf14*^{null} intercrosses. Dissections were performed at E17.5 in the same manner as previously described (Section 2.3.3). Placenta and embryonic wet weights were recorded. Half of each placenta was preserved for cryo-histology as described earlier (Section 2.3.4). Portions of the remaining half were taken for genotyping, gene expression or lipid content analysis. Placental triacylglyeride content was measured as previously described (Section 2.3.6). Placental layer fractions were determined using the ratio of the average JZ and LZ area determined by random grid sampling of a single central placental section for each sample. Comparisons were made between wild-type, heterozygous and null placentas using students t-test and/or Rank-sum tests.

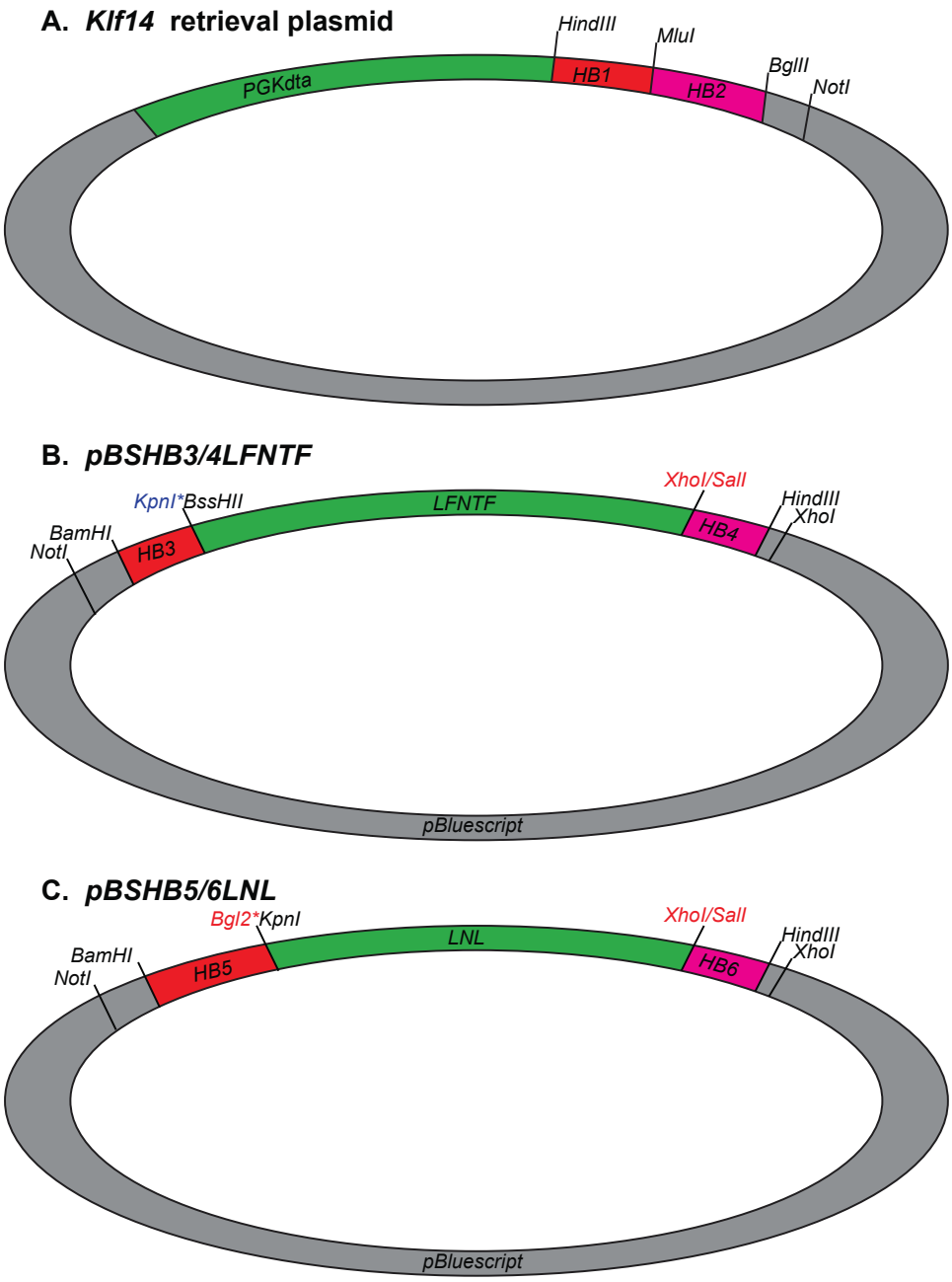

Figure 40. Recombineering plasmids. (A) Plasmid used to retrieve 13.5Kb region around *Klf14* from bMQ6044J02. (B) Plasmid used to place 3′ LFNTF selectable marker on the targeting construct. (C) Plasmid used to place a 5′ LNL selectable marker on the targeting construct.′

4.4 RESULTS

4.4.1 Confirmation of *Klf14* null allele

I engineered a novel targeting construct using recombineering to produce a targeted deletion of *Klf14* in mice (Figure 41A). Chimeric floxed allele mice were initially generated by blastocyst injection of 129Sv strain homologous recombinant ESCs into wild-type B6 blastocysts. Chimeric male offspring were crossed with B6 females and screened for passage of the *agouti* fur color trait indicating germline passage of the recombinant J1 ESCs. Offspring were then screened for the presence of a $Klf14^{flox}$ allele by Southern blot consisting of a BglII restriction digest and an external 5′ probe (Figure 41B). The wild-type BglII band is 4.9kb whereas the floxed allele is 9.2kb (Figure 41B). Full incorporation of the targeting construct was confirmed by Southern blot with KpnI digestion and an external 3′ probe to differentiate the 16.1kb wild-type allele and the13.2 kb floxed allele (Data not shown). Confirmed heterozygous $Klf14^{flox}$ males were mated to Sox2:CRE transgenic females to generate $Klf14^{null}$ heterozygous offspring (Figure 41A). The presence of a $Klf14^{null}$ allele was confirmed by Southern blot with ScaI restriction digest and the same external 5′ probe. The wild-type ScaI band is 11kb whereas the null allele is 6kb (Figure 41C). Semi-nested genomic PCR was used to assess genotyping of offspring as both the floxed and null alleles were backcrossed onto inbred 129Sv and B6 mouse strains. Using this strategy, the wild-type allele amplified a 200bp band from primer pairs *b* and c, whereas the floxed allele generated a 300bp doublet from primer pairs *b* and *c*, and the null allele generated a 400bp

fragment from primers *a* and *c* (Figure 41D). These genotyping results clearly show the generation and stable inheritance of floxed and null *Klf14* alleles.

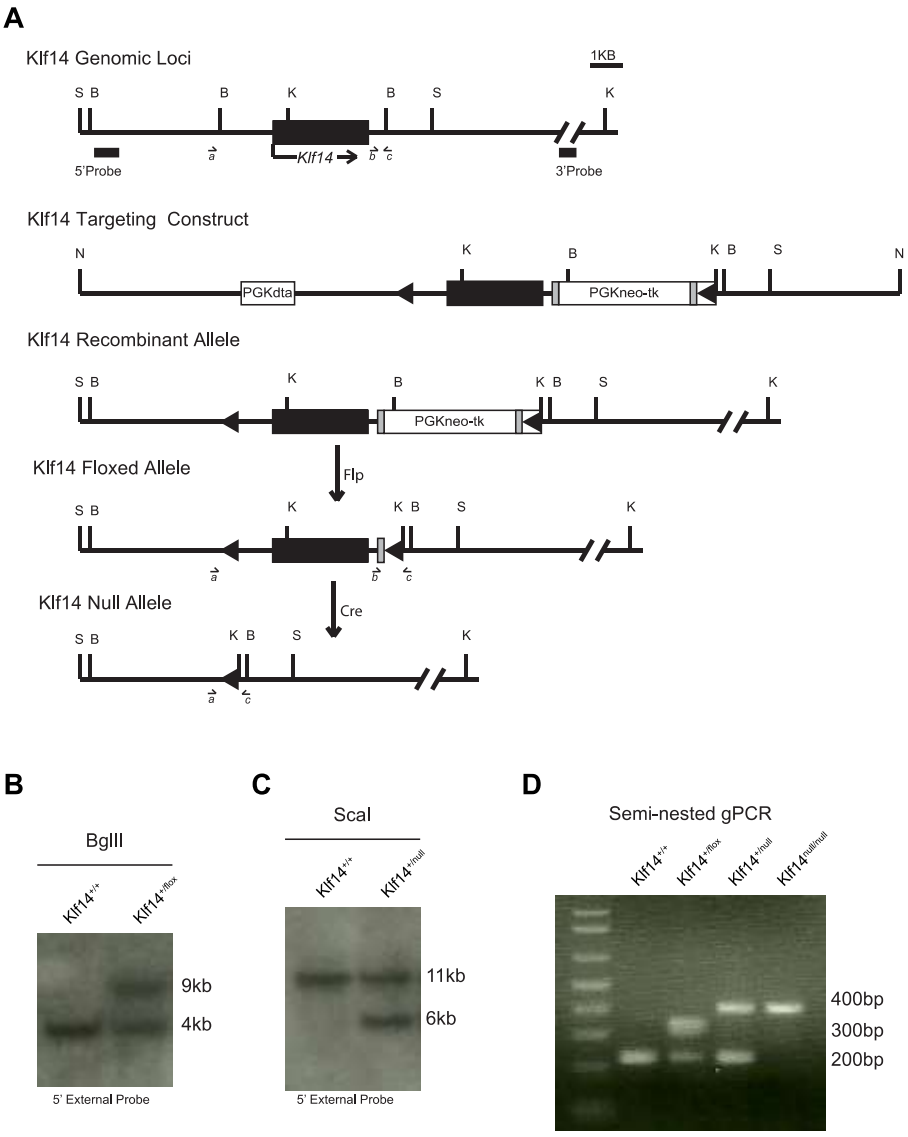

Figure 41. Targeted deletion of *Klf14* in mice. (A) Design and targeting of *Klf14*. (B) Southern blot confirming floxed allele in mice. (C) Southern blot confirming null allele in mice. (D) Genotyping PCR confirming flox and null alleles in mouse. Key: rectangles represent gene elements *Klf14* gene, PGK-neomycin-thymidine kinase cassette, PGK-diptheria toxin cassette; triangles represent loxp sites Abbreviations: S-ScalI, B-BglII, K-KpnI, N-NotI; a,b and c- semi-nested PCR primers. Scale bar is 1kb.

4.4.2 *Klf14* is an imprinted gene expressed in the placenta

I measured *Klf14* expression in an array of fetal and adult tissues by RT-PCR and found that expression levels were highest in yolk sac, fetal intestine and placenta and to a lesser degree in fetal brain, fetal liver, adult kidney and adult heart. However, *Klf14* expression was not detected in adult spleen, adult liver and homozygous null placenta (Figure 42A). Next, I sought to genetically confirm reports that *Klf14* expression is exclusively from the maternal allele in the mouse placenta. To these ends I compared expression of *Klf14* in wild-type ($Klf14^{+/+}$), maternal null ($Klf14^{null/+,}$), paternal null ($Klf14^{+/null}$), and homozygous null ($Klf14^{null/null}$) placentas using RT-PCR. Half of the offspring from heterozygous null dams crossed to wild-type males were $Klf14^{null/+}$ and had no detectable expression of *Kl1f14* after 35 RT-PCR cycles, and were queivalent in placental *Klf14* gene expression to that of $Klf14^{null/null}$ placentas derived from offspring of interbred heterozygotes (Figure 42A). Expression of *Klf14* in $Klf14^{+/null}$ placentas on the other hand were observed to be at or near $Klf14^{+/+}$ levels. These results provide definitive proof that *Klf14* is a maternally expressed gene within the mouse placenta.

To determine whether imprinting at the *Mest* DMD was altered in $Klf14^{null/null}$ placentas I assayed DNA methylation by COBRA and BGS. Bisulfite conversion and PCR amplification of a 550bp region of the *Mest* DMD yields two BstBI restriction sites, however if C→T conversion is blocked by DNA methylation these sites will not be generated. Approximately half of the bisulfite PCR product in $Klf14^{+/+}$ samples was undigested by BstBI, indicating roughly 50% methylation. Similar results were found in $Klf14^{null/null}$ placentas suggesting no changes in *Mest* DMD methylation in $Klf14^{null}$ transgenic placenta. However nearly all amplicons recovered from $Dnmt1^{c/c}$ ESCs were undigested by BstBI, indicative of the low methylation state of these cells.

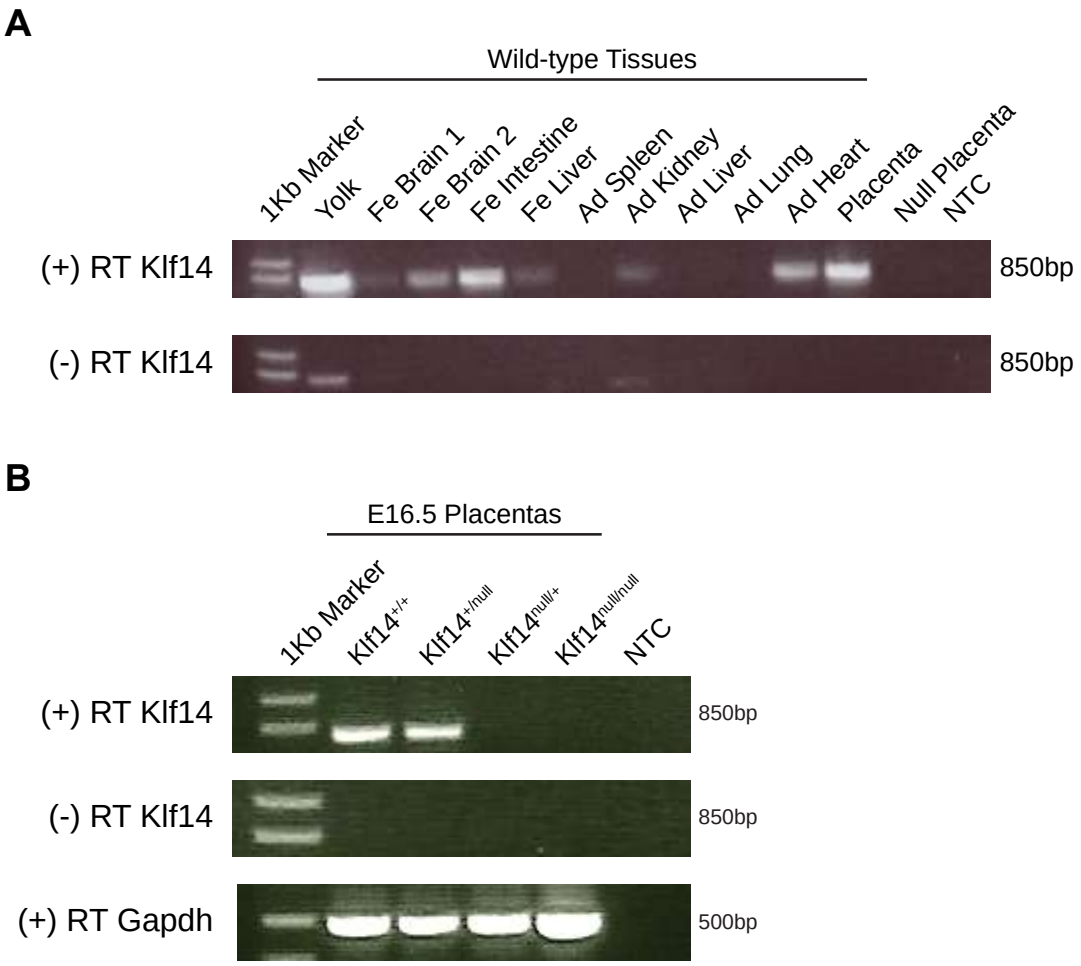

Figure 42. *Klf14* is expressed in the mouse placenta and is an imprinted gene. (A) RT-PCR based expression assay for *Klf14* in an array of fetal (Fe) and adult (Ad) tissues as well as extraembryonic tissue including homozygous null placenta. (B) Expression of *Klf14* in wild-type, heterozygous null and homozygous null E16.6 placentas. NTC-no template control.

I confirmed the COBRA assays by sequencing 16 cloned bisulfite converted PCR amplicons of the *Mest* DMD from *Klf14*$^{+/+}$ and *Klf14*$^{null/null}$ placentas (Figure 43A). Wild-type samples revealed the expected pattern of containing both fully methylated and fully unmethylated alleles. The average wild-type methylation value was 57.6%. Homozygous null placentas showed a similar pattern of *Mest* DMD methylation with both fully methylated and completely unmethylated alleles. The average *Mest* DMD CpG methylation in *Klf14*$^{null/null}$ placentas was 54.6%. These results further confirm that *Mest* DMD methylation is not altered by deletion of *Klf14*

Due to the tissue specific expression patterns of *Klf14* and the location of a CGI overlapping the *Klf14* transcriptional start site and 5′-end of the gene I hypothesized that there may be tissue specific methylation at this region. The EagI and MluI CpG methylation sensitive restriction enzymes have unique restriction sites within the *Klf14* coding region (Figure 43C). The EagI site falls within the CGI whereas the MluI site falls 3′ of it. Genomic DNA from an array of wild-type tissues was digested with ScaI in combination with either MluI or EagI, and probed with a 5′ internal radioprobe. The fetal liver was the only tissue in which partial digestion was observed in the ScaI-EagI double digest indicating partial methylation of the CGGCCG EagI CGI site (Figure 43C). Partial digestion was observed in genomic DNA derived from placental and adult liver samples suggesting partial methylation of the ACGCGT restriction sequence within the *Klf14* gene body (Figure 43C). I interpret these results as evidence that the *Klf14* CGI and gene body are generally hypomethylated but may have some tissue specific DNA methylation patterns

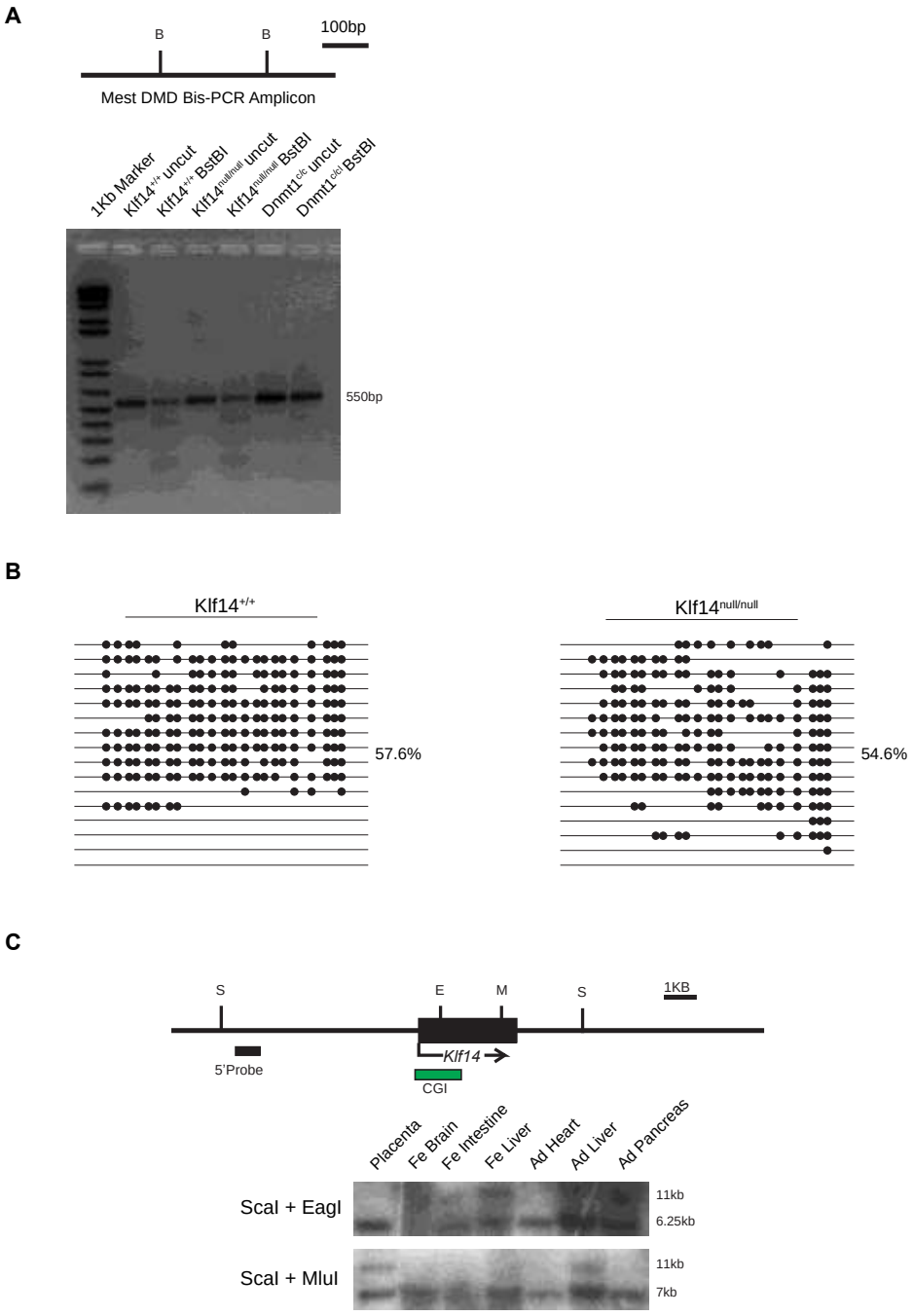

Figure 43. DNA methylation at the *Mest* DMD is normal in homozygous *Klf14* null placentas. (A) *Mest* DMD COBRA assay. (B) *Mest* DMD bisulfite genomice sequencing of 16 wild-type and *Klf14*$^{null/null}$ alleles. (C) Methylation-sensitive Southern blotting of the *Klf14* CGI and gene body. Abbreviations B-BstBI, S-ScaI, E-EagI, M-MluI.

4.4.3 *Klf14* null mice are viable and fertile

Heterozygous null mice were both viable and fertile regardless of sex, strain background or parent-of-origin of the *Klf14* null allele. The offspring of heterozygous intercrosses were found to contain wild-type, heterozygous null and homozygous null genotypes at near mendelian 1:2:1 frequency (Tables 8 and 9, Chi-square test P>0.05). Moreover, homozygous null mice of both sexes were viable and fertile on 129Sv and B6 strains. No differences were observed in the growth curves of wild-type, heterozygous and homozygous null littermates from weaning through postnatal day 90 (Data not shown). These results suggest that *Klf14* is not essential for murine development or reproduction, but do not rule out more sublte developmental or metabolic defects in null mice. Therefore, it was still important to determine if any abnormalities were present in developing *Klf14* null placentas.

Genotype	Obs	Exp		Genotype	Obs	Exp
Wild-type	37	27		Female Wild-type	18	13.5
Heterozygous Null	50	54		Female Heterozygous Null	26	27
Homozygous Null	21	27		Female Homozygous Null	11	13.5
Total	108	108		Male Wild-type	19	13.5
Chi-Square (df = 2)	5.33 (P>0.05)			Male Heterozygous Null	24	27
				Male Homozygous Null	10	13.5
				Total	108	108
				Chi-Square (df = 5)	5.48 (P>0.05)	

Table 8. Near Mendelian inheritance of the *Klf14* null allele in 129Sv strain heterozygous intercrosses. (Left) Chi-square analysis without gender influence. (Right) Chi-square analysis including gender. Abbreviations: Obs, Observed; Exp, Expected; df, degrees freedom; P, P-value.

Genotype	Obs	Exp		Genotype	Obs	Exp
Wild-type	20	16.5		Female Wild-type	8	8.25
Heterozygous Null	29	33		Female Heterozygous Null	18	16.5
Homozygous Null	18	16.5		Female Homozygous Null	9	8.25
Total	66	66		Male Wild-type	13	8.25
Chi-Square (df = 2)	1.36 (P>0.05)			Male Heterozygous Null	11	16.5
				Male Homozygous Null	8	8.25
				Total	66	66
				Chi-Square (df = 5)	4.79 (P>0.05)	

Table 9. Near Mendelian inheritance of the *Klf14* null allele in B6 strain heterozygous intercrosses. (Left) Chi-square analysis without gender influence. (Right) Chi-square analysis including gender. Abbreviations: Obs, Observed; Exp, Expected; df, degrees freedom; P, P-value.

4.4.4 Overgrowth in homozygous *Klf14* null placentas

Even though homozygous *Klf14* null animals were viable and fertile we examine E17.5 litters to determine if there were any growth effects on either heterozygous or homozygous null embryos and placentas. Average placental and fetal weights from wild-type and mutant offspring from litters of heterozygous *Klf14* null intercrosses are displayed in Figure 44. Homozygous null placentas were approximately 10% heavier than wild-type littermates ($P<0.05$; Figure 44A). The intermediate phenotype observed in heterozygous *Klf14* null placenta is most likely due to equal distributions of $Klf14^{+/null}$ and $Klf14^{null/+}$ that either had a functional or non-functional *Klf14*. Although the standard error of the mean (SEM) placenta weight is lower in heterozygotes than either wild-type or homozygous null littermates the standard error (uncorrected for sample size) is larger in heterozygotes. No difference in fetal weights was observed between genotypes from these crosses (Figure 44).

To determine whether there was an imprinting effect on placental development in heterozygous offspring I analyzed E17.5 litters of *Klf14*$^{null/+}$ mated to wild-type 129Sv males. Average placental and fetal weights from wild-type and *Klf14*$^{-/+}$ offspring are shown in Figure 45. The maternal null placentas were significantly heavier than wild-type littermates ($P<0.05$; Figure 45A). These results are interpreted as evidence rejecting a role for *Klf14* within the mother from influencing placental size. Rather the data suggest loss of active maternal *Klf14* in offspring autonomously enhances fetal growth. Similar to the offspring of heterozygous intercrosses no significant difference in fetal weights was detected in the offspring of *Klf14*$^{null/+}$ dams (Figure 45B).

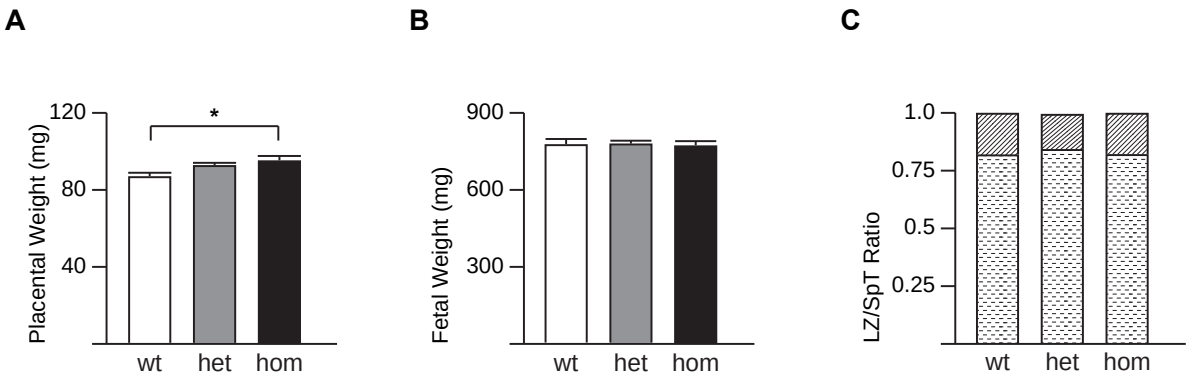

Figure 44. E17.5 Placental and fetal weights in offspring of heterozygous *Klf14* null intercrosses. (A) Wet placental weight of wild-type (wt, n=17), heterozygous (het, n=43) and homozygous null (hom, n=12) littermates (B) Corresponding fetal weights (C) Placental layer fractions *P<0.05 2-way Students T-Test.

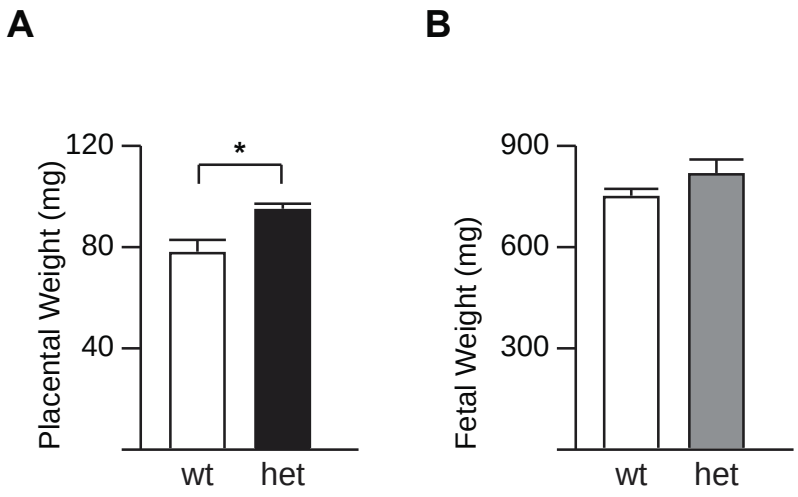

Figure 45. E17.5 Placental and fetal weights in offspring of maternal *Klf14* null dams. (A) Wet placental weight of wild-type (wt, n=9), and maternal null heterozygous (het, n=10) littermates (B) Corresponding fetal weights (C) Placental layer fractions *P<0.05 2-way Students T-Test.

4.4.5 Placenta layer structure in *Klf14* null placentas

I chose to further investigate the placental overgrowth phenotype using histological methods in order to determine if there were any structural abnormalities. The LZ and JZ layer fractions of homozygous and heterozygous *Klf14* null placentas from heterozygous intercrosses were not significantly different from wild-type littermates (44C). These results indicate that the observed placental overgrowth is evenly distributed between layers rather than attributable to expansion of either JZ or LZ.

4.4.6 Placental lipid content increased by high fat diet in *Klf14* null placentas

In the prior chapter loss of imprinting at the *Mest* cluster was determined to be associated with increased lipid content in the *Dnmt1*$^{\Delta 1o}$ maternal effect model. Therefore, it was important to determine if the increased placenta weight in the *Klf14* null model was due to lipid accumulation. However, I observed no difference in placental triacylglyceride concentrations in wild-type and *Klf14*$^{-/-}$ placentas (Figure 46). I challenged wild-type and *Klf14*$^{-/-}$ females with a high fat diet (HFD) for 6-weeks prior to and then during pregnancy to determine if placental lipid content was contingent on diet. Placentas recovered from pregnant *Klf14*$^{-/-}$ females challenged with HFD were significantly higher than those from wild-type dams fed with normal chow (Figure 46). However, no difference was found in wild-type litters fed with HFD nor was there a significant difference between offspring of *Klf14*$^{-/-}$ females compared with wild-type HFD offspring. These preliminary data suggest *Klf14* may regulate placental lipids in the context of HFD.

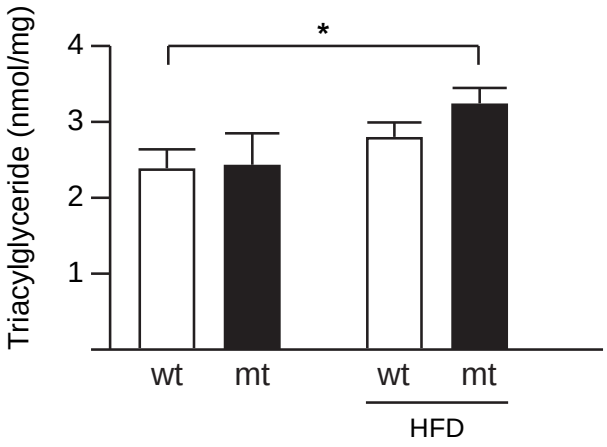

Figure 46. Lipid Accumulation in *Klf14* null offspring. Comparison of litters from wild-type and homozygous null females fed either normal or high fat diet (HFD) chow. *P<0.05 2-tailed Students T-Test

4.5 DISCUSSION

4.5.1 Opposing effects of *Klf14* and *Mest* on placental growth

The results presented in this section that show *Klf14* influences placental growth suggest that its loss of expression in the DNMT1o-deficient model may be in part responsible for the associations between loss of imprinting at the *Mest* cluster and placental phenotypes. In DNMT1o-deficient placentas the expression of *Klf14* is decreased more than 2-fold at E9.5, E15.5 and E17.5 whereas *Mest* expression is increased significantly only at the two later time points (Figure 28). Although the reciprocal changes in *Klf14* and *Mest* were concomitant, only *Mest* was identified by linear regression as associated with DNMT1o-deficient placental efficiency suggesting that *Mest* is either a marker of highly vascularized efficient placentas or that loss of imprinting of *Mest* influences the ratio of fetal and placental weight. Although fetal growth was unaffected in *Klf14* null mice, the E/P placental efficiency ratio was not significantly decreased despite the moderate placenta overgrowth (data not shown). Congruent placental and fetal growth restriction is observed in mice with a paternally inherited *Mest* null allele (*274*). Therefore, it is expected, although unconfirmed, that *Mest* overexpression would increase placental and fetal growth evenly. Based on my results regarding the *Klf14* null and the aforementioned *Mest* null model it is likely that the collective loss of imprinting at the *Mest* cluster integrates disparately towards fetal overgrowth. My results also show that *Klf14* and *Mest* have opposing influences on placental growth.

In Chapter 3 I revealed novel associations between loss of *Mest* DMD methylation and accumulation of spongiotrophoblast at E15.5, and accumulation of placental triacylglycerides at E17.5. The latter phenotype is particularly relevant given my findings in this section that placental lipid accumulation occurred in offspring of homozygous null *Klf14* females maintained on HFD during and six weeks prior to pregnancy. However, the lipid accumulation in DNMT1o-deficient placentas was more pronounced and occurred without HFD administration. I interpret these results to indicate that mosaic loss of DMD methylation in the context of *Mest* DMD hypomethylation and HFD in the context of maternal *Klf14null* development are insults to placental metabolism that result in excess lipid deposition. Based on my research herein, a further investigation into the role of genes within the *Mest* imprinting cluster with a focus on *Klf14* and *Mest* in fetal endothelial, syncytiotrophoblast and adipose lipid metabolism is warranted.

Klf14 null mice did not recapitulate the altered layer development observed in DNMT1o-deficient placentas. Despite the increase in spongiotrophoblast associated with loss of *Mest* DMD methylation in DNMT1o-deficient placentas I did not observe any changes in SpT layer fraction in E16.5 homozygous null placentas compared to littermates. Similarly, no difference in placental structure was observed in the growth restricted *Mest* null placentas. This suggests that either another gene within the *Mest* cluster was responsible for this phenotype or that epistatic interactions within the *Mest* loci or between the *Mest* loci and other clusters. Previously it has been pointed out that the components of the *H19, Grb10, Kcnq1* and *Plagl1* clusters are involved in SpT development and are part of a larger integrated network of imprinted genes to which *Klf14* and *Mest* may belong.

4.5.2 Placental and maternal influence on metabolism

Placental function and maternal environment during prenatal development has strong influences on the lifelong health of individuals. The association between adult metabolic disease and SNPs upstream of *Klf14* could be mediated by long lasting effects due to either maternal *Klf14* susceptibility alleles in either mother or placenta. Therefore, it was particularly of interest that homozygous null *Klf14* females when fed HFD had offspring with placentas enriched in triacylglycerides. These results show that *Klf14* may modulate lipid metabolism in pregnant females in a way that alters placental lipid deposition. This is exemplary of environmental influences being integrated through a genetic pathway. Further studies should be performed to validate my findings using a greater sample number of wild-type and homozygous *Klf14* null females. In addition, it would be interesting to determine if heterozygous maternal null or paternal null (*i.e.* $Klf14^{null/+}$ or $Klf14^{+/null}$) dams mated to wild-type males and fed HFD also yield increased placenta triacylglycerides in either wild-type or heterozygous offspring. Such a study would confirm that placental triacylglyceride accumulation is the result of HFD plus maternal *Klf14* deletion or provide evidence that the phenotype is caused by HFD plus placental *Klf14* deletion. Lastly, it might be interesting to perform a uterine transfer of wild-type embryos into homozygous *Klf14* null females to verify that lipid accumulation occurs independent of offspring genotype.

4.5.3 Comparison with other targeted *Klf14* models

During the time I was investigating the role of *Klf14* in placenta biology three different groups published reports on the effects of *Klf14* deletion in mouse (*433-435*). However, none of these

studies examined *in utero* fetal or placental development. These three groups utilized different targeted deletion models and examined diverse facets of mouse biology influenced by *Klf14* ranging from sphingosine-1-phosphate signaling in the liver, hepatic cholesterol metabolism, and centromere amplification (*433-435*). The fact that each of these groups published findings on homozygous *Klf14* null mice confirms my finding that *Klf14* is not an essential gene.

A group from the Mayo clinic utilized a neomycin insertion-deletion mouse available from the KOMP repository at UC Davis in their study of hepatic sphingosine kinase-1 (*Sk1*) transcriptional regulation (*435*). Using a luciferase assay this group observed that FGF2/FGFR1 induced *Sk1* promoter activity is dependent on GC rich sequences overlying KLF14 binding sites (*435*). They found that in HUVEC cells that *Klf14* siRNA reduces FGF2 stimulated *Sk1* expression, whereas *Klf14* overexpression increases basal and FGF2 stimulated *Sk1* expression (*435*). They also showed that KLF14 dependent FGF2 stimulation resulted in accumulation of activating histone marks (increased H4K8ac and H3K14ac) and a decrease in repressive marks (decreased H3k9me3 and H3K27me) at the *Sk1* promoter (*435*). Furthermore, they showed that epitope tagged KLF14 binds the endogenous *Sk1* promoter and interacts directly with the histone acetyltransferase p300 (*435*). This study provides firm genetic proof that KLF14 is a transcriptional regulator that can interact with more than just SIN3A, and is a mediator of FGF2 signaling.

Following up on the role of *Klf14* in liver a second group generated a liver-specific conditional null by mating a floxed *Klf14* allele with an *Albumin:CRE* mouse (*433*). They initially became interested in *Klf14* due to the GWAS studies linking it to T2D and HDL levels and their preliminary findings that *Klf14* expression is decreased in HFD fed wild-type mice, *Apoe* null coronary heart disease mouse model and in the leptin deficient (*ob*/*ob*) murine obesity

model (*433*). Overexpression of *Klf14* by adenoviral infection *in vivo* resulted in increased HDL-C and APO-A1 (*433*). Hepatocyte *in vitro* adenoviral induced *Klf14* overexpression showed a clear increase in *ApoA1* transcription that was dependent on two CACCC boxes bound by *Klf14* within the *ApoA1* promoter (*433*). Furthermore, *Klf14* expression was increased in perhexaline treated Apoe homozygous null mice and partially rescued the cardiac plaque phenotype in a manner independent of carnitine palmitoyltransferase1 inhibition by perhexaline (*433*). These results are particularly interesting given my findings that placentas derived from homozygous null *Klf14* dams are more susceptible to lipid accumulation. In addition, it was noted in DNMT1o-deficient placentas that mitochondrial carnitine efflux was highly distorted (*414*).

A third *Klf14* null model was developed using TALON zinc finger nucleases (*434*). This group became interested in *Klf14* when they discovered that it encodes a transcription factor that binds to and represses polo-like kinase-4 (*Plk4*) (*434*). It has previously been established that overexpression of *Plk4* induces centrosome amplification (*434*). They found that 13-14 month old homozygous *Klf14* null mice had more frequent tumors of the lung, lymph and spleen than wild-type (*434*). Homozygous *Klf14* null mice were also more susceptible to azoxymethane chemically induced colon tumors (*434*). They established homozygous *Klf14* null murine embryonic fibroblast cultures and found that roughly 12% of cells were polyploid. Additionally, they found that siRNA knockdown of *Klf14* in HeLa cells resulted in increased *Plk4* expression, centrosome amplification and misaligned metaphase plates, whereas *Klf14* overexpression provoked mitotic catastrophe (*434*). These results may in part explain why imprinting of *Klf14* is beneficial due to hazards of overexpression While I did not find any evidence of tumors in my *Klf14* null colony, I did not observe them beyond 9 months.

5.0 OVERALL DISCUSSION

5.1 SUMMARY AND SIGNIFICANCE

In Chapter 2 I described an array of abnormal placental phenotypes present in the *Dnmt1*$^{\Delta 1o}$ maternal effect offspring. Early in development trophoblast differentiation was severely disrupted leading to diminished LZ development and increased TGC abundance. Many of the abnormal placentas found at E12.5 could not support a viable fetus and lacked fetal vasculature in the placental labyrinth. The phenotypes in late gestation DNMT1o-placentas were very different. Although at E15.5 placental layers were not significantly different than wt, by E17.5 the fraction of JZ relative to LZ was increased. I observed extensions of SpT into the LZ in many E15.5 and E17.5 DNMT1o-deficient placentas. I also found that DNMT1o-deficient placentas recovered at E15.5 and E17.5 were enriched in glycogen deposits and lipid droplets. At E17.5 the ratio of fetal and placenta growth was highly dysregulated and revealed that both high and low E/P ratio placentas had unique gene expression profiles. Taken together these results demonstrate the strong effects on placenta development that occur in the the *Dnmt1*$^{\Delta 1o}$ maternal effect model.

In Chapter 3 I described the breadth of loss of imprinting in DNMT1o-deficient placentas and correlated these molecular changes with placental abnormalities. In DNMT1o-deficient placenta imprinted gene expression was disrupted across gestation. At later gestational ages the

directionality of imprinted gene expression changes was not always congruent with the changes expected with loss of DMD methylation. Novel associations between *Mest* and *Ascl2* expression levels and E/P ratio were revealed. A broad survey of 15 imprinted DMDs in DNMT1o-deficient placentas confirmed the epigenetic mosaicism previously postulated to occur in this model. DMD methylation was higher in the E17.5 than E12.5 placental cohorts suggesting selection against certain hypomethylated epigenotypes. In addition, methylation at some DMDs (*e.g. Dlk1* and *Nespas*) appeared less mutable than others. Ultimately, I used regression analysis to reveal novel associations between individual DMDs and placental phenotypes. Amongst the more notable associations were: a relationship between loss of *Peg10* DMD methylation and both reduced fetal viability and diminished labyrinth central volume at E12.5; a relationship between loss of *Kcnq1* DMD methylation and TGC accumulation at E12.5; and a relationship between loss of *Mest* DMD methylation and triacylglyceride accumulation at E17.5. These results provide an impetus to further dissect these three imprinting clusters for roles in placental development.

In my final results section, Chapter 4, I focused on the generation and study of a novel targeted deletion of the imprinted *Klf14* gene. I used this model to confirm previous assertions that *Klf14* is an imprinted gene expressed in the placenta. Although *Klf14* null mice were viable and fertile even in homozygous genotypes, I observed changes in the placenta. Both homozygous conceuptuses from heterozygous intercrosses, and heterozygous conceptuses from homozygous maternal null dams had significantly heavier placentas at E17.5 than wild-type littermates. In addition, placentas from homozygous null dams fed HFD were enriched in lipids. These results suggest a role for *Klf14* in regulating placental growth and metabolism and highlight the need for further investigation of this model.

The results presented within my dissertation significantly add to the scientific understanding of the role of genomic imprints in placental development. In characterizing the range of phenotypic and molecular abnormalities seen in DNMT1o-deficient placentas I have explicitly demonstrated that disruption of the inheritance of genomic imprinting has direct biological effects on trophoblast differentiation and metabolism and the balance of placental and fetal growth. Using this data, I was able to reveal novel associations between individual imprinted DMDs and specific placental phenotypes. This analysis revealed particular importance of the *Kcnq1*, *Peg10*, and *Mest* imprinting clusters for placental development. This study demonstrates the feasibility and importance of epigenotype-phenotype association studies. Lastly, my work developing and studying the imprinted *Klf14* gene revealed its role in regulating placental growth. My findings are summarized in Figure 47 demonstrate that mosaic loss of imprinting in the *Dnmt1*$^{\Delta 1o}$ maternal effect model lead to placental abnormalities, some of which can be replicated by deletion of *Klf14*.

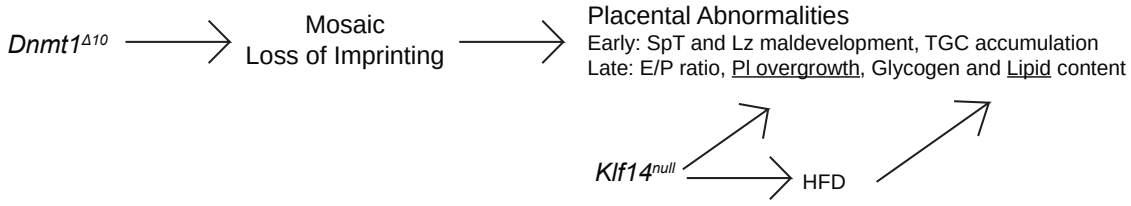

Figure 47. Dissertation summary model. The *Dnmt1*$^{\Delta 1o}$ maternal effect model results in partial and mosaic loss of genomic imprinting early in embryonic development. This influences abnormal placental development at early and late gestational time points resultin in specific phenotypes. Deletion of the *Klf14* gene also results in late gestation placenta overgrowth and when confronted with high fat diet increases lipid stores.

5.2 FUTURE DIRECTIONS

5.2.1 Coevolution of genomic imprinting and placentation

Genomic imprinting is a fascinating molecular phenomenon that has co-evolved with mammalian placentation. It is of note that prototheria (monotremes), metatheria (marsupials) and eutherian (placental mammals) have an increasing number of genomic imprints and reliance on *in utero* gestation (*436*). Furthermore, the boundaries of imprinted clusters are expanded to impose parent-of-origin specific expression to additional neighboring genes in extraembryonic tissues including the placenta and vitelline yolk sac (*307, 309*). For example, in extraembryonic tissues the *Igf2R* imprinted cluster includes *Slc22a1* and *Slc22a3*, the *Kcnq1* imprinted cluster includes *Th, Ascl2, Tspan32, Nap1l4,* and *Osbpl5*, the *Peg10* imprinted cluster includes *Tfpi2, Ppp1r9a, Pon2* and *Pon3*, the *H19* imprinted cluster includes *Ins2* and the *Grb10* cluster inclues *Cobl* (*307, 309*). The mechanisms by which this expansion occurs may have to do with unique nuclear architecture and chromatin topology in extraembryonic lineages that enable long distance interactions of ICs with expanded sets of imprinted genes and distant enhancers and repressors (*437*). Revealing the full scope of genomic imprinting within the placenta and the mechanisms that enable the expansion of imprinting boundaries will aide in the effort to ascribe placental functions to imprinted loci.

By understanding the evolutionary history of genomic imprinting we should be better equipped to understand the function of genomic imprints in mammalian biology. Therefore, I

think it is important to better grasp what placental physiological adaptations coincide with the acquisition of specific imprints. For example, the *H19* imprint (and paternal allele-specific *Igf2* expression) originated in the common ancestor of metatherian and eutherians possibly reflecting the changes in maternal/offspring resource allocation with the evolutionary acquisition of placentation (*438-440*). *Peg10* (but neither *Sgce* nor *Ppp1r9a*) and *Mest* are also imprinted in metatherians, but members of the *Snrpn, Kcnq1* and *Dlk1* cluster are not, suggesting the former are involved in early placentation while the latter are involved in eutherian-specific phenomena such as prolonged *in utero* development (*441, 442*). Furthermore, the *Impact* and *Zrsr1* imprints are specific to rodents (*442*). Intriguingly, strict *IGF2R* allele specific expression has been lost in primates, despite retention of imprinted *IGF2R* DMD methylation, perhaps indicative of changes in placental and fetal growth and maternal resource allocation in extended gestation of single conceptuses (*383, 439*). It is interesting to question whether the relaxation of *Igf2r* imprinting was due to a different adaptation to limit its expression, or changes in the threshold of IGF2 signaling, or to differences in the recognition of imprints in primates versus other mammals. The answers to these questions and more should help us understand our own genome and aid in the era of genomic medicine

The expansion of imprinted clusters to regulate additional genes in murine extraembryonic lineages is not conserved in humans. For example, in humans, the *Igf2r* DMD is maternally imprinted but expression of *IGF2R, SLC22A2* and *SLC22A3* is polymorphic and only imprinted in some but not all human term placentas (*383*). The expanded placenta-specific imprinting within the *Kcnq1* cluster is also lost in humans resulting in only the core *KCNQ1* cluster (*KCNQ1ot, KCNQ1, PHLDA2* and *CDKN1C*) and not the centromeric (*NAP1/4* and *OSBPL5*) nor telomeric (*CD81, TSPAN32* and ASCL2) adjacent genes retaining monoallelic

expression in trophoblast cells *in vivo* and *in vitro* (*383, 443*). Similarly, the extraembryonic paternally imprinted X chromosome inactivation phenomenon found in rodents is not conserved in humans, rather random inactivation analogous to the embryo proper occurs (*444*). The commonality of extraembryonic imprinted X-chromosome inactivation and expanded extraembryonic imprinted clusters processes suggests a co-evolution of an extraembryonic-specific imprinting mechanism that was lost during human evolution (*436*). The possibility of a mechanism involving ncRNA and repressive histone modifications that spread imprinting beyond core loci is particularly attractive (*436*).

There are three theories that explain how genomic imprinting arose during evolution (*440*). Each one postulates in its own way a selective advantage to the inheritance of parent-of-origin specific epigenetic information (*440*). The most prominent theory is the kinship theory in which a conflict of interest over maximizing reproductive fitness in maternal and paternal genomes exists (*411, 440*). In this paradigm the maternally inherited genome will be most successful if there are a large number of siblings across multiple litters from the same mother and favors an allocation of maternal resources that limits fetal growth so that it is not an impedance on future litters (*411, 440*). Paternally inherited genomes, particularly in non-monogamous mammals such as mice, maximize reproductive fitness by producing large vigorous offspring at the expense of future litters from the mother (*411, 440*). The kinship theory thus predicts and is validated by the fact that paternally expressed genes promote growth (*e.g. Igf2, Peg1*), whereas maternally expressed genes restrict growth (*e.g. Grb10*, *Phlda2*, *Cdkn1c*, *Igf2r*) (*440*). However, kinship theory is contradicted by the findings that many paternal UPDs result in growth restriction and/or embryonic lethality (*261*). Another argument against kinship theory is that it invokes a teleological argument that animates maternal and paternal genomes to selfishly direct

their own evolution towards different reproductive strategies. Theoretically, it is in the best interest of the species as a whole to have a balance of intra-litter and inter-litter fecundity to maximize species vitality.

The ovarian bomb theory is an alternative explanation to the evolution of genomic imprints (*445*). The central tenet to this theory is that genomic imprinting arose to prevent parthenogenetic oocyte activation from producing viable conceptuses or invasive trophoblastic diseases (*i.e.* ovarian teratomas) (*445*). This would limit trophoblastic disease to those derived from pregnancy (*i.e.* choriocarcinomas and molar pregnancies) (*445*). Like kinship theory, the ovarian bomb theory predicts that maternally expressed genes are growth limiting, and paternally expressed genes are growth promoting in order to overcome limitations the maternal genome has to promote growth (*445*). While this theory limits active selection to those genes involved in trophoblast development it does allow for new imprints to be acquired as passengers due to proximity or sequence similarity (*445*).

The authors of both the kinship and ovarian bomb theories focus entirely on the function of maternally and paternally expressed genes rather than the genomic imprints (*i.e.* DMD methylation) *per se* because the maternal imprints (*e.g. Kcnq1*, *Grb10*, and *Igf2r*) associate with expression of maternal genes and paternal imprints (e.g. *H19*) associate with expression of paternal genes often through indirect ncRNA or secondary epigenetic mechanisms. The evolution of maternal genomic imprints may have had as much to do with silencing of repressive ncRNAs (*e.g. Kcnq1ot*) than with the maternally expressed genes themselves. Similarly, the *H19* and *Dlk1* paternal imprints may have formed to silence the *H19* and *Meg3* ncRNAs rather than to promote the neighboring paternally expressed genes. I suggest that it may be more informative to ask how DMD methylation itself influences life history strategies to determine how genomic

imprints evolved. My results showed that loss of the maternal *Kcnq1* imprint was associated with TGC accumulation which in many ways looks like hydatidiform molar trophoblastic disease. This evidence fits the ovarian bomb theory better than the kinship theory. However, loss of the *Peg10* maternal imprint in DNMT1o-deficient mice results in diminished LZ development and fetal lethality, a result that neither the kinship nor ovarian bomb theory can adequately explain, suggesting that both theories may be too rigid.

A third theory on the evolution of genomic imprints suggests that haploid (monoallelic) expression enables rapid gene evolution (*446*). This theory is not mutually exclusive with the prior two. It is generally accepted among biologists that one of the benefits of diploid genomes is the robustness imparted by having two copies of each gene. However, when one allele is masked it can be mutated in compound fashion and bypass recessive lethal intermediates by not being expressed for multiple generations (*446*). In fact, it has been determined that many imprinted genes, including *Klf14*, are undergoing rapid evolution (*270*). It is also of note, although somewhat circumstantial, that most tissue-specific imprinted genes are either involved in placenta or the brain, the two fastest evolving organs in mammals (*447*).

Regardless of how genomic imprints initially evolved and what their selective fitness benefits are, they are clearly involved in reproductive isolation (*448*). In deer mice (*Peromyscus*) hybrids of *Peromyscus maniculatus* and *P. polionotus* have reciprocal parent-of origin effects (*448-451*). In crosses of *P.maniculatus* females with *P. polionotus* males offspring are viable but growth restricted and their JZ is reduced at E13 (*449-451*). In contrast, the reciprocal cross of *P. polionotus* females with *P.maniculatus* males are overgrown and dysmorphic with altered E/P ratio and disorganized hemorrhaging labyrinth (*449-451*). These overgrown mice have abnormal imprinting at the *Peg3*, *Mest*, *Snrpn*, *H19* and *Plagl1* imprinting clusters (*450, 451*). It has been

suggested due to the broad nature of loss of imprinting that there is a maternal effect locus (possibly *Dnmt1o* or *Dnmt3l*) responsible for the interspecific hybrid phenotypes (*450*). Furthermore, the placental dysplasia resulting from loss of imprinting is the main reason for the reproductive isolation of these two species (*448*). One explanation for these findings of incomplete loss of imprinting is that a differential expression difference in DNMT1o protein and interacting maternal/zygotic partners (*e.g.* DMAP1 or ZFP57) in the two species when interbred do not reach a sufficient threshold to maintain more sensitive imprints.

Many imprinted genes arose through retrotransposition. This mechanism generates new genes by reverse transcribing mRNA and integrating the resulting cDNA into the genome at a new site. This process is mediated by LTRs that flank transposable elements and are recognized by retroviral transposases. Essentially, these gene duplications events enabled the evolution of novel functions and/or or expression profiles. There are three classes of imprinted retrotransposed genes. The first class are transposed copies or endogenous retroviral genes (ERVs) that have been coopted to serve unique mammalian function (*e.g. Peg10, Rtl1*) (*289, 290, 373*). A second class of retrotransposed imprinted gene were derived from X-chromosome parent genes and inserted within introns of host genes (*e.g*. *Nap1l5* and *Zrsr1*) (*452*). A third class of retrotransposed imprinted gene as exemplified by Klf14 are intronless transposed copies of autosomal genes (*270*). Each of these types of imprinted genes acquired imprinting following transposition.

Both *Peg10* and *Rtl1* are copies of a Ty3/gypsy retrotransposon most similar to the Sushi-ichi retrotransposon family found in other vertebrates (*289, 290*). Of the 9 mammalian Sushi-like retrotransponons 5 are located on the X chromosome, 2 are imprinted and 2 are autosomal non-imprinted (*289*). It is likely that *Peg10* initiated the formation of an imprinted loci to block its

expression after transposition, although the Peg10 DMD sequence does not have homology to other Sushi-ichi family members (*289*). The *Peg10* locus is present in eutherian and marsupial mammals but not in monotremes further suggesting a link with placental evolution (*453*). *Rtl1* does contain a CGI, however there is no evidence of parent-specific methylation (*289*). *Rtl1* retrotransposition was an ancestral event to the acquisition of the intergenic DMD regulating the *Dlk1* cluster and insertion of miRNAs and snoRNAs in eutherians (*368*).

Retrotransposition of *Nap1l5* and *Zrsr1* resulted in novel micro imprinted domains that imposed parent-of-origin transcriptional effects on their host genes (*454*). The rodent-specific retrotransposition of *Zrsr1* led to direct imprinting of *Commd1*. In the case of *Nap1l5* retrotransposition resulted in imprinted allele-specific polyadenylation of *Herc3*. The *Nnat* microimprinted domain is similar in structure to *Nap1l5* and *Zrsr1,* and imprints its host gene *Bclap*. No ancestral gene has been identified, although a *Nnat* pseudogene exists on mouse chromosome 7 (*239, 454, 455*). It is perhaps not coincidental that alternative polyadenylation and transcriptional interference that occurs in these less complicated imprinted domains also occurs in the larger *Kcnq1, Mest*, and *Igf2r* domains. These findings on microimprinted domains have been interpreted as suggesting that such retrotranspositon events may have been the impetus for the earliest genomic imprints in eutherian development. My results showed that the *Nnat, Nap1l5*, and *Zrsr1* DMDs are approximately 40- 60% methylated in wild-type placentas which is in line with expected levels of a genomic imprint (Figures 32 Q-S). However, only the *Zrsr1* DMD had significant loss of methylation in DNMT1o-deficient placentas indicating that the *Nnat* and *Nap1l5* DMDs are either insensitive to loss of preimplantation maintenance methyltransferase activity or that they are absolutely required for TE development.

The final class of retrotransposed imprinted genes are copies of autosomal parent genes. For example, *Klf14* most likely acquired imprinting status upon its transposition in proximity of *Mest*, which may have been beneficial to limit the dosage of the ancestral gene product *Klf16* and enable its rapid evolution (*270*). Furthermore, retrotransposition of other genes have been vital to placental development in particular the syncytins *SynA* and *SynB* were coopted from viral envelope proteins to enable cell fusion of SynT progenitors within the labyrinth (*210, 211*). The syncytin 5′ LTR sequences are promoters dynamically regulated by DNA methylation in the human placenta (*456*).

It is also of note that species specific ERVs, or portions of their LTRs, are present in the promoters of many trophoblast expressed genes. These ERV promoters are enriched in binding sites for the placenta master transcriptional regulators ELF5, CDX2 and EOMES (*457*). These findings suggest a relationship between intergenic ERV transposition and adoption of trophoblast specific expression in mammalian genomes. It is clear from the above findings that retrotransposition had a strong impact on the evolution of both placentation and genomic imprinting. The placenta is a suitable target for live retroviruses and ERVs as it enables direct passage between generations as well as enabling horizontal transfer from heterozygous individuals to littermates *in utero* (*458*). In addition, the placenta may provide access to germline integration (*458*). ERVs once established would be maintained by positive selection if they were coopted to unique functions, efficiently silenced or genetically degraded (*458*). Retrotranspostition may be a key in the evolution of genomic imprinting because DNA methylation evolved as host genome defense mechanism used to silence transposable elements (*459, 460*). While not all imprinted loci contain transposed elements it is possible they are recognized by the same methylation machinery due to sequence similarities. It is still unclear

how imprinted DMDs, unlike the majority of the genome (including most ERVs), escape erasure and *de novo* DNA methylation during reprogramming.

5.2.2 Imprint-like sequences

Recently, imprint-like sequences that convey heritable epigenetic information from parental gametes have been identified. Methylation at these regions are similar to imprints in that they acquire parent-specific methylation patterns and are protected from DNA demethylation during preimplantation development. Much of the evidence of imprint-like sequences comes from the study of TET-off *Dnmt1* cell culture model of early perimplantation development (*110, 111*). In the TET-off system addition of tetracycline reduces genomic DNA methylation in ES cells within days of tetracycline application, however DNA methylation is also lost at imprinted DMDs (*110, 111*). After removal of tetracycline, genomic DNA methylation gradually recovers due to the combined activity of *de novo* and DNMT1 methyltransferase activity. However, genomic imprints and a larger group of imprint-like sequences do not recover DNA methylation to prior levels (*111*). Among 90 genomic loci that have greater than 80% reduction in DNA methylation following transient DNMT1 inactivation in ESCs as measured by RRBS 15 are imprinted loci and the remainder are imprint-like sequences (*111*). *Zfp787* is one imprint-like gene previously identified as a transient maternal DMD using the *Dnmt3l* maternal effect model (*98*). *Zfp787* is maternally imprinted in gametes and is protected from preimplantation demethylation, but acquires paternal methylation methylation at implantation such that embryonic livers are biallelically methylated by E9.5 (*98*). Unfortunately, the *Zfp787* DMD methylation status has not been determined in any extraembryonic lineage. A number of other

loci were co-identified in the TET-off and *Dnmt3l* maternal effect models but have not been further validated as imprinted DMDs or transient DMDs (*98, 111*).

DNA methylation at a limited set of these imprint-like sequence was measured in DNMT1o-deficient embryos and placentas to determine if the loci identified in the TET-off system are similarly effected by loss of maintenance methyltransferase activity during early reprogramming events (*111*). Many of these loci showed partial loss of methylation in both compartments (e.g. *Rnf216, Bbs9, Stk10* and *Zfp676*) while others showed loss of methylation only in the placenta (e.g. *Xlr4a, Xlr4b,* and *Prdm1*) or in the embryo (*1700018B08rik*) (*111*). This may indicate that the epigenetic status of some transient DMDs are inherited exclusively in embryonic or extraembryonic lineages while others are perpetuated in all lineages and are likely true DMDs. Intriguingly, *Prdm1* is a transcriptional repressor that is critical for differentiation of SpA-TGCs (*461*). I propose to identify the full set of imprinted DMDs and imprint-like sequences that is disrupted in *Dnmt1*$^{\Delta 1o}$ maternal effect offspring (both fetal and placenta tissues) using a global DNA methylation analysis method such as RRBS. This data may even be used to determine if any of the imprint-like sequences associate with placental phenotypes.

5.2.3 Role of placenta in imprinting disorders

It was my hope that some of my dissertation results would shed light on human imprinting disorders. Many imprinting disorders alter prenatal and/or postnatal growth rates. For example, BWS manifests as overgrowth and sometimes occurs with placentomegaly (*114*). This syndrome can have epigenetic etiologies based on loss of methylation of the *Kcnq1* DMD and gain of methylation of the *H19* DMD (*114*). My results showed a correlation with loss of *Ascl2* expression in DNMT1o-deficient placentas and increased E/P ratio suggesting loss of imprinting

within the *Kcnq1* cluster may increase placental efficiency in late gestation (Figure 29A). It was also intriguing that late gestation expression of both *Ascl2* and *Phlda2* was increased in DNMT1o-deficient placentas, as opposed to the decrease of expression expected with loss of *Kcnq1*DMD methylation, suggesting compensatory mechanisms that may alter late gestation loss of imprinting expression profiles and fetal and placental growth trajectories. I observed a strong correlation between loss of *Kcnq1* methylation and TGC accumulation during mid-gestation was made (Table 4 and 36G). and it would be interesting to determine if the abundance of the analogous extravillous cytotrophoblast in BWS cases is altered.

The SRS growth restriction clinical phenotype is due to loss of methylation at the *H19* DMD in the majority of cases and due to matUP7 or gain of *Mest* DMD methylation in a minority of cases (*125, 130*). I showed that loss of maintenance methyltransferase activity in DNMT1o-deficient conceptuses results in mosaic loss of *Igf2* expression in the placental compartment (Figures 4 and 28). However, I did not find an association between *H19* DMD methylation with either placental or fetal weight. I did however find an association between loss of *H19* DMD methylation and JZ layer development at E12.5 (Table 4). In addition, higher E/P ratio was associated with increased *Mest* expression and loss of *Mest* DMD methylation was associated with placental lipid accumulation (Figures 29B and 39). These results in combination with the placental overgrowth phenotype observed in the *Klf14* deletion (Figures 44A and 45A) suggest that the *Mest* cluster is involved in the growth phenotype of matUPD7 SRS cases where one would expect increased genetic dosage of *Klf14* and decreased *Mest* expression. It would certainly be worthwhile to examine SRS associated placentas for changes in cytotrophoblast histology and in sycytiotrophoblast lipid content.

The imprinting diseases PHPIa and Ib are caused by loss of imprinting at the *Nespas* and *Gnas* locus (*148*). I was intrigued to find that the *Nespas* DMD methylation was largely immutable in DNMT1o-deficient placenta, perhaps suggesting a developmental requirement (Figures 32M and 32N). While the placenta takes on some functions of thyroid and kidney during prenatal development it remains unclear what if any function the imprinted genes in this cluster do in the placenta. I revealed a positive association between loss of *Nespas* DMD methylation and spongiotrophoblast at E12.5 (Table 4).

Similarly, no known placental functions for the PWS/AS loci containing the *SNRPN* imprinting cluster have been described. My results using stepwise linear regression modeling suggest that both *Kcnq1* and *Snrpn* are informative to predicting TGC accumulation (Table 5). Although it is possible that the *Snrpn* association is due to close linkage with *Kcnq1* it may be informative to examine placentas associated with PWS/AS for abnormal extravillous trophoblast proliferation. Recently it has been shown that snoRNAs from the *Snrpn* cluster regulate alternative splicing of the serotonin receptor *5Htr2c*, and separately that the placenta is a transient source of serotonin during early forebrain development (*324, 462-464*). I conjecture based on those two lines of evidence that the *SNRPN* cluster may regulate serotonin levels during prenatal development and be altered in *PWS/AS* conceptuses. It would be interesting to examine fetal and placental serotonin receptor isoform expression and serotonin levels in DNMT1o-deficient offspring (with loss of *Snrpn* DMD methylation) and in *Snrpn* locus targeted mutation models (e.g. *Snrpn* DMD deletion, *Snord114/116* deletion). I also propose that some imprinting disorders cases may be caused by failure to maintain imprints during preimplantaion. The findings of mosaic loss of imprinting, particularly in BWS and SRS cases, suggests that the severity of phenotypes may be based on the degree of mosaicism and the tissue types (including

the placenta) in which loss of imprinting is found. Finally, I suggest that there may be distinct epi-alleles in the population that are more prone to loss of imprinting during preimplantation development due to environmental factors and maternal effects.

The separation of placental and fetal phenotypes in the DNMT1o-model is difficult due to the entanglement and codependence of their development. One tool to better ascertain the placenta autonomous phenotypes from those that are intertwined or the result of fetal maldevelopment is through tetrapoloid trophoblast complementation. It would be informative to determine if the partial fetal lethality observed at E12.5 in DNMT1o-deficient placentas could be rescued by tetrapolid complementation of *Dnmt1*$^{\Delta 1o}$ maternal effect blastocysts. If survival to late gestation and neonatal time points was observed at a greater frequency, placental phenotypes could firmly be attributed as the main antagonist of early fetal lethality associated with loss of imprinting. Similarly, the reciprocal experiment could be performed and normal ES cells injected into *Dnmt1*$^{\Delta 1o}$ maternal effect blastocysts and examined for developmental outcome. If abnormal wild-type fetal development was observed in such conceptuses it would be arguably caused by placental imprinting defects, however this system would likely result in at least partially chimeric fetuses with some cells having partial loss of imprinting. I also suggest the development of both ESC and TSC lines from DNMT1o-deficient conceptuses that have loss of imprinting at a small number of loci with clinical relevance (*e.g. Snrpn, H19, Kcnq1, Mest, Plagl1, Nespas*). These cell lines could be studied for their potential to generate normal chimeric fetal or trophoblast tissue after blastocyst injection. The experiments I have proposed above may yield results that are informative on the contribution of genomic imprinting in the placenta on fetal development.

5.2.4 Reproductive technologies

It has been reported that within the population of BWS patients there is enrichment for individuals conceived by assisted reproductive technologies (ART) (*465-468*). Although this suggests an increased incidence of imprinted diseases associated with ART, not all clinical research corroborates these findings (recently reviewed by (*469, 470*)). Nearly all cases of BWS associated with ART are concomitant with loss of methylation at IC1 (KCNQ1), whereas this is the case for only half of all BWS cases in the naturally conceived population (*114, 471*). Furthermore, loss of methylation in BWS cases from children born after ART is observed at a broad range of DMDs including *Mest*, *Snrpn* and *Plagl1* (*471, 472*). This multigenic, and sometimes mosaic effect suggests that loss of imprinting occurs post-fertilization within the embryo. It is important for future studies to calculate the ART associated risk of SRS and TNDM1, which are most commonly associated with loss of methylation at the *H19* and *PLAGL1* loci respectively (*469*). The gamete and embryo manipulation performed in ART procedures such as superovulation, *in vitro* fertilization and intra-cytoplasmic sperm injection directly expose both gametes and embryos during the window of time crucial for the maintenance of genomic imprints (*473, 474*). My results clearly show that the majority of DMDs, including *Kcnq1*, *H19*, *Mest* and *Plagl1* can be affected, either in isolation or in tandem, by loss of DNMT1o activity Therefore, it is rather intuitive to suggest that ART may be detrimental to DNMT1o maintenance methyltransferase activity.

Similarly, both ART and cloning in mouse alter imprinted DMD methylation. Mouse embryos generated from IVF and cultured during preimplantation development in Whittens medium have lower levels of *H19* methylation, and their placenta are afflicted with loss of imprinting to a greater degree than the fetus, showing biallelic expression of *H19*, *Snrpn*, *Ascl2*

and *Peg3* (*475, 476*). Likewise, aberrant imprinted gene expression is observed in preimplantation embryos cultured in M16+FBS (*477*). Blastocysts, mid-gestation embryos and placentas derived from superovulated oocytes developing *in vivo* have a modest partial loss of imprinting at the *Snrpn* and *H19* loci (*478, 479*). Both biallelic expression and loss of DMD methylation is greater in the placental compartment than in the embryo proper (*478*). Superovulated oocytes harbor normal imprinted DMD methylation ruling out superovulation induced effects on the establishment of imprints (*480*). Imprinted genes are overrepresented in those transcripts whose expression is increased or decreased more than 2-fold in placentas derived from *in vitro* fertilized superovulated oocytes (*481*). These results taken together suggest that environmental influences subject the early embryo to loss of imprinting during preimplantation development and that the maintenance of imprints is less robust in the TE than the ICM. It would certainly be of interest to determine the amount of DNMT1o present in superovulated oocytes and its activity in preimplantation *in vitro* culture.

Reconstitution of an enucleated oocyte with a donor nucleus (either ES or somatic cell) reformats the epigenetic state of the donor genome to one that emulates a nascent zygote in a process known as “reprograming” (*482, 483*). Cloning by nuclear transfer is an inefficient process (*484*). Only10-20% of ES cell nuclear donors and 50-70% of somatic cell nuclear donors mature into blastocysts (*484*). Of uterine transferred blastocysts 5-20% of ES nuclear donor and 1-3% of somatic nuclear donors survive to term and even fewer to adulthood (*484*). The majority of clones develop abnormally with fetal and placental overgrowth concomitant with altered imprinted gene expression and DMD methylation (*484-487*). Cloned placentas are overgrown almost 2-fold, have an expanded JZ enriched with GCs with SpT extensions into the LZ, have enlarged TGCs and a disorganized LZ (*488*). ESCs cultured from SCNT derived blastocysts are

epigentically equivalent to naturally fertilized blastocyst derived ESCs and can produce all fetal lineages when complemented with tetraploid TE further suggesting that extraembryonic development is the limiting factor in reproductive cloning (*489, 490*). The similarities between cloned mice and the JZ and GC expansions I observed in late gestation DNMT1o-deficient placentas is striking.

My results also showed a disruption of E/P ratio and a general overgrowth of DNMT1o-deficient placentas and fetuses surviving to late gestation which mirrors the findings in cloned animals and suggest that abnormal maintenance of imprints during preimplantation may be the central cause of cloning developmental failures. The work on reproductive cloning has implications for the large offspring syndrome observed in cloned livestock and in conservation efforts to restore native fauna and endangered species (*491, 492*). Interestingly, SCNT porcine embryos undergo replication dependent preimplantation partial demethylation of the *H19* DMD (*493*). Because this demethylation occurs during the first two cell cycles and is mimicked by *DNMT1* GV oocyte RNAi injection it implies that maternal DNMT1s activity is decreased in SCNT embryos (*493*). The above results taken together indicate that it is critical for reproductive biologists to better understand the details of maintenance methyltransferase activity in preimplantation development to improve the safety and efficacy of clinical ART and animal cloning. It would be insightful to determine if DNMT1o activity is altered in ART or nuclear transfer in mice, and whether ART or oocyte reconstitution can modulate the $Dnmt1^{\Delta 1o}$ maternal effect.

Reprogramming of somatic nuclei can also be carried out by transfection of the 4 Yamanaka pluripotency factors (*Oct3/4*, *c-Myc*, *Sox2* and *Klf4*) (*494*). A small percentage of these induced pluripotent stem (iPSCs) cells can generate high percentage chimerism when

injected into blastocysts and yield all iPSC pups from tetraploid TE complementation (*495, 496*). The most prominent transcriptional difference between iPSCs incapable of generating all iPSC pups via tetraploid complementation and genetically identical ESCs is found in the expression levels of maternally expressed *Meg3* and *Rian* transcripts within the *Dlk1* imprinting cluster (*380, 381*). Biallelic *Dlk1* DMD methylation represses maternal ncRNA transcription in these iPSCs (*380, 381*). However, the subset of iPSCs that are competent to generate chimeras and all iPSC tetraploid complemented offspring have normal monoallelic methylation and *Meg3* expression (*380, 381*). The incompetent iPSCs can be made to generate all iPSC offspring by the addition of the HDAC inhibitor valproic acid (*381*). Lastly, the addition of ascorbic acid (vitamin C), a potent histone methyltranferase and TET enzyme cofactor, during iPSC induction prevents *Dlk1* DMD hypermethylation and yields developmentally competent iPSCs (*497*). The fact that the *Dlk1* DMD becomes biallecially methylated during iPSC reprogramming suggests that there are molecular mechanisms during *in vivo* reprogramming that prevent *de novo* methylation at this locus. My results that *Dlk1* DMD methylation is invariable in DNMT1o-deficient placentas is in line with these findings and suggests an early selection against loss or gain of methylation at the *Dlk1* DMD (Figures 32O and 32P). Furthermore, parthenogenetic development can be induced with inheritance of one allele of Dlk1 and *H19* DMD deletion (both of which mimic the paternal imprinted state). I interpret these results to suggest that paternal imprints are required for embryonic development and as supporting evidence to the ovarian bomb theory.

The limited developmental potential of SCNT and iPSCs is perhaps not surprising given that ES cells themselves, particularly inbred and long term passaged lines, are restricted in their fetal chimera contribution when injected into host blastocysts or complemented with tetrapoloid TE (*484, 498, 499*). Mice derived from ES cells are often overgrown and riddled with epigenetic

defects including at imprinted loci (*498*, *499*). Clearly these results suggest that the maintenance of genomic imprints during reprogramming is a requirement for full embryonic developmental potential. It would be interesting to determine the extraembryonic developmental potential of ES, SCNT and iPSCs with imprinting defects that have been transformed via iRas to a TSC like state.

5.2.5 Mechanisms of imprinting

There are a number of unresolved issues regarding the molecular mechanisms involved in the maintenance of genomic imprints during preimplantation development. I have presented a summary of the factors present in the imprinting maintenance machinery including DNMT1, UHRF1, DNMT3, DMAP, ZFP57, TRIM28, and histone modifiers (Section 1.1.2). The maintenance of parent-of-origin specific monoallelic methylation during the dynamic genomic demethylation and remethylation events that occur with preimplantation reprogramming require that imprinted alleles be protected from demethylation and faithfully propagated, and the non-imprinted allele to be resistant to *de novo* methylation. Genetic ablation of the factors involved in these processes effects imprinted DNA methylation. Deletion of either *Zfp57* or *Trim28* results in partial loss of DMD methylation with certain loci more affected than others (*71, 72*, *74*). It is therefore reasonable to hypothesize that different imprinted loci have unique effectors and epigenetic readout, and that some are more robust than others. Furthermore, the maternal-zygotic lethality of compound *Dnmt1*^{v} and *Dmap* null alleles suggests that the interaction between DMAP and maternal DNMT1s is essential for early reprogramming either via maintenance of imprints or the formation of the TIP60 epigenetic complex (*107*). Detailed clarification of the

epigenetic components involved in preimplantation and their interactions although difficult to procure from early embryos will be essential to fully elucidate this process.

The role of ncRNA in the establishment, maintenance and expansion of genomic imprints is also unresolved (*500-502*). The macro long ncRNAs *Kcnq1ot, Airn,* and *Nespas* have been implicated to act *in cis* to silence neighboring genes directly by transcriptional interference and through recruitment of heterochromatin factors including EHMT2 (*500*). The expansion of the *Airn* and *Kcnq1ot* ncRNA spread across chromatin in extraembryonic tissue is one plausible explanation for larger imprinted domains at the *Igf2r* and *Kcnq1* clusters in placenta (*500*). In addition, the ncRNA may function in modulating nuclear architecture and long range chromatin interactions (*437*). Both the *Kcnq1ot* and *Airn* ncRNA are expressed in spermatagonia where the X-chromsome is imprinted via the *Xist* ncRNA and may share a common mechanism in regulation of their promoter (*436*).

Other imprinted ncRNAs like the snoRNAs and miRNAs in the *Snrpn* and *Dlk1* cluster likely function in trans to modulate alternative splicing, mRNA editing and overall gene expression levels of important developmental factors. For example, the miRNAs processed from the extended *Meg3* transcript have are thought to modulate PRC2 components that influence expression of numerous genes (*380*). The snoRNA genes *Snord114* and *Snord116* within the *Snrpn* cluster alter alternative splicing and mediate prominent PWS/AS phenotypes (*324, 325, 464*). The role of snoRNAs derived from *Meg8* within the *Dlk1* cluster nor the role of miRNAs from the same cluster are well defined. The snoRNAs from both the *Dlk1* and *Snrpn* clusters form unique imprinted chromatin architecture in which one allele is transcriptionally active and produces long transcripts that are found at nuclear foci near their respective imprinted domains, that are spliced into snoRNA products and distributed throughout the nucleus (*503*). The *H19*

ncRNA is processed into *Mir675*, a miRNA that influences placental development (*306*). Other ncRNA antisense transcripts including *Peg3as, Mestit,* and *Nespas* are even less studied. Furthermore, the large primate specific C19MC miRNA cluster is imprinted and is involved in placental exosome mediated fetal and maternal immunity (*504, 505*). I conjecture that future research will better define the functional roles of imprinted ncRNAs in health and disease.

5.2.6 Role of the *Kcnq1* cluster in TGC development

One of the major findings in my dissertation was an association between loss of methylation at the *Kcnq1* and *Snrpn* DMDs and accumulation of TGCs (Tables 4 and 5; Figures 36G and 36H). The TGC accumulation phenotype mimicked the *Dnmt3l* maternal effect and *Ascl2* targeted deletion models suggesting that loss of *Aslc2* expression in trophoblast is the underlying cause. In humans, *Ascl2* is expressed highly by intervillous and extravillous trophoblast but is not imprinted (*506, 507*). Complete hydatidiform molar pregnancies (which have a diploid paternally inherited genome) that are noninvasive do not express *ASCL2*, whereas invasive complete hydatidiform molar pregnancies do express *ASCL2* (*506*). Although the lack of *ASCL2* expression in the noninvasive molar pregnancies suggests paternal imprinting, it is more likely due to the predominance of microvillous-like cysts containing SynT and villous cytotrophoblast and the lack of extravillous cytotrophoblast which do not express *ASCL2*. The expression of *ASCL2* in intervillous cytotrophoblast is congruent with *Ascl2* expression in murine SpT, where it acts to repress TGC differentiation, but its expression in extravillous cytotrophoblst seems contradictory given their similar to TGCs. It would be interesting to determine if *ASCL2* is absent from more specialized endovascular extravillous cytotrophoblast subtypes.

Other members of the *KCNQ1* imprinted cluster that are imprinted in mouse extraembryonic lineages are not imprinted in humans including *CD81, TSSC4, NAP1/4* and *CARS* (*383*). However, *CDKN1C* and *PHLDA2* that are closer to the *KCNQ1* imprinting center are ubiquitously imprinted in human and are normally expressed in various cytotrophoblast lineages (*383, 508, 509*). In complete hydatidiform moles neither *CDKN1C* nor *PHLDA2* are not expressed (*508, 509*). Their expression is also limited in incomplete hydatidiform moles (triploid with diploid paternal and haploid maternal chromosome set) due to the single active maternal allele (*508, 509*). Although these correlative results suggest a possible role in molar pregnancies more profound evidence would be needed to rule out coincidental or passive associations. Many of the DNMT1o-deficient placentas collected at E9.5 presented hydatidiform molar-like cysts when viewed under the dissecting microscope (data not shown). I suspect that these may have been similar to the samples with expanded TGCs and flattened labyrinths, and diminish *Ascl2* and *Phlda2* expression (Figure 4). Based on the E9.5 DNMT1o-deficient phenotypes and the E12.5 associations between loss of *Kcnq1* DMD methylation and TGC accumulation along with the above hydatidiform molar molecular imprinting abnormalities I infer that loss of the *KCNQ1* imprint contributes to hydatidiform molar pregnancies.

The role of P-TGCs in mouse placenta development is to form a protective barrier between maternal endometrium and produce placental hormones (*231, 232*). Specifically, TGCs secrete choriogonadotropin hormone and the related family of prolactins (*225, 227*). In rodents this family of hormones has grown to include of 23 members in a large cluster and 3 additional members in a smaller cluster on mouse chromosome 13qA1 (*225, 227, 236*). While humans have a more limited set of prolactins their function in placenta development are poorly understood. The extravillous cytotrophoblast are similar to mouse TGCs and are polypoloid, but not to the

same extent as TGCs. Extravillous cytotrophoblast are however more invasive than their mouse counterparts extending into and taking up residence in the myometrium where they integrate into the maternal vascular system (*177*). Most studies on extravillous trophoblast have focused on their angiogenic and vascular remodeling properties in health and disease (*e.g*. PE). I think there may be crucial insights to be gained by studying their proliferation and secretion in loss of imprinting disorders. Given that placentomegaly is a common feature of BWS it would be pertinent to examine BWS associated placentas with loss of IC1 loss of methylation for extravillous cytotrophoblast numbers and examine whether *Ascl2* expression is disrupted.

5.2.7 Role of the *Peg10* cluster in labyrinth development and fetal viability

My regression studies revealed associations between loss of the maternal *Peg10* imprint and diminished labyrinth development and embryonic lethality at E12.5 (Table 4; Figure 36E). While deletion of *Peg10* results in similar neonatal lethality, loss of methylation is expected to lead to biallelic transcription of *Peg10* and *Sgce* and suppression of paternal *Pon2*, *Pon3* and *Ppp1r9a* transcription (*288*, *293*). In fact, I found that *Pon2* was significantly down regulated at E9.5 (Figure 28). The study of commercially available *Pon2, Pon3*, and *Ppp1r9a* targeted deletion mouse models for placental phenotypes may be informative. I also suggest the generation of a *Peg10* DMD deletion model which would likely replicate the imprinted allele due to the deletion of *Peg10* and *Sgce* promoter elements, and phenocopy embryonic lethality in the paternal *Peg10* null and 6q bimaternal translocation models. The *Peg10* DMD deletion may also reveal additional phenotypes from biallelic expression of maternally expressed genes in this cluster, particularly if crossed with a single copy *Peg10* transgene to rescue early lethality. Transgenic overexpression of *Peg10* and *Sgce* could mimic the loss of *Peg10* DMD methylation phenotypes

observed in DNMT1o-deficient placentas and would be worthwhile to pursue. Lastly it has been presented in the literature that the *Peg10* DMD regulates an expanded set of imprinted genes in extraembryonic tissues including *Ppp19ra,* and possibly other genes (*e.g. Dlx5*, *Calcr* and *Asb4*), therefore it is imperative to determine the exact boundaries of the *Peg10* imprinted cluster in mouse placenta (*263, 510*). This could be done by examining expression of genes in proximity of *Peg10* in DNMT1o-deficient E9.5 placentas with near complete loss of *Peg10* DMD methylation.

5.2.8 Identification of KLF14 transcriptional targets in mouse.

My results in Chapter 4 show that *Klf14* is an imprinted negative regulator of placental growth and that its deletion results in a significant increase in placental weight. It is important to determine what transcriptional targets are regulated by *Klf14* during placental development. To these ends I am currently working on comparing the genome-wide gene expression profiles of *Klf14* homozygous null and wild-type littermate placentas derived from heterozygous null intercrosses. Once significantly altered genes are identified I will test for enrichment of gene ontology pathways. I will also examine the promoters of up and down regulated genes for the presence of CACCC KLF14 DNA-binding sequence motifs. Transcriptional targets could be confirmed using luciferase reporter assays in trophoblast stem cells co-transfected with *Klf14* and luciferase reporters driven by the promoter of putative KLF14 targets. Additionally, it would be of interest to examine the presence of the KLF14 interacting partners SIN3A and p300 as well as various histone modification at target genes of interest in homozygous null and wild-type placentas using chromatin immunoprecipitation. These experiments should further reveal the functional role of *Klf14* in placental development.

During my thesis research I was unable to determine where in the placenta *Klf14* is expressed. It has been reported that *Klf14* is present in the placental labyrinth, which is an amalgam of trophoblast and fetal derived cells. I attempted to use commercially available polyclonal antibodies to identify KLF14 localization by immunofluorescence to no avail (data not shown). I had mixed results using these antibodies in western blotting as well (data not shown). Here I propose three different experiments to determine whether *Klf14* is expressed in trophoblast or fetal derived labyrinth cells. Heterozygous $Klf14^{flox}$ females could be crossed to male *Sox2:CRE* transgenics to generate epiblast specific *Klf14* maternal null conceptuses. If the fetal vascular endothelial cells in the labyrinth are the only cell type that express *Klf14* then fetuses that are heterozygous *Klf14* null would lack placental *Klf14* expression. Additionally, I could generate a trophoblast specific conditional deletion by crossing heterozygous $Klf14^{flox}$ females with *Cyp19*, *Tpbpa*, or *Gcm1* driven *CRE* transgenic males to generate ubiquitous trophoblast specific deletion or targeted deletion within SpT or SynT layer II respectively (*511*). A second method to generate trophoblast specific null mice is through the use of peripheral blastocyst lentiviral CRE infection (a new technique that specifically targets the mural and polar TE at the blastocyst stage) (*512*). Finally, I could attempt to isolate either SynT or fetal endothelial cells by using various cell capture methods (*ie.* antigen specific magnetic bead capture, or flow cytometry) and examine *Klf14* expression.

I also propose the construction of additional models to determine the role of the *Mest* imprinting cluster at large within the placenta. I think it would of interest to attempt to develop a *Klf14* transgenic overexpression model, although this may be difficult given the mitotic catastrophe revealed in HeLa cell *Klf14* overexpression (*434*). Engineering a targeted *Mest* DMD deletion model, while complicated due to the overlap with exon 1 and intron 1, would be

expected to generate an allele that replicates the methylated maternal allele. Paternal inheritance of a *Mest* DMD null might influence fetal and placental growth given the expected decrease in *Mest* expression and increase in *Klf14*. It is also important to define the function of MEST using biochemical *in vitro* experiments to determine putative hydrolase substrates. A *Mest* overexpression transgenic model may recapitulate the DNMT1o-deficient placental lipid accumulation phenotype and be insightful to determine causative mechanisms in a less heterogenous model. It would also be of particular interest to delete the placenta specific *Mest* promoter and/or exon and investigate whether placenta and/or fetal growth restriction still occurs similarly to the constitutive deletion. Each of these models suggested here could also be fed HFD to see whether metabolic phenotypes can be induced. Although I have focused on placental biology, it is likely that the *Mest* imprinting cluster has important roles in other organs.

5.3 CONCLUDING REMARKS

In conclusion, I have surveyed the placental morphological and epigenetic abnormalities in DNMT1o-deficient placentas and revealed unique roles for the *Kcnq1*, *Peg10* and *Mest* imprinting clusters. My work to generate and study a targeted deletion of *Klf14* has demonstrated a role for it in regulating placental growth. These findings add to the growing body of evidence that genomic imprints are vital for placental development. I hope that my dissertation research has added to our understanding of the mammalian genome. I look forward to further investigations by myself and others that resolve the functional roles and mechanisms involving the phenomenon known as genomic imprinting.

APPENDIX A

Primer Name	Primer Sequence
***Dnmt1o* Genotyping**	
Egg6	AGGAAAACAGTGGAGGAAC
Egg7	TACTTTGCACAGGGCTGTCCT
Sex Genotyping	
ZFYfwd	CCTATTGCATGGACAGCAGCTTATG
ZFYrev	GACTAGACATGTCTTAACATCTGTCC
***Sox2:CRE* Genotyping**	
SOX2fwd	AGGTGTAGAGAAGGCACTTAGC
SOX2rev	CTAATCGCCATCTTCCAGCAGG
***Klf14* Genotyping**	
HB3fwd	CTGCTCTTCCTTTCCTCACT
HB4rev	GAGAGACTTTTCTTCGCAGC
HB6rev	TGATTAGGAGGGGGAAAACAC

APPENDIX B

Primer Name	Primer Sequence	
qPCR		
Peg10	TGCTTGCACAGAGCTACAGTC	CTGAATCCAGCCATGTGGTAGA
Sgce	CGGATTCTTTGAAAAGCCGAGA	GTCTGTGTGCATGGGAGGTAT
Pon2	GCTCTGAGTTTGCTGGGCAT	GGCAGTTTGGAAGGTCTACAGAT
Dlk1	GGAACCATGGCAGTGCATCT	CGAACGTCTATTTCGCAGAATTT
Meg3	TCCTCACCTCCAATTTCCCCT	GAGCGAGAGCCGTTCGATG
Rtl1	CCTGTGCCAGGGGCTCAACG	CTTGGGCGCGACTCAGGTGG
Igf2	GTGCTGCATCGCTGCTTAC	ACGTCCCTCTCGGACTTGG
H19	GAACAGAAGCATTCTAGGCTGG	TTCTAAGTGAATTACGGTGGGTG
Igf2r	AGCCTCGGCAGATTTATTTT	CCCCATTGGTCCTCATGTCT
Slc22a2	GAACGCTGAGCTGTACCCTACA	GGGCAGAGCACACCATCAT
Mest	TCTCCAAAAGCTCCTCAAAG	ATGAATGGGGATGGACACAG
Klf14	CTCCGTGTGCCTCAACTAGC	CAGGCGCATCCAGGATAGC
Phlda2	CTCCGACGAGATCCTTTGCG	ACACGTACTTAGAGGTGTGCTC
Ascl2	AAGCACACCTTGACTGGTACG	AAGTGGACGTTTGCACCTTCA
Grb10	CCTGCCAAGCATGATGTCAAA	CCAGGCACCTCTCTAATCCCA
RT-PCR		
Klf14	TGGACACCCTCTCCAAAGTC	AAGCGACATCAGTGCTCCTT-

APPENDIX C

Primer Name	Primer Sequence	
Bisulfite Genomic Sequencing (nested)		
H19_R1	GAGTATTTAGGAGGTATAAGAATT	ATCAAAAACTAACATAAACCCT
H19_R2	GTAAGGAGATTATGTTTATTTTTG	CCTCATTAATCCCATAACTAT
Kcnq_R1	GGTTTAAAGGGTTTTAAGATTATTTTTG	CTTCTTTTCCCTCTATAsTAATTCTAC
Kcnq_R2	GTTTTTGTAAGTTTGGGTTATAAAG	AACTTTTCTATTCAACTTAATTCCC
Snrpn_R1	TATGTAATATGATATAGTTTAGAAATTAG	AATAAACCCAAATCTAAAATATTTTAATC
Snrpn_R2	AATTTGTGTGATGTTTGTAATTATTTGG	ATAAAATACACTTTCACTACTAAAATCC
Mest_R1	GATTTGGGATATAAAAGGTTAATGAG	TCATTAAAAACACAAACCTCCTTTAC
Mest_R2	TTTTAGATTTTGAGGGTTTTAGGTTG	AATCCCTTAAAAATCATCTTTCACAC

APPENDIX D

Primer Name	**Primer Sequence for EpiTYPER Mass Array**		
Primer 5′ tag			
	5' FWD Tag	AGGAAGAGAG	
	5' REV Tag (T7)	CAGTAATACGACTCACTATAGGGAGAAGGCT	
Imprinted gDMR		**Sequence (5' to 3')**	**Genomic Coordinates (GRCm38)**
Dlk1.A	FWD	ATAGTATTGGTTTGGTATATATGGATG	12:109527424-109527853
	REV	CCATAACATAAACATAAAAATCCACAA	
Dlk1.B	FWD	GATGTGTTGTGGATTTAGGTTGTAG	12:109528138-109528138
	REV	ATCCCCTATACTCAAAACATTCTCC	
Grb10	FWD	AGGAGTTGTTTATTATTTGGATTATTGT	11:12025702-12026046
	REV	CTCTAAACTCCAAAACCCTTTTTCT	
H19(*)	FWD	GTTGATGGTTTTAGAATTTTATAAGTTAG	7:142581609-142581931
	REV	CACAATACCACTAAAAAAACAAAACA	
Igf2r	FWD	GATAGGAGGATTTAGAGGGTTTTGT	17:12742752-12743024
	REV	AACCCCATTATCTACAACTCAAACA	
Impact.A	FWD	TTTGTATTAAGTAGGTTGTTTTAGGG	18:12972913-12973111
	REV	ACAACCAAACTAAAATTAACCAAACAA	
Impact.B	FWD	TTGTTTGGTTAATTTTAGTTTGGTT	18:12973084-12973497
	REV	TCATATAACAATACAACAAAACCTACTC	
Kcnq1	FWD	TGGAGAGTTTTTTTGTTTAGTTTGG	7:150481809 -150481430
	REV	CAAAACCACCCCTACTTCTATAAAC	
Nespas.A	FWD	TGGGGGTTTTTGATTTTTTTATTTTG	2:174295281-174295599
	REV	TAAATCTCAACCACTAACCCACTCC	
Nespas.B	FWD	TTTTTTTTAGGGTTTTGTAGGTTAGATTTG	2:174295985-174296393
	REV	CCCCTCCTCCTTCTATTATAAACACC	
Mest	FWD	ATATGTTGGGGAGGGATTTTTTTAG	6:30737763-30738178
	REV	CAACAAAAACAACAAACAACAACTC	
Peg3	FWD	GATTTTGTTTGGGGGTTTTTAATATTGAT	7:6683342 -6683054
	REV	CCACCAACCCAAAATAAACATCTCT	
Plagl1	FWD	TATTTTTGTGGGGATGGAGGAATTA	10:13090467-13090791

	REV	ATCCCAACCCAAACTAAATAACAAA	
Peg10	FWD	TTAGGATTTGGTTATTGAAGGTTTG	6:4697732 -4697319
	REV	CCCCTCCTAAAATCTCTCTATATAAAAC	
Snrpn	FWD	TGTGATGTTTGTAATTATTTGGGAG	7:67150146 -67149901
	REV	CTAAAATCCACAAACCCAACTAACC	
Nnat	FWD	TTTAGGTGGTAAGAGGGTATTTAAGG	2:157560062-157560273
	REV	AATACATACTCACCTACAACAACAC	
Nap1l5	FWD	AGTTTGGAATTTTTTGTTAAATTTGG	6:58906694-58907060
	REV	CAACTACAAAACCTCTCTAAACCAAC	
Zrsr1	FWD	GGTAAGGTAGATAATTATTGTTTTAGTTGT	11:22972131-22972559
	REV	CATAAACCTACCCATACAATTACCC	

(*) From McGraw et al (2013)

BIBLIOGRAPHY

1. S. C. Barton, M. A. Surani, M. L. Norris, Role of paternal and maternal genomes in mouse development. *Nature* **311**, 374-376 (1984).

2. M. A. Surani, S. C. Barton, M. L. Norris, Development of reconstituted mouse eggs suggests imprinting of the genome during gametogenesis. *Nature* **308**, 548-550 (1984).

3. M. A. Surani, S. C. Barton, M. L. Norris, Nuclear transplantation in the mouse: heritable differences between parental genomes after activation of the embryonic genome. *Cell* **45**, 127-136 (1986).

4. J. McGrath, D. Solter, Completion of mouse embryogenesis requires both the maternal and paternal genomes. *Cell* **37**, 179-183 (1984).

5. M. H. Kaufman, S. C. Barton, M. A. Surani, Normal postimplantation development of mouse parthenogenetic embryos to the forelimb bud stage. *Nature* **265**, 53-55 (1977).

6. C. L. Markert, Parthenogenesis, homozygosity, and cloning in mammals. *J Hered* **73**, 390-397 (1982).

7. M. A. Surani, S. C. Barton, Development of gynogenetic eggs in the mouse: implications for parthenogenetic embryos. *Science* **222**, 1034-1036 (1983).

8. T. Kajii, K. Ohama, Androgenetic origin of hydatidiform mole. *Nature* **268**, 633-634 (1977).

9. K. Ohama *et al.*, Dispermic origin of XY hydatidiform moles. *Nature* **292**, 551-552 (1981).

10. B. M. Cattanach, Parental origin effects in mice. *Journal of embryology and experimental morphology* **97 Suppl**, 137-150 (1986).

11. A. G. Searle, C. V. Beechey, Complementation studies with mouse translocations. *Cytogenet Cell Genet* **20**, 282-303 (1978).

12. B. M. Cattanach, M. Kirk, Differential activity of maternally and paternally derived chromosome regions in mice. *Nature* **315**, 496-498 (1985).

13. A. G. Searle, C. V. Beechey, The use of Robertsonian translocations in the mouse for studies on non-disjunction. *Cytogenet Cell Genet* **33**, 81-87 (1982).

14. B. M. Cattanach, C. V. Beechey, Autosomal and X-chromosome imprinting. *Development*, 63-72 (1990).

15. B. M. Cattanach, M. D. Burtenshaw, C. Rasberry, E. P. Evans, Large deletions and other gross forms of chromosome imbalance compatible with viability and fertility in the mouse. *Nature genetics* **3**, 56-61 (1993).

16. M. A. Surani, W. Reik, M. L. Norris, S. C. Barton, Influence of germline modifications of homologous chromosomes on mouse development. *Journal of embryology and experimental morphology* **97 Suppl**, 123-136 (1986).

17. J. R. Chaillet, D. S. Bader, P. Leder, Regulation of genomic imprinting by gametic and embryonic processes. *Genes Dev* **9**, 1177-1187 (1995).

18. J. R. Chaillet, T. F. Vogt, D. R. Beier, P. Leder, Parental-specific methylation of an imprinted transgene is established during gametogenesis and progressively changes during embryogenesis. *Cell* **66**, 77-83 (1991).

19. W. Reik, A. Collick, M. L. Norris, S. C. Barton, M. A. Surani, Genomic imprinting determines methylation of parental alleles in transgenic mice. *Nature* **328**, 248-251 (1987).

20. C. Sapienza, J. Paquette, T. H. Tran, A. Peterson, Epigenetic and genetic factors affect transgene methylation imprinting. *Development* **107**, 165-168 (1989).

21. H. Sasaki *et al.*, Inherited type of allelic methylation variations in a mouse chromosome region where an integrated transgene shows methylation imprinting. *Development* **111**, 573-581 (1991).

22. J. L. Swain, T. A. Stewart, P. Leder, Parental legacy determines methylation and expression of an autosomal transgene: a molecular mechanism for parental imprinting. *Cell* **50**, 719-727 (1987).

23. C. Williamson, Blake A, Thomas S, Beechey CV, Hancock J, Cattanach BM, Peters J. . (MRC Harwell, Oxfordshire, 2013).

24. B. Reinhart, J. R. Chaillet, Genomic imprinting: cis-acting sequences and regional control. *Int Rev Cytol* **243**, 173-213 (2005).

25. B. Reinhart, A. Paoloni-Giacobino, J. R. Chaillet, Specific differentially methylated domain sequences direct the maintenance of methylation at imprinted genes. *Mol Cell Biol* **26**, 8347-8356 (2006).

26. W. A. MacDonald, M. R. Mann, Epigenetic regulation of genomic imprinting from germ line to preimplantation. *Mol Reprod Dev* **81**, 126-140 (2014).

27. T. H. Bestor, The DNA methyltransferases of mammals. *Hum Mol Genet* **9**, 2395-2402 (2000).

28. A. Bird, DNA methylation patterns and epigenetic memory. *Genes Dev* **16**, 6-21 (2002).

29. M. Monk, M. Boubelik, S. Lehnert, Temporal and regional changes in DNA methylation in the embryonic, extraembryonic and germ cell lineages during mouse embryo development. *Development* **99**, 371-382 (1987).

30. Z. D. Smith *et al.*, A unique regulatory phase of DNA methylation in the early mammalian embryo. *Nature* **484**, 339-344 (2012).

31. T. H. Bestor, J. R. Edwards, M. Boulard, Notes on the role of dynamic DNA methylation in mammalian development. *Proc Natl Acad Sci U S A* **112**, 6796-6799 (2015).

32. S. A. Smallwood *et al.*, Dynamic CpG island methylation landscape in oocytes and preimplantation embryos. *Nature genetics* **43**, 811-814 (2011).

33. M. M. Suzuki, A. Bird, DNA methylation landscapes: provocative insights from epigenomics. *Nat Rev Genet* **9**, 465-476 (2008).

34. C. P. Walsh, J. R. Chaillet, T. H. Bestor, Transcription of IAP endogenous retroviruses is constrained by cytosine methylation. *Nature genetics* **20**, 116-117 (1998).

35. J. A. Yoder, C. P. Walsh, T. H. Bestor, Cytosine methylation and the ecology of intragenomic parasites. *Trends Genet* **13**, 335-340 (1997).

36. A. M. Deaton, A. Bird, CpG islands and the regulation of transcription. *Genes Dev* **25**, 1010-1022 (2011).

37. S. Augui, E. P. Nora, E. Heard, Regulation of X-chromosome inactivation by the X-inactivation centre. *Nat Rev Genet* **12**, 429-442 (2011).

38. D. P. Barlow, M. S. Bartolomei, Genomic imprinting in mammals. *Cold Spring Harb Perspect Biol* **6**, (2014).

39. D. N. Ciccone *et al.*, KDM1B is a histone H3K4 demethylase required to establish maternal genomic imprints. *Nature* **461**, 415-U115 (2009).

40. D. Leung *et al.*, Regulation of DNA methylation turnover at LTR retrotransposons and imprinted loci by the histone methyltransferase Setdb1. *P Natl Acad Sci USA* **111**, 6690-6695 (2014).

41. Z. X. Chen, A. D. Riggs, DNA methylation and demethylation in mammals. *J Biol Chem* **286**, 18347-18353 (2011).

42. K. Williams, J. Christensen, K. Helin, DNA methylation: TET proteins-guardians of CpG islands? *EMBO Rep* **13**, 28-35 (2012).

43. M. Ginsburg, M. H. Snow, A. McLaren, Primordial germ cells in the mouse embryo during gastrulation. *Development* **110**, 521-528 (1990).

44. A. McLaren, Primordial germ cells in the mouse. *Dev Biol* **262**, 1-15 (2003).

45. P. Hajkova *et al.*, Epigenetic reprogramming in mouse primordial germ cells. *Mech Dev* **117**, 15-23 (2002).

46. B. J. Lesch, D. C. Page, Genetics of germ cell development. *Nat Rev Genet* **13**, 781-794 (2012).

47. M. Saitou, S. C. Barton, M. A. Surani, A molecular programme for the specification of germ cell fate in mice. *Nature* **418**, 293-300 (2002).

48. P. Hajkova *et al.*, Genome-wide reprogramming in the mouse germ line entails the base excision repair pathway. *Science* **329**, 78-82 (2010).

49. C. Popp *et al.*, Genome-wide erasure of DNA methylation in mouse primordial germ cells is affected by AID deficiency. *Nature* **463**, 1101-1105 (2010).

50. Y. F. He *et al.*, Tet-mediated formation of 5-carboxylcytosine and its excision by TDG in mammalian DNA. *Science* **333**, 1303-1307 (2011).

51. S. Ito *et al.*, Tet proteins can convert 5-methylcytosine to 5-formylcytosine and 5-carboxylcytosine. *Science* **333**, 1300-1303 (2011).

52. M. Tahiliani *et al.*, Conversion of 5-methylcytosine to 5-hydroxymethylcytosine in mammalian DNA by MLL partner TET1. *Science* **324**, 930-935 (2009).

53. J. M. Trasler, Gamete imprinting: setting epigenetic patterns for the next generation. *Reprod Fertil Dev* **18**, 63-69 (2006).

54. T. L. Davis, J. M. Trasler, S. B. Moss, G. J. Yang, M. S. Bartolomei, Acquisition of the H19 methylation imprint occurs differentially on the parental alleles during spermatogenesis. *Genomics* **58**, 18-28 (1999).

55. C. C. Oakes, S. La Salle, D. J. Smiraglia, B. Robaire, J. M. Trasler, Developmental acquisition of genome-wide DNA methylation occurs prior to meiosis in male germ cells. *Dev Biol* **307**, 368-379 (2007).

56. D. Lucifero, C. Mertineit, H. J. Clarke, T. H. Bestor, J. M. Trasler, Methylation dynamics of imprinted genes in mouse germ cells. *Genomics* **79**, 530-538 (2002).

57. S. K. Howlett, W. Reik, Methylation levels of maternal and paternal genomes during preimplantation development. *Development* **113**, 119-127 (1991).

58. S. Tomizawa *et al.*, Dynamic stage-specific changes in imprinted differentially methylated regions during early mammalian development and prevalence of non-CpG methylation in oocytes. *Development* **138**, 811-820 (2011).

59. H. Kobayashi *et al.*, Contribution of intragenic DNA methylation in mouse gametic DNA methylomes to establish oocyte-specific heritable marks. *PLoS Genet* **8**, e1002440 (2012).

60. M. C. Cirio *et al.*, Preimplantation expression of the somatic form of Dnmt1 suggests a role in the inheritance of genomic imprints. *BMC Dev Biol* **8**, 9 (2008).

61. R. Hirasawa *et al.*, Maternal and zygotic Dnmt1 are necessary and sufficient for the maintenance of DNA methylation imprints during preimplantation development. *Genes Dev* **22**, 1607-1616 (2008).

62. C. Mertineit *et al.*, Sex-specific exons control DNA methyltransferase in mammalian germ cells. *Development* **125**, 889-897 (1998).

63. S. Ratnam *et al.*, Dynamics of Dnmt1 methyltransferase expression and intracellular localization during oogenesis and preimplantation development. *Dev Biol* **245**, 304-314 (2002).

64. S. Gkountela, A. T. Clark, A big surprise in the little zygote: the curious business of losing methylated cytosines. *Cell Stem Cell* **15**, 393-394 (2014).

65. M. Wossidlo *et al.*, 5-Hydroxymethylcytosine in the mammalian zygote is linked with epigenetic reprogramming. *Nat Commun* **2**, 241 (2011).

66. K. Iqbal, S. G. Jin, G. P. Pfeifer, P. E. Szabo, Reprogramming of the paternal genome upon fertilization involves genome-wide oxidation of 5-methylcytosine. *Proc Natl Acad Sci U S A* **108**, 3642-3647 (2011).

67. F. Guo *et al.*, Active and passive demethylation of male and female pronuclear DNA in the mammalian zygote. *Cell Stem Cell* **15**, 447-458 (2014).

68. L. Shen *et al.*, Tet3 and DNA replication mediate demethylation of both the maternal and paternal genomes in mouse zygotes. *Cell Stem Cell* **15**, 459-470 (2014).

69. T. Nakamura *et al.*, PGC7/Stella protects against DNA demethylation in early embryogenesis. *Nat Cell Biol* **9**, 64-71 (2007).

70. T. Nakamura *et al.*, PGC7 binds histone H3K9me2 to protect against conversion of 5mC to 5hmC in early embryos. *Nature* **486**, 415-419 (2012).

71. R. Hirasawa, R. Feil, A KRAB domain zinc finger protein in imprinting and disease. *Dev Cell* **15**, 487-488 (2008).

72. X. Li *et al.*, A maternal-zygotic effect gene, Zfp57, maintains both maternal and paternal imprints. *Dev Cell* **15**, 547-557 (2008).

73. Y. Liu, H. Toh, H. Sasaki, X. Zhang, X. Cheng, An atomic model of Zfp57 recognition of CpG methylation within a specific DNA sequence. *Genes Dev* **26**, 2374-2379 (2012).

74. D. M. Messerschmidt *et al.*, Trim28 is required for epigenetic stability during mouse oocyte to embryo transition. *Science* **335**, 1499-1502 (2012).

75. S. Quenneville *et al.*, In embryonic stem cells, ZFP57/KAP1 recognize a methylated hexanucleotide to affect chromatin and DNA methylation of imprinting control regions. *Mol Cell* **44**, 361-372 (2011).

76. X. Zuo *et al.*, Zinc finger protein ZFP57 requires its co-factor to recruit DNA methyltransferases and maintains DNA methylation imprint in embryonic stem cells via its transcriptional repression domain. *J Biol Chem* **287**, 2107-2118 (2012).

77. P. Hajkova, Epigenetic reprogramming--taking a lesson from the embryo. *Curr Opin Cell Biol* **22**, 342-350 (2010).

78. Z. D. Smith, A. Meissner, DNA methylation: roles in mammalian development. *Nat Rev Genet* **14**, 204-220 (2013).

79. H. D. Morgan, F. Santos, K. Green, W. Dean, W. Reik, Epigenetic reprogramming in mammals. *Hum Mol Genet* **14 Spec No 1**, R47-58 (2005).

80. J. Borgel *et al.*, Targets and dynamics of promoter DNA methylation during early mouse development. *Nature genetics* **42**, 1093-1100 (2010).

81. C. R. Farthing *et al.*, Global mapping of DNA methylation in mouse promoters reveals epigenetic reprogramming of pluripotency genes. *PLoS Genet* **4**, e1000116 (2008).

82. M. G. Goll, T. H. Bestor, Eukaryotic cytosine methyltransferases. *Annu Rev Biochem* **74**, 481-514 (2005).

83. J. Song, O. Rechkoblit, T. H. Bestor, D. J. Patel, Structure of DNMT1-DNA complex reveals a role for autoinhibition in maintenance DNA methylation. *Science* **331**, 1036-1040 (2011).

84. J. Song, M. Teplova, S. Ishibe-Murakami, D. J. Patel, Structure-based mechanistic insights into DNMT1-mediated maintenance DNA methylation. *Science* **335**, 709-712 (2012).

85. K. Takeshita *et al.*, Structural insight into maintenance methylation by mouse DNA methyltransferase 1 (Dnmt1). *Proc Natl Acad Sci U S A* **108**, 9055-9059 (2011).

86. K. Fellinger, U. Rothbauer, M. Felle, G. Langst, H. Leonhardt, Dimerization of DNA methyltransferase 1 is mediated by its regulatory domain. *J Cell Biochem* **106**, 521-528 (2009).

87. Z. X. Chen, J. R. Mann, C. L. Hsieh, A. D. Riggs, F. Chedin, Physical and functional interactions between the human DNMT3L protein and members of the de novo methyltransferase family. *J Cell Biochem* **95**, 902-917 (2005).

88. S. K. Ooi *et al.*, DNMT3L connects unmethylated lysine 4 of histone H3 to de novo methylation of DNA. *Nature* **448**, 714-717 (2007).

89. C. Qiu, K. Sawada, X. Zhang, X. Cheng, The PWWP domain of mammalian DNA methyltransferase Dnmt3b defines a new family of DNA-binding folds. *Nat Struct Biol* **9**, 217-224 (2002).

90. F. Chedin, M. R. Lieber, C. L. Hsieh, The DNA methyltransferase-like protein DNMT3L stimulates de novo methylation by Dnmt3a. *Proc Natl Acad Sci U S A* **99**, 16916-16921 (2002).

91. K. Hata, M. Okano, H. Lei, E. Li, Dnmt3L cooperates with the Dnmt3 family of de novo DNA methyltransferases to establish maternal imprints in mice. *Development* **129**, 1983-1993 (2002).

92. D. Jia, R. Z. Jurkowska, X. Zhang, A. Jeltsch, X. Cheng, Structure of Dnmt3a bound to Dnmt3L suggests a model for de novo DNA methylation. *Nature* **449**, 248-251 (2007).

93. M. Okano, D. W. Bell, D. A. Haber, E. Li, DNA methyltransferases Dnmt3a and Dnmt3b are essential for de novo methylation and mammalian development. *Cell* **99**, 247-257 (1999).

94. D. Bourc'his, G. L. Xu, C. S. Lin, B. Bollman, T. H. Bestor, Dnmt3L and the establishment of maternal genomic imprints. *Science* **294**, 2536-2539 (2001).

95. D. Bourc'his, T. H. Bestor, Meiotic catastrophe and retrotransposon reactivation in male germ cells lacking Dnmt3L. *Nature* **431**, 96-99 (2004).

96. S. La Salle *et al.*, Loss of spermatogonia and wide-spread DNA methylation defects in newborn male mice deficient in DNMT3L. *BMC Dev Biol* **7**, 104 (2007).

97. T. Arima *et al.*, Loss of the maternal imprint in Dnmt3Lmat-/- mice leads to a differentiation defect in the extraembryonic tissue. *Dev Biol* **297**, 361-373 (2006).

98. C. Proudhon *et al.*, Protection against de novo methylation is instrumental in maintaining parent-of-origin methylation inherited from the gametes. *Mol Cell* **47**, 909-920 (2012).

99. R. Schulz *et al.*, The parental non-equivalence of imprinting control regions during mammalian development and evolution. *PLoS Genet* **6**, e1001214 (2010).

100. M. Kaneda *et al.*, Essential role for de novo DNA methyltransferase Dnmt3a in paternal and maternal imprinting. *Nature* **429**, 900-903 (2004).

101. E. Li, T. H. Bestor, R. Jaenisch, Targeted mutation of the DNA methyltransferase gene results in embryonic lethality. *Cell* **69**, 915-926 (1992).

102. E. Li, C. Beard, R. Jaenisch, Role for DNA methylation in genomic imprinting. *Nature* **366**, 362-365 (1993).

103. H. Lei *et al.*, De novo DNA cytosine methyltransferase activities in mouse embryonic stem cells. *Development* **122**, 3195-3205 (1996).

104. C. Y. Howell *et al.*, Genomic imprinting disrupted by a maternal effect mutation in the Dnmt1 gene. *Cell* **104**, 829-838 (2001).

105. M. Toppings *et al.*, Profound phenotypic variation among mice deficient in the maintenance of genomic imprints. *Hum Reprod* **23**, 807-818 (2008).

106. F. Ding, J. R. Chaillet, In vivo stabilization of the Dnmt1 (cytosine-5)-methyltransferase protein. *Proc Natl Acad Sci U S A* **99**, 14861-14866 (2002).

107. K. N. Mohan, F. Ding, J. R. Chaillet, Distinct roles of DMAP1 in mouse development. *Mol Cell Biol* **31**, 1861-1869 (2011).

108. K. L. Tucker *et al.*, Germ-line passage is required for establishment of methylation and expression patterns of imprinted but not of nonimprinted genes. *Genes Dev* **10**, 1008-1020 (1996).

109. K. L. Tucker, D. Talbot, M. A. Lee, H. Leonhardt, R. Jaenisch, Complementation of methylation deficiency in embryonic stem cells by a DNA methyltransferase minigene. *Proc Natl Acad Sci U S A* **93**, 12920-12925 (1996).

110. E. Borowczyk, K. N. Mohan, L. D'Aiuto, M. C. Cirio, J. R. Chaillet, Identification of a region of the DNMT1 methyltransferase that regulates the maintenance of genomic imprints. *Proc Natl Acad Sci U S A* **106**, 20806-20811 (2009).

111. S. McGraw *et al.*, Transient DNMT1 suppression reveals hidden heritable marks in the genome. *Nucleic acids research* **43**, 1485-1497 (2015).

112. B. Shaffer *et al.*, The DNMT1 intrinsically disordered domain regulates genomic methylation during development. *Genetics* **199**, 533-541 (2015).

113. J. H. U. McKusick-Nathans Institue of Genetic Medicine. (Baltimore, MD), vol. 2015.

114. R. Weksberg, C. Shuman, J. B. Beckwith, Beckwith-Wiedemann syndrome. *Eur J Hum Genet* **18**, 8-14 (2010).

115. R. Weksberg, A. C. Smith, J. Squire, P. Sadowski, Beckwith-Wiedemann syndrome demonstrates a role for epigenetic control of normal development. *Hum Mol Genet* **12 Spec No 1**, R61-68 (2003).

116. F. Cerrato *et al.*, The two-domain hypothesis in Beckwith-Wiedemann syndrome: autonomous imprinting of the telomeric domain of the distal chromosome 7 cluster. *Hum Mol Genet* **14**, 503-511 (2005).

117. R. Weksberg, D. R. Shen, Y. L. Fei, Q. L. Song, J. Squire, Disruption of insulin-like growth factor 2 imprinting in Beckwith-Wiedemann syndrome. *Nature genetics* **5**, 143-150 (1993).

118. S. Engemann *et al.*, Sequence and functional comparison in the Beckwith-Wiedemann region: implications for a novel imprinting centre and extended imprinting. *Hum Mol Genet* **9**, 2691-2706 (2000).

119. M. P. Lee, R. J. Hu, L. A. Johnson, A. P. Feinberg, Human KVLQT1 gene shows tissue-specific imprinting and encompasses Beckwith-Wiedemann syndrome chromosomal rearrangements. *Nature genetics* **15**, 181-185 (1997).

120. N. J. Smilinich *et al.*, A maternally methylated CpG island in KvLQT1 is associated with an antisense paternal transcript and loss of imprinting in Beckwith-Wiedemann syndrome. *Proc Natl Acad Sci U S A* **96**, 8064-8069 (1999).

121. R. Weksberg *et al.*, Discordant KCNQ1OT1 imprinting in sets of monozygotic twins discordant for Beckwith-Wiedemann syndrome. *Hum Mol Genet* **11**, 1317-1325 (2002).

122. I. Hatada *et al.*, An imprinted gene p57KIP2 is mutated in Beckwith-Wiedemann syndrome. *Nature genetics* **14**, 171-173 (1996).

123. T. Eggermann *et al.*, Broad clinical spectrum in Silver-Russell syndrome and consequences for genetic testing in growth retardation. *Pediatrics* **123**, e929-931 (2009).

124. S. M. Price, R. Stanhope, C. Garrett, M. A. Preece, R. C. Trembath, The spectrum of Silver-Russell syndrome: a clinical and molecular genetic study and new diagnostic criteria. *Journal of medical genetics* **36**, 837-842 (1999).

125. S. Abu-Amero *et al.*, The genetic aetiology of Silver-Russell syndrome. *Journal of medical genetics* **45**, 193-199 (2008).

126. S. Abu-Amero *et al.*, Epigenetic signatures of Silver-Russell syndrome. *Journal of medical genetics* **47**, 150-154 (2010).

127. T. Eggermann *et al.*, Epigenetic mutations in 11p15 in Silver-Russell syndrome are restricted to the telomeric imprinting domain. *Journal of medical genetics* **43**, 615-616 (2006).

128. A. M. Fisher *et al.*, Duplications of chromosome 11p15 of maternal origin result in a phenotype that includes growth retardation. *Hum Genet* **111**, 290-296 (2002).

129. E. L. Wakeling *et al.*, Epigenotype-phenotype correlations in Silver-Russell syndrome. *Journal of medical genetics* **47**, 760-768 (2010).

130. T. Eggermann, K. Eggermann, N. Schonherr, Growth retardation versus overgrowth: Silver-Russell syndrome is genetically opposite to Beckwith-Wiedemann syndrome. *Trends Genet* **24**, 195-204 (2008).

131. D. Monk *et al.*, Chromosome 7p disruptions in Silver Russell syndrome: delineating an imprinted candidate gene region. *Hum Genet* **111**, 376-387 (2002).

132. D. Monk *et al.*, Duplication of 7p11.2-p13, including GRB10, in Silver-Russell syndrome. *Am J Hum Genet* **66**, 36-46 (2000).

133. K. Hannula, M. Lipsanen-Nyman, T. Kontiokari, J. Kere, A narrow segment of maternal uniparental disomy of chromosome 7q31-qter in Silver-Russell syndrome delimits a candidate gene region. *Am J Hum Genet* **68**, 247-253 (2001).

134. S. Azzi *et al.*, Complex tissue-specific epigenotypes in Russell-Silver Syndrome associated with 11p15 ICR1 hypomethylation. *Hum Mutat* **35**, 1211-1220 (2014).

135. D. J. Mackay *et al.*, Multilocus methylation defects in imprinting disorders. *Biomol Concepts* **6**, 47-57 (2015).

136. K. Buiting, Prader-Willi syndrome and Angelman syndrome. *Am J Med Genet C Semin Med Genet* **154C**, 365-376 (2010).

137. S. B. Cassidy, S. Schwartz, J. L. Miller, D. J. Driscoll, Prader-Willi syndrome. *Genet Med* **14**, 10-26 (2012).

138. S. Malcolm *et al.*, Uniparental paternal disomy in Angelman's syndrome. *Lancet* **337**, 694-697 (1991).

139. R. D. Nicholls, J. H. Knoll, M. G. Butler, S. Karam, M. Lalande, Genetic imprinting suggested by maternal heterodisomy in nondeletion Prader-Willi syndrome. *Nature* **342**, 281-285 (1989).

140. K. Buiting, C. Lich, S. Cottrell, A. Barnicoat, B. Horsthemke, A 5-kb imprinting center deletion in a family with Angelman syndrome reduces the shortest region of deletion overlap to 880 bp. *Hum Genet* **105**, 665-666 (1999).

141. R. D. Nicholls, S. Saitoh, B. Horsthemke, Imprinting in Prader-Willi and Angelman syndromes. *Trends Genet* **14**, 194-200 (1998).

142. T. Ohta *et al.*, Imprinting-mutation mechanisms in Prader-Willi syndrome. *Am J Hum Genet* **64**, 397-413 (1999).

143. S. Saitoh *et al.*, Minimal definition of the imprinting center and fixation of chromosome 15q11-q13 epigenotype by imprinting mutations. *Proc Natl Acad Sci U S A* **93**, 7811-7815 (1996).

144. T. Kishino, M. Lalande, J. Wagstaff, UBE3A/E6-AP mutations cause Angelman syndrome. *Nature genetics* **15**, 70-73 (1997).

145. T. Matsuura *et al.*, De novo truncating mutations in E6-AP ubiquitin-protein ligase gene (UBE3A) in Angelman syndrome. *Nature genetics* **15**, 74-77 (1997).

146. A. J. de Smith *et al.*, A deletion of the HBII-85 class of small nucleolar RNAs (snoRNAs) is associated with hyperphagia, obesity and hypogonadism. *Hum Mol Genet* **18**, 3257-3265 (2009).

147. T. Sahoo *et al.*, Prader-Willi phenotype caused by paternal deficiency for the HBII-85 C/D box small nucleolar RNA cluster. *Nature genetics* **40**, 719-721 (2008).

148. G. Kelsey, Imprinting on chromosome 20: tissue-specific imprinting and imprinting mutations in the GNAS locus. *Am J Med Genet C Semin Med Genet* **154C**, 377-386 (2010).

149. C. M. Williamson *et al.*, Glomerular-specific imprinting of the mouse gsalpha gene: how does this relate to hormone resistance in albright hereditary osteodystrophy? *Genomics* **36**, 280-287 (1996).

150. E. M. Shore *et al.*, Paternally inherited inactivating mutations of the GNAS1 gene in progressive osseous heteroplasia. *N Engl J Med* **346**, 99-106 (2002).

151. J. Liu *et al.*, A GNAS1 imprinting defect in pseudohypoparathyroidism type IB. *J Clin Invest* **106**, 1167-1174 (2000).

152. D. J. Mackay, I. K. Temple, Transient neonatal diabetes mellitus type 1. *Am J Med Genet C Semin Med Genet* **154C**, 335-342 (2010).

153. R. J. Gardner *et al.*, An imprinted locus associated with transient neonatal diabetes mellitus. *Hum Mol Genet* **9**, 589-596 (2000).

154. M. Kamiya *et al.*, The cell cycle control gene ZAC/PLAGL1 is imprinted--a strong candidate gene for transient neonatal diabetes. *Hum Mol Genet* **9**, 453-460 (2000).

155. I. Iglesias-Platas *et al.*, Altered expression of the imprinted transcription factor PLAGL1 deregulates a network of genes in the human IUGR placenta. *Hum Mol Genet* **23**, 6275-6285 (2014).

156. J. R. Lupski, Genomic disorders: structural features of the genome can lead to DNA rearrangements and human disease traits. *Trends Genet* **14**, 417-422 (1998).

157. E. M. Torres, B. R. Williams, A. Amon, Aneuploidy: cells losing their balance. *Genetics* **179**, 737-746 (2008).

158. T. Hassold, H. Hall, P. Hunt, The origin of human aneuploidy: where we have been, where we are going. *Hum Mol Genet* **16 Spec No. 2**, R203-208 (2007).

159. T. Hassold, P. Hunt, To err (meiotically) is human: the genesis of human aneuploidy. *Nat Rev Genet* **2**, 280-291 (2001).

160. D. J. Barker, P. M. Clark, Fetal undernutrition and disease in later life. *Rev Reprod* **2**, 105-112 (1997).

161. D. Maulik, Fetal growth restriction: the etiology. *Clin Obstet Gynecol* **49**, 228-235 (2006).

162. J. M. Rogers, Tobacco and pregnancy: overview of exposures and effects. *Birth Defects Res C Embryo Today* **84**, 1-15 (2008).

163. E. P. Riley, M. A. Infante, K. R. Warren, Fetal alcohol spectrum disorders: an overview. *Neuropsychol Rev* **21**, 73-80 (2011).

164. S. M. Pinto *et al.*, Substance abuse during pregnancy: effect on pregnancy outcomes. *Eur J Obstet Gynecol Reprod Biol* **150**, 137-141 (2010).

165. G. Valsamakis, C. Kanaka-Gantenbein, A. Malamitsi-Puchner, G. Mastorakos, Causes of intrauterine growth restriction and the postnatal development of the metabolic syndrome. *Ann N Y Acad Sci* **1092**, 138-147 (2006).

166. D. B. Dunger, C. J. Petry, K. K. Ong, Genetic variations and normal fetal growth. *Horm Res* **65 Suppl 3**, 34-40 (2006).

167. J. M. Roberts, Preeclampsia: what we know and what we do not know. *Semin Perinatol* **24**, 24-28 (2000).

168. J. Zhang, M. A. Klebanoff, J. M. Roberts, Prediction of adverse outcomes by common definitions of hypertension in pregnancy. *Obstet Gynecol* **97**, 261-267 (2001).

169. J. M. Roberts, D. W. Cooper, Pathogenesis and genetics of pre-eclampsia. *Lancet* **357**, 53-56 (2001).

170. J. M. Roberts, C. A. Hubel, The two stage model of preeclampsia: variations on the theme. *Placenta* **30 Suppl A**, S32-37 (2009).

171. S. T. Chelbi, D. Vaiman, Genetic and epigenetic factors contribute to the onset of preeclampsia. *Mol Cell Endocrinol* **282**, 120-129 (2008).

172. P. M. Catalano, Obesity, insulin resistance, and pregnancy outcome. *Reproduction* **140**, 365-371 (2010).

173. D. J. Barker, The developmental origins of chronic adult disease. *Acta Paediatr Suppl* **93**, 26-33 (2004).

174. D. J. Barker, Sir Richard Doll Lecture. Developmental origins of chronic disease. *Public Health* **126**, 185-189 (2012).

175. P. D. Gluckman, M. A. Hanson, T. Buklijas, A conceptual framework for the developmental origins of health and disease. *J Dev Orig Health Dis* **1**, 6-18 (2010).

176. D. J. Barker, K. L. Thornburg, Placental programming of chronic diseases, cancer and lifespan: a review. *Placenta* **34**, 841-845 (2013).

177. P. Georgiades, A. C. Ferguson-Smith, G. J. Burton, Comparative developmental anatomy of the murine and human definitive placentae. *Placenta* **23**, 3-19 (2002).

178. A. Malassine, J. L. Frendo, D. Evain-Brion, A comparison of placental development and endocrine functions between the human and mouse model. *Hum Reprod Update* **9**, 531-539 (2003).

179. N. Malti *et al.*, Oxidative stress and maternal obesity: feto-placental unit interaction. *Placenta* **35**, 411-416 (2014).

180. F. Gundogan *et al.*, Impaired placentation in fetal alcohol syndrome. *Placenta* **29**, 148-157 (2008).

181. B. Cox *et al.*, Comparative systems biology of human and mouse as a tool to guide the modeling of human placental pathology. *Mol Syst Biol* **5**, 279 (2009).

182. K. Knox, J. C. Baker, Genomic evolution of the placenta using co-option and duplication and divergence. *Genome Res* **18**, 695-705 (2008).

183. K. Cockburn, J. Rossant, Making the blastocyst: lessons from the mouse. *J Clin Invest* **120**, 995-1003 (2010).

184. P. A. Latos, M. Hemberger, Review: the transcriptional and signalling networks of mouse trophoblast stem cells. *Placenta* **35 Suppl**, S81-85 (2014).

185. P. L. Pfeffer, D. J. Pearton, Trophoblast development. *Reproduction* **143**, 231-246 (2012).

186. R. M. Roberts, S. J. Fisher, Trophoblast stem cells. *Biol Reprod* **84**, 412-421 (2011).

187. C. E. Senner, M. Hemberger, Regulation of early trophoblast differentiation - lessons from the mouse. *Placenta* **31**, 944-950 (2010).

188. D. G. Simmons, J. C. Cross, Determinants of trophoblast lineage and cell subtype specification in the mouse placenta. *Dev Biol* **284**, 12-24 (2005).

189. R. Rugh, *The Mouse: Its reproduction and development*. (Oxford University Press, New York, 1993).

190. A. Ralston, J. Rossant, Cdx2 acts downstream of cell polarization to cell-autonomously promote trophectoderm fate in the early mouse embryo. *Dev Biol* **313**, 614-629 (2008).

191. A. Suwinska, R. Czolowska, W. Ozdzenski, A. K. Tarkowski, Blastomeres of the mouse embryo lose totipotency after the fifth cleavage division: expression of Cdx2 and Oct4 and developmental potential of inner and outer blastomeres of 16- and 32-cell embryos. *Dev Biol* **322**, 133-144 (2008).

192. N. Nishioka *et al.*, The Hippo signaling pathway components Lats and Yap pattern Tead4 activity to distinguish mouse trophectoderm from inner cell mass. *Dev Cell* **16**, 398-410 (2009).

193. N. Nishioka *et al.*, Tead4 is required for specification of trophectoderm in pre-implantation mouse embryos. *Mech Dev* **125**, 270-283 (2008).

194. A. Ralston *et al.*, Gata3 regulates trophoblast development downstream of Tead4 and in parallel to Cdx2. *Development* **137**, 395-403 (2010).

195. J. Rossant, Stem cells and early lineage development. *Cell* **132**, 527-531 (2008).

196. S. Tanaka, T. Kunath, A. K. Hadjantonakis, A. Nagy, J. Rossant, Promotion of trophoblast stem cell proliferation by FGF4. *Science* **282**, 2072-2075 (1998).

197. M. Guzman-Ayala, N. Ben-Haim, S. Beck, D. B. Constam, Nodal protein processing and fibroblast growth factor 4 synergize to maintain a trophoblast stem cell microenvironment. *Proc Natl Acad Sci U S A* **101**, 15656-15660 (2004).

198. C. W. Lu *et al.*, Ras-MAPK signaling promotes trophectoderm formation from embryonic stem cells and mouse embryos. *Nature genetics* **40**, 921-926 (2008).

199. F. Cambuli *et al.*, Epigenetic memory of the first cell fate decision prevents complete ES cell reprogramming into trophoblast. *Nat Commun* **5**, 5538 (2014).

200. M. J. Large, F. J. DeMayo, The regulation of embryo implantation and endometrial decidualization by progesterone receptor signaling. *Mol Cell Endocrinol* **358**, 155-165 (2012).

201. A. Rai, J. C. Cross, Development of the hemochorial maternal vascular spaces in the placenta through endothelial and vasculogenic mimicry. *Dev Biol* **387**, 131-141 (2014).

202. J. Rossant, J. C. Cross, Placental development: lessons from mouse mutants. *Nat Rev Genet* **2**, 538-548 (2001).

203. J. C. Cross, How to make a placenta: mechanisms of trophoblast cell differentiation in mice--a review. *Placenta* **26 Suppl A**, S3-9 (2005).

204. D. G. Simmons *et al.*, Early patterning of the chorion leads to the trilaminar trophoblast cell structure in the placental labyrinth. *Development* **135**, 2083-2091 (2008).

205. J. Rinkenberger, Z. Werb, The labyrinthine placenta. *Nature genetics* **25**, 248-250 (2000).

206. D. Goldman-Wohl, S. Yagel, United we stand not dividing: the syncytiotrophoblast and cell senescence. *Placenta* **35**, 341-344 (2014).

207. S. L. Adamson *et al.*, Interactions between trophoblast cells and the maternal and fetal circulation in the mouse placenta. *Dev Biol* **250**, 358-373 (2002).

208. L. Anson-Cartwright *et al.*, The glial cells missing-1 protein is essential for branching morphogenesis in the chorioallantoic placenta. *Nature genetics* **25**, 311-314 (2000).

209. S. A. Bainbridge *et al.*, Effects of reduced Gcm1 expression on trophoblast morphology, fetoplacental vascularity, and pregnancy outcomes in mice. *Hypertension* **59**, 732-739 (2012).

210. A. Dupressoir *et al.*, Syncytin-A and syncytin-B, two fusogenic placenta-specific murine envelope genes of retroviral origin conserved in Muridae. *Proc Natl Acad Sci U S A* **102**, 725-730 (2005).

211. A. Dupressoir *et al.*, A pair of co-opted retroviral envelope syncytin genes is required for formation of the two-layered murine placental syncytiotrophoblast. *Proc Natl Acad Sci U S A* **108**, E1164-1173 (2011).

212. R. Arora, V. E. Papaioannou, The murine allantois: a model system for the study of blood vessel formation. *Blood* **120**, 2562-2572 (2012).

213. S. Giroux *et al.*, Embryonic death of Mek1-deficient mice reveals a role for this kinase in angiogenesis in the labyrinthine region of the placenta. *Curr Biol* **9**, 369-372 (1999).

214. B. M. Zeigler *et al.*, The allantois and chorion, when isolated before circulation or chorio-allantoic fusion, have hematopoietic potential. *Development* **133**, 4183-4192 (2006).

215. H. N. Jones, T. L. Powell, T. Jansson, Regulation of placental nutrient transport--a review. *Placenta* **28**, 763-774 (2007).

216. A. K. Duttaroy, Transport of fatty acids across the human placenta: a review. *Prog Lipid Res* **48**, 52-61 (2009).

217. Y. Barak, Y. Sadovsky, T. Shalom-Barak, PPAR Signaling in Placental Development and Function. *PPAR Res* **2008**, 142082 (2008).

218. Y. Barak *et al.*, PPAR gamma is required for placental, cardiac, and adipose tissue development. *Mol Cell* **4**, 585-595 (1999).

219. T. Shalom-Barak *et al.*, Peroxisome proliferator-activated receptor gamma controls Muc1 transcription in trophoblasts. *Mol Cell Biol* **24**, 10661-10669 (2004).

220. Y. Barak *et al.*, Effects of peroxisome proliferator-activated receptor delta on placentation, adiposity, and colorectal cancer. *Proc Natl Acad Sci U S A* **99**, 303-308 (2002).

221. V. Sapin, P. Dolle, C. Hindelang, P. Kastner, P. Chambon, Defects of the chorioallantoic placenta in mouse RXRalpha null fetuses. *Dev Biol* **191**, 29-41 (1997).

222. F. Guillemot, A. Nagy, A. Auerbach, J. Rossant, A. L. Joyner, Essential role of Mash-2 in extraembryonic development. *Nature* **371**, 333-336 (1994).

223. M. Tanaka, M. Gertsenstein, J. Rossant, A. Nagy, Mash2 acts cell autonomously in mouse spongiotrophoblast development. *Dev Biol* **190**, 55-65 (1997).

224. G. T. Ma *et al.*, Nodal regulates trophoblast differentiation and placental development. *Dev Biol* **236**, 124-135 (2001).

225. M. J. Soares, The prolactin and growth hormone families: pregnancy-specific hormones/cytokines at the maternal-fetal interface. *Reprod Biol Endocrinol* **2**, 51 (2004).

226. Y. He *et al.*, Alternative splicing of vascular endothelial growth factor (VEGF)-R1 (FLT-1) pre-mRNA is important for the regulation of VEGF activity. *Mol Endocrinol* **13**, 537-545 (1999).

227. M. J. Soares, T. Konno, S. M. Alam, The prolactin family: effectors of pregnancy-dependent adaptations. *Trends Endocrinol Metab* **18**, 114-121 (2007).

228. S. Bouillot, C. Rampon, E. Tillet, P. Huber, Tracing the glycogen cells with protocadherin 12 during mouse placenta development. *Placenta* **27**, 882-888 (2006).

229. P. M. Coan, N. Conroy, G. J. Burton, A. C. Ferguson-Smith, Origin and characteristics of glycogen cells in the developing murine placenta. *Dev Dyn* **235**, 3280-3294 (2006).

230. S. J. Tunster, A. B. Jensen, R. M. John, Imprinted genes in mouse placental development and the regulation of fetal energy stores. *Reproduction* **145**, R117-137 (2013).

231. D. Hu, J. C. Cross, Development and function of trophoblast giant cells in the rodent placenta. *Int J Dev Biol* **54**, 341-354 (2010).

232. D. G. Simmons, A. L. Fortier, J. C. Cross, Diverse subtypes and developmental origins of trophoblast giant cells in the mouse placenta. *Dev Biol* **304**, 567-578 (2007).

233. P. Riley, L. Anson-Cartwright, J. C. Cross, The Hand1 bHLH transcription factor is essential for placentation and cardiac morphogenesis. *Nature genetics* **18**, 271-275 (1998).

234. I. C. Scott, L. Anson-Cartwright, P. Riley, D. Reda, J. C. Cross, The HAND1 basic helix-loop-helix transcription factor regulates trophoblast differentiation via multiple mechanisms. *Mol Cell Biol* **20**, 530-541 (2000).

235. M. Hughes *et al.*, The Hand1, Stra13 and Gcm1 transcription factors override FGF signaling to promote terminal differentiation of trophoblast stem cells. *Dev Biol* **271**, 26-37 (2004).

236. D. G. Simmons, S. Rawn, A. Davies, M. Hughes, J. C. Cross, Spatial and temporal expression of the 23 murine Prolactin/Placental Lactogen-related genes is not associated with their position in the locus. *BMC Genomics* **9**, 352 (2008).

237. R. L. Hannibal, J. C. Baker, Selective Amplification of the Genome Surrounding Key Placental Genes in Trophoblast Giant Cells. *Curr Biol* **26**, 230-236 (2016).

238. T. Z. Zybina, Eugenia, Genome variation in the trophoblast cell lifespan: Diploidy, polyteny, depolytenization, genome segregation. *World Journal of Medical Genetics* **4**, 77-93 (2014).

239. H. K. Evans, A. A. Wylie, S. K. Murphy, R. L. Jirtle, The neuronatin gene resides in a "micro-imprinted" domain on human chromosome 20q11.2. *Genomics* **77**, 99-104 (2001).

240. D. Dou, R. Joseph, Cloning of human neuronatin gene and its localization to chromosome-20q 11.2-12: the deduced protein is a novel "proteolipid'. *Brain Res* **723**, 8-22 (1996).

241. F. Kagitani *et al.*, Peg5/Neuronatin is an imprinted gene located on sub-distal chromosome 2 in the mouse. *Nucleic acids research* **25**, 3428-3432 (1997).

242. C. M. Williamson *et al.*, Localisation of the imprinted gene neuronatin, Nnat, confirms and refines the location of a second imprinting region on mouse chromosome 2. *Cytogenet Cell Genet* **81**, 73-78 (1998).

243. N. Kikyo *et al.*, Genetic and functional analysis of neuronatin in mice with maternal or paternal duplication of distal Chr 2. *Dev Biol* **190**, 66-77 (1997).

244. J. Hubertus *et al.*, Selective methylation of CpGs at regulatory binding sites controls NNAT expression in Wilms tumors. *PLoS One* **8**, e67605 (2013).

245. H. Miki *et al.*, Birth of mice produced by germ cell nuclear transfer. *Genesis* **41**, 81-86 (2005).

246. R. M. Joseph, Neuronatin gene: Imprinted and misfolded: Studies in Lafora disease, diabetes and cancer may implicate NNAT-aggregates as a common downstream participant in neuronal loss. *Genomics* **103**, 183-188 (2014).

247. T. Gu *et al.*, Molecular characterization of the Neuronatin gene in the porcine placenta. *PLoS One* **7**, e43325 (2012).

248. J. Peters *et al.*, A cluster of oppositely imprinted transcripts at the Gnas locus in the distal imprinting region of mouse chromosome 2. *Proc Natl Acad Sci U S A* **96**, 3830-3835 (1999).

249. S. F. Wroe *et al.*, An imprinted transcript, antisense to Nesp, adds complexity to the cluster of imprinted genes at the mouse Gnas locus. *Proc Natl Acad Sci U S A* **97**, 3342-3346 (2000).

250. M. Klemke, R. H. Kehlenbach, W. B. Huttner, Two overlapping reading frames in a single exon encode interacting proteins--a novel way of gene usage. *EMBO J* **20**, 3849-3860 (2001).

251. T. Xie *et al.*, The alternative stimulatory G protein alpha-subunit XLalphas is a critical regulator of energy and glucose metabolism and sympathetic nerve activity in adult mice. *J Biol Chem* **281**, 18989-18999 (2006).

252. A. Plagge *et al.*, The imprinted signaling protein XL alpha s is required for postnatal adaptation to feeding. *Nature genetics* **36**, 818-826 (2004).

253. S. Yu *et al.*, Variable and tissue-specific hormone resistance in heterotrimeric Gs protein alpha-subunit (Gsalpha) knockout mice is due to tissue-specific imprinting of the gsalpha gene. *Proc Natl Acad Sci U S A* **95**, 8715-8720 (1998).

254. L. S. Weinstein, S. Yu, C. A. Ecelbarger, Variable imprinting of the heterotrimeric G protein G(s) alpha-subunit within different segments of the nephron. *Am J Physiol Renal Physiol* **278**, F507-514 (2000).

255. S. A. Eaton *et al.*, New mutations at the imprinted Gnas cluster show gene dosage effects of Gsalpha in postnatal growth and implicate XLalphas in bone and fat metabolism but not in suckling. *Mol Cell Biol* **32**, 1017-1029 (2012).

256. C. Coombes *et al.*, Epigenetic properties and identification of an imprint mark in the Nesp-Gnasxl domain of the mouse Gnas imprinted locus. *Mol Cell Biol* **23**, 5475-5488 (2003).

257. J. Liu *et al.*, Identification of the control region for tissue-specific imprinting of the stimulatory G protein alpha-subunit. *Proc Natl Acad Sci U S A* **102**, 5513-5518 (2005).

258. C. M. Williamson *et al.*, A cis-acting control region is required exclusively for the tissue-specific imprinting of Gnas. *Nature genetics* **36**, 894-899 (2004).

259. C. M. Williamson *et al.*, Identification of an imprinting control region affecting the expression of all transcripts in the Gnas cluster. *Nature genetics* **38**, 350-355 (2006).

260. C. M. Williamson *et al.*, Uncoupling antisense-mediated silencing and DNA methylation in the imprinted Gnas cluster. *PLoS Genet* **7**, e1001347 (2011).

261. B. M. Cattanach, Beechey CV, in *Genomic Imprinting: Frontiers in Molecular Biology,* S. V. Reik W., Ed. (IRL Press, Oxford, 1997), vol. 18, pp. 118-145.

262. C. V. Beechey, Peg1/Mest locates distal to the currently defined imprinting region on mouse proximal chromosome 6 and identifies a new imprinting region affecting growth. *Cytogenet Cell Genet* **90**, 309-314 (2000).

263. C. V. Beechey, A reassessment of imprinting regions and phenotypes on mouse chromosome 6: Nap1l5 locates within the currently defined sub-proximal imprinting region. *Cytogenet Genome Res* **107**, 108-114 (2004).

264. K. Hannula-Jouppi *et al.*, Differentially methylated regions in maternal and paternal uniparental disomy for chromosome 7. *Epigenetics : official journal of the DNA Methylation Society* **9**, 351-365 (2014).

265. L. Lefebvre, S. Viville, S. C. Barton, F. Ishino, M. A. Surani, Genomic structure and parent-of-origin-specific methylation of Peg1. *Hum Mol Genet* **6**, 1907-1915 (1997).

266. Y. Nishita, T. Sado, I. Yoshida, N. Takagi, Effect of CpG methylation on expression of the mouse imprinted gene Mest. *Gene* **226**, 199-209 (1999).

267. L. Bentley *et al.*, The imprinted region on human chromosome 7q32 extends to the carboxypeptidase A gene cluster: an imprinted candidate for Silver-Russell syndrome. *Journal of medical genetics* **40**, 249-256 (2003).

268. T. Kaneko-Ishino *et al.*, Peg1/Mest imprinted gene on chromosome 6 identified by cDNA subtraction hybridization. *Nature genetics* **11**, 52-59 (1995).

269. T. Kayashima *et al.*, The novel imprinted carboxypeptidase A4 gene (CPA4) in the 7q32 imprinting domain. *Hum Genet* **112**, 220-226 (2003).

270. L. Parker-Katiraee *et al.*, Identification of the imprinted KLF14 transcription factor undergoing human-specific accelerated evolution. *PLoS Genet* **3**, e65 (2007).

271. Y. Nishita, I. Yoshida, T. Sado, N. Takagi, Genomic imprinting and chromosomal localization of the human MEST gene. *Genomics* **36**, 539-542 (1996).

272. N. N. Sado T., Tada M., Nobuo T., A novel mesoderm-sepcific cDNA isolated from a mouse embryonal carcinoma cell line. *Develop. Grwoth & Differ.* **35**, 551-560 (1993).

273. S. Kobayashi *et al.*, Human PEG1/MEST, an imprinted gene on chromosome 7. *Hum Mol Genet* **6**, 781-786 (1997).

274. L. Lefebvre *et al.*, Abnormal maternal behaviour and growth retardation associated with loss of the imprinted gene Mest. *Nature genetics* **20**, 163-169 (1998).

275. W. Mayer *et al.*, Expression of the imprinted genes MEST/Mest in human and murine placenta suggests a role in angiogenesis. *Dev Dyn* **217**, 1-10 (2000).

276. J. McMinn, M. Wei, Y. Sadovsky, H. M. Thaker, B. Tycko, Imprinting of PEG1/MEST isoform 2 in human placenta. *Placenta* **27**, 119-126 (2006).

277. W. Shi *et al.*, Loss-of-imprinting of Peg1 in mouse interspecies hybrids is correlated with altered growth. *Genesis* **39**, 65-72 (2004).

278. J. L. MacIsaac, A. B. Bogutz, A. S. Morrissy, L. Lefebvre, Tissue-specific alternative polyadenylation at the imprinted gene Mest regulates allelic usage at Copg2. *Nucleic acids research* **40**, 1523-1535 (2012).

279. A. Kong *et al.*, Parental origin of sequence variants associated with complex diseases. *Nature* **462**, 868-874 (2009).

280. T. M. Teslovich *et al.*, Biological, clinical and population relevance of 95 loci for blood lipids. *Nature* **466**, 707-713 (2010).

281. B. F. Voight *et al.*, Twelve type 2 diabetes susceptibility loci identified through large-scale association analysis. *Nature genetics* **42**, 579-589 (2010).

282. M. Civelek, A. J. Lusis, Conducting the metabolic syndrome orchestra. *Nature genetics* **43**, 506-508 (2011).

283. K. S. Small *et al.*, Identification of an imprinted master trans regulator at the KLF14 locus related to multiple metabolic phenotypes. *Nature genetics* **43**, 561-564 (2011).

284. W. Davies, R. J. Smith, G. Kelsey, L. S. Wilkinson, Expression patterns of the novel imprinted genes Nap1l5 and Peg13 and their non-imprinted host genes in the adult mouse brain. *Gene Expr Patterns* **4**, 741-747 (2004).

285. R. J. Smith, W. Dean, G. Konfortova, G. Kelsey, Identification of novel imprinted genes in a genome-wide screen for maternal methylation. *Genome Res* **13**, 558-569 (2003).

286. M. Cowley, A. J. Wood, S. Bohm, R. Schulz, R. J. Oakey, Epigenetic control of alternative mRNA processing at the imprinted Herc3/Nap1l5 locus. *Nucleic acids research* **40**, 8917-8926 (2012).

287. R. Ono *et al.*, A retrotransposon-derived gene, PEG10, is a novel imprinted gene located on human chromosome 7q21. *Genomics* **73**, 232-237 (2001).

288. R. Ono *et al.*, Identification of a large novel imprinted gene cluster on mouse proximal chromosome 6. *Genome Res* **13**, 1696-1705 (2003).

289. N. A. Youngson, S. Kocialkowski, N. Peel, A. C. Ferguson-Smith, A small family of sushi-class retrotransposon-derived genes in mammals and their relation to genomic imprinting. *Journal of Molecular Evolution* **61**, 481-490 (2005).

290. J. Brandt *et al.*, Transposable elements as a source of genetic innovation: expression and evolution of a family of retrotransposon-derived neogenes in mammals. *Gene* **345**, 101-111 (2005).

291. K. Shigemoto *et al.*, Identification and characterisation of a developmentally regulated mammalian gene that utilises -1 programmed ribosomal frameshifting. *Nucleic acids research* **29**, 4079-4088 (2001).

292. C. Henke *et al.*, Regulation of murine placentogenesis by the retroviral genes Syncytin-A, Syncytin-B and Peg10. *Differentiation* **85**, 150-160 (2013).

293. R. Ono *et al.*, Deletion of Peg10, an imprinted gene acquired from a retrotransposon, causes early embryonic lethality. *Nature genetics* **38**, 101-106 (2006).

294. A. C. Ferguson-Smith, B. M. Cattanach, S. C. Barton, C. V. Beechey, M. A. Surani, Embryological and molecular investigations of parental imprinting on mouse chromosome 7. *Nature* **351**, 667-670 (1991).

295. M. S. Bartolomei, A. L. Webber, M. E. Brunkow, S. M. Tilghman, Epigenetic mechanisms underlying the imprinting of the mouse H19 gene. *Genes Dev* **7**, 1663-1673 (1993).

296. A. C. Ferguson-Smith, H. Sasaki, B. M. Cattanach, M. A. Surani, Parental-origin-specific epigenetic modification of the mouse H19 gene. *Nature* **362**, 751-755 (1993).

297. J. L. Thorvaldsen, K. L. Duran, M. S. Bartolomei, Deletion of the H19 differentially methylated domain results in loss of imprinted expression of H19 and Igf2. *Genes Dev* **12**, 3693-3702 (1998).

298. V. Pant *et al.*, Mutation of a single CTCF target site within the H19 imprinting control region leads to loss of Igf2 imprinting and complex patterns of de novo methylation upon maternal inheritance. *Mol Cell Biol* **24**, 3497-3504 (2004).

299. S. Kurukuti *et al.*, CTCF binding at the H19 imprinting control region mediates maternally inherited higher-order chromatin conformation to restrict enhancer access to Igf2. *Proc Natl Acad Sci U S A* **103**, 10684-10689 (2006).

300. T. M. DeChiara, E. J. Robertson, A. Efstratiadis, Parental imprinting of the mouse insulin-like growth factor II gene. *Cell* **64**, 849-859 (1991).

301. F. L. Sun, W. L. Dean, G. Kelsey, N. D. Allen, W. Reik, Transactivation of Igf2 in a mouse model of Beckwith-Wiedemann syndrome. *Nature* **389**, 809-815 (1997).

302. M. Constancia *et al.*, Placental-specific IGF-II is a major modulator of placental and fetal growth. *Nature* **417**, 945-948 (2002).

303. P. M. Coan *et al.*, Disproportional effects of Igf2 knockout on placental morphology and diffusional exchange characteristics in the mouse. *J Physiol* **586**, 5023-5032 (2008).

304. D. R. Esquiliano, W. Guo, L. Liang, P. Dikkes, M. F. Lopez, Placental glycogen stores are increased in mice with H19 null mutations but not in those with insulin or IGF type 1 receptor mutations. *Placenta* **30**, 693-699 (2009).

305. P. A. Leighton, R. S. Ingram, J. Eggenschwiler, A. Efstratiadis, S. M. Tilghman, Disruption of imprinting caused by deletion of the H19 gene region in mice. *Nature* **375**, 34-39 (1995).

306. A. Keniry *et al.*, The H19 lincRNA is a developmental reservoir of miR-675 that suppresses growth and Igf1r. *Nat Cell Biol* **14**, 659-665 (2012).

307. Q. J. Hudson *et al.*, Extra-embryonic-specific imprinted expression is restricted to defined lineages in the post-implantation embryo. *Dev Biol* **353**, 420-431 (2011).

308. D. Mancini-DiNardo, S. J. Steele, R. S. Ingram, S. M. Tilghman, A differentially methylated region within the gene Kcnq1 functions as an imprinted promoter and silencer. *Hum Mol Genet* **12**, 283-294 (2003).

309. T. M. Kulinski, D. P. Barlow, Q. J. Hudson, Imprinted silencing is extended over broad chromosomal domains in mouse extra-embryonic lineages. *Curr Opin Cell Biol* **25**, 297-304 (2013).

310. G. V. Fitzpatrick, P. D. Soloway, M. J. Higgins, Regional loss of imprinting and growth deficiency in mice with a targeted deletion of KvDMR1. *Nature genetics* **32**, 426-431 (2002).

311. R. Oh-McGinnis, A. B. Bogutz, L. Lefebvre, Partial loss of Ascl2 function affects all three layers of the mature placenta and causes intrauterine growth restriction. *Dev Biol* **351**, 277-286 (2011).

312. D. Frank *et al.*, Placental overgrowth in mice lacking the imprinted gene Ipl. *Proc Natl Acad Sci U S A* **99**, 7490-7495 (2002).

313. S. J. Tunster, M. Van de Pette, R. M. John, Fetal overgrowth in the Cdkn1c mouse model of Beckwith-Wiedemann syndrome. *Dis Model Mech* **4**, 814-821 (2011).

314. S. C. Andrews *et al.*, Cdkn1c (p57Kip2) is the major regulator of embryonic growth within its imprinted domain on mouse distal chromosome 7. *BMC Dev Biol* **7**, 53 (2007).

315. M. Salas *et al.*, Placental growth retardation due to loss of imprinting of Phlda2. *Mech Dev* **121**, 1199-1210 (2004).

316. S. J. Tunster, B. Tycko, R. M. John, The imprinted Phlda2 gene regulates extraembryonic energy stores. *Mol Cell Biol* **30**, 295-306 (2010).

317. S. J. Tunster, H. D. Creeth, R. M. John, The imprinted Phlda2 gene modulates a major endocrine compartment of the placenta to regulate placental demands for maternal resources. *Dev Biol* **409**, 251-260 (2016).

318. B. M. Cattanach *et al.*, A candidate mouse model for Prader-Willi syndrome which shows an absence of Snrpn expression. *Nature genetics* **2**, 270-274 (1992).

319. J. L. Resnick, R. D. Nicholls, R. Wevrick, G. Prader-Willi Syndrome Animal Models Working, Recommendations for the investigation of animal models of Prader-Willi syndrome. *Mamm Genome* **24**, 165-178 (2013).

320. T. Yang *et al.*, A mouse model for Prader-Willi syndrome imprinting-centre mutations. *Nature genetics* **19**, 25-31 (1998).

321. T. A. Gray, S. Saitoh, R. D. Nicholls, An imprinted, mammalian bicistronic transcript encodes two independent proteins. *Proc Natl Acad Sci U S A* **96**, 5616-5621 (1999).

322. M. Stefan *et al.*, Hormonal and metabolic defects in a prader-willi syndrome mouse model with neonatal failure to thrive. *Endocrinology* **146**, 4377-4385 (2005).

323. M. Stefan *et al.*, Global deficits in development, function, and gene expression in the endocrine pancreas in a deletion mouse model of Prader-Willi syndrome. *Am J Physiol Endocrinol Metab* **300**, E909-922 (2011).

324. S. Kishore *et al.*, The snoRNA MBII-52 (SNORD 115) is processed into smaller RNAs and regulates alternative splicing. *Hum Mol Genet* **19**, 1153-1164 (2010).

325. F. Ding *et al.*, SnoRNA Snord116 (Pwcr1/MBII-85) deletion causes growth deficiency and hyperphagia in mice. *PLoS One* **3**, e1709 (2008).

326. Y. Kuroiwa *et al.*, Peg3 imprinted gene on proximal chromosome 7 encodes for a zinc finger protein. *Nature genetics* **12**, 186-190 (1996).

327. S. K. Murphy, A. A. Wylie, R. L. Jirtle, Imprinting of PEG3, the human homologue of a mouse gene involved in nurturing behavior. *Genomics* **71**, 110-117 (2001).

328. J. Kim, L. Ashworth, E. Branscomb, L. Stubbs, The human homolog of a mouse-imprinted gene, Peg3, maps to a zinc finger gene-rich region of human chromosome 19q13.4. *Genome Res* **7**, 532-540 (1997).

329. H. He, J. Kim, Regulation and function of the peg3 imprinted domain. *Genomics Inform* **12**, 105-113 (2014).

330. J. Kim *et al.*, Discovery of a novel, paternally expressed ubiquitin-specific processing protease gene through comparative analysis of an imprinted region of mouse chromosome 7 and human chromosome 19q13.4. *Genome Res* **10**, 1138-1147 (2000).

331. J. Kim, X. Lu, L. Stubbs, Zim1, a maternally expressed mouse Kruppel-type zinc-finger gene located in proximal chromosome 7. *Hum Mol Genet* **8**, 847-854 (1999).

332. M. M. Thiaville *et al.*, DNA-binding motif and target genes of the imprinted transcription factor PEG3. *Gene* **512**, 314-320 (2013).

333. J. M. Huang, J. Kim, DNA methylation analysis of the mammalian PEG3 imprinted domain. *Gene* **442**, 18-25 (2009).

334. L. Li *et al.*, Regulation of maternal behavior and offspring growth by paternally expressed Peg3. *Science* **284**, 330-333 (1999).

335. J. P. Curley *et al.*, Increased body fat in mice with a targeted mutation of the paternally expressed imprinted gene Peg3. *FASEB J* **19**, 1302-1304 (2005).

336. J. Kim *et al.*, Peg3 mutational effects on reproduction and placenta-specific gene families. *PLoS One* **8**, e83359 (2013).

337. J. Kim *et al.*, Imprinting control region (ICR) of the Peg3 domain. *Hum Mol Genet* **21**, 2677-2687 (2012).

338. R. J. Smith *et al.*, The mouse Zac1 locus: basis for imprinting and comparison with human ZAC. *Gene* **292**, 101-112 (2002).

339. I. Iglesias-Platas *et al.*, Imprinting at the PLAGL1 domain is contained within a 70-kb CTCF/cohesin-mediated non-allelic chromatin loop. *Nucleic acids research* **41**, 2171-2179 (2013).

340. D. Ma *et al.*, Impaired glucose homeostasis in transgenic mice expressing the human transient neonatal diabetes mellitus locus, TNDM. *J Clin Invest* **114**, 339-348 (2004).

341. A. Varrault *et al.*, Zac1 regulates an imprinted gene network critically involved in the control of embryonic growth. *Dev Cell* **11**, 711-722 (2006).

342. N. Miyoshi *et al.*, Identification of the Meg1/Grb10 imprinted gene on mouse proximal chromosome 11, a candidate for the Silver-Russell syndrome gene. *Proc Natl Acad Sci U S A* **95**, 1102-1107 (1998).

343. B. M. Cattanach, C. V. Beechey, C. Rasberry, J. Jones, D. Papworth, Time of initiation and site of action of the mouse chromosome 11 imprinting effects. *Genet Res* **68**, 35-44 (1996).

344. D. Monk *et al.*, Reciprocal imprinting of human GRB10 in placental trophoblast and brain: evolutionary conservation of reversed allelic expression. *Hum Mol Genet* **18**, 3066-3074 (2009).

345. H. Shiura *et al.*, Paternal deletion of Meg1/Grb10 DMR causes maternalization of the Meg1/Grb10 cluster in mouse proximal Chromosome 11 leading to severe pre- and postnatal growth retardation. *Hum Mol Genet* **18**, 1424-1438 (2009).

346. M. Charalambous *et al.*, Disruption of the imprinted Grb10 gene leads to disproportionate overgrowth by an Igf2-independent mechanism. *Proc Natl Acad Sci U S A* **100**, 8292-8297 (2003).

347. M. Charalambous *et al.*, Maternally-inherited Grb10 reduces placental size and efficiency. *Dev Biol* **337**, 1-8 (2010).

348. F. M. Smith *et al.*, Mice with a disruption of the imprinted Grb10 gene exhibit altered body composition, glucose homeostasis, and insulin signaling during postnatal life. *Mol Cell Biol* **27**, 5871-5886 (2007).

349. P. Arnaud *et al.*, Conserved methylation imprints in the human and mouse GRB10 genes with divergent allelic expression suggests differential reading of the same mark. *Hum Mol Genet* **12**, 1005-1019 (2003).

350. T. Hikichi, T. Kohda, T. Kaneko-Ishino, F. Ishino, Imprinting regulation of the murine Meg1/Grb10 and human GRB10 genes; roles of brain-specific promoters and mouse-specific CTCF-binding sites. *Nucleic acids research* **31**, 1398-1406 (2003).

351. L. A. Sanz *et al.*, A mono-allelic bivalent chromatin domain controls tissue-specific imprinting at Grb10. *EMBO J* **27**, 2523-2532 (2008).

352. Y. Yamasaki-Ishizaki *et al.*, Role of DNA methylation and histone H3 lysine 27 methylation in tissue-specific imprinting of mouse Grb10. *Mol Cell Biol* **27**, 732-742 (2007).

353. I. Hatada *et al.*, Allele-specific methylation and expression of an imprinted U2af1-rs1 (SP2) gene. *Nucleic acids research* **23**, 36-41 (1995).

354. A. Nabetani, I. Hatada, H. Morisaki, M. Oshimura, T. Mukai, Mouse U2af1-rs1 is a neomorphic imprinted gene. *Mol Cell Biol* **17**, 789-798 (1997).

355. Z. Zhang *et al.*, Comparative analyses of genomic imprinting and CpG island-methylation in mouse Murr1 and human MURR1 loci revealed a putative imprinting control region in mice. *Gene* **366**, 77-86 (2006).

356. Y. Wang *et al.*, The mouse Murr1 gene is imprinted in the adult brain, presumably due to transcriptional interference by the antisense-oriented U2af1-rs1 gene. *Mol Cell Biol* **24**, 270-279 (2004).

357. K. Joh, H. Yatsuki, K. Higashimoto, T. Mukai, H. Soejima, Antisense transcription occurs at the promoter of a mouse imprinted gene, commd1, on the repressed paternal allele. *J Biochem* **146**, 771-774 (2009).

358. B. van de Sluis *et al.*, Increased activity of hypoxia-inducible factor 1 is associated with early embryonic lethality in Commd1 null mice. *Mol Cell Biol* **27**, 4142-4156 (2007).

359. G. N. Maine, E. Burstein, COMMD proteins: COMMing to the scene. *Cell Mol Life Sci* **64**, 1997-2005 (2007).

360. P. Georgiades, M. Watkins, M. A. Surani, A. C. Ferguson-Smith, Parental origin-specific developmental defects in mice with uniparental disomy for chromosome 12. *Development* **127**, 4719-4728 (2000).

361. M. Tevendale, M. Watkins, C. Rasberry, B. Cattanach, A. C. Ferguson-Smith, Analysis of mouse conceptuses with uniparental duplication/deficiency for distal chromosome 12: comparison with chromosome 12 uniparental disomy and implications for genomic imprinting. *Cytogenet Genome Res* **113**, 215-222 (2006).

362. M. Kagami *et al.*, Deletions and epimutations affecting the human 14q32.2 imprinted region in individuals with paternal and maternal upd(14)-like phenotypes. *Nature genetics* **40**, 237-242 (2008).

363. T. Ogata, M. Kagami, A. C. Ferguson-Smith, Molecular mechanisms regulating phenotypic outcome in paternal and maternal uniparental disomy for chromosome 14. *Epigenetics : official journal of the DNA Methylation Society* **3**, 181-187 (2008).

364. J. V. Schmidt, P. G. Matteson, B. K. Jones, X. J. Guan, S. M. Tilghman, The Dlk1 and Gtl2 genes are linked and reciprocally imprinted. *Genes Dev* **14**, 1997-2002 (2000).

365. S. Takada *et al.*, Delta-like and gtl2 are reciprocally expressed, differentially methylated linked imprinted genes on mouse chromosome 12. *Curr Biol* **10**, 1135-1138 (2000).

366. J. P. Hagan, B. L. O'Neill, C. L. Stewart, S. V. Kozlov, C. M. Croce, At least ten genes define the imprinted Dlk1-Dio3 cluster on mouse chromosome 12qF1. *PLoS One* **4**, e4352 (2009).

367. S. P. Lin *et al.*, Asymmetric regulation of imprinting on the maternal and paternal chromosomes at the Dlk1-Gtl2 imprinted cluster on mouse chromosome 12. *Nature genetics* **35**, 97-102 (2003).

368. C. A. Edwards *et al.*, The evolution of the DLK1-DIO3 imprinted domain in mammals. *PLoS Biol* **6**, e135 (2008).

369. C. M. Smas, L. Chen, H. S. Sul, Cleavage of membrane-associated pref-1 generates a soluble inhibitor of adipocyte differentiation. *Mol Cell Biol* **17**, 977-988 (1997).

370. A. Yevtodiyenko, J. V. Schmidt, Dlk1 expression marks developing endothelium and sites of branching morphogenesis in the mouse embryo and placenta. *Dev Dyn* **235**, 1115-1123 (2006).

371. Y. S. Moon *et al.*, Mice lacking paternally expressed Pref-1/Dlk1 display growth retardation and accelerated adiposity. *Mol Cell Biol* **22**, 5585-5592 (2002).

372. J. N. Waddell *et al.*, Dlk1 is necessary for proper skeletal muscle development and regeneration. *PLoS One* **5**, e15055 (2010).

373. J. Volff, C. Korting, M. Schartl, Ty3/Gypsy retrotransposon fossils in mammalian genomes: did they evolve into new cellular functions? *Mol Biol Evol* **18**, 266-270 (2001).

374. Y. Sekita *et al.*, Role of retrotransposon-derived imprinted gene, Rtl1, in the feto-maternal interface of mouse placenta. *Nature genetics* **40**, 243-248 (2008).

375. K. Schuster-Gossler, P. Bilinski, T. Sado, A. Ferguson-Smith, A. Gossler, The mouse Gtl2 gene is differentially expressed during embryonic development, encodes multiple alternatively spliced transcripts, and may act as an RNA. *Dev Dyn* **212**, 214-228 (1998).

376. H. Seitz *et al.*, A large imprinted microRNA gene cluster at the mouse Dlk1-Gtl2 domain. *Genome Res* **14**, 1741-1748 (2004).

377. N. Takahashi *et al.*, Deletion of Gtl2, imprinted non-coding RNA, with its differentially methylated region induces lethal parent-origin-dependent defects in mice. *Hum Mol Genet* **18**, 1879-1888 (2009).

378. H. Takeda *et al.*, The callipyge mutation enhances bidirectional long-range DLK1-GTL2 intergenic transcription in cis. *Proc Natl Acad Sci U S A* **103**, 8119-8124 (2006).

379. M. Kawahara *et al.*, High-frequency generation of viable mice from engineered bi-maternal embryos. *Nat Biotechnol* **25**, 1045-1050 (2007).

380. L. Liu *et al.*, Activation of the imprinted Dlk1-Dio3 region correlates with pluripotency levels of mouse stem cells. *J Biol Chem* **285**, 19483-19490 (2010).

381. M. Stadtfeld *et al.*, Aberrant silencing of imprinted genes on chromosome 12qF1 in mouse induced pluripotent stem cells. *Nature* **465**, 175-181 (2010).

382. D. P. Barlow, R. Stoger, B. G. Herrmann, K. Saito, N. Schweifer, The mouse insulin-like growth factor type-2 receptor is imprinted and closely linked to the Tme locus. *Nature* **349**, 84-87 (1991).

383. D. Monk *et al.*, Limited evolutionary conservation of imprinting in the human placenta. *Proc Natl Acad Sci U S A* **103**, 6623-6628 (2006).

384. R. Stoger *et al.*, Maternal-specific methylation of the imprinted mouse Igf2r locus identifies the expressed locus as carrying the imprinting signal. *Cell* **73**, 61-71 (1993).

385. A. Wutz *et al.*, Imprinted expression of the Igf2r gene depends on an intronic CpG island. *Nature* **389**, 745-749 (1997).

386. R. Lyle *et al.*, The imprinted antisense RNA at the Igf2r locus overlaps but does not imprint Mas1. *Nature genetics* **25**, 19-21 (2000).

387. P. A. Latos *et al.*, Airn transcriptional overlap, but not its lncRNA products, induces imprinted Igf2r silencing. *Science* **338**, 1469-1472 (2012).

388. F. Sleutels, R. Zwart, D. P. Barlow, The non-coding Air RNA is required for silencing autosomal imprinted genes. *Nature* **415**, 810-813 (2002).

389. T. Nagano *et al.*, The Air noncoding RNA epigenetically silences transcription by targeting G9a to chromatin. *Science* **322**, 1717-1720 (2008).

390. R. Zwart, F. Sleutels, A. Wutz, A. H. Schinkel, D. P. Barlow, Bidirectional action of the Igf2r imprint control element on upstream and downstream imprinted genes. *Genes Dev* **15**, 2361-2366 (2001).

391. L. K. Harris, I. P. Crocker, P. N. Baker, J. D. Aplin, M. Westwood, IGF2 actions on trophoblast in human placenta are regulated by the insulin-like growth factor 2 receptor, which can function as both a signaling and clearance receptor. *Biol Reprod* **84**, 440-446 (2011).

392. M. M. Lau *et al.*, Loss of the imprinted IGF2/cation-independent mannose 6-phosphate receptor results in fetal overgrowth and perinatal lethality. *Genes Dev* **8**, 2953-2963 (1994).

393. A. A. Wylie *et al.*, Tissue-specific inactivation of murine M6P/IGF2R. *Am J Pathol* **162**, 321-328 (2003).

394. A. Wutz *et al.*, Non-imprinted Igf2r expression decreases growth and rescues the Tme mutation in mice. *Development* **128**, 1881-1887 (2001).

395. Y. Hagiwara *et al.*, Screening for imprinted genes by allelic message display: identification of a paternally expressed gene impact on mouse chromosome 18. *Proc Natl Acad Sci U S A* **94**, 9249-9254 (1997).

396. R. J. Oakey, P. G. Matteson, S. Litwin, S. M. Tilghman, R. L. Nussbaum, Nondisjunction rates and abnormal embryonic development in a mouse cross between heterozygotes carrying a (7, 18) robertsonian translocation chromosome. *Genetics* **141**, 667-674 (1995).

397. K. Okamura *et al.*, Comparative genome analysis of the mouse imprinted gene impact and its nonimprinted human homolog IMPACT: toward the structural basis for species-specific imprinting. *Genome Res* **10**, 1878-1889 (2000).

398. K. Okamura, Y. Yamada, Y. Sakaki, T. Ito, An evolutionary scenario for genomic imprinting of Impact lying between nonimprinted neighbors. *DNA Res* **11**, 381-390 (2004).

399. K. Okamura, Y. Sakaki, T. Ito, Comparative genomics approach toward critical determinants for the imprinting of an evolutionarily conserved gene Impact. *Biochem Biophys Res Commun* **329**, 824-830 (2005).

400. C. M. Pereira *et al.*, IMPACT, a protein preferentially expressed in the mouse brain, binds GCN1 and inhibits GCN2 activation. *J Biol Chem* **280**, 28316-28323 (2005).

401. M. Roffe, G. N. M. Hajj, H. F. Azevedo, V. S. Alves, B. A. Castilho, IMPACT Is a Developmentally Regulated Protein in Neurons That Opposes the Eukaryotic Initiation Factor 2 alpha Kinase GCN2 in the modulation of Neurite Outgrowth. *Journal of Biological Chemistry* **288**, 10860-10869 (2013).

402. M. C. Cirio *et al.*, DNA methyltransferase 1o functions during preimplantation development to preclude a profound level of epigenetic variation. *Dev Biol* **324**, 139-150 (2008).

403. H. Leonhardt, A. W. Page, H. U. Weier, T. H. Bestor, A targeting sequence directs DNA methyltransferase to sites of DNA replication in mammalian nuclei. *Cell* **71**, 865-873 (1992).

404. L. L. Carlson, A. W. Page, T. H. Bestor, Properties and localization of DNA methyltransferase in preimplantation mouse embryos: implications for genomic imprinting. *Genes Dev* **6**, 2536-2541 (1992).

405. K. Ohsawa, Y. Imai, D. Ito, S. Kohsaka, Molecular cloning and characterization of annexin V-binding proteins with highly hydrophilic peptide structure. *J Neurochem* **67**, 89-97 (1996).

406. M. C. Cardoso, H. Leonhardt, DNA methyltransferase is actively retained in the cytoplasm during early development. *J Cell Biol* **147**, 25-32 (1999).

407. J. Martel, Fortier A., Lopes F., Cirio C., Chaillet J., Trasler J., paper presented at the 41st Annual Meeting of the Society for the Study of Reproduction, Kailua-Kona, Hawaii, 2008.

408. S. McGraw *et al.*, Loss of DNMT1o disrupts imprinted X chromosome inactivation and accentuates placental defects in females. *PLoS Genet* **9**, e1003873 (2013).

409. K. P. Himes, E. Koppes, J. R. Chaillet, Generalized disruption of inherited genomic imprints leads to wide-ranging placental defects and dysregulated fetal growth. *Dev Biol* **373**, 72-82 (2013).

410. E. Koppes, K. P. Himes, J. R. Chaillet, Partial Loss of Genomic Imprinting Reveals Important Roles for Kcnq1 and Peg10 Imprinted Domains in Placental Development. *PLoS One* **10**, e0135202 (2015).

411. T. Moore, D. Haig, Genomic imprinting in mammalian development: a parental tug-of-war. *Trends Genet* **7**, 45-49 (1991).

412. A. L. Fowden, A. N. Sferruzzi-Perri, P. M. Coan, M. Constancia, G. J. Burton, Placental efficiency and adaptation: endocrine regulation. *J Physiol* **587**, 3459-3472 (2009).

413. A. L. Fowden, J. W. Ward, F. P. Wooding, A. J. Forhead, M. Constancia, Programming placental nutrient transport capacity. *J Physiol* **572**, 5-15 (2006).

414. K. P. Himes *et al.*, Loss of inherited genomic imprints in mice leads to severe disruption in placental lipid metabolism. *Placenta* **36**, 389-396 (2015).

415. K. Green *et al.*, A developmental window of opportunity for imprinted gene silencing mediated by DNA methylation and the Kcnq1ot1 noncoding RNA. *Mamm Genome* **18**, 32-42 (2007).

416. M. Frommer *et al.*, A genomic sequencing protocol that yields a positive display of 5-methylcytosine residues in individual DNA strands. *Proc Natl Acad Sci U S A* **89**, 1827-1831 (1992).

417. Z. Xiong, P. W. Laird, COBRA: a sensitive and quantitative DNA methylation assay. *Nucleic acids research* **25**, 2532-2534 (1997).

418. M. Ehrich *et al.*, Quantitative high-throughput analysis of DNA methylation patterns by base-specific cleavage and mass spectrometry. *Proc Natl Acad Sci U S A* **102**, 15785-15790 (2005).

419. M. Bibikova *et al.*, High density DNA methylation array with single CpG site resolution. *Genomics* **98**, 288-295 (2011).

420. A. Meissner *et al.*, Reduced representation bisulfite sequencing for comparative high-resolution DNA methylation analysis. *Nucleic acids research* **33**, 5868-5877 (2005).

421. T. D. Schmittgen, K. J. Livak, Analyzing real-time PCR data by the comparative C(T) method. *Nat Protoc* **3**, 1101-1108 (2008).

422. J. M. Frost, G. E. Moore, The importance of imprinting in the human placenta. *PLoS Genet* **6**, e1001015 (2010).

423. S. Choufani *et al.*, A novel approach identifies new differentially methylated regions (DMRs) associated with imprinted genes. *Genome Research* **21**, 465-476 (2011).

424. F. Court *et al.*, Genome-wide parent-of-origin DNA methylation analysis reveals the intricacies of human imprinting and suggests a germline methylation-independent mechanism of establishment. *Genome Research* **24**, 554-569 (2014).

425. B. B. McConnell, V. W. Yang, Mammalian Kruppel-like factors in health and diseases. *Physiol Rev* **90**, 1337-1381 (2010).

426. S. K. Swamynathan, Kruppel-like factors: three fingers in control. *Hum Genomics* **4**, 263-270 (2010).

427. Y. Belacortu, R. Weiss, S. Kadener, N. Paricio, Transcriptional activity and nuclear localization of Cabut, the Drosophila ortholog of vertebrate TGF-beta-inducible early-response gene (TIEG) proteins. *PLoS One* **7**, e32004 (2012).

428. G. Lomberk *et al.*, Kruppel-like factor 11 regulates the expression of metabolic genes via an evolutionarily conserved protein interaction domain functionally disrupted in maturity onset diabetes of the young. *J Biol Chem* **288**, 17745-17758 (2013).

429. M. J. Truty, G. Lomberk, M. E. Fernandez-Zapico, R. Urrutia, Silencing of the transforming growth factor-beta (TGFbeta) receptor II by Kruppel-like factor 14 underscores the importance of a negative feedback mechanism in TGFbeta signaling. *J Biol Chem* **284**, 6291-6300 (2009).

430. C. R. Gonzalez, S. S. Vallcaneras, R. S. Calandra, S. I. Gonzalez Calvar, Involvement of KLF14 and egr-1 in the TGF-beta1 action on Leydig cell proliferation. *Cytokine* **61**, 670-675 (2013).

431. N. G. Copeland, N. A. Jenkins, D. L. Court, Recombineering: a powerful new tool for mouse functional genomics. *Nat Rev Genet* **2**, 769-779 (2001).

432. P. Liu, N. A. Jenkins, N. G. Copeland, A highly efficient recombineering-based method for generating conditional knockout mutations. *Genome Res* **13**, 476-484 (2003).

433. Y. Guo *et al.*, Perhexiline activates KLF14 and reduces atherosclerosis by modulating ApoA-I production. *J Clin Invest* **125**, 3819-3830 (2015).

434. G. Fan *et al.*, Loss of KLF14 triggers centrosome amplification and tumorigenesis. *Nat Commun* **6**, 8450 (2015).

435. T. M. de Assuncao *et al.*, New role for Kruppel-like factor 14 as a transcriptional activator involved in the generation of signaling lipids. *J Biol Chem* **289**, 15798-15809 (2014).

436. W. Reik, A. Lewis, Co-evolution of X-chromosome inactivation and imprinting in mammals. *Nat Rev Genet* **6**, 403-410 (2005).

437. W. A. MacDonald, S. S. Sachani, C. R. White, M. R. Mann, A role for chromatin topology in imprinted domain regulation. *Biochem Cell Biol* **94**, 43-55 (2016).

438. G. Smits *et al.*, Conservation of the H19 noncoding RNA and H19-IGF2 imprinting mechanism in therians. *Nature genetics* **40**, 971-976 (2008).

439. K. Sterner, Jameson, N., and Wildman D., in *Building babies: Primate development in proximate and ultimate perspective,* C. K.B.H, Ed. (Springer Science, New York, 2013).

440. J. F. Wilkins, D. Haig, What good is genomic imprinting: the function of parent-specific gene expression. *Nat Rev Genet* **4**, 359-368 (2003).

441. M. B. Renfree, E. I. Ager, G. Shaw, A. J. Pask, Genomic imprinting in marsupial placentation. *Reproduction* **136**, 523-531 (2008).

442. M. B. Renfree, S. Suzuki, T. Kaneko-Ishino, The origin and evolution of genomic imprinting and viviparity in mammals. *Philos Trans R Soc Lond B Biol Sci* **368**, 20120151 (2013).

443. J. M. Frost, R. Udayashankar, H. D. Moore, G. E. Moore, Telomeric NAP1L4 and OSBPL5 of the KCNQ1 cluster, and the DECORIN gene are not imprinted in human trophoblast stem cells. *PLoS One* **5**, e11595 (2010).

444. S. M. Zeng, J. Yankowitz, X-inactivation patterns in human embryonic and extra-embryonic tissues. *Placenta* **24**, 270-275 (2003).

445. S. Varmuza, M. Mann, Genomic imprinting--defusing the ovarian time bomb. *Trends Genet* **10**, 118-123 (1994).

446. R. A. McGowan, C. C. Martin, DNA methylation and genome imprinting in the zebrafish, Danio rerio: some evolutionary ramifications. *Biochem Cell Biol* **75**, 499-506 (1997).

447. A. R. Prickett, R. J. Oakey, A survey of tissue-specific genomic imprinting in mammals. *Mol Genet Genomics* **287**, 621-630 (2012).

448. P. B. Vrana, Genomic imprinting as a mechanism of reproductive isolation in mammals. *J Mammal* **88**, 5-23 (2007).

449. A. R. Duselis, P. B. Vrana, Aberrant growth and pattern formation in Peromyscus hybrid placental development. *Biol Reprod* **83**, 988-996 (2010).

450. A. R. Duselis, C. D. Wiley, M. J. O'Neill, P. B. Vrana, Genetic evidence for a maternal effect locus controlling genomic imprinting and growth. *Genesis* **43**, 155-165 (2005).

451. M. Loschiavo, Q. K. Nguyen, A. R. Duselis, P. B. Vrana, Mapping and identification of candidate loci responsible for Peromyscus hybrid overgrowth. *Mamm Genome* **18**, 75-85 (2007).

452. R. B. McCole *et al.*, A Case-by-Case Evolutionary Analysis of Four Imprinted Retrogenes. *Evolution* **65**, 1413-1427 (2011).

453. S. Suzuki *et al.*, Retrotransposon silencing by DNA methylation can drive mammalian genomic imprinting. *PLoS Genet* **3**, e55 (2007).

454. R. B. McCole, R. J. Oakey, Unwitting hosts fall victim to imprinting. *Epigenetics : official journal of the DNA Methylation Society* **3**, 258-260 (2008).

455. H. K. Evans, J. R. Weidman, D. O. Cowley, R. L. Jirtle, Comparative phylogenetic analysis of blcap/nnat reveals eutherian-specific imprinted gene. *Mol Biol Evol* **22**, 1740-1748 (2005).

456. J. Gimenez *et al.*, Comparative methylation of ERVWE1/syncytin-1 and other human endogenous retrovirus LTRs in placenta tissues. *DNA Res* **16**, 195-211 (2009).

457. E. B. Chuong, M. A. Rumi, M. J. Soares, J. C. Baker, Endogenous retroviruses function as species-specific enhancer elements in the placenta. *Nature genetics* **45**, 325-329 (2013).

458. D. Haig, Retroviruses and the placenta. *Curr Biol* **22**, R609-613 (2012).

459. D. P. Barlow, Methylation and imprinting: from host defense to gene regulation? *Science* **260**, 309-310 (1993).

460. J. F. McDonald, M. A. Matzke, A. J. Matzke, Host defenses to transposable elements and the evolution of genomic imprinting. *Cytogenet Genome Res* **110**, 242-249 (2005).

461. A. Mould, M. A. Morgan, L. Li, E. K. Bikoff, E. J. Robertson, Blimp1/Prdm1 governs terminal differentiation of endovascular trophoblast giant cells and defines multipotent progenitors in the developing placenta. *Genes Dev* **26**, 2063-2074 (2012).

462. A. Bonnin *et al.*, A transient placental source of serotonin for the fetal forebrain. *Nature* **472**, 347-350 (2011).

463. A. Bonnin, P. Levitt, Fetal, maternal, and placental sources of serotonin and new implications for developmental programming of the brain. *Neuroscience* **197**, 1-7 (2011).

464. S. Kishore, S. Stamm, The snoRNA HBII-52 regulates alternative splicing of the serotonin receptor 2C. *Science* **311**, 230-232 (2006).

465. M. R. DeBaun, E. L. Niemitz, A. P. Feinberg, Association of in vitro fertilization with Beckwith-Wiedemann syndrome and epigenetic alterations of LIT1 and H19. *Am J Hum Genet* **72**, 156-160 (2003).

466. C. Gicquel *et al.*, In vitro fertilization may increase the risk of Beckwith-Wiedemann syndrome related to the abnormal imprinting of the KCN1OT gene. *Am J Hum Genet* **72**, 1338-1341 (2003).

467. J. Halliday, K. Oke, S. Breheny, E. Algar, J. A. D, Beckwith-Wiedemann syndrome and IVF: a case-control study. *Am J Hum Genet* **75**, 526-528 (2004).

468. E. R. Maher *et al.*, Beckwith-Wiedemann syndrome and assisted reproduction technology (ART). *Journal of medical genetics* **40**, 62-64 (2003).

469. D. J. Amor, J. Halliday, A review of known imprinting syndromes and their association with assisted reproduction technologies. *Hum Reprod* **23**, 2826-2834 (2008).

470. A. Uyar, E. Seli, The impact of assisted reproductive technologies on genomic imprinting and imprinting disorders. *Curr Opin Obstet Gynecol* **26**, 210-221 (2014).

471. D. Lim *et al.*, Clinical and molecular genetic features of Beckwith-Wiedemann syndrome associated with assisted reproductive technologies. *Hum Reprod* **24**, 741-747 (2009).

472. S. Rossignol *et al.*, The epigenetic imprinting defect of patients with Beckwith-Wiedemann syndrome born after assisted reproductive technology is not restricted to the 11p15 region. *Journal of medical genetics* **43**, 902-907 (2006).

473. D. Lucifero, J. R. Chaillet, J. M. Trasler, Potential significance of genomic imprinting defects for reproduction and assisted reproductive technology. *Hum Reprod Update* **10**, 3-18 (2004).

474. A. Paoloni-Giacobino, J. R. Chaillet, Genomic imprinting and assisted reproduction. *Reprod Health* **1**, 6 (2004).

475. A. S. Doherty, M. R. Mann, K. D. Tremblay, M. S. Bartolomei, R. M. Schultz, Differential effects of culture on imprinted H19 expression in the preimplantation mouse embryo. *Biol Reprod* **62**, 1526-1535 (2000).

476. M. R. Mann *et al.*, Selective loss of imprinting in the placenta following preimplantation development in culture. *Development* **131**, 3727-3735 (2004).

477. S. Khosla, W. Dean, D. Brown, W. Reik, R. Feil, Culture of preimplantation mouse embryos affects fetal development and the expression of imprinted genes. *Biol Reprod* **64**, 918-926 (2001).

478. A. L. Fortier, F. L. Lopes, N. Darricarrere, J. Martel, J. M. Trasler, Superovulation alters the expression of imprinted genes in the midgestation mouse placenta. *Human Molecular Genetics* **17**, 1653-1665 (2008).

479. B. A. Market-Velker, L. Y. Zhang, L. S. Magri, A. C. Bonvissuto, M. R. W. Mann, Dual effects of superovulation: loss of maternal and paternal imprinted methylation in a dose-dependent manner. *Human Molecular Genetics* **19**, 36-51 (2010).

480. M. M. Denomme, L. Y. Zhang, M. R. W. Mann, Embryonic imprinting perturbations do not originate from superovulation-induced defects in DNA methylation acquisition. *Fertil Steril* **96**, 734-U268 (2011).

481. P. Fauque *et al.*, In vitro fertilization and embryo culture strongly impact the placental transcriptome in the mouse model. *PLoS One* **5**, e9218 (2010).

482. S. Markoulaki, A. Meissner, R. Jaenisch, Somatic cell nuclear transfer and derivation of embryonic stem cells in the mouse. *Methods* **45**, 101-114 (2008).

483. K. Hochedlinger, R. Jaenisch, Nuclear reprogramming and pluripotency. *Nature* **441**, 1061-1067 (2006).

484. W. M. Rideout, 3rd, K. Eggan, R. Jaenisch, Nuclear cloning and epigenetic reprogramming of the genome. *Science* **293**, 1093-1098 (2001).

485. D. Humpherys *et al.*, Abnormal gene expression in cloned mice derived from embryonic stem cell and cumulus cell nuclei. *Proc Natl Acad Sci U S A* **99**, 12889-12894 (2002).

486. D. Humpherys *et al.*, Epigenetic instability in ES cells and cloned mice. *Science* **293**, 95-97 (2001).

487. M. R. Mann *et al.*, Disruption of imprinted gene methylation and expression in cloned preimplantation stage mouse embryos. *Biol Reprod* **69**, 902-914 (2003).

488. S. Tanaka *et al.*, Placentomegaly in cloned mouse concepti caused by expansion of the spongiotrophoblast layer. *Biol Reprod* **65**, 1813-1821 (2001).

489. T. Brambrink, K. Hochedlinger, G. Bell, R. Jaenisch, ES cells derived from cloned and fertilized blastocysts are transcriptionally and functionally indistinguishable. *Proc Natl Acad Sci U S A* **103**, 933-938 (2006).

490. S. Wakayama *et al.*, Equivalency of nuclear transfer-derived embryonic stem cells to those derived from fertilized mouse blastocysts. *Stem Cells* **24**, 2023-2033 (2006).

491. W. V. Holt, A. R. Pickard, R. S. Prather, Wildlife conservation and reproductive cloning. *Reproduction* **127**, 317-324 (2004).

492. L. E. Young, K. D. Sinclair, I. Wilmut, Large offspring syndrome in cattle and sheep. *Rev Reprod* **3**, 155-163 (1998).

493. Y. Wei *et al.*, Unfaithful maintenance of methylation imprints due to loss of maternal nuclear Dnmt1 during somatic cell nuclear transfer. *PLoS One* **6**, e20154 (2011).

494. K. Takahashi, S. Yamanaka, Induction of pluripotent stem cells from mouse embryonic and adult fibroblast cultures by defined factors. *Cell* **126**, 663-676 (2006).

495. M. J. Boland *et al.*, Adult mice generated from induced pluripotent stem cells. *Nature* **461**, 91-94 (2009).

496. X. Y. Zhao *et al.*, iPS cells produce viable mice through tetraploid complementation. *Nature* **461**, 86-90 (2009).

497. M. Stadtfeld *et al.*, Ascorbic acid prevents loss of Dlk1-Dio3 imprinting and facilitates generation of all-iPS cell mice from terminally differentiated B cells. *Nature genetics* **44**, 398-405, S391-392 (2012).

498. W. Dean *et al.*, Altered imprinted gene methylation and expression in completely ES cell-derived mouse fetuses: association with aberrant phenotypes. *Development* **125**, 2273-2282 (1998).

499. K. Eggan *et al.*, Hybrid vigor, fetal overgrowth, and viability of mice derived by nuclear cloning and tetraploid embryo complementation. *Proc Natl Acad Sci U S A* **98**, 6209-6214 (2001).

500. P. M. Guenzl, D. P. Barlow, Macro lncRNAs: a new layer of cis-regulatory information in the mammalian genome. *RNA Biol* **9**, 731-741 (2012).

501. F. M. Pauler, M. V. Koerner, D. P. Barlow, Silencing by imprinted noncoding RNAs: is transcription the answer? *Trends Genet* **23**, 284-292 (2007).

502. H. Royo, J. Cavaille, Non-coding RNAs in imprinted gene clusters. *Biol Cell* **100**, 149-166 (2008).

503. P. Vitali, H. Royo, V. Marty, M. L. Bortolin-Cavaille, J. Cavaille, Long nuclear-retained non-coding RNAs and allele-specific higher-order chromatin organization at imprinted snoRNA gene arrays. *J Cell Sci* **123**, 70-83 (2010).

504. E. Delorme-Axford *et al.*, Human placental trophoblasts confer viral resistance to recipient cells. *Proc Natl Acad Sci U S A* **110**, 12048-12053 (2013).

505. M. Noguer-Dance *et al.*, The primate-specific microRNA gene cluster (C19MC) is imprinted in the placenta. *Hum Mol Genet* **19**, 3566-3582 (2010).

506. M. Alders *et al.*, The human Achaete-Scute homologue 2 (ASCL2,HASH2) maps to chromosome 11p15.5, close to IGF2 and is expressed in extravillus trophoblasts. *Hum Mol Genet* **6**, 859-867 (1997).

507. T. Miyamoto *et al.*, The human ASCL2 gene escaping genomic imprinting and its expression pattern. *J Assist Reprod Genet* **19**, 240-244 (2002).

508. M. Fukunaga, Immunohistochemical characterization of p57(KIP2) expression in early hydatidiform moles. *Hum Pathol* **33**, 1188-1192 (2002).

509. A. Saxena *et al.*, The product of the imprinted gene IPL marks human villous cytotrophoblast and is lost in complete hydatidiform mole. *Placenta* **24**, 835-842 (2003).

510. K. Nakabayashi *et al.*, Genomic imprinting of PPP1R9A encoding neurabin I in skeletal muscle and extra-embryonic tissues. *Journal of medical genetics* **41**, 601-608 (2004).

511. H. Li, H.-K. Sung, D. Qu, A. Nagy, S. L. Adamson, Conditional Gene Deletion in the Placenta Using the Cre-loxP System. *The Guide to Investigation of Mouse Pregnancy*, 309 (2013).

512. Y. Morioka, A. Isotani, R. G. Oshima, M. Okabe, M. Ikawa, Placenta-specific gene activation and inactivation using integrase-defective lentiviral vectors with the Cre/LoxP system. *Genesis* **47**, 793-798 (2009).